Geochemical (elemental and isotopic) constraints on the genesis of the Mississippi Valley-type zinc-lead deposit of San Vicente, central Peru

Spangenberg, Jorge Enrique

UNIVERSITÉ DE GENÈVE
Département de Minéralogie

FACULTÉ DES SCIENCES
Professeur Lluís Fontboté

Geochemical (elemental and isotopic) constraints on the genesis of the Mississippi Valley-type zinc-lead deposit of San Vicente, central Peru

THÈSE

présentée à la Faculté des Sciences de l'Université de Genève pour obtenir le grade de Docteur ès Sciences, mention Sciences de la Terre

par

Jorge Enrique SPANGENBERG
de Montevideo (Uruguay)

Thèse No 2745

Genève
1995

La Faculté des Sciences, sur le préavis de Messieurs L. FONTBOTÉ, professeur ordinaire et directeur de thèse (Département de minéralogie), J. HUNZIKER, professeur (Université de Lausanne - Institut de minéralogie, BFSH 2), G. ANDERSON, professeur (Université de Toronto - Département de géologie), D. FONTIGNIE, docteur (Département de minéralogie) et Z. SHARP, docteur (Université de Lausanne - Institut de minéralogie, BFSH 2), autorise l'impression de la présente thèse, sans exprimer d'opinion sur les propositions qui y sont énoncées.

Genève, le 23 mars 1995

Thèse - 2745 -

Le Doyen, Pierre MOESCHLER

Spangenberg, J. E.: Geochemical (elemental and isotopic) constraints on the genesis of the Mississippi Valley-type zinc-lead deposit of San Vicente, central Peru.

Terre & Environnement, vol. 1, xii + 123 pp. (1995)

ISBN 2-940153-00-0
Section des Sciences de la Terre, Université de Genève, 13 rue des Maraîchers, CH-1211 Genève 4, Suisse
Téléphone: ++41-22-702-6111, Télefax: ++41-22-320-5732

TABLE OF CONTENTS

[1] This chapter "Introduction and summary of the results" is written in French in accordance with the instructions for publication of PhD theses of the Faculté des Sciences, Université de Genève.

ACKNOWLEDGMENTS

I would like to thank Prof. L. Fontboté for introducing me to the project topic and to the Mississippi Valley-type district of San Vicente. I am also thankful for his supervision, suggestions and fruitful discussions throughout the work.

I am particularly indebted to Prof. G.M. Anderson, Prof. J. Hunziker, Dr. Z. Sharp, and Dr. D. Fontignie for critical reading and improvement of the manuscript.

I am grateful to the San Ignacio de Morococha S.A. Mining Company and the staff of the Geology Department of San Vicente mine for their help in the field work, especially L. Oldham, Ing. R. Tejada, Ing. D. Dávila, Ing. O. Febres, Ing. L. Guillén, Ing. C. Vallejo, Ing. R. Ligarda, Ing. J. Motta, Ing. M. Castañeda, Ing. C. Salinas, Ing. H. Aspajo, and Ing. W. Flores.

A significant part of this work was carried out at the Stable Isotope Laboratory of the University of Lausanne. I acknowledge the help, assistance and collaboration of Prof. J. Hunziker, and all the "stable isotope colleagues". I am specially grateful to Dr. Z. Sharp for introducing me in the analytical procedures and for stimulating discussions.

I would also like to thank Prof. J.-R. Disnar of the University of Orléans for the Rock-Eval analyses and his valuable contribution on geochemical aspects of the organic matter associated to the San Vicente ore.

I would also like to express my thanks for help in analytical work to Dr. F. Bussy, University of Lausanne (microprobe analyses); Dr. Ph. Thélin, University of Lausanne (XRD-analyses), Dr. H.-R. Pfeifer and J.-C. Lavanchy, Centre d'Analyse Minérale, University of Lausanne (coulometric determination of C_{org}), Dr. P. Voldet, Mineralogy Department, University of Geneva (Rb determination), Dr. D. Fontignie, Dr. R. Moritz and M. Falcheri, Mineralogy Department, University of Geneva (Sr isotopes), Prof. J. Buffle, Dr. J.-C. Negre, and M.-R. Martin, Chemical and analytical Department, University of Geneva (ICP-AES analysis), Dr. R. Martini, Geology Department, University of Geneva (cathodoluminescence microscopy).

I am grateful to all the faculty and staff of the Earth Sciences Section of the University of Geneva, especially Prof. M. Delaloye and Prof. R. Chessex, heads of the Department of Mineralogy, Mrs. J. Berthoud for their help and support throughout this work, V. Cornut and J.M. Bocard for excellent thin and polished sections, J. Metzger for his help in the preparation of the illustrations, Prof. M. Dungan for correction of the English abstract, F. Capponi, Mrs. N. Rihs, and Dr. P. Kunz for their assistance. I would also like to thank my friends and colleagues of the Universities of Geneva and Lausanne, particularly M. Doppler, R. Marschik, M. Ferrés, S. Jordi, F. Lieben, and O. Parlak for friendly contributions to this work.

I would like to express my thanks to Dr. S. Rosas for making available prior publication the necessary sedimentological background for this study. Blanca, Lionel, Norma and Pilar Rosas provided hospitality in Lima.

I acknowledge the financial support of the Swiss National Science Foundation (Grant no 20-36397.92).

Last but not least I deeply thank the support, encouragement, and patience of my wife Delphine and my children Solène and Adrien, and the support and stimulations of my parents, Emilia and Gustavo, and my brother Germán during all my studies.

ABSTRACT

Geochemical (elemental and isotopic) constraints on the genesis of the Mississippi Valley-type zinc-lead deposit of San Vicente, central Peru

Mississippi Valley-type (MVT) zinc-lead deposits and ore occurrences of the San Vicente belt are hosted in dolostones of the eastern Upper Triassic to Lower Jurassic Pucará basin, central Peru. The elemental (Ca, Mg, Fe, Mn, Sr, Na, Ba, Zn, C_{org}, S and rare earth elements) and isotopic (C and O) compositions of the host and gangue carbonates from 20 localities, including the San Vicente main deposit, minor ore occurrences, and barren localities are used to constrain fluid path-ways, ore precipitation mechanisms, and changes in Eh-pH conditions during mineralization.

The altered replacement dolomite (I) and the white sparry dolomite (II) are both depleted in Fe and REE, and enriched in Mn compared to the host dolomite. They display, at least in the samples of the main deposit, negative Ce and Eu anomalies. These results suggest that the incoming ore fluid was slightly oxidizing, acidic, and poor in REE and Fe and therefore had had limited previous interaction with the carbonate host rocks. This is consistent with its migration along an oxidizing main aquifer, such as the Red Sandstones and other clastic units at the base of the basin.

Mixing between an incoming hot, saline, slightly acidic and oxidizing radiogenic (Pb, Sr) fluid and the native intra-formational alkaline reducing waters explains the overall isotopic variation (-11.5 to 2.5‰ $\delta^{13}C$, -12.5 to -6.4‰ PDB $\delta^{18}O$) and the distribution of REE and other trace elements in the different generations of hydrothermal carbonates (I, II, and III). The mixing of these two different fluids determines the evolving composition of the mineralizing fluid(s).

The ore-stage altered host dolomite and hydrothermal carbonates show narrower isotopic ranges (0.2 to 1.7 ‰ $\delta^{13}C$, -11.4 to -7.3 ‰ PDB $\delta^{18}O$). These patterns are similar throughout the studied area. The measured isotopic covariations of the hydrothermal carbonates, which are consistent with the REE data, indicate that two mechanisms were responsible for precipitation of the ore-stage carbonates and associated sphalerite:

a) Temperature-dependent interaction of the mineralizing fluids and the carbonate host rocks explain the alteration and replacement of the dark dolomite (I) and precipitation of early sphalerite (I) and (II). Subsequently, a second generation of hydrothermal white sparry dolomite (II) and sphalerite (II) formed overgrowths on the altered dolomite (I) by filling secondary porosity under fluid-buffered conditions. This main mineralizing stage was the result of prolonged fluid-rock interaction coupled with minor CO_2 degassing.

b) Pressure fall leading to outgassing of CO_2 and consequent increase in the pH of the ore fluid caused precipitation of late sparry carbonates (dolomite and calcite III) and, likely, sphalerite (III).

The regionally uniform isotopic and elemental patterns, coupled with the mineralogical and petrographic similarities among the different MVT occurrences, reflect that similar mineralizing processes occurs in the entire San Vicente belt. This implies the existence of an interconnected mineralizing hydrothermal system. In addition, the limited isotopic and elemental equilibration between the incoming fluid and the Pucará rocks indicates that access of the corrosive ore fluid to the mineralized zones was likely by permeable channel-ways (faults, basement highs).

The results of the Rock-Eval pyrolisis indicate the occurrence of two types of organic matter in the gangue carbonates of San Vicente: a hyper-mature kerogen (T_{max} about 515°C), which likely is thermally altered native organic matter, and an allochtonous thermally labile soluble bitumen (T_{max} about 230°C). The presence of native sulfur associated with extremely carbon-light calcites replacing evaporitic sulfates (up to -11.5‰ $\delta^{13}C$), altered native organic matter, and heavier hydrothermal bitumen (from -27.5 to

-23.3‰ $\delta^{13}C$) point to thermochemical reduction of sulfate and / or thiosulfate. The Rock-Eval results combined with carbon isotope data suggest that the native organic matter was the main source of reductants in the mineralizing fluid. Alteration of the organic matter disseminated in the host dolomite by the incoming ore fluid liberated hydrocarbons which locally produced reducing conditions that led to sulfate reduction (and reduction of Eu^{+3} to Eu^{+2}). After further thermal cracking, water-washing, and polymerization of the released hydrocarbons, solid aggregates of hydrothermal bitumen precipitated. Thus, the main flow type of the fluid during ore precipitation was pervasive and, consequently, the ore distribution controlled by porosity (primary or secondary).

The Fe-Mn covariations combined with the Eu anomalies of the hydrothermal carbonates are consistent with a change from a reducing ore-forming stage to oxidizing conditions following ore deposition. The REE enrichment, the Mn depletion, and the positive Eu anomalies of the late-stage vug-filling carbonates indicate that the post-ore "residual" acidic fluids were again oxidizing due to continuous influx of fresh basinal waters. Late REE-rich dolomite III (or calcite) and associated sphalerite III formed from the slightly acidic ore fluid during CO_2 degassing, caused in turn by an enhanced hydrothermal porosity. The widespread hydraulic brecciation, upward "escape" veins, and other structures indicate that the fluid was overpressured. An abrupt pressure drop could favor CO_2 degassing and therefore may play a major role in the ore precipitation during the late hydrothermal events in San Vicente.

RÉSUMÉ

Contraintes géochimiques (élémentaires et isotopiques) lors de la genèse du gisement zinc-plomb de type Mississippi Valley de San Vicente, Pérou central

Les gisements et occurrences de type Mississippi Valley (MVT) du district minier zinc-plomb de San Vicente se trouvent dans des dolomies de l'est du bassin de Pucará (Triasique supérieur - Jurassique inférieur), Pérou central. La composition élémentaire (Ca, Mg, Fe, Mn, Sr, Na, Ba, Zn, C_{org}, S et terres rares) et la composition isotopique (C et O) des carbonates de gangue de vingt localités -dont la mine de San Vicente, indices minéralisés et zones stériles- ont été étudiées pour contraindre géochimiquement le chemin des fluides minéralisateurs, le mécanismes des précipitations des sulfures et les variations de conditions pH-Eh pendant la minéralisation.

La dolomie noire de remplacement (I) et la dolomie blanche baroque (II) sont appauvries en fer et en terres rares et enrichies en Mn par rapport à la dolomie hôte. Les dolomies hydrothermales présentent, au moins dans les échantillons de la mine de San Vicente, des anomalies négatives en Ce et Eu. Ces résultats suggèrent que le fluide minéralisateur était relativement oxydant, acide et pauvre en terres rares et en fer, ce qui implique que le fluide a eu un échange préliminaire très restreint avec les carbonates hôtes. Par conséquent, on peut conclure que le fluide a circulé le long d'un aquifère oxydant, probablement les grès rouges (*Red Sandstone*) et d'autres unités détritiques à la base du bassin.

Le mélange d'un fluide extra-formationnel chaud, salin, légèrement acide, oxydant et radiogénique (Pb, Sr) avec des eaux intra-formationelles alcalines et réductrices, explique la variation isotopique totale (-11.5 à 2.5‰ $\delta^{13}C$, -12.5 à -6.4‰ PDB $\delta^{18}O$) et la distribution des terres rares et des autres éléments en traces dans les carbonates hydrothermaux.

Les valeurs de $\delta^{13}C$ et $\delta^{18}O$ de la dolomie hôte altérée et des carbonates hydrothermaux (0.2 à 1.7 ‰ $\delta^{13}C$, -11.4 à -7.3 ‰ PDB $\delta^{18}O$) et la composition isotopique de carbone (-23.3 à -27.5 ‰ $\delta^{13}C$) de la matière organique associée aux carbonates, ont une distribution similaire dans tout le district étudié.

Deux mécanismes sont supposés être responsables de la précipitation des carbonates de gangue et de la sphalérite:

a) L'interaction du fluide minéralisateur avec les carbonates hôtes explique l'altération et le remplacement de la dolomie noire (I) et la précipitation de la sphalérite (I et II). Postérieurement, une deuxième génération de dolomie hydrothermale baroque (II) et de sphalérite (II) forme des encroûtements sur la dolomie (I) altérée, ainsi que de colmatage de la porosité secondaire. Cette phase minéralisante principale, caractérisée par des réactions tamponnées par le fluide, est le résultat d'une interaction prolongée fluide-roche, combinée au dégazage du CO_2.

b) Le dégazage du CO_2, en partie provoquée par une diminution de la pression, conduit à l'augmentation du pH du fluide minéralisant et provoque la précipitation de la dernière génération des carbonates baroques (dolomie ou calcite III) et, probablement, de la sphalérite (III).

L'uniformité isotopique et élémentaire à l'échelle régionale, combinée avec les similitudes minéralogiques et pétrographiques des différentes occurrences de type MVT, indique que les processus minéralisants ont été similaires dans tout le district de San Vicente, ce qui implique l'existence d'un système hydrothermal minéralisant interconnecté. En outre, l'absence d'équilibre isotopique et élémentaire limité entre le fluide et les roches de Pucará suggère que l'accès du fluide minéralisateur aux zones minéralisées fut probablement par des canaux très perméables (failles et/ou hauts du socle).

Les résultats de la pyrolyse Rock-Eval indiquent que deux types de matière organique se trouvent dans les carbonates de gangue de San Vicente: un kérogène hyper-mature (T_{max}

de 515°C), vraisemblablement une matière organique native altérée, et un bitume soluble thermiquement labile (T_{max} de 230°C). La présence de soufre natif associé à la calcite très légère (jusqu'à 11.5‰ $\delta^{13}C$) dans des pseudomorphes des sulfates, de matière organique altérée et de bitume solide hydrothermal plus lourd (de -27.0 à -23.0‰ $\delta^{13}C$) évoque la réduction thermochimique de sulfates ou de thiosulfates. Les résultats Rock-Eval, combinés avec les données isotopiques, suggèrent que la matière organique disséminée dans la dolomie hôte a constitué la principale source d'agents réducteurs dans le fluide minéralisateur. L'altération de la matière organique disséminée dans la dolomie hôte par le fluide minéralisateur a libéré des hydrocarbures qui produisent localement des conditions réductrices, conduisant à la réduction des sulfates (et réduction de Eu^{+3} à Eu^{+2}). Par conséquent, le flux du fluide minéralisateur pendant la précipitation de la sphalérite fut pervasif; la porosité (primaire ou secondaire) détermine donc la distribution de la minéralisation. Après avoir été continuellement soumis à un cracking thermique, à un "water-washing" et à une polymérisation, les hydrocarbure libérés forment un résidu organique solide (bitume hydrothermal).

Les covariations de Fe-Mn et le changement de signe des anomalies en Eu indiquent que les conditions oxydo-réductrices du système fluide-roche, réductrices pendant la minéralisation, sont devenues légèrement oxydantes pendant la phase de post-minéralisation. L'enrichissement en terres rares, l'appauvrissement en Mn et l'anomalie positive en Eu des carbonates tardifs (II) de remplissage indiquent que le fluide résiduel post-minéralisation était à nouveau oxydant en raison de l'apport de fluides du bassin. Les carbonates tardifs (dolomie ou calcite III), riches en terres rares et la sphalérite III ont précipité à partir d'un fluide légèrement acide pendant le dégazage du CO_2, partiellement provoqué par une augmentation de la porosité hydrothermale. La bréchification hydraulique très répandue et les "veines d'échappement" orientées vers le haut ainsi que d'autres structures indiquent que le fluide a été en surpression. Une chute abrupte de la pression favoriserait le dégazage du CO_2 et aurait donc joué un rôle principal dans la précipitation de la sphalérite pendant les événements hydrothermaux tardifs de San Vicente.

RESUMEN

Restricciones geoquímicas (elementales e isotópicas) en la génesis de los yacimientos zinc-plomo de tipo Mississippi Valley de San Vicente, Perú central

Los yacimientos y ocurrencias de tipo Mississippi Valley (MVT) del distrito de San Vicente están hospedadas en dolomías del este de la cuenca Pucará (Triásico superior - Liásico), en el centro de Perú. La composición elemental (Ca, Mg, Fe, Mn, Sr, Na, Ba, Zn, C_{org}, S y tierras raras) e isotópica (C y O) de los carbonatos de ganga de 20 localidades -incluyendo la mina San Vicente, ocurrencias minerales menores y áreas estériles- han sido estudiadas para restringir geoquímicamente el camino de los fluidos mineralizantes, los mecanismos de precipitación de sulfuros y las variaciones de pH y Eh durante la mineralización.

La dolomía negra de remplazamiento (dolomita I) y la dolomita blanca espática (dolomita II) están ambas empobrecidas en Fe y tierras raras y enriquecidas en Mn comparadas con la dolomía de caja. Las dolomías hidrotermales tienen, por lo menos en las muestras de la mina San Vicente, anomalías negativas en Ce y Eu. Estos resultados sugieren que el fluido mineralizante fue relativamente oxidante, ácido, y pobre en tierras raras y Fe, lo que indica que el fluido tuvo previamente una interacción muy limitada con los carbonatos de la roca de caja. Esto es consistente con una circulación del fluido a lo largo de un acuífero oxidante, probablemente las areniscas rojas (*Red Sandstone*) y otras unidades clásticas en la base de la cuenca.

La mezcla de un fluido extra-formacional caliente, salino, ligeramente ácido, oxidante y radiogénico (Pb, Sr) con aguas intra-formacionales alcalinas y reductoras explica la variación isotópica total (-11.5 a 2.5‰ $\delta^{13}C$ y -12.5 a -6.4‰ PDB $\delta^{18}O$) y la distribución de las tierras raras y otros elementos traza en los carbonatos hidrotermales.

Los valores de $\delta^{13}C$ y $\delta^{18}O$ de la dolomita de caja alterada y de los carbonatos hidrotermales (0.2 a 1.7 ‰ $\delta^{13}C$ y -11.4 a -7.3 ‰ PDB $\delta^{18}O$), y la composición isotópica del carbono (-23.3 a -27.5 ‰ $\delta^{13}C$) de la materia orgánica asociada a estos carbonatos, muestra una distribución similar a lo largo de toda el área estudiada.

Dos mecanismos se condideran responsables de la precipitación de los carbonatos de ganga y de la esfalerita asociada:

a) La interacción del fluido mineralizante con los carbonatos de caja explica la alteración y remplazamiento de la dolomía negra (I) y la precipitación de la esfalerita (I) y (II). Posteriormente una segunda generación de dolomita hidrotermal blanca espática (II) y esfalerita (II) formaron sobrecrecimientos sobre la dolomía (I) alterada, rellenando porosidad secundaria. Esta fase mineralizante principal, caracterizada por mecanismos tamponeados por el fluido fue el resultado de prolongada interacción fluido-roca combinada con desgasificación de CO_2.

b) La desgasificación de CO_2 en parte provocada por una disminución de la presión, condujo al aumento del pH del fluido mineralizante y causó la precipitación de la última generación de carbonatos espáticos (dolomita o calcita III) y, probablemente esfalerita (III).

La uniformidad isotópica y elemental a escala regional, combinada con las similitudes mineralógicas y petrográficas de las distintas ocurrencias del tipo MVT, refleja que los procesos mineralizantes fueron similares en todo el distrito de San Vicente. Esto implica la existencia de un sistema hidrotermal mineralizante inter-conectado. Además, la ausencia de equilibrio isotópico y elemental entre el fluido y las rocas de la cuenca de Pucará indican que el acceso del fluido corrosivo a las áreas mineralizadas fue probablemente por canales muy permeables (fallas, altos estructurales).

Los resultados de la pirólisis Rock-Eval indican la ocurrencia de dos tipos de materia orgánica en los carbonatos de ganga de San Vicente: un querógeno hipermaduro (T_{max} de 515°C) -probablemente la materia orgánica nativa alterada- y un bitumen alóctono térmicamente labil y soluble (T_{max} de 230°C). La presencia de sulfuro nativo asociado a

calcita de carbono muy liviano (hasta -11.5‰ $\delta^{13}C$) reemplazando sulfatos evaporíticos, materia orgánica nativa alterada y bitumen hidrotermal más pesado (de -27.0 a -23.0‰ $\delta^{13}C$) evoca la reducción termoquímica de sulfato o tiosulfato. Los resultados de la pirólisis Rock-Eval combinados con los datos de isótopos de carbono sugieren que la materia orgánica nativa fue la fuente principal de agentes reductores en el fluido mineralizante. La alteración de la materia orgánica diseminada en la dolomía caja por el fluido mineralizante liberó hidrocarburos que produjeron localmente las condiciones reductoras necesarias para la reducción de sulfatos (y reducción de Eu^{+3} a Eu^{+2}). En consecuencia, el flujo del fluido mineralizante durante la precipitación de sulfuros fue pervasivo, y la porosidad (primaria o secundaria) determinó la distribución de la mineralización. La continuación del cracking térmico, del "water-washing" y de la polimerización de estos hidrocarburos fueron responsables de la formación de un residuo orgánico sólido (bitumen hidrotermal).

Las covariaciones de Fe y Mn combinadas con las anomalías de Eu de los carbonatos hidrotermales sugieren un cambio de condiciones reductoras durante la fase mineralizante principal a oxidantes en fases post-mineralización. El enriquecimiento en tierras raras, empobrecimiento en Mn, y la anomalía positiva de Eu de los carbonatos tardíos de relleno indican que el fluido "residual" post-mineralización fue nuevamente oxidante debido a un flujo continuo de salmueras de la cuenca. Los carbonatos tardíos (dolomita o calcita III), ricos en tierras raras, y la esfalerita III se formaron a partir de un fluido ligeramente ácido durante la desgasificación de CO_2, ocasionada en parte por un aumento de la porosidad hidrotermal. La extensa brechificación hidráulica, venas de escape ascendentes y otras estructuras indican que el fluido estaba en sobre-presión. Un brusco descenso de la presión favorecería la desgasificación de CO_2 y tendría un rol principal en la precipitación de sulfuros durante los eventos hidrotermales tardíos en San Vicente.

CHAPTER 1

INTRODUCTION ET RÉSUMÉ DES RÉSULTATS[1]

1.1 Introduction

1.1.1 Considérations générales

Le district minier zinc-plomb de San Vicente est le meilleur exemple sud-américain de gisements de type Mississippi Valley (MVT). Il se trouve dans le Pérou central, à 328 km à l'est de Lima, dans la province de Chanchamayo. D'un point de vue morphostructural, San Vicente se trouve dans la zone subandine entre le versant oriental de la cordillère des Andes et le piémont amazonien (Fig. 1.1). Cette région nommée Ceja de Selva est caractérisée par

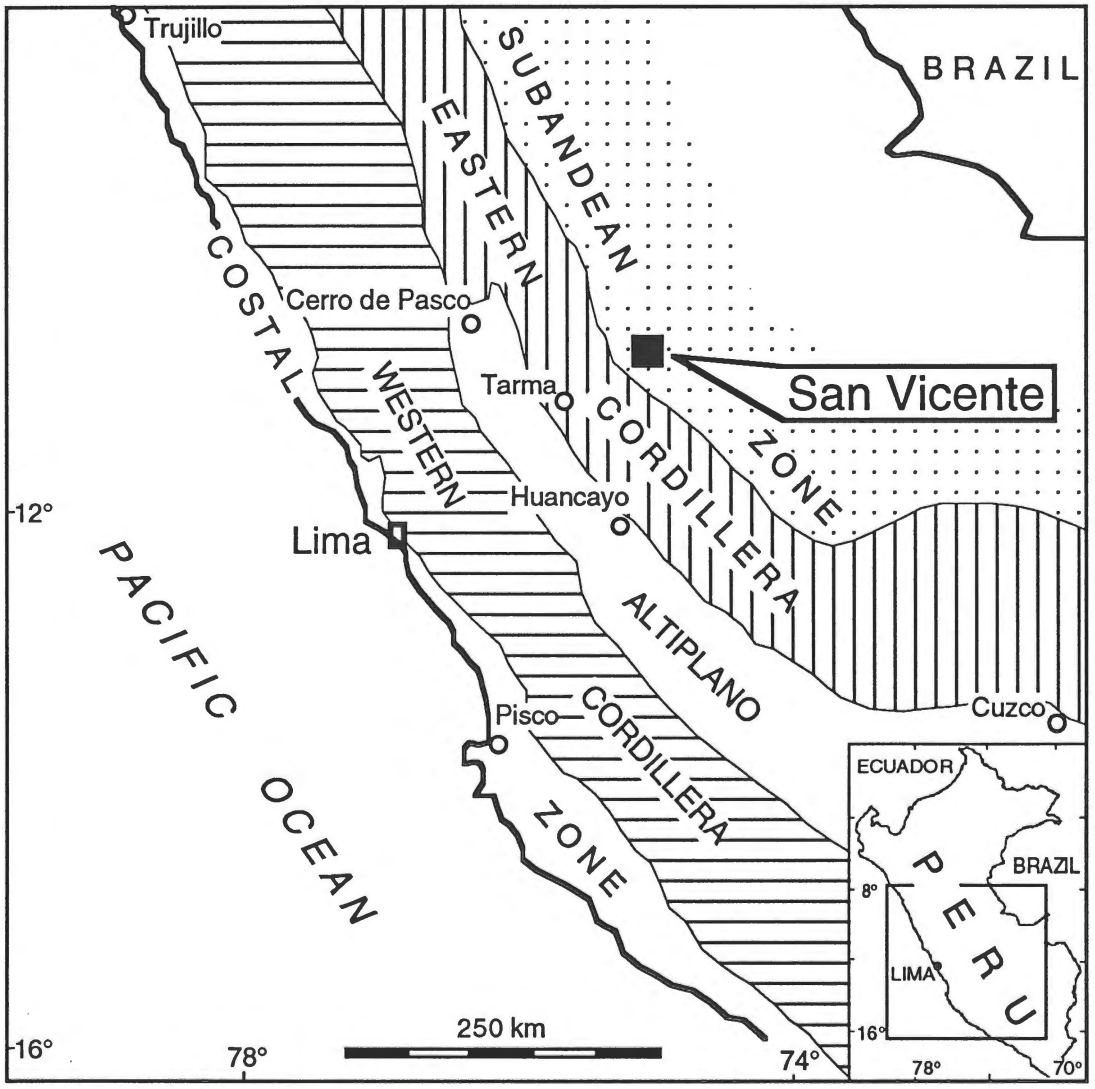

Figure 1.1. Geographical sketch map showing the location of the San Vicente Mississippi Valley-type zinc-lead district and the morphostructural units of central Peru after Mégard (1976).
Schéma géographique montrant la localisation du district minié zinc-plomb de San Vicente de type Mississippi Valley et la zonation morphostructurale du Pérou Central d'après Mégard (1976).

---

[1] This chapter "Introduction and summary of the results" is written in French in accordance with the instructions for publication of PhD theses of the Faculté des Sciences, Université de Genève.

un relief très accidenté avec des crêtes dépassant parfois 3000 m et un climat très chaud et humide; une végétation tropicale la recouvre jusqu'à 3500 m. Les gisements de San Vicente ainsi que d'autres gisements mineurs et occurrences du même type sont encaissés dans la partie est du bassin de Pucará (Fig. 1.2), d'âge Triasique supérieur - Jurassique inférieur. Le gisement majeur, c'est-à-dire San Vicente même, est le seul gisement de la partie est du bassin de Pucará actuellement en production et est exploité par la compagnie minière San Ignacio de Morococha (SIMSA). La somme de la production et des réserves totalise 20 millions de tonnes de minerai à une teneur en zinc de 11 % et en plomb de 0.8 %. Il est le deuxième producteur de zinc du Pérou, après les gisements de Cerro de Pasco.

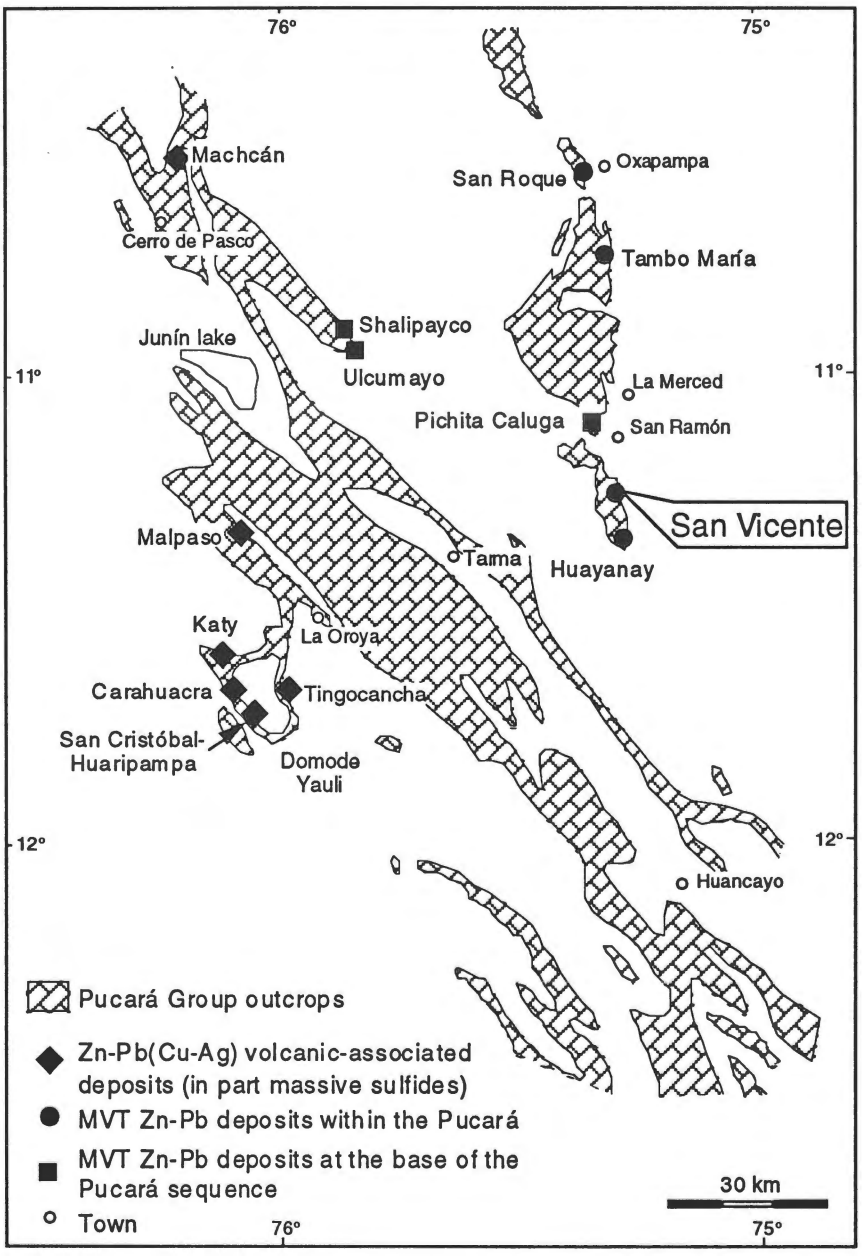

Figure 1.2. Outcrop map of the Pucará Group showing the location of the San Vicente district and the ore deposits and occurrences associated with the Pucará rocks (after Fontboté, 1990).
Carte des affleurements du groupe Pucará montrant le district minier de San Vicente ainsi que d'autres gisements et occurrences associés aux roches du Pucará (d'après Fontboté, 1990).

Différents aspects du gisement de San Vicente ont été traités par Schulz (1971), Levin (1975), Lavado (1980), Fontboté (1981), Gonzalez (1987), Gorzawski (1989), Fontboté et Gorzawski (1990), Gorzawski et al. (1990), Moritz et al. (1993) et Spangenberg et al. (1994, 1995).

Selon Fontboté et Gorzawski (1990), le gisement de San Vicente s'est formé à un enfouissement maximal de 2 km, à une température comprise entre 70 et 100°C par introduction de saumures riches en zinc et plomb caractérisées par du strontium et du plomb ragiogéniques. Ces fluides minéralisateurs ont altéré les carbonates hôtes et précipité les sulfures et carbonates. L'altération des carbonates hôtes est caractérisée par les éléments suivants: textures de remplacement (dissolution/précipitation), strontium plus radiogénique, carbone et oxygène plus légers, enrichissement en manganèse et appauvrissement en fer.

1.1.2 But et organisation du travail

L'objectif du travail est de caractériser les carbonates de gangue du gisement de San Vicente en utilisant différentes méthodes géochimiques (élémentaires et isotopiques).

Étant donné la récente extension des opérations minières vers le nord et les intenses travaux d'exploration dans le district entier, de nouvelles zones, non étudiées par Fontboté et Gorzawski (1990), ont été ouvertes à l'échantillonnage, tant dans les affleurements en surface que dans la mine et dans les sondages carottés. Un échantillonnage systématique a donc permis d'obtenir une image tridimensionnelle de la signature géochimique des carbonates de gangue en accord avec la position relative des gisements et des occurrences connus. Cette approche géochimique, soutenue par l'information de terrain et l'information pétrographique entend détecter les effets du fluide(s) minéralisateur(s) sur la roche hôte. En se basant sur la géochimie des carbonates de gangue, on essaiera d'apporter des réponses aux questions encore ouvertes sur la genèse de San Vicente. Ces questions sont les suivantes:

1. Quelles sont la source et la composition des fluides minéralisants?
2. Quel chemin ont suivi ces fluides?
3. Dans quelles conditions physico-chimiques se sont précipités le minerai et la gangue?
4. Quel est le processus minéralisateur prépondérant et ses interrelations: l'interaction du fluide minéralisant avec la roche hôte, le mélange des fluides ou la dégazification du fluide?

Ce travail se présente de la façon suivante. Tout d'abord seront traités dans ce premier chapitre le cadre géologique régional ainsi qu'un résumé des résultats de l'étude. Les trois chapitres suivants (chapitre 2, 3 et 4) sont des manuscrits en cours de publication et comprennent chacun un aspect principal du travail. Le chapitre 2 est d'intérêt méthodologique et se réfère aux distorsions trouvées lors de l'analyse des isotopes de carbone et d'oxygène dans les carbonates riches en matière organique et soufre; le manuscrit est intitulé *"Apparent stable isotope heterogeneities in gangue carbonates of the Mississippi Valley-type Zn-Pb deposit, central Peru"* (auteurs: Spangenberg, J, Sharp, Z., et Fontboté, L., *Mineralium Deposita*, v. 30, p. 67-74 (1995). Les variations de la composition des isotopes stables sont abordées dans le chapitre 3; le manuscrit est intitulé *"Carbon and oxygen isotope study of hydrothermal carbonates in the zinc-lead deposits of the San Vicente district, central Peru"* (auteurs: Spangenberg, J., Fontboté, L., Sharp, Z., et Hunziker, J.). Les résultats de la géochimie des éléments en traces, dont les terres rares sont présentés dans le chapitre 4, dans le manuscrit *"Rare-earth and trace elements in hydrothermal carbonates of the San Vicente Mississippi Valley-type district, central Peru"* (auteurs: Spangenberg, J. et Fontboté, L.). Et, enfin, le dernier chapitre est consacré aux résultats préliminaires de la géochimie de la matière organique associée aux carbonates de San Vicente.

1.2 Aspects géologiques

1.2.1 Aspects géologiques régionaux

Le bassin de Pucará (Norien-Toarcien) est une plate-forme carbonatée dans la marge

occidentale du bouclier brésilien (Pérou central et nord jusqu'à 45° S, voir Fig. 1.1). Il s'est formé pendant le cycle andin par transgression marine sur des roches détritiques et des roches volcaniques alcalines à sub-alcalines du Groupe de Mitu, d'âge permien à triasique inférieur (Fontboté, 1990). Les aspects régionaux, métallogénétiques et sédimentologiques du Groupe de Pucará sont détaillés en Mégard (1978, 1987), Fontboté (1990) et Rosas (1994) ainsi que dans les références citées dans ces études.

Le Groupe de Pucará (Fig. 1.3) est constitué, de bas en haut, de trois formations: la Formation Chambará, la Formation Aramachay et la Formation Condorsinga (Fontboté, 1990; Rosas, 1994), qui se caractérisent par des sédiments néritiques. La *Formation Chambará* (Norian à Rhaetian; presque de 1000 m d'épaisseur) est constituée principalement de faciès de barrière d'eau peu profonde, supra/intertidal, lagunaire et infratidal à prédominance dolomitique. La *Formation Aramachay* (Hettangien à Sinémurien, presque de 150 m d'épaisseur) est caractérisée par des faciès plus profonds. Dans la partie ouest du bassin, cette formation est constituée de sédiments argileux et siliceux à grain très fin (shales) fortement recristallisés; le contenu en carbonates est variable. Quant à la partie est, dans la région de San Vicente, elle est caractérisée par des faciès plus anoxiques: shales bitumineux, grès, chert et roches phosphatées et elle est plus riche en carbonates. La *Formation Condorsinga* (Pliensbachian à Toarcian, presque de 350 m d'épaisseur) est représentée principalement par des calcaires bio-clastiques et chertiques. Les Formations Chambará et Condorsinga se caractérisent par des faciès d'eau peu profonde avec des évaporites et des barrières oolithiques. Elles sont, dans la partie est du bassin, les hôtes de plusieurs gisements MVT (Fig. 1.3). Les gisements les plus importants sont Shalipayco, à la base de la séquence carbonatée et San Vicente dans la partie centrale de la séquence (Fontboté, 1990).

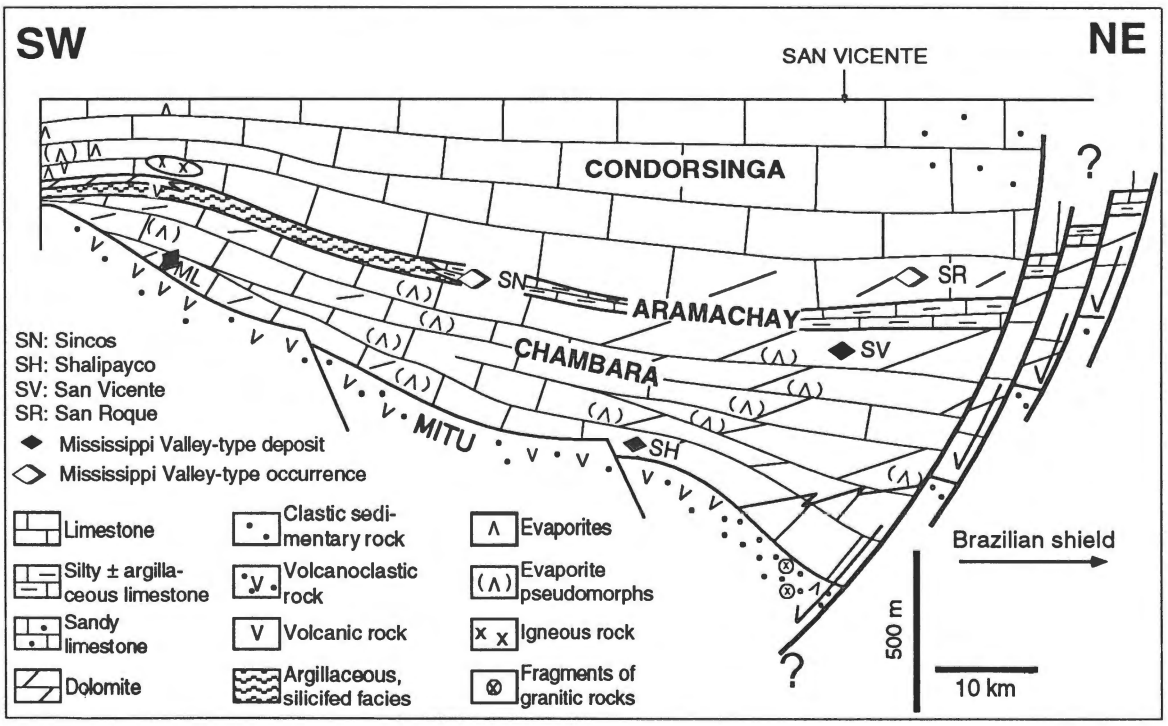

Figure 1.3. Schematic SW-NE cross-section in the southern Pucará basin (Upper Triassic - Lower Jurassic) showing the location of some MVT deposits (from Rosas, 1994).
Coupe schématique SW-NE à travers la partie sud du bassin de Pucará (Trias supérieur - Jurassique inférieur) montrant la localisation de quelques gisements MVT (d'après Rosas, 1994).

1.2.2 Le Groupe de Pucará à San Vicente

Dans la région de San Vicente (Fig. 1.4), les roches les plus anciennes sont des mica

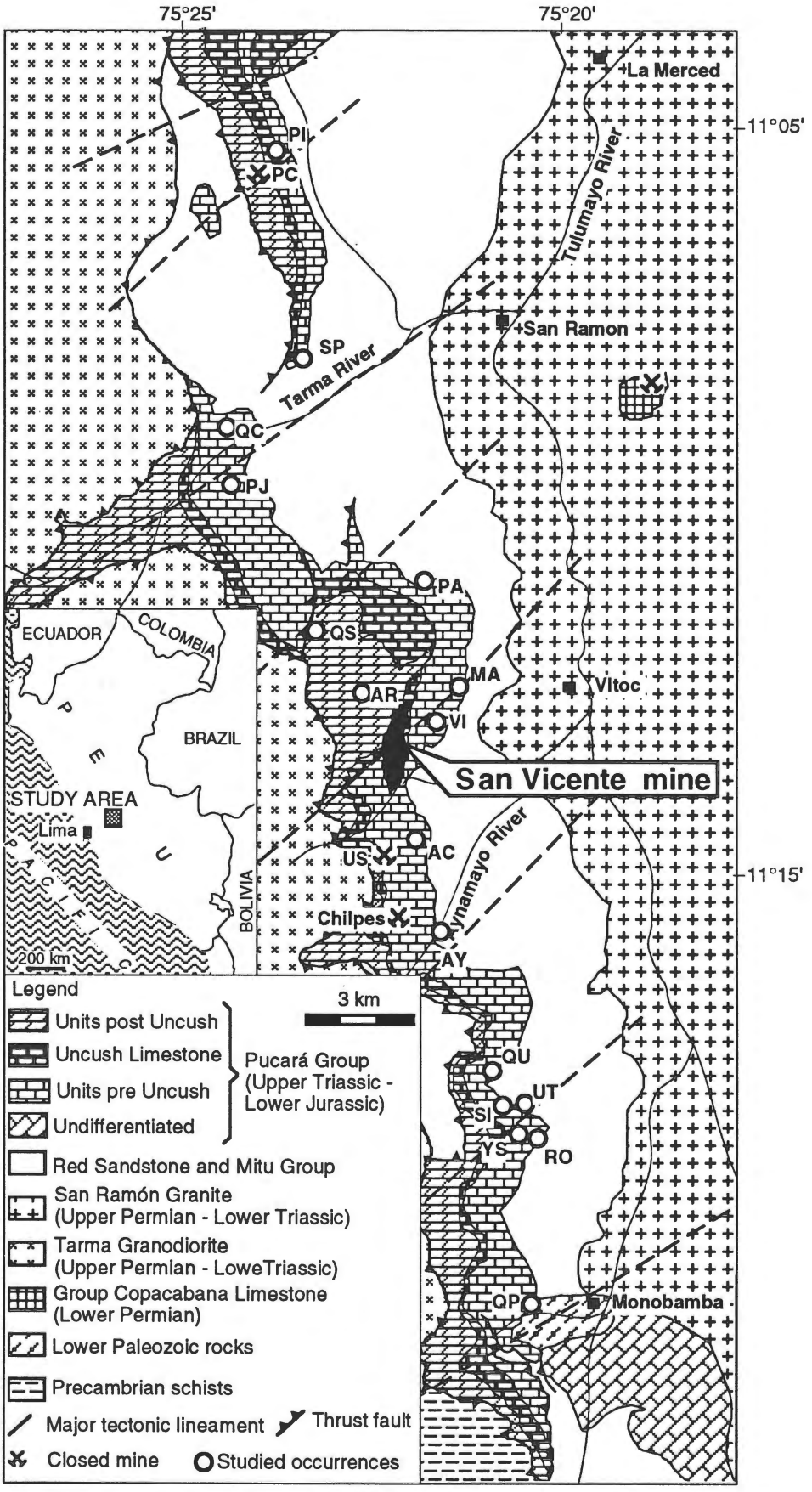

Figure 1.4. Geological map of San Vicente belt showing the studied localities (barren and mineralized areas). QP = Quebrada Piñon; RO = Rondayacu; YS = Yanachuro Sur; UT = Utcuyacu; QU=Quebrada Utcuyacu; AY = Aynamayo; CH = Chilpes; AC = Afloramiento Campana; US = Uncush Sur; SV = San Vicente mine; VI = Vilcapoma; AR = Arcopunco MA = Machuyacu; QS = Quebrada Seca; PA = Palmapata; PJ = Puntayacu Junior; QC = Quebrada Cascas; SP = Sur Pichita; PI = Pichita.

Carte géologique de la région de San Vicente montrant les localités étudiées.

schistes et gneiss précambriens ainsi que des roches du Paléozoïque inférieur, qui se présentent sous un faciès flyschoïde (Mégard, 1978). Elles sont recouvertes de carbonates du groupe Copacabana d'âge permien inférieur et de séquences terrigènes typiquement molassiques (conglomérats, grès conglomératiques, grès grossiers) du Groupe de Mitu (Permien supérieur - Trias inférieur). Deux granitoïdes d'âge Permien supérieur - Trias inférieur affleurent dans le district de San Vicente: la granodiorite de Tarma et le granite San Ramón.

Aux séries détritiques et volcano-clastiques de couleur rouge du Mitu succèdent les calcaires triassico-jurassiques de Pucará (Fig. 1.5). Dans la zone du gîte de San Vicente, l'épaisseur de la séquence de Pucará est de presque 1400 m de Norien à l'Hettangien. La succession stratigraphique est la suivante: (1) grès rouges (*Red Sandstone*); (2) séquence de calcaire de base; (3) dolomie San Judas; (4) calcaire Neptuno; (5) dolomie San Vicente; (6) calcaire bitumineux à silex Uncush; (7) dolomie Alfonso. Les unités (2) à (5) sont de la Formation Chambará, la (6) de la Formation Aramachay, et la (7) de la Formation Condorsinga. Dans le district de San Vicente, on distingue localement les unités appelées calcaires de Arcopunco et dolomies Colca sur la dolomie Alfonso (Rosas, 1994).

Une série de failles normales et de linéaments tectoniques de direction générale NE-SW, NW-SE et N-S coupe la séquence carbonatée dans la proximité des gisements et des occurrences minérales (Fig. 1.5). Ce système de failles et les hauts du socle (p.e., roches paléozoïques prés de village Monobamba) ont sûrement joué un rôle important dans la circulation des fluide(s) minéralisateur(s).

Les minerais apparaissent sous forme de corps lenticulaires, localement appelés mantos, qui sont concordants avec la stratification à l'échelle du gisement. Ces corps minéralisés sont de 100 à 400 m de long (exceptionnellement jusqu'à 1.3 km , p.e. "manto San Vicente techo "), de 200 à 300 m de large et de seulement quelques mètres d'épaisseur. La minéralisation apparaît le plus souvent comme remplaçant des grainstones oolithiques dolomitisés, soit en tant que minerai zébré, soit en tant que ciment en brèche ou veinules (Figs. 1.6a, 1.6b; Fontboté and Gorzawski, 1990; Spangenberg et al., 1995).

1.2.3 Carbonates de gangue

Dans les unités des dolomies encaissant la minéralisation de San Vicente, dolomie Alfonso, dolomie San Vicente et dolomie San Judas, apparaissent différentes générations de carbonates de gangue qui ont été décrites par Fontboté et Gorzawski (1990). Ceci comprend de la dolomie noire de remplacement (dark replacement dolomite = DRD, I), de la dolomie baroque (white sparry dolomite = WSD, II), de la dolomie tardive (late filling dolomite = LFD, III) et de la calcite (late filling calcite = LFC, III) tardive, et des carbonates remplaçant du sulfate evaporitique (EP). Les études géochimiques, surtout celles des isotopes de carbone et oxygène, nous ont permis d'affiner la classification des carbonates hydrothermaux en relation avec le degré d'interaction entre la dolomie noire de remplacement et le fluide minéralisateur (Tableau 1.1 et Figs. 1.6c-h, 1.7a-h, 1.8).

Dans la DRD on distingue trois sous-générations selon le degré de recristallisation et de préservation des textures primaires (oolithes): "Ivf" dolomie à grain très fin à oolithes ; "If" dolomie à grain fin; et "Im" dolomie à grain moyen (Tableau 1.1 et Figs. 1.7a-1.7f). La sous-génération Ivf est la dolomie la moins altérée, accessible à l'échantillonnage à San Vicente. Cette dolomie a été remplacée de façon pervasive par une première génération de sphalérite (sl I) et de dolomie blanche (Figs. 1.7g, 1.7h). Pendant la phase principale de minéralisation, le fluide précipite de la sphalérite II et de la dolomie baroque II qui remplissent partiellement les pores (formant par répétition une texture zébra) ainsi que les

Figure 1.5. Stratigraphic column of the Pucará Group in the San Vicente mining area (after Rosas, 1994). 1 = red sandstone; 2 = marly limestone; 3 = marly dolomite; 4 = limestone; 5 = dolomite; 6 = dolomite with white sparry dolomite (WSD); 7 = partly dedolomitized dolomite; 8 = bituminous silty limestone; 9 = volcanic rocks; 10 = lenses of gypsum; 11 = ore.
Coupe stratigraphique du groupe de Pucará dans la mine de San Vicente.

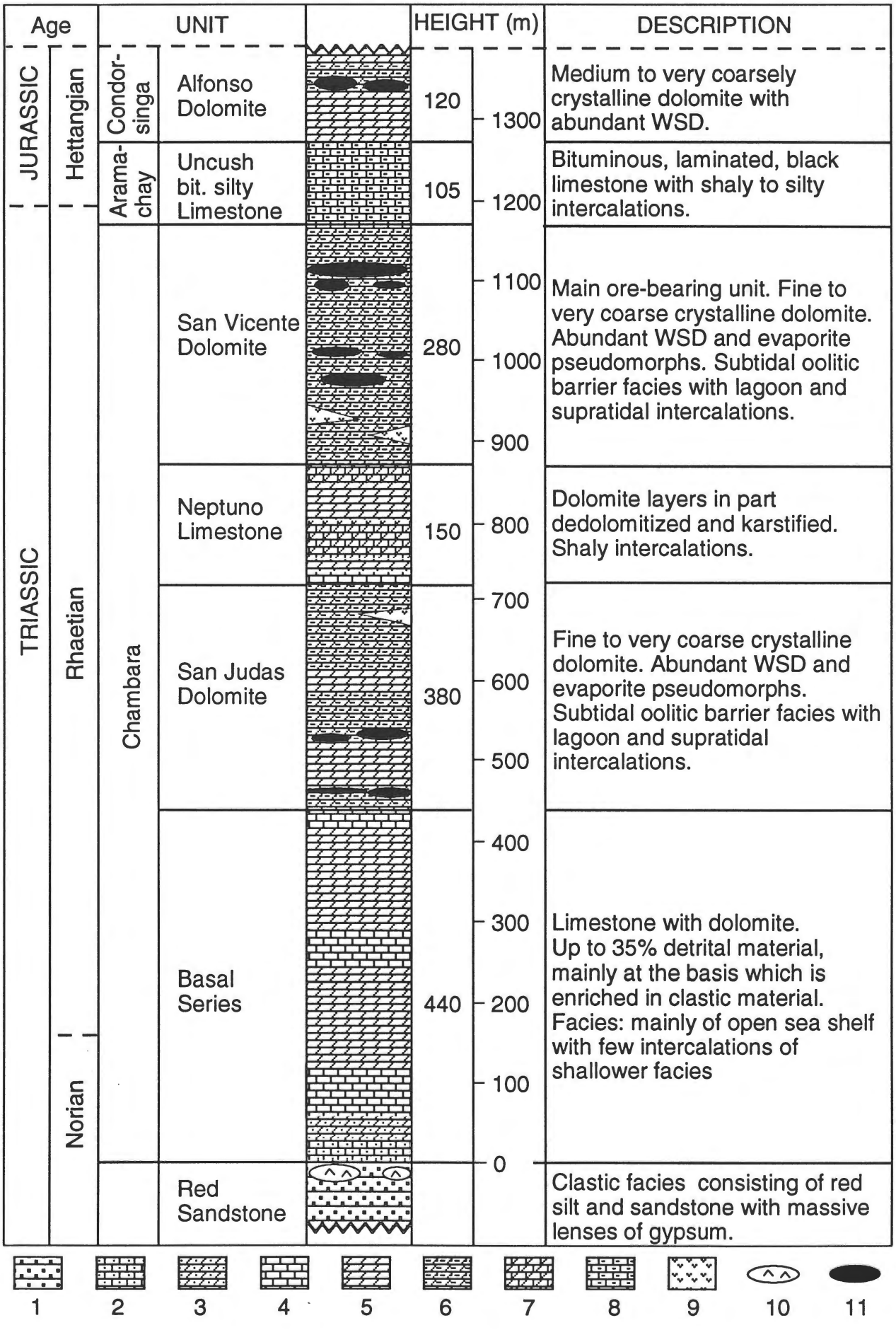
Age
UNIT
HEIGHT (m)
DESCRIPTION
JURASSIC
TRIASSIC
Hettangian
Rhaetian
Norian
Condor-singa
Arama-chay
Chambara
Alfonso Dolomite
120
Medium to very coarsely crystalline dolomite with abundant WSD.
Uncush bit. silty Limestone
105
Bituminous, laminated, black limestone with shaly to silty intercalations.
San Vicente Dolomite
280
Main ore-bearing unit. Fine to very coarse crystalline dolomite. Abundant WSD and evaporite pseudomorphs. Subtidal oolitic barrier facies with lagoon and supratidal intercalations.
Neptuno Limestone
150
Dolomite layers in part dedolomitized and karstified. Shaly intercalations.
San Judas Dolomite
380
Fine to very coarse crystalline dolomite. Abundant WSD and evaporite pseudomorphs. Subtidal oolitic barrier facies with lagoon and supratidal intercalations.
Basal Series
440
Limestone with dolomite. Up to 35% detrital material, mainly at the basis which is enriched in clastic material. Facies: mainly of open sea shelf with few intercalations of shallower facies
Red Sandstone
Clastic facies consisting of red silt and sandstone with massive lenses of gypsum.
1300
1200
1100
1000
900
800
700
600
500
400
300
200
100
0
1
2
3
4
5
6
7
8
9
10
11

Table 1.1. Studied host and gangue minerals from San Vicente MVT district
Carbonates de gangue étudiés dans le district MVT de San Vicente

Lithologic unit	Generation/ Subgeneration	Description
San Judas Dolomite, San Vicente Dolomite, Alfonso Dolomite		
	I	dark replacement dolomite
	Ivf	very fine-grained dolomite I (size 15 to 60 μm)
	If	fine-grained dolomite I (size 40 to 100 μm)
	Im	medium-grained dolomite I (size 100 to 400 μm)
	Iom	organic matter disseminated in dolomite I
	II	White sparry dolomite
	IIt1	spots of dolomite II
	IIt2	fine veinlets of dolomite II
	IIt3	ordered bands of dolomite II
	IIt4	zebra texture
	IIt5	broad crosscutting veins of dolomite II
	IIt6	dolomite II in hydraulic breccia
	III	late-stage filling carbonate
	IIId	late-stage filling dolomite
	IIIc	late-stage filling calcite
	IIIbit	allochtonous hydrothermal bitumen
	EP	carbonate as evaporite pseudomorph
	EPd	dolomite replacing sulfate evaporites
	EPc	calcite replacing sulfate evaporite
Uncush bituminous silty Limestone (UL)		
	UL	host calcite
	ULom	organic matter disseminated in UL

espaces vides en brèches hydrauliques. Une génération tardive de dolomie III et calcite III remplit les espaces vides dans la dolomie baroque. Sphalérite III et galène sont associées à ces carbonates tardifs. La pyrite se trouve en trace dans toutes les phases de la minéralisation et dans le cas de la dolomie hôte (DRD Ivf), elle est présente en grains très fins associée au quartz. Dans la bordure nord du gisement ("manto San Vicente techo") se trouvent des

Figure 1.6. a. Zebra ore and hydraulic breccias and different carbonate generations (San Vicente N mine, manto Ayala, level 1570, cut 600). The mineralization consists mainly of sphalerite (I and II) and galena. **b.** Mine wall (tunnel Uncush, level 1455) showing sphalerite III as breccia cement. **c.** Hand specimen (manto 3, sample FSV-657B) showing different carbonate generations: dark replacement dolomite (DRD, I) and subgenerations of white sparry dolomite (WSD, II). 1 = millimetric sized spots of WSD in mottled DRD (subgeneration t1), 2 = fine veinlets of WSD (subgeneration t2), 3 = ordered millimetric to centimetric thick bands of WSD (subgeneration t3). **d.** Hand specimen (manto Ayala, level 1570, cut 500, sample FSV-663) of zebra ore showing repetition of DRD and WSD (subgeneration t4), yellow sphalerite II, and late filling dolomite III (irregular white bands). **e.** Hand specimen (manto 3p, level 1750, gallery 255NW, sample FSV-029) showing crosscutting veins of WSD (subgeneration t5), late calcite III, and calcite replacing evaporitic sulfate. **f.** Hand specimen (tunnel Uncush, level 1455, sample FSV-1092) showing subgeneration t6 of the white dolomite II (greyish bands) as oriented overgrowths of breccias, and late-stage filling white calcite III. **g.** Mine wall view (manto Jesus, level 1750, crosscut 1310E) of calcite replacing sulfate evaporites. **h.** Solid hydrothermal bitumen (IIIbit) occurs as void filling, and appears to be younger than calcite III (manto Ayala, level 1750, crosscut 1240E).
Vues des parois de la mine et photos des échantillons montrant les différentes générations de carbonates hydrothermaux.

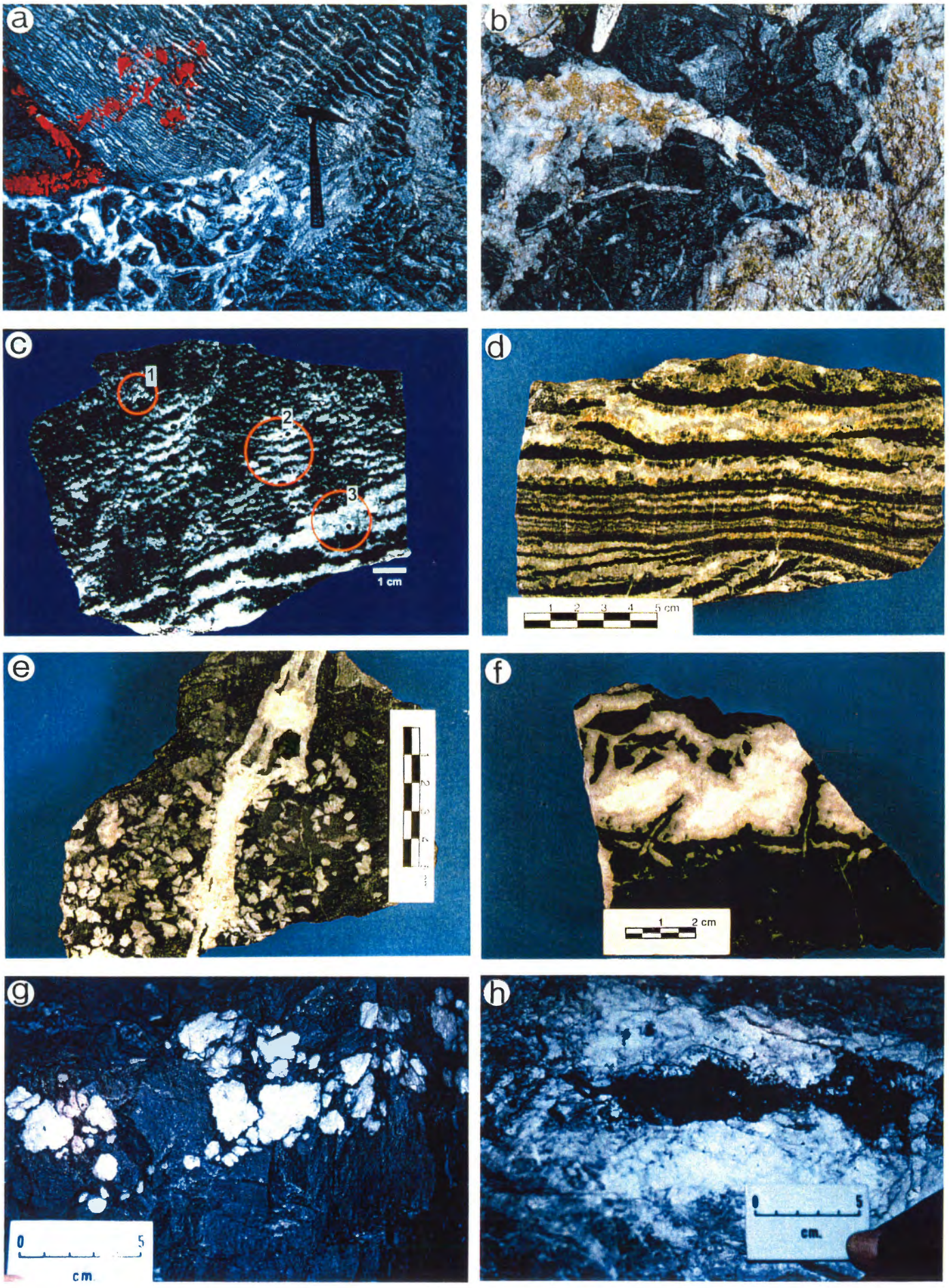
a
b
c
1
2
3
1 cm
d
1 2 3 4 5 cm
e
f
1 2 cm
g
0 5
cm
h
0 5
cm

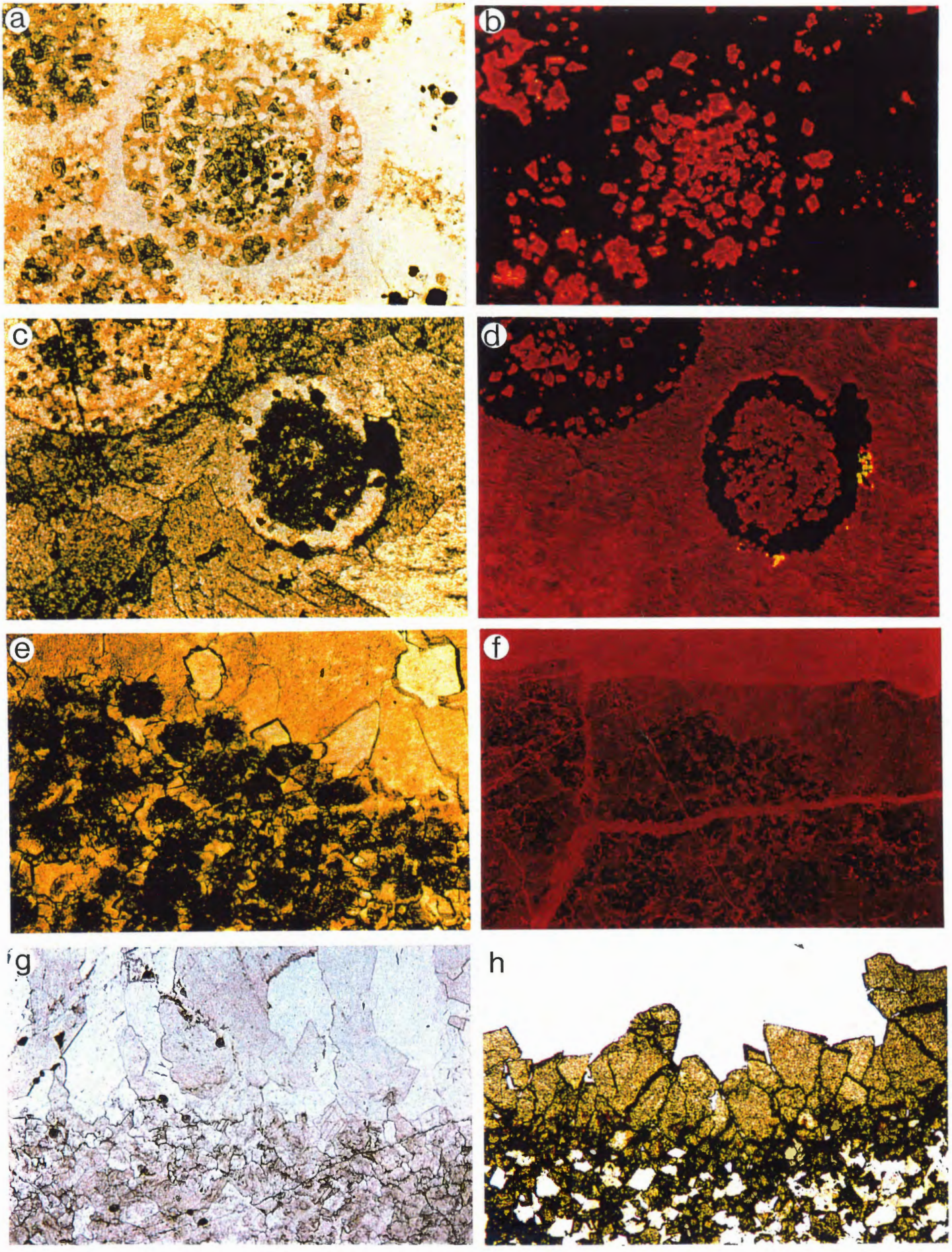
a
b
c
d
e
f
g
h

niveaux centimétriques de pyrite massive.

Une autre phase carbonatée est la calcite ou dolomite remplaçant les sulfates évaporitiques (Fig. 1.6g). Occasionnellement du soufre natif apparaît, associé à ces pseudomorphes de sulfates.

Deux types de matière organique sont disséminés dans les carbonates de gangue: la matière organique (kerogen) associée à la dolomite hôte et du bitume solide allochtone (aussi appelé bitume hydrothermal) associé surtout à la calcite hydrothermale tardive (Fig. 1.6h).

1.3 Méthodes

1.3.1 Échantillonnage

L'échantillonnage a été effectué en septembre-octobre 1992 et juin 1994 suivant un schéma hiérarchique qui considère différents niveaux de variations: district, gisement, manto, affleurement et échantillon de main.

District de San Vicente

124 échantillons ont été prélevés dans 20 localités le long d'un travers N-S d'à peu prés 33 km de long, centré sur le gisement de San Vicente (Fig. 1. 4). Pour 14 d'entre eux, les conditions d'affleurement et les sondages d'exploration nous ont permis de faire des profils à travers la séquence de Pucará.

Gisement de San Vicente

Le gisement de San Vicente a été échantillonné en détail, qui comprend 96 échantillons représentant aprox. 500 m à travers la séquence, et 11 mantos dans les trois dolomies (Alfonso, San Vicente, San Judas) le long de 2600 m parallèles à la stratification.

Manto

Deux mantos ("manto Alfonso" et "manto San Vicente Techo") furent échantillonnés selon des profils en croix de direction aprox. NS et EW sur une surface de 400x100 m^2 (32 échantillons) et 700x100 m^2 respectivement (23 échantillons), comprenant la zone minéralisée et la projection stérile dans le même horizon. Le pas d'échantillonnage dans ces profils fut irrégulier, variant entre 5 et 50 m. Le but principal de l'échantillonnage à l'échellede la mine et du manto était de détecter une possible zonalité (horizontale ou verticale) dans le gisement, qui aurait pu indiquer le chemin du fluide minéralisant.

Figure 1.7. Photomicrographs of the dark replacement dolomite (DRD) of the San Vicente dolostones showing the three subgenerations defined by the degree of hydrothermal alteration. **a.** Very fine-grained DRD (Ivf) exhibiting oolites under normal light (sample FSV-811; uncrossed polars). **b.** Same field as in **a** under cathodoluminescence. Note replacement of the black non-luminescent host by a dull red luminescence. The yellow rims indicate the recrystallization boundaries. **c.** Fine-grained DRD (If) with oolites, partially replaced by dolomite II (sample FSV-811; uncrossed polars). **d.** Same field of view as in **b** under cathodoluminescence. The dull-red luminescent dolomite replaced the dolomite I from the center outwards. Bright yellow luminescence likely indicate exsolved organic matter. **e.** Medium-grained DRD (Im). The host dolomite was pervasive replaced by the white (red luminescent) dolomite (sample FSV-905; uncrossed polars). **f.** Same field as in **e** under cathodoluminescence. Note ghosts of oolites. **g.** Thin section (manto Ayala, level 1570, cut 600, sample FSV-914; parallel nicols) showing the pervasively altered dark replacement dolomite (Im) and the open space filling dolomite II. **h.** Thin section (manto Ayala, level 1570, cut 600, sample FSV-915; parallel nicols). Sphalerite (brown grains) is in the same paragenetic situation as white dolomite: (I) as fine-crystalline anhedral sphalerite intergrown with recrystallized dolomite I; and (II) as coarse open-space filling subhedral sphalerite predating and/or intergrown with the white sparry dolomite II on the pervasive altered dark dolomite I. For photos a-f witdth is 1.7 mm, for photos g-h width is 4.2 mm.
Photo-micrographies de la dolomie noire de remplacement montrant les trois sous-générations définies selon le degré d'altération hydrothermale.

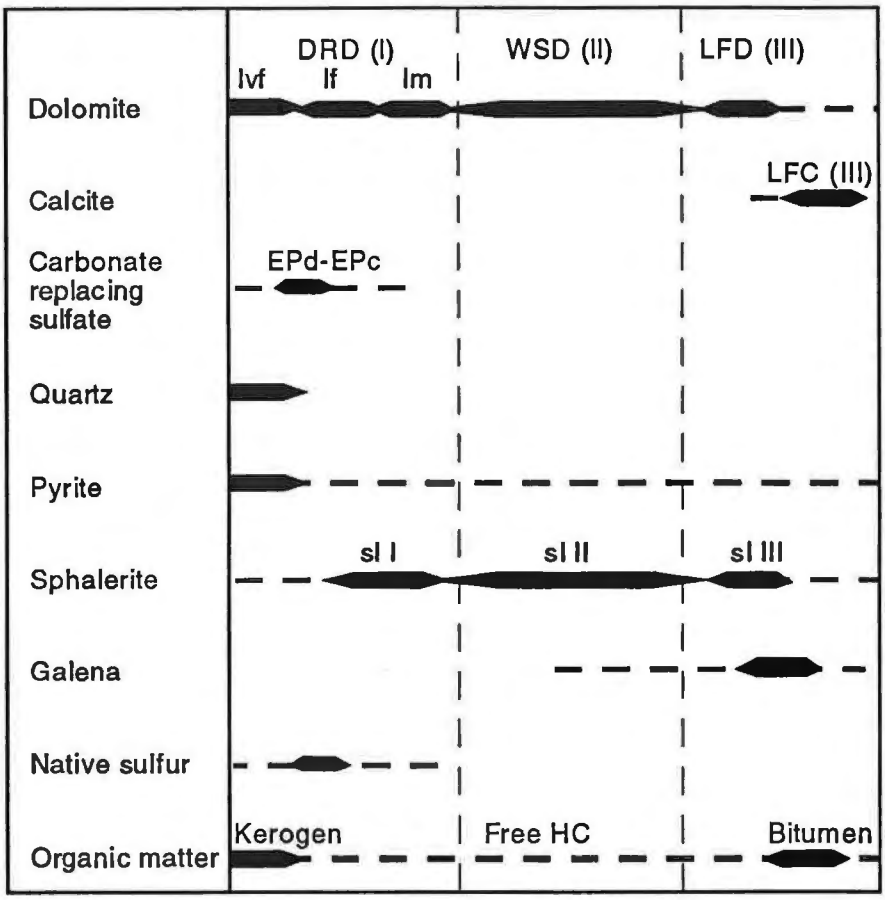

Figure 1.8. Paragenetic sequence of the hydrothermal gangue minerals and ore in the Mississippi Valley-type district of San Vicente. Abbreviations: DRD = dark replacement dolomite ("Ivf" very fine-grained, "If" fine-grained, "Im" medium-grained; WSD = white sparry dolomite; LFD = late filling dolomite; LFC = late filling calcite; sl I, sl II and sl III = generations of sphalerite; EPd or EPc= dolomite or calcite replacing evaporitic sulfate; HC = hydrocarbons. Modified from Fontboté and Gorzawski (1990).
Séquence paragénétique des minéraux de gangue et sulfures dans le district de San Vicente du type Mississippi Valley. Modifié d'après Fontboté et Gorzawski (1990).

Affleurement et échantillon de main

Deux affleurements, un dans le "manto Jesus" (n=12) et un dans le "manto Ayala" (n=11), ont été sélectionnés pour l'échantillonnage en détail des différentes sous-générations texturelles de la dolomie noire I (Ivf à Im) et de la dolomie baroque II (t1 à t6).

La variation géochimique à l'échelle d'échantillon a été étudiée dans des échantillons représentatifs du minerai zébré (FSV-924) et de la brèche hydraulique (FSV-919).

1.3.2 Approche géochimique

Tous les échantillons ont été sciés en plaques afin de faciliter le prélèvement sélectif des différentes générations de carbonates de gangue. 54 sections polies ont été étudiées par méthodes pétrographiques courantes et quelques unes par cathodoluminescence afin de garantir la classification correcte des générations de carbonates, en particulier les sous-générations de la dolomie de remplacement noire (DRD). Les différentes générations de carbonates ont été prélevées en utilisant une fraiseuse de dentiste (échantillons de <100 mg)

ou une perceuse de table (échantillons de >1g) à mèches de diamants. La composition minéralogique de plus de 100 échantillons a été contrôlée par diffractométrie aux rayons X à l'Université de Lausanne.

Les carbonates ont été étudiés par différentes méthodes géochimiques: analyses isotopiques de carbone et oxygène (Laboratoire de Géologie Isotopique de l'Université de Lausanne), analyses de Ca, Mg, Fe, Mn, Na, Sr et Zn par microsonde électronique (LAME de l'Université de Lausanne), analyses par ICP-AES de Ca, Mg, Fe, Mn, Na, Sr, Zn et Ba (Département de Chimie Minérale de l'Université de Genève), analyses des terres rares par ICP-MS et INAA (laboratoire XRAL), analyses d'isotopes de strontium (Université de Genève), analyses du carbone total et du soufre total par titration coulométrique et pyrolyse LECO (CAM de l'Université de Lausanne, et laboratoire XRAL), ainsi que pyrolyse Rock-Eval (Laboratoire de Géologie de la Matière Organique, Université d'Orléans).

1.4 Résumé des résultats

1.4.1 Isotopes de carbone et oxygène

Plus de 250 échantillons de carbonates de gangue et matière organique ont été analysés pour des rapports d'isotopes stables. Les valeurs de $\delta^{13}C$ et $\delta^{18}O$ de la dolomie hôte altérée et des carbonates hydrothermaux mettent en évidence une forte homogénéité régionale. Celle-ci, en considérant aussi les grandes similitudes minéralogiques et pétrographiques des différentes occurrences de type MVT, permettent de conclure que les processus minéralisants ont été similaires dans tout le district de San Vicente, ce qui suggère l'existence d'un système minéralisant hydrothermal avec des "*plumbing*" interconnectés. Un modèle quantitatif des mélanges d'un fluide légèrement acide avec l'eau intra- formationnelle native expliquerait les covariations globales des isotopes de carbone et oxygène ($\delta^{13}C$ = -11.5 à 2.5 ‰, $\delta^{18}O$ = -12.5 à -6.4 ‰) dans les différentes générations de carbonates. Les dolomites précipitées pendant la phase principale de la minéralisation montrent un intervalle de variation étroit ($\delta^{13}C$ = -0.1à 1.7 ‰, $\delta^{18}O$ = -11.8 à -7.3 ‰) qui est expliqué en termes d'interaction fluide-roche et de dégazification de CO_2.

On constate que du soufre natif est associé à de la calcite très légère (p.e. $\delta^{13}C$ = -11.5) dans les pseudomorphes de sulfates et de bitume solide hydrothermale plus lourd que la matière organique (kerogen) disséminée dans la dolomie hôte (de -27.0 à -23.0 ‰ $\delta^{13}C$). Cela suggère que l'altération de la matière organique et la réduction thermochimique des sulfates évaporitiques ont été liées aux phénomènes de minéralisation et ont constitué une source de soufre réduit.

1.4.2 Éléments mineurs et traces, terres rares inclues

La géochimie en éléments majeurs et traces (Ca, Mg, Fe, Mn, Sr, Na, Ba et Zn) inclus les terres rares (TR) des carbonates hydrothermaux permet de restreindre le chemin suivi par le fluide minéralisant et les changements de conditions pH-Eh pendant la minéralisation. Les dolomies hydrothermales liées à la minéralisation sont appauvries en Fe et TR et enrichies en Mn par rapport à la dolomie hôte. Les dolomies hydrothermales dans la mine présentent une anomalie négative en Ce. Ces résultats indiquent que le fluide minéralisant était légèrement oxydant et acide et pauvre en TR et Fe. Cela suggère que le fluide minéralisant a circulé par un aquifère principal, s'agissant probablement d'unités détritiques à la base de la séquence de Pucará et qui ont eu un échange très limité avec les carbonates hôtes. De plus, les dolomies hydrothermales ont une chimie très semblable dans tout le district de San Vicente, ce qui renforce l'hypothèse basée sur l'homogénéité régionale des isotopes stables dans les carbonates hydrothermaux, que le fluide minéralisant a eu accès aux sites de minéralisation par canaux structuraux (failles et hauts du socle) interconnectés. Les covariations de Fe-Mn et le changement de signe des anomalies en Eu indiquent que les conditions oxydo-réductrices du système fluide-roche sont passées de réductrices pendant la minéralisation à légèrement oxydantes dans la phase de post-minéralisation.

1.4.4 Matière organique

La pyrolyse Rock-Eval de la dolomie hôte et les calcaires de Uncush indiquent que deux types de matière organique (MO) se trouvent dans les carbonates de gangue de San Vicente: un kerogen hyper-mature (T_{max} > 500°C), vraisemblablement la matière organique native altérée, et un bitume soluble thermiquement labile (T_{max} varient de 235 à 243 °C). L'altération de la MO disséminée dans la dolomie hôte par les fluides minéralisants a libéré des hydrocarbures, qui sont continuellement soumis à un cracking thermique, au "water-washing" et à une polymérisation responsables de la formation d'un résidu de MO solide (bitume hydrothermal).

Références

Fontboté, L. (1981) Strata-bound Zn-Pb-F-Ba deposits in carbonate rocks: New aspects of paleogeographic location, facies factors and diagenetic evolution. (With a comparison of occurrences from the Triassic of southern Spain, the Triassic/Liassic of central Peru and other localities). Unpub. Ph.D. dissert., Univ. Heidelberg, 193 p.

Fontboté, L. (1990) Stratabound ore deposits in the Pucará basin. An overview. In: Fontboté, L., Amstutz, G.C., Cardozo, M., Cedillo, E., and Frutos, J. (Editors) Stratabound Ore Deposits in the Andes, Springer-Verlag, Berlin, Heidelberg, p. 253-266.

Fontboté, L., and Gorzawski, H. (1990) Genesis of the Mississippi Valley-type Zn-Pb deposit of San Vicente, Central Peru: geological and isotopic (Sr, O, C, S) evidences. Economic Geology, v. 85, p. 1402-1437.

González, E. (1987) Petrographische und geochemische Untersuchungen an einem gesamt-Profil durch die schichtgebundene Zn-Pb-Lagerstätte San Vicente, Perú. Unpub. Diplomarbeit, Uni. Heidelberg, 128 p.

Gorzawski, H., Fontboté, L., Field, C.W., and Tejada, R. (1990) Sulfur isotope studies in the zinc-lead mine Vicente, Central Perú. In: Fontboté, L., Amstutz, G.C., Cardozo, M., Cedillo, E., and Frutos, J. (Editors) Stratabound Ore Deposits in the Andes, Springer-Verlag, Berlin, Heidelberg, p. 305-312.

Gorzawski, H., Fontboté, L., Sureau, A., and Calvez, J.Y. (1989) Strontium isotope trends during diagenesis in ore-bearing carbonate basins. Geologische Rundschau, v. 78, p. 269-290.

Moritz, R., Spangenberg, J., and Fontboté, L. (1993) Evaluation of fluid mixing and fluid-rock interaction processes during genesis of the San Vicente Zn-Pb MVT deposit, central Peru, based on Sr, O, and C isotopic covariations. In: Fenoll Hach-Ali, P., Torres-Ruiz, J., and Gervilla, F. (Editors) Current reseach in geology applied to ore deposits. Proceedings of the Second Biennial SGA Meeting, Granada, Spain, Sept. 9-13, 1993, p. 355-359.

Rosas, S. (1994) Facies, diagenetic evolution, and sequence analysis along a SW-NE profile in the southern Pucará Basin (Upper Triassic-Lower Jurassic), central Peru. Heidelberger Geowissenschaftliche Abhandlungen, v. 80, 337 p.

Schulz, G.C. (1971) Die schichtgebundene Zinkblende Lagerstätte San Vicente in Ost-Perú und ihr geologischer Rahmen. Unpub. Ph.D. dissert., Univ. Aachen, 167 p.

Spangenberg, J., Fontboté, L., Sharp, Z., and Hunziker, J. (1994) Stable isotope (C, O) constraints on the genesis of the Mississippi Valley-type zinc-lead deposit of San Vicente, central Peru. 7° Congreso Geológico Chileno, 17-21 octubre de 1994, Concepción, Chile. Abstracts volume II, p. 1532-1536.

Spangenberg, J., Sharp, Z., and Fontboté, L. (1995) Apparent carbon and oxygen isotope variations of carbonate gangue minerals Mississippi Valley-type Zn-Pb of San Vicente deposit, central Peru: the effect of organic matter and sulphides. Mineralium Deposita, v. 30, p. 67-74.

CHAPTER 2

APPARENT STABLE ISOTOPE HETEROGENEITIES IN GANGUE CARBONATES OF THE MISSISSIPPI VALLEY-TYPE ZINC-LEAD DEPOSIT OF SAN VICENTE, CENTRAL PERU

Abstract

The aim of the present communication is to emphasize that some variations of the measured $\delta^{13}C$ and $\delta^{18}O$ values are *apparent*, and due to analytical interferences caused by the presence of sulfur and organosulfur compounds in the analyzed carbonates. This is particularly relevant for isotopic studies on carbonate-hosted mineral deposits, where the nearly ubiquitous association of the host carbonates with organic matter and sulfides can certainly affect the metallogenetic interpretations. In this work two methods were used to overcome the disturbing effects of sulfides and organic matter: (1) sample pretreatment following the method proposed by Charef and Sheppard (1984), combining the oxidation of organic matter with sodium hypochlorite and trapping of the sulfur species with silver phosphate, and (2) laser-based microprobe extraction. Apparent isotopic variations in sparry dolomite from a single hand sample of zebra ore from the MVT Zn-Pb deposit, San Vicente, central Peru, are as large as 6‰ $\delta^{13}C$ and 4‰ $\delta^{18}O$. These variations are reduced to several tenths of a per mil when the samples are pretreated. A careful examination of the effects of treatment with NaOCl and/or Ag_3PO_4 in relation to the concentration of sulfide inclusions indicates that the main disturbing effects for $\delta^{13}C$ values are the presence of sulfur species and organic matter, whereas the $\delta^{18}O$ values are mainly affected by the presence of sulfides. Fine- and medium-grained replacement carbonates from MVT and other sediment-hosted base metal deposits are potentially the most affected during isotope analysis due to the common presence of organic matter and sulfides. Using *in situ* laser microprobe techniques, it is possible to determine isotopic variations at a sub-millimeter scale. Our results show that laser extraction analysis allows a more precise sampling of the carbonate minerals, and minimizes contamination of the sample with sulfides and to some extent with intergrown organic matter. However, there is an isotopic shift associated with the laser extraction technique, of the order of 0.5-1‰ for $\delta^{13}C$ and $\delta^{18}O$ values.

2.1 Introduction

Changes in the stable isotope composition of host and gangue carbonates of Mississippi Valley-type (MVT) Pb-Zn deposits are mainly explained as an effect of changing fluid composition, temperature, water/rock ratio, or some combination of these effects (e.g. Hall and Friedman, 1969; Pinckney and Rye, 1972; Sverjensky, 1981; Hannah and Stein, 1984; Machel, 1987; Gregg and Shelton, 1989; Rowan and Leach, 1989; Frank and Lohman, 1986; Ghazban, et al., 1990). In general, it has been observed that with advancing diagenetic stages, the carbon and oxygen isotope ratios are lowered (Machel, 1987; Banner et al., 1988; Kaufman et al., 1990, 1991; Fontboté and Gorzawski, 1990; Moritz et al., 1993).

In the course of an ongoing investigation on the geochemical zonation in gangue carbonates of the Mississippi Valley-type Zn-Pb district San Vicente, central Peru, we attempt to trace potential small carbon and oxygen isotopic variations (e.g. less than 2‰) at the deposit and the district scale that could reflect basinal brine migration. For this purpose, defined carbonate generations have been sampled and analyzed from different parts of the district. Preliminary results confirm the general tendency toward lower isotope ratios with advancing diagenetic stages, but reveal variations within single hand specimens of the same order as those observed over the entire deposit (in the range of -4.1 to 2‰ $\delta^{13}C$ and -10.3 to -5.9‰ $\delta^{18}O$, see Fontboté

and Gorzawski, 1990). These major isotopic heterogeneities at hand specimen scale may preclude the recognition of subtle isotopic variations at orebody, deposit, or district scale.

The aim of the present communication is to demonstrate that some of the variations of the measured $\delta^{13}C$ and $\delta^{18}O$ may be *apparent*, and due to analytical interferences caused by the presence of sulfides and organic matter in the analyzed carbonates. Sulfides and organic matter, which are abundant in most carbonate-hosted base metal deposits, can strongly affect the carbon and oxygen isotope analyses (e.g. Smith and Croxford, 1975; Weber et al., 1976; Rye and Williams, 1981; Charef and Sheppard, 1984), and may account for the large isotopic variations at a small scale. We want to emphasize the need for controlling the influence of organic, organosulfur, and sulfur species of the measured $\delta^{13}C$ and $\delta^{18}O$ values of carbonates. This is particularly relevant for isotopic studies on carbonate-hosted mineral deposits, where the nearly ubiquitous association of the host carbonates with organic matter and sulfides can certainly affect the metallogenetic interpretations.

In this work two methods were used to overcome the disturbing effects of sulfides and organic matter: (1) sample pretreatment following the method proposed by Charef and Sheppard (1984), combining the oxidation of organic matter with sodium hypochlorite and trapping of the sulfur species with silver phosphate; and (2) laser-based microprobe extraction.

The isotopic variations at the centimeter to sub-millimeter scale were evaluated with a combination of a systematic detailed sampling using conventional and *in situ* laser methods. Treatment for organic matter and sulfur allows us to recognize slight variations of isotopic ratios (i.e., less than 0.5‰) in a defined generation of the host carbonates in San Vicente through the ore-bodies, ore deposits, or ore district, which otherwise might be overlooked.

2.2 Geologic background

The geology and genetic aspects of the San Vicente Zn-Pb deposit, including Sr, C, and O isotope studies in the carbonate gangue minerals are discussed in Fontboté and Gorzawski (1990) and Moritz et al. (1993). The ore occurs as lens-shaped bodies, generally concordant with the bedding, and displays a characteristic rhythmic banding, known as zebra rock or diagenetic crystallization rhythmites (Fontboté and Gorzawski, 1990; Fontboté, 1993). The main ore minerals, sphalerite and galena, are interbanded with white sparry dolomite and grey replacement dolomite. Three distinct dolomite types occur in the host rocks: dark grey replacement dolomite, ore-stage sparry dolomite, and late-stage void-filling dolomite.

The early stage replacement dolomite, referred to as generation I in Fontboté and Gorzawski (1990), is a very fine- to medium-grained, dark grey dolomite, with abundant inclusions of organic matter. In some ore-bearing samples this stage I dolomite is completely replaced by sphalerite and, less commonly, by galena. The total organic carbon and sulfur contents in this dark replacement dolomite are up to 5.2 wt. % and 2.1 wt. %, respectively (Table 2.1).

The sparry dolomite consists of coarse or very coarse, subhedral, light grey to white or light brown dolomite, and corresponds to generation II of Fontboté and Gorzawski (1990). This dolomite type occurs as cement in moldic and vuggy porosity, or as bands between the dark replacement dolomite, giving the characteristic rhythmic banding of the zebra rock (Fig. 2.1). Zonal crystal growth can often be recognized as a simple color difference, due to a low amount of disseminated sulfides (up to 0.08 wt.% total sulfur) and organic matter (up to 0.09 wt.% total organic carbon). The precipitation of sparry dolomite is interpreted as a late diagenetic event, having formed from highly saline basinal brines (Fontboté and Gorzawski, 1990; Moritz et al., 1993). Sphalerite mineralization is mainly paragenetically associated with this sparry dolomite generation.

Late-stage open-space filling dolomite is a coarse- to very coarse-grained, milky-white, xenomorphic dolomite, virtually free of organic matter and sulfides (Table 2.1). It occludes voids in white sparry dolomite, and correlates with the generation III dolomite of Fontboté and Gorzawski (1990). Locally, this late-stage diagenetic crystallization generation consist of calcite,

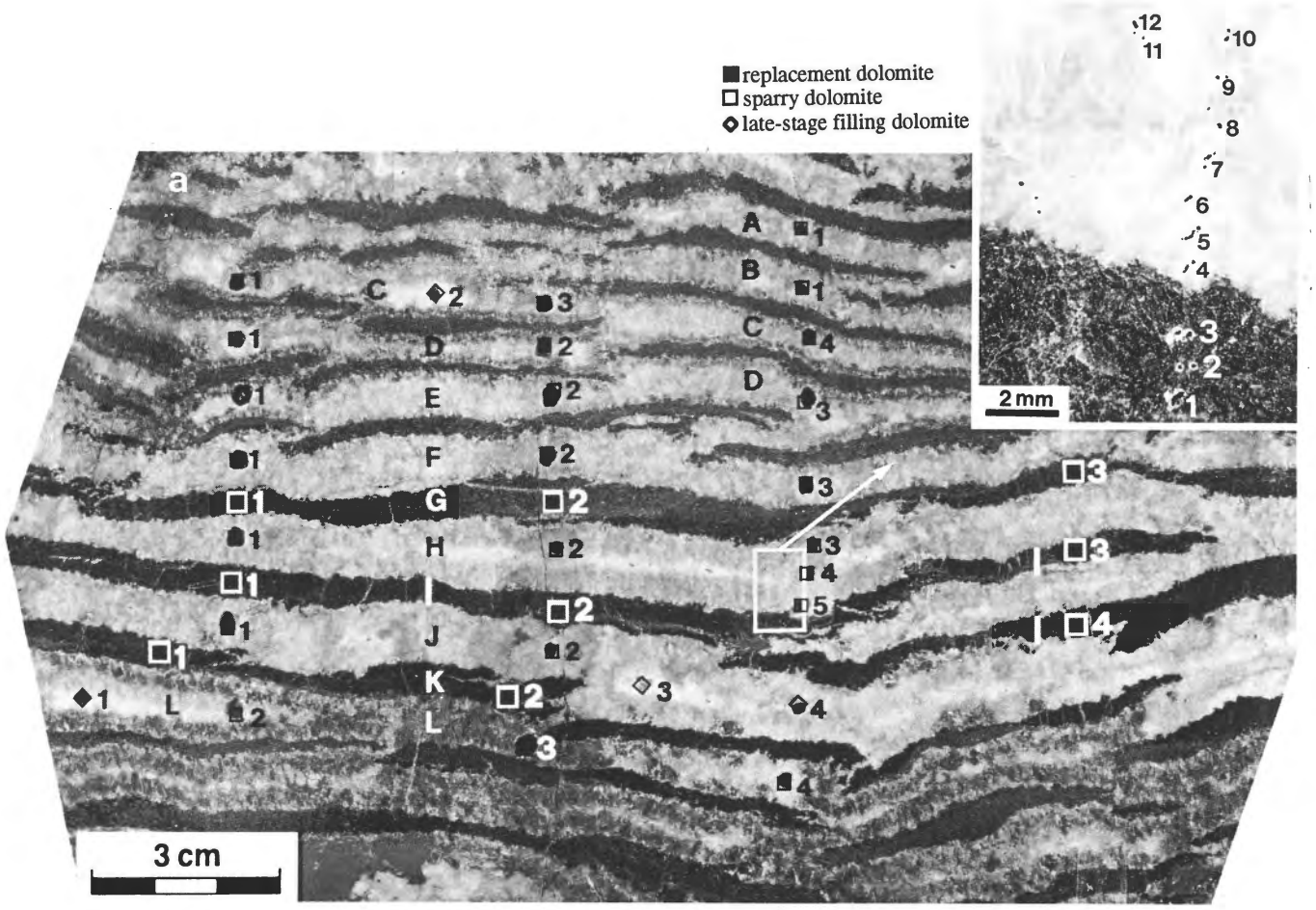

Figure 2.1. Representative hand sample (FSV-924) of zebra ore showing the sampled sites. Detail of the *in situ* laser microsampled area. Individual bands (*letters*) and specific analysis locations (*numbers*) correspond with sample names in tables.

galena, or bitumen instead of dolomite. In the samples selected for this study the filling carbonate is exclusively dolomite.

Table 2.1. Range of organic carbon and sulfur contents of gangue carbonates in the San Vicente MVT deposit. The number of analyzed samples (by LECO pyrolisis) is given in parentheses

Carbonate generation	C_{org} (wt.%)	S (wt.%)
Dark replacement dolomite (5)	0.09-5.2	0.13-2.1
White sparry dolomite (5)	<0.01-0.09	0.07-0.08
Late filling carbonate (3)	<0.01-0.05	<0.01-0.02

2.3 Analytical procedures

Three different analytical procedures have been compared: (1) conventional acid CO_2-extraction without pretreatment; 2) conventional CO_2-extraction with sodium hypochlorite and silver phosphate pretreatment; and 3) *in situ* laser microprobe CO_2-extraction without treatment.

Treatment of laser-extracted CO_2 with silver phosphate was attempted, but a successful method was not found.

2.3.1 Conventional method

Individual dolomite types were selectively sampled from roughly polished slabs using a drilling device. The holes of a diameter of about 1-3 mm were aligned along profiles covering the different dolomite generations.

All isotope analyses were carried out at the Laboratory of Isotopic Geochemistry at the University of Lausanne. Carbon and oxygen isotope analyses were performed following standard carbon dioxide extraction techniques of McCrea (1950). Approximately 10 mg of fine-grained dolomite was dissolved in vacuum at 50°C by 100% phosphoric acid. The released carbon dioxide was trapped in liquid nitrogen and cleaned by means of a fractionate sublimation using a dry ice-ethanol mixture. The gas was measured on a Finnigan® MAT-251 mass spectrometer. Data were corrected for fractionation using the carbonate-acid fractionation factor for dolomite of 1.01065 (Rosenbaum and Sheppard, 1986) and are expressed conventionally in the δ notation as the variation in per mil relative to the PDB standard. Analytical reproducibility, reported as standard deviations of replicate analyses of the laboratory working standard Binn Dolomite is better than $\pm$ 0.05‰ for carbon and $\pm$ 0.1‰ for oxygen.

2.3.2 Sodium hypochlorite and silver phosphate pretreatment

Earlier publications report the oxidation of organic matter by sodium hypochlorite (e.g. Weber et al., 1976; Land et al, 1977) and the removal of acid-volatile sulfur compounds by a silver phosphate pretreatment (e.g. Smith and Croxford, 1975; Rye and Williams, 1981). We have used the pretreatment procedure proposed by Charef and Sheppard (1984) to minimize the effects of organosulfur species. It consists of the combined oxidation of organic matter by sodium hypochlorite (NaOCl) followed by silver phosphate (Ag_3PO_4) treatment of the phosphoric acid evolved gas.

The powdered samples were reacted with 5% fresh NaOCl solution for 15 h. at room temperature, filtered, washed several times with distilled water, and dried at 80°C for 4 h. The gas released by the phosphoric acid was exposed to coarsely powdered Ag_3PO_4 at room temperature for 10 min to eliminate the evolved H_2S. The Ag_3PO_4 was dried at 150°C for 30 min and left in the vacuum line for at least another 30 min prior to extraction.

No significant differences of the isotope ratios of the laboratory dolomite standard were observed by using the Ag_3PO_4- or the combined NaOCl+Ag_3PO_4 pretreatment, within the analytical precision of $\pm$0.05‰ for $\delta^{13}C$ and $\pm$0.1‰ for $\delta^{18}O$ (Table 2.2). As stated by Charef and Sheppard (1984), the sodium hypochlorite treatment does not necessarily remove all types of organic carbon in the carbonate samples, but it certainly destabilizes all 'active' organosulfur compounds, sensitive to oxidation by the 5% NaOCl solution, leaving only stable organic carbon species.

Table 2.2. Average and standard deviation of conventional carbon and oxygen isotope analyses of laboratory standard Binn Dolomite

Pretreatment (n)	$\delta^{13}C$ ‰ PDB	$\delta^{18}O$ ‰ PDB
None (21)	1.55 (0.04)	-9.41 (0.10)
NaOCl+Ag_3PO_4 (8)	1.61 (0.03)	-9.46 (0.06)
Ag_3PO_4 (8)	1.61 (0.05)	-9.48 (0.10)

2.3.3 In situ laser microprobe determination

In situ laser measurements, following the procedure of Sharp (1992) were made at the University of Lausanne to study the isotopic zonation at sub-millimeter scale across a single 1 cm thick band of white sparry dolomite. The CO_2-extractions were carried out at 100% laser power (20 W). Twenty laser shots, each of 30 ms duration, performed in two closely neighboring sites, produced 150-200 µm-diameter holes (Fig. 2.1). The evolved CO_2 was trapped with liquid N_2, cryogenically purified, and then transferred on-line to the mass spectrometer for isotopic analysis. The precision of the oxygen and carbon isotope ratios reported for homogeneous samples is better than ± 0.1‰ and ± 0.2‰, respectively (Sharp, 1992).

The procedure for the *in situ* measurements with Ag_3PO_4 treatment were identical to the conventional *in situ* method except that a cold finger with Ag_3PO_4 was included in the extraction line. The Ag_3PO_4 treatment was similar to that described for conventional analyses. Various methods of heating and degassing of the Ag_3PO_4 were attempted in order to remove the isotopic shift caused by the phosphate interaction; none was found to alleviate the problem.

2.4 Results and discussion

Two representative ore-bearing hand specimens with megascopically recognizable different dolomite crystallization generations from the San Vicente mine have been analyzed in detail. The isotopic analyses of a zebra ore sample with typical rhythmic banding are given in Fig. 2.1 and Tables 2.3 and 2.4. Three sets of analyses are compared: conventional acid extraction method without pretreatment, with pretreatment, and laser extraction.

A comparison between the results of the conventional isotopic analyses with and without pretreatment (Fig. 2.2 and Table 2.4) shows a dramatic difference. The use of the combined NaOCl+Ag_3PO_4 pretreatment for the replacement dolomite and of the Ag_3PO_4 trap for the sparry dolomite and late-stage void-filling dolomite eliminates most of the heterogeneities found in the non-treated samples. Without pretreatment, the dark replacement dolomite displays a strong variation of $\delta^{13}C$ (between 1.4 and 8.4‰) and $\delta^{18}O$ (between -8.4 and -6.3‰). The two most erratic $\delta^{13}C$ values (7.9‰ and 8.4‰) are probably mainly due to the presence of sulfur species as shown by the strong decrease of the values achieved with the Ag_3PO_4-only treatment. In these same two samples the oxygen isotope ratios are clearly lowered with the Ag_3PO_4 pretreatment. The use of the combined pretreatment decreases slightly but consistently the $\delta^{13}C$ values and has no clear influence on the $\delta^{18}O$ values, suggesting that the main disturbing effects for the carbon isotopic ratios are due to the presence of organic matter and sulfur whereas the oxygen isotope ratios are disturbed mainly by the presence of sulfides.

The light grey sparry dolomite is virtually free of organic matter but bears variable amounts of sulfides. Accordingly, important differences are already achieved with the Ag_3PO_4-only treatment, with the help of which, for instance, instead of the erratically heavy $\delta^{13}C$ value of 18.7‰ a ratio of 0.7‰ is obtained. The results show that the treatment with NaOCl is not necessary for this dolomite generation.

The use of the above described pretreatment produces less important changes in the isotopic values of the very clean void-filling dolomite, but eliminates the still significant disturbances (see Table 2.3 and Fig. 2.1).

Variations in the $\delta^{13}C$ and $\delta^{18}O$ values at a sub-millimeter scale were evaluated with the *in situ* laser extraction technique. The range in the $\delta^{18}O$ values for the dark replacement dolomite and light grey sparry dolomite are small (-7.9 to -7.2‰, except for one anomalously high value at the contact between these two carbonate generations, Table 2.4). As expected, the $\delta^{18}O$ values for the late-stage dolomite are 3‰ lighter than the earlier dolomite generations. The $\delta^{13}C$ values for the sparry dolomite are in good agreement with the conventional pretreated analyses, while the $\delta^{13}C$ values for the dark replacement dolomite are closer to the unpretreated

Table 2.3. Variation of $\delta^{13}C$ and $\delta^{18}O$ values of gangue dolomites of a zebra ore sample[a] with method of pretreatment

Sample name	$\delta^{13}C$ ‰ PDB Pretreatment			$\delta^{18}O$ ‰ PDB Pretreatment		
	None	NaOCl + Ag_3PO_4	Ag_3PO_4	None	NaOCl + Ag_3PO_4	Ag_3PO_4
			Dark replacement dolomite			
G1	7.9	0.0	1.1	-7.0	-8.7	-8.3
I1	1.5	0.8	1.2	-7.9	-8.1	-8.5
K1	2.0	0.7		-8.4	-8.9	
G3	8.4	0.3	1.3	-6.3	-8.7	-8.6
I3	1.7	1.1		-7.2	-7.7	
I4	1.4	0.7		-8.4	-8.5	
G2		0.4			-8.9	
I2		0.4			-8.0	
K2		1.0			-8.6	
average	3.8	0.6	1.2	-7.5	-8.4	-8.5
(1σ)	(3.4)	(0.4)	(0.1)	(0.8)	(0.4)	(0.2)
			Light-grey sparry dolomite			
C1	2.0		0.8	-7.1		-7.8
D1	1.3	0.7	0.7	-8.0	-8.0	-9.1
E1	18.7[b]	0.5	0.7	-4.1	-8.0	-8.0
F1	1.5	1.1	1.3	-8.2	-8.1	-8.3
H1	1.3	1.0	1.3	-8.2	-8.3	-8.2
J1	1.4	1.0	1.3	-7.6	-8.1	-7.7
L2	1.5		1.3	-7.8		-8.1
C3	1.3	0.7	1.2	-7.9	-9.4	-8.1
D2	5.4	0.7	1.2	-6.5	-8.1	-7.7
E2	3.1	0.8	1.0	-5.2	-8.0	-7.7
F2	1.3	0.9	1.0	-8.7	-9.1	-9.3
H2			0.8			-9.0
J2			1.2			-8.4
A1			1.2			-8.2
B1			1.2			-8.8
C4			1.1			-8.1
D3			0.7			-8.5
F3			1.5			-8.4
H3			1.3			-8.4
H4			1.2			-7.8
H5			1.0			-8.3
L4			1.3			-8.2
average	2.0	0.8	1.1	-7.2	-8.3	-8.3
(1σ)	(1.3)	(0.2)	(0.3)	(1.4)	(0.5)	(0.4)
			White late-stage void-filling dolomite			
L1	1.1		1.0	-11.5		-11.6
C2	1.3		1.1	-10.8		-11.3
J3	1.7		1.1	-10.0		-11.2
J4			1.1			-11.1
average	1.4		1.1	-10.8		-11.3
(1σ)	(0.3)		(0.1)	(0.7)		(0.2)

[a] Sample FSV-924 from San Vicente N mine, level 1570 , local coordinates 20602 N and 19797 E

[b] Value excluded from average and from Fig. 2.2

Table 2.4. *In situ* stable isotope analyses of the zebra ore sample using a laser extraction technique

Analysis number[a]	$\delta^{13}C$ ‰ PDB	$\delta^{18}O$ ‰ PDB
	Dark replacement dolomite	
1 LC43-15	1.5	-7.4
2 LC43-3	1.3	-7.3
3 LC43-4	1.5	-7.4
average (1σ)	1.4 (0.2)	-7.4 (0.1)
	Light-grey sparry dolomite	
4 LC43-5	1.1	-6.3
5 LC43-6	0.9	-7.6
6 LC43-9	0.8	-7.9
7 LC43-8	0.7	-7.2
8 LC43-10	0.8	-7.9
10 LC43-12[b]	1.5	-7.9
13 LC43-2	1.3	-7.9
average (1σ)	1.0 (0.3)	-7.5 (0.6)
	White late-stage void-filling dolomite	
9 LC43-11[c]	0.5	-10.6
11 LC43-14	0.3	-11.1
12 LC43-13[c]	0.6	-10.3
average (1σ)	0.5 (0.2)	-10.7 (0.4)

[a] Location of the analysed microsamples are shown in Fig. 2.1

[b] Sample site rich in sphalerite

[c] Possibly contaminated by sparry dolomite

values. The late-stage void-filling dolomite is depleted in ^{13}C relative to the conventional analyses.

The following conclusions can be drawn regarding the *in situ* laser analyses of sulfides- and organic matter-rich carbonates (Table 2.5): (1) In samples rich in organic matter (e.g. dark replacement dolomite) the $\delta^{13}C$ and $\delta^{18}O$ values are equivalent to conventional analyses, but different from samples pretreated to remove the disturbing effects of sulfur species and organic contaminants; (2) in samples rich only in sulfides (e.g. light-grey sparry dolomite) the $\delta^{13}C$ values are correct, but the $\delta^{18}O$ values are elevated by ~1‰ to those obtained with pretreatment; (3) the lower $\delta^{13}C$ values for the late-stage dolomite may reflect kinetic fractionation effects common to all laser analyses (Sharp, 1992) or may be explained by a more precise micro-sampling than can be obtained with conventional drilling; (4) simple Ag_3PO_4 treatment does not alleviate the problem of sulfur contamination.

The results of a second representative hand specimen are presented in Table 2.6 and Fig. 2.3. The combined NaOCl and Ag_3PO_4 pretreatment was used for the analyses of the dark replacement dolomite. The sparry dolomite and the late-stage filling dolomite were only subjected to the pretreatment with Ag_3PO_4. Consistent clear trends without erratic values are illustrated, for example, in profiles D-E and E'-A across the three dolomite generations (Fig. 2.4). The white sparry dolomite exhibits significantly lighter $\delta^{13}C$ and $\delta^{18}O$ values than the early stage replacement dolomite, and heavier values than the paragenetically later open space filling dolomite. The decreasing isotopic ratios with increasing distance relative to the replacement dolomite may be explained by changes in the water to rock ratio, having precipitated the late-stage dolomite from an isotopic lighter fluid with a smaller contribution from the original replacement dolomite.

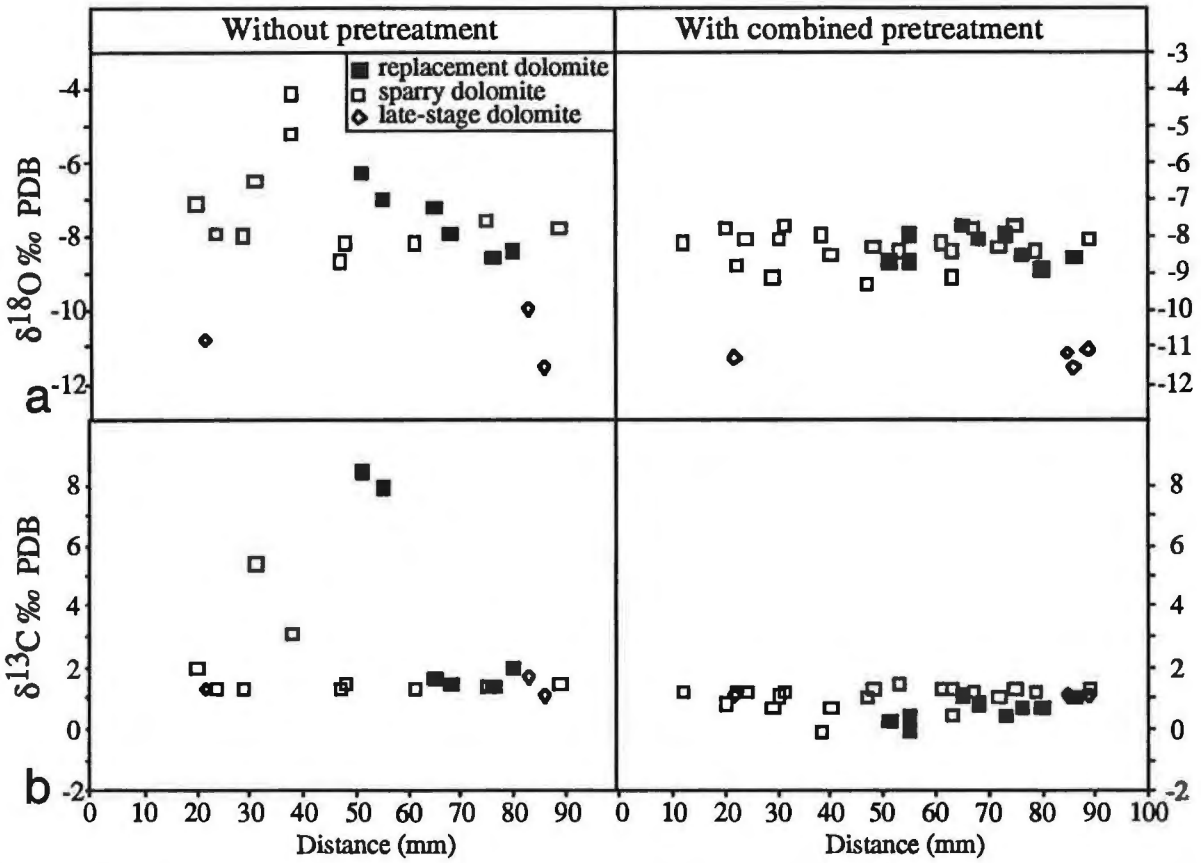

Figure 2.2. Variations of $\delta^{13}C$ (**a**) and $\delta^{18}O$ (**b**) values in replacement dolomite, sparry dolomite and late-stage void-filling dolomite of a zebra ore hand sample (FSV-924) using conventional acid extraction with and without pretreatment. Distances are referred to the lower edge of the sample, as illustrated in Fig. 2.1.

Table 2.5. Summary of the average $\delta^{13}C$ and $\delta^{18}O$ values and 1σ of the gangue dolomites analysed with different procedure

Dolomite generation (Sanple FSV-924)	Analytical procedure	$\delta^{13}C$ ‰ PDB	$\delta^{18}O$ ‰ PDB
Dark replacement dolomite	Conventional	3.8 (3.4)	-7.5 (0.8)
	$NaOCl+Ag_3PO_4$	0.6 (0.4)	-8.4 (0.4)
	Ag_3PO_4	1.2 (0.3)	-8.5 (0.2)
	In situ	1.4 (0.1)	-7.4 (0.1)
Light grey sparry dolomite	Conventional	2.0 (1.3)	-7.2 (1.4)
	$NaOCl+Ag_3PO_4$	0.8 (0.2)	-8.3 (0.5)
	Ag_3PO_4	1.1 (0.3)	-8.3 (0.4)
	In situ	1.0 (0.3)	-7.5 (0.6)
White late-stage filling dolomite	Conventional	1.4 (0.3)	-10.8 (0.7)
	$NaOCl+Ag_3PO_4$		
	Ag_3PO_4	1.1 (0.1)	-11.3 (0.2)
	In situ	0.5 (0.2)	-10.7 (0.4)

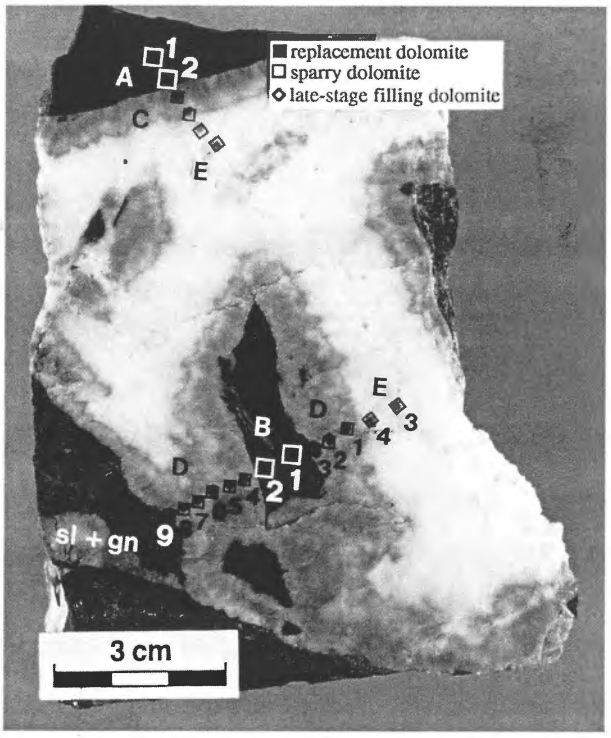

Figure 2.3. Hydraulic breccia (sample FSV-919) with grey-white sparry dolomite (*C* and *D*) surrounding the dark replacement dolomite (*A* and *B*), and milky white dolomiten (*E*) filling the open spaces.

Table 2.6. Isotopic composition of the different stage dolomites of an ore sample[a] using the combined pretreatment

Sample name	$\delta^{13}C$ ‰ PDB	$\delta^{18}O$ ‰ PDB
	Dark replacement dolomite[b]	
A1	1.4	-8.3
A2	1.3	-8.2
B1	1.0	-9.2
B2	1.2	-8.8
average (1σ)	1.2 (0.2)	-8.6 (0.5)
	Light-grey sparry dolomite[c]	
C1	0.7	-10.8
C2	0.6	-10.7
D1	0.4	-10.6
D2	0.5	-10.8
D3	1.0	-10.2
D4	0.7	-11.1
D5	0.5	-11.8
D6	0.9	-11.2
D7	0.8	-11.1
D8	1.0	-10.4
D9	1.0	-10.4
average (1σ)	0.7 (0.2)	-10.8 (0.5)

continued

Table 2.6. Continued

Sample name	$\delta^{13}C$ ‰ PDB	$\delta^{18}O$ ‰ PDB
	White late-stage void-filling dolomite[c]	
E1	0.0	-10.9
E2	-0.2	-12.5
E4	0.1	-12.4
E3	0.1	-12.2
average (1σ)	0.0 (0.1)	-12.0 (0.7)

[a] Sample FSV-919 from San Vicente N mine, level 1570, local coordinates 20561.5 N and 19795 E

[b] $NaOCl+Ag_3PO_4$ - pretreatment

[c] Only Ag_3PO_4 - pretreatment

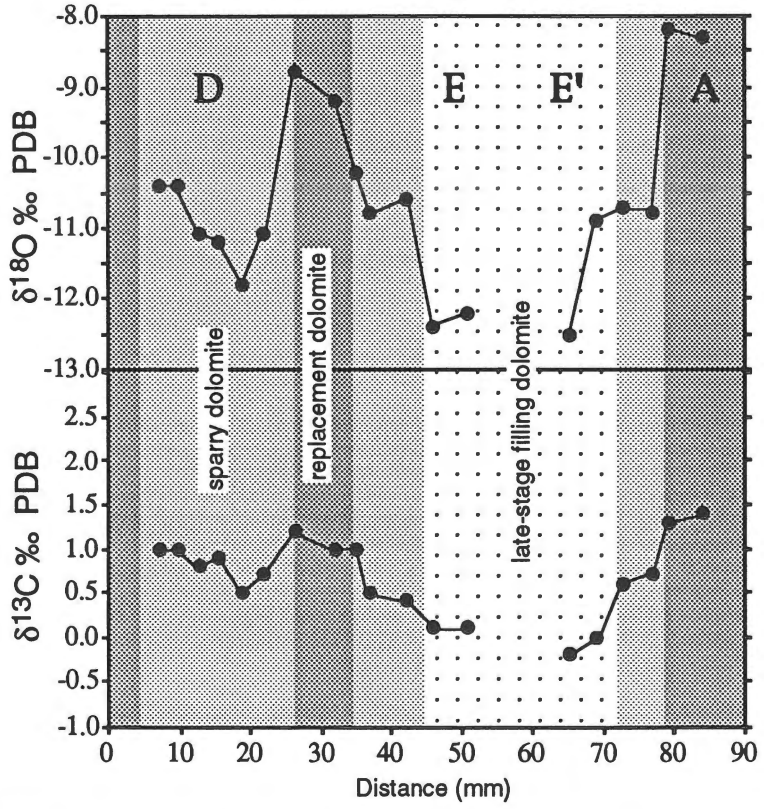

Figure 2.4. Cross section (*D-E* and *E'-A*, see Fig. 2.3) of carbon and oxygen isotope ratios, covering dark replacement dolomite ($NaOCl + Ag_3PO_4$ pretreatment), grey white sparry dolomite and late-stage filling dolomite (both Ag_3PO_4 pretreatment).

2.5 Conclusions

1. Our results show that small scale isotopic variations in the MVT gangue carbonates of San Vicente deposit are mainly due to the presence of sulfides in the carbonate sample, and that the associated organic matter plays a minor role.

2. The combined sodium hypochlorite and silver phosphate pretreatment, proposed by Charef and Sheppard (1984) is necessary for the accurate isotopic analysis of samples containing organic matter and sulfides, i.e. most fine- and medium-grained carbonate samples from MVT and other sediment-hosted base metal deposits.
3. For the isotopic analyses of white sparry and open space filling dolomite, which are virtually free of organic matter, the treatment with silver phosphate is sufficient.
4. Using this methodology the total variation of the $\delta^{13}C$ and $\delta^{18}O$ values of a defined carbonate generation in a hand specimen can be lowered to the global analytical and sampling error, i.e. not larger than ±0.1 to 0.4‰. Without this pretreatment an additional error in the range of +1 to +2‰, and occasionally up to +10‰ may be introduced.
5. There is an isotopic shift associated with the *in situ* laser technique. The $\delta^{13}C$ and $\delta^{18}O$ values are elevated relative to conventional pretreated samples by 0.5 to 1‰. The *in situ* method yields reproducible results. These data indicate that there is no appreciable isotopic variations at the sub-millimeter scale within any of the three carbonate generations.
6. In the samples studied in the present work, the variations of the stable isotope compositions within and between bands of a defined carbonate generation are very small (±0.1 to 0.4‰ $\delta^{13}C$ and 0.2 to 0.7 ‰ $\delta^{18}O$), suggesting uniform chemical and physicochemical conditions during precipitation of a given carbonate generation, at least at a centimeter scale.
7. The pretreatment methodology allows us to recognize subtle isotopic variations in the gangue carbonates that can be relevant for tracing basinal fluid pathways, and that would otherwise go unnoticed without pretreatment.

Acknowledgements

We acknowledge the financial support of the Swiss National Science Foundation (Grant n° 20-36397.92). This study is a contribution to IGC Project n° 342 *Age and Isotopes of South American Ores*. Thanks are due to the San Ignacio de Morococha S.A. Mining Company, and in particular the staffs of the Geology and Exploration Departments for their help in the field work. The manuscript benefited from critical comments by a anonymous reviewer of Mineralium Deposita. We also gratefully acknowledge J. Hunziker (University of Lausanne) and R. Moritz (University of Geneva) for their suggestions during this study, and M. Doppler and J. Metzger (University of Geneva) for their help in the preparation of the illustrations.

References

Banner, J.L., Hanson, G.N., and Meyers, W.J. (1988) Water-rock interaction history of riegonally extensive dolomites of the Burlington-Keokuk Formation (Mississippian): isotopic evidence. In: Shukla, V., and Baker, P.A. (Editors) Sedimentology and Geochemistry of Dolostones. Society of Economic Paleontologists and Mineralogists Special Publication No. 43, p. 97-113.

Charef, A., and Sheppard, M.F. (1984) Carbon and oxygen isotope analysis of calcite or dolomite associated with organic matter. Isotope Geoscience, v. 2, p. 325-333.

Frank, M.H., and Lohmann, K.C. (1986) Textural and chemical alteration of dolomite: interaction of mineralizing fluids and host rock in a Mississippi Valley-type deposit, Bonneterre Formation, Viburnum Trend. In: Hagni, R.D. (Editor) Process mineralogy VI: The metallurgical society, Warrendale, Pennsylvania, p. 103-116.

Fontboté, L., and Gorzawski, H. (1990) Genesis of the Mississippi Valley-type Zn-Pb deposit of San Vicente, Central Peru: geologic and isotopic (Sr, O, C, S) evidence. Economic Geology, v. 85, p. 1402-1437.

Fontboté, L. (1993) Self-organization fabrics in carbonate-hosted ore deposits: the example of diagenetic crystallization rhythmites (DCRs). In: Fenoll Hach-Ali, P., Torres-Ruiz, J., and Gervilla, F. (Editors) Current research in geolgy applied to ore deposits.

Proceedings of the Second Biennial SGA Meeting, Sept. 9-13, 1993, Granada, Spain, p. 11-14.

Ghazban, F., Schwarcz, H.P. and Ford, D.C. (1990) Carbon and sulfur isotope evidence for in situ reduction of sulfate, Nanisivik lead-zinc deposit, Northwest Territories, Baffin Island, Canada. Economic Geology, v. 85, p. 360-375.

Gregg, J.M., and Shelton, K.L. (1989) Geochemical and petrographic evidence for fluid sources and pathways during dolomitization and lead-zinc mineralization in Southeast Missouri: a review. Carbonates and Evaporites, v. 4, p. 153-175.

Hall, W.E., and Friedman, I. (1969) Oxygen and carbon isotopic composition of ore and host rock of selected Mississippi Valley deposits. U.S. Geol. Survey Prof Paper 650-C, p. C140-C148.

Hannah, J.L., and Stein, H.J. (1984) Evidence for changing ore fluid composition: stable isotope analyses of secondary carbonates, Bonneterre Formation, Missouri. Econ. Geol., v. 79, p. 1930-1935.

Kaufman, J., Meyers, W.J. and Hanson, G.N. (1990) Burial cementation in the Swan Hills formation (Devonian), Rosevear field, Alberta, Canada. Journal of Sedimentary Petrology, v. 60, p. 918-936.

Kaufman, J., Hanson, G.N., and Meyers, W.J. (1991) Dolomitization of the Devonian Swan Hills formation, Rosevear field, Alberta, Canada. Sedimentology, v. 38, p.41-66.

Land, L.S., Lang, J.C., and Barnes, D.J. (1977) On the stable carbon and oxygen isotopic composition of some shallow water, ahermatypic, scleractinian coral sceletons. Geochimica et Cosmochimica Acta, v. 41, p. 169-172.

Machel, H.-G. (1987) Saddle dolomite as a by-product of chemical compaction and thermochemical sulfate reduction. Geology, v. 15, p. 936-940.

McCrea, J.M. (1950) On the isotopic chemistry of carbonates and a paleotemperature scale. Journal of Chemical Physics, v. 18, p. 849-857.

Moritz, R., Fontboté, L., Spangenberg, J. Fontignie, D., Sharp, Z.D., and Rosas, S. (1993) Brine evolution and formation of Mississippi Valley-type deposits in the Pucará Basin, central Peru: Sr, C, and O isotopic evidence. In: Parnell, J., Ruffell, A.H., and Moles, N.R. (Editors) Geofluids '93, 4th-7th May 1993, Torquay, England, p. 309-312.

Pinckney, D.M. and Rye, R.O. (1972) Variation of O^{18}/O^{16}, C^{13}/C^{12}, texture, and mineralogy in altered limestone in the Hill Mine, Cave-in-District, Illinois. Economic Geology, v. 67, p. 1-18.

Rosenbaum, J., and Sheppard, S.M.F. (1986) An isotopic study of siderites, dolomites and ankerites at high temperatures. Geochimica et Cosmochimica Acta, v. 50, p. 1147-1150.

Rowan, E.L., and Leach, D.L. (1989) Constraints from fluid inclusions and sulfide precipitation mechanisms and ore fluid migration in the Viburnum Trend lead district, Missouri. Economic Geology, v. 84, p. 1948-1965.

Rye, D.M., and Williams, N. (1981) Studies of the base metal sulfide deposits at McArthur River, Northern Territory, Australia: III. The stable isotope geochemistry of the H.Y.C., Ridge, and Cooley Deposits. Economic Geology, v. 76, p. 1-26.

Sharp, Z.D. (1992) In situ laser microprobe techniques for stable isotope analysis. Chemical Geology (Isotope Geoscience Section), v. 101, p. 3-19.

Smith, J.W., and Croxford, R.J.W. (1975) An isotopic investigation of the environment of deposition of the McArthur mineralization. Mineralium Deposita, v. 10, p. 269-276.

Sverjensky, D.A. (1981) Isotopic alteration of carbonate host rocks as a function of water to rock ratio. An example from the Upper Mississippi Valley Zinc-Lead District. Economic Geology, v. 76, p. 154-172.

Weber, J.N, Deines, P., Weber, P.H., and Baker, P.A. (1976) Depth related changes in the $^{13}C/^{12}C$ ratio of skeletal carbonate deposited by the Caribbean reef-frame building coral *Montastrea annularis*: further implications of a model for stable isotope fractionation by scleractinian corals. Geochimica Cosmochimica Acta, v. 40, p. 31-39.

CHAPTER 3

CARBON AND OXYGEN ISOTOPE STUDY OF HYDROTHERMAL CARBONATES IN THE ZINC-LEAD DEPOSITS OF THE SAN VICENTE DISTRICT, CENTRAL PERU

Abstract

Mississippi Valley-type zinc-lead deposits and ore occurrences of the San Vicente belt are hosted in dolostones of the eastern part of the Upper Triassic to Lower Jurassic Pucará basin, central Peru. C and O isotope studies of the host and gangue carbonates from fifteen localities, including the San Vicente main deposit, minor ore occurrences and barren localities were used to constrain models of the ore forming processes. The $\delta^{13}C$ and $\delta^{18}O$ values of the altered host dolostone and hydrothermal carbonates, and the carbon isotope composition of the associated organic matter show a strong regional homogeneity. These results coupled with the strong mineralogical and petrographic similarities of the different MVT occurrences perhaps reflects the fact that the mineralizing processes were similar in the whole San Vicente belt, suggesting the existence of a common regional mineralizing hydrothermal system with interconnected plumbing.

A mixing model between an incoming hot saline slightly acidic radiogenic (Pb, Sr) fluid and the native formation water explains the overall isotopic variation ($\delta^{13}C$ = -11.5 to 2.5‰ and $\delta^{18}O$ = -12.5 to -6.4‰) of the carbonate generations. The dolomites formed during the main ore stage show a narrower range ($\delta^{13}C$ = -0.1 to 1.7‰ and $\delta^{18}O$ = -11.8 to -7.3‰) which is explained by exchange between the mineralizing fluids and the host carbonates combined with changes in temperature and pressure. This model of fluid-rock interaction explains the pervasive alteration of the host dolomite I and precipitation of sphalerite I. The open-space filling hydrothermal white sparry dolomite and the coexisting sphalerite II formed in previously prepared secondary porosity as overgrowths on the altered dolomite I by prolonged fluid-rock interaction and limited CO_2 degassing. Late filling dolomite III (or calcite) and the associated sphalerite III formed from the slightly acidic ore fluid during CO_2 degassing. Consequently, pressure variability plays a major role in the ore precipitation during the late hydrothermal events in San Vicente.

The results support a model that involves two ore forming mechanism: (1) alteration of the dolomite I and deposition of sphalerite I and II by temperature-dependent water-rock interaction between the mineralizing fluids and the preexisting carbonate host rocks, and (2) pressure drop likely as a result of dissolution-brecciation caused outgassing of CO_2 and consequent increase in pH of the ore fluid which in turn precipitated late sparry dolomite and sphalerite III. The presence of native sulfur associated with extremely carbon-light calcites replacing evaporitic sulfates (e.g., $\delta^{13}C$ = -11.5‰), altered native organic matter and heavier hydrothermal bitumen (from -27.0 to -23.0‰ $\delta^{13}C$) points to thermochemical reduction of sulfate and / or thiosulfate.

3.1 Introduction

Stable isotope studies of carbonates from Mississippi Valley-type (MVT) deposits can provide valuable information on sources of the mineralizing solutions, temperature of the mineralization and fluid pathways (e.g., Haefner et al., 1988; Hannah and Stein, 1984; Gregg and Shelton, 1989; Nesbitt and Muehlenbachs, 1994). Furthermore, they may put physicochemical constraints on the mechanism of precipitation of ore and gangue carbonates, chemical evolution of the mineralizing fluids, and on fluid-mixing and fluid-rock interaction processes (e.g., Garvin and Ludvigson, 1993; Ghazban et al., 1991; Gregg, 1985; Frank and Lohmann, 1986; Shelton et al., 1986; Gregg and Shelton, 1989; Banner et al., 1988; Farr, 1992; Qing and Mountjoy, 1992; Sverjensky, 1981).

San Vicente is the main ore field in a MVT zinc-lead belt located in the eastern part of the Upper Triassic - Lower Jurassic carbonate Pucará basin in central Peru. This contribution is part of a larger investigation which comprises trace and minor element studies (Spangenberg and Fontboté, 1995; Spangenberg and Fontboté, in prep.), strontium (Spangenberg et al., in prep.), sulfur and lead isotope studies, fluid inclusion studies, and geochemical studies of the associated organic matter (Spangenberg, 1995). Previous work on the San Vicente deposit includes Fontboté and Gorzawski (1990), Gorzawski et al. (1990), and Spangenberg et al. (1995). Moritz et al. (in press) present Sr, C and O isotope data on mineralized and barren carbonate rocks of the Pucará basin.

This study reports results of a carbon and oxygen isotopic investigation of the host and gangue carbonates from the San Vicente district. The aim is to put constraints on the chemistry of the ore solutions, the fluid-flow types, and the processes involved during sulfide precipitation. Quantitative modeling of the measured C and O isotope covariation in the different carbonate generations are used to characterize the geochemical mixing processes (fluid-fluid or fluid-rock) and the changes in temperature and pressure. In particular it will be shown that the main ore-stage mechanism of sulfide precipitation involved interaction of an extraformational incoming hot slightly acidic fluid with the dolomite host rock, and that a dissolution-driven pressure increase, followed by fracturing, and consequent CO_2 degassing may account for the precipitation of late-stage sulfides.

3.2 Geological setting

The San Vicente Mississippi Valley-type (MVT) Zn-Pb district is located 300 km east of Lima in central Peru, between 1000 and 2500 m altitude, in the so-called "Ceja de Selva", i.e., the eastern flank of the Andes covered by tropical rain forest. It has an accumulated production of about 14 million metric tons, and reserves exceeding 5 million tons ore of 11 wt. % zinc and 0.8 wt. % lead.

The Upper Triassic - Lower Jurassic Pucará basin, host of the San Vicente deposit and other non-mined MVT occurrences (Fig. 3.1), is a carbonate platform at the western margin of the Brazilian Shield developed at the beginning of the Andean cycle by marine transgression over clastic sediments and volcanic and volcaniclastic rocks of the Upper Permian to Lower Triassic Mitu Group (Fontboté, 1990; Rosas, 1994).

Recent sedimentological, Sr, C and O isotope and metallogenetic studies of the Pucará basin are discussed in Fontboté (1990), Rosas (1994) and Moritz et al. (in press). The geology of the San Vicente main deposit was described in detail by Fontboté and Gorzawski (1990, and references therein). In the San Vicente mining area the carbonate sequence of the Pucará Group has a thickness of about 1300 m and ranges in age from Norian to Hettangian (Fig. 3.2). Three dolomitic units, the San Judas Dolomite (SJD), the San Vicente Dolomite (SVD), and the Alfonso Dolomite (AD), host the orebodies. Most of the economic mineralization is contained within the San Vicente Dolomite. A series of normal faults and tectonic lineaments of general direction NE-SW, NW-SE, and N-S cut the carbonate units in the proximity to the orebodies. These fault systems and the basement highs may play an important role in the genesis of San Vicente ore as channel ways of the mineralizing solutions.

The ore occurs mainly as lens-shaped bodies (mantos) commonly conformable with bedding at the deposit scale. They are up to 1.3 km long, 200-300 m width, and several meters thick. The mineralization largely replaces dolomitized subtidal oolitic grainstones interlayered with dolomitized mudstones rich in organic matter and bearing evaporitic sulfate pseudomorphs (sabkha facies). It appears as zebra ore and occasionally as cement in breccias or veinlets (Figs. 1.6a, 1.6b; Fontboté and Gorzawski, 1990; Spangenberg et al., 1995). White sparry dolomite (WSD) is the main hydrothermal carbonate. Typically, WSD

Figure 3.1. Map of San Vicente MVT district showing the studied localities (barren and mineralized areas). QP=Quebrada Piñon; RO=Rondayacu; YS=Yanachuro Sur; UT=Utcuyacu; QU=Quebrada Utcuyacu; AY=Aynamayo; CH=Chilpes; US= Uncush Sur; AC=Afloramiento Campana; SV=San Vicente mine; AR=Arcopunco; MA=Machuyacu; PA=Palmapata; PJ=Puntayacu Junior; PS=Pichita Sur.

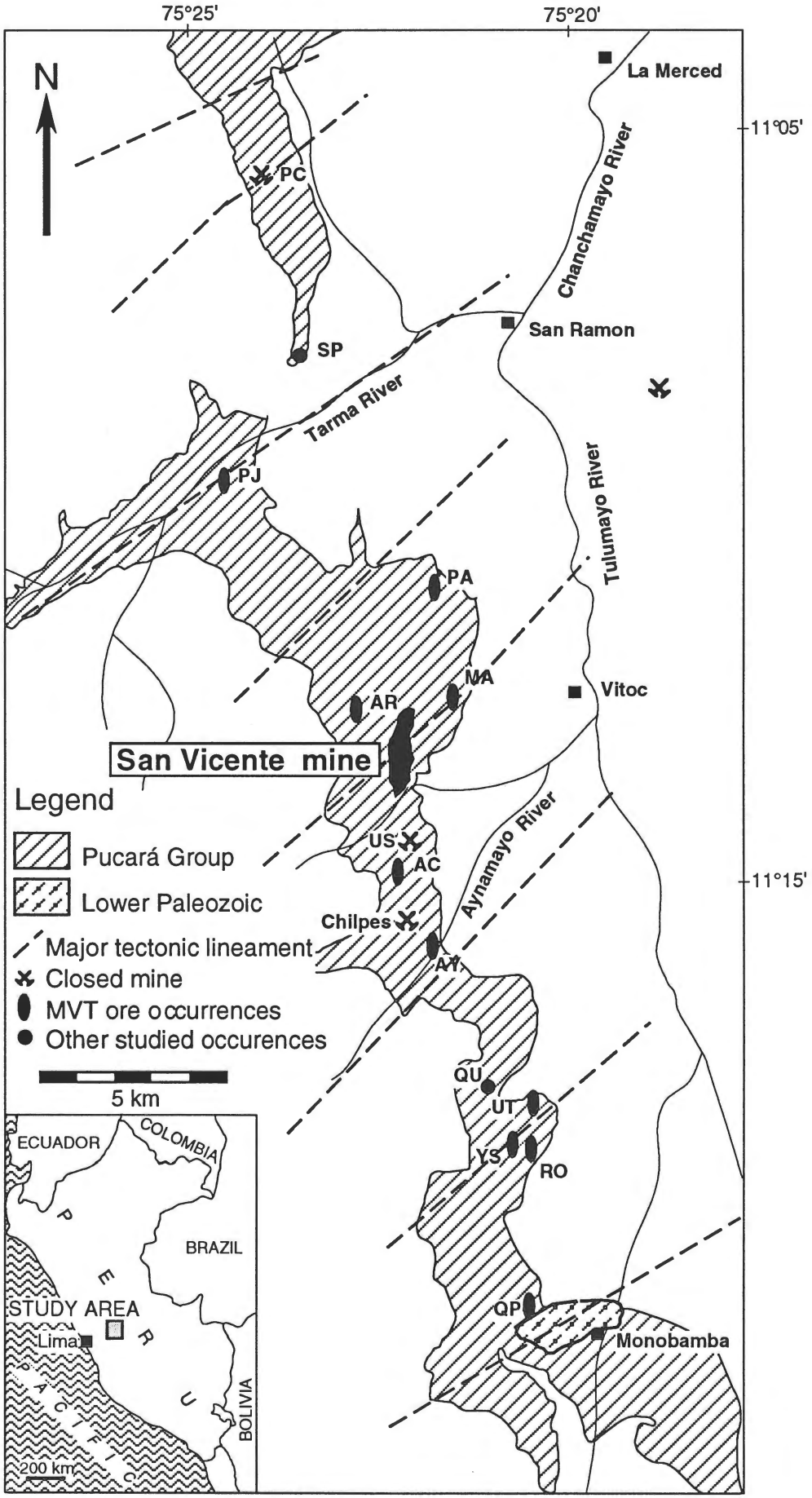
75°25'
75°20'
N
La Merced
11°05'
PC
Chanchamayo River
SP
San Ramon
Tarma River
PJ
Tulumayo River
PA
MA
AR
Vitoc
San Vicente mine
Legend
Pucará Group
Lower Paleozoic
Major tectonic lineament
Closed mine
MVT ore occurrences
Other studied occurences
US
AC
Aynamayo River
11°15'
Chilpes
AY
5 km
QU
UT
YS
RO
ECUADOR
COLOMBIA
BRAZIL
STUDY AREA
Lima
QP
Monobamba
BOLIVIA
200 km

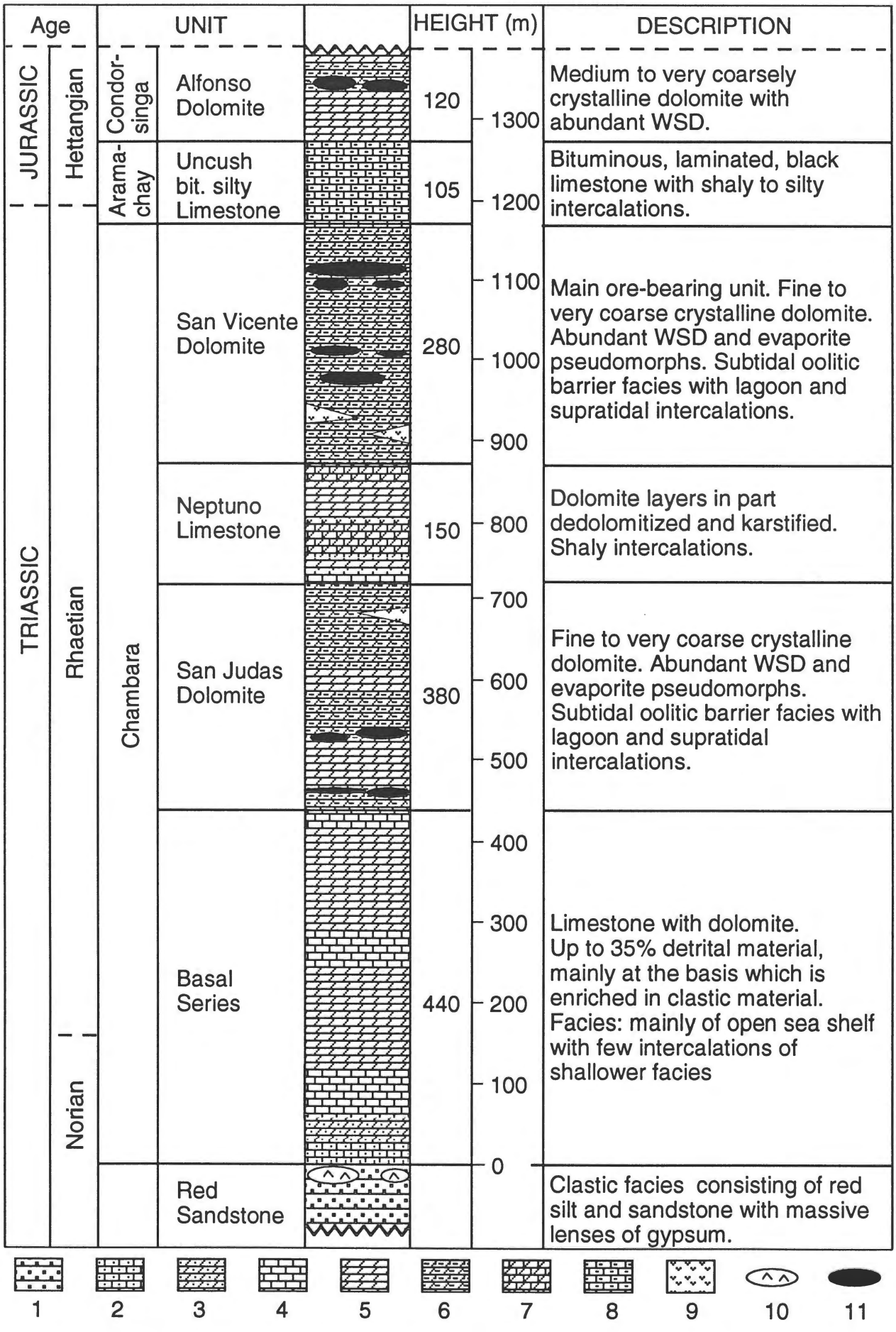
Age
UNIT
HEIGHT (m)
DESCRIPTION
JURASSIC
TRIASSIC
Hettangian
Rhaetian
Norian
Condor-singa
Arama-chay
Chambara
Alfonso Dolomite
120
Medium to very coarsely crystalline dolomite with abundant WSD.
Uncush bit. silty Limestone
105
Bituminous, laminated, black limestone with shaly to silty intercalations.
San Vicente Dolomite
280
Main ore-bearing unit. Fine to very coarse crystalline dolomite. Abundant WSD and evaporite pseudomorphs. Subtidal oolitic barrier facies with lagoon and supratidal intercalations.
Neptuno Limestone
150
Dolomite layers in part dedolomitized and karstified. Shaly intercalations.
San Judas Dolomite
380
Fine to very coarse crystalline dolomite. Abundant WSD and evaporite pseudomorphs. Subtidal oolitic barrier facies with lagoon and supratidal intercalations.
Basal Series
440
Limestone with dolomite. Up to 35% detrital material, mainly at the basis which is enriched in clastic material. Facies: mainly of open sea shelf with few intercalations of shallower facies
Red Sandstone
Clastic facies consisting of red silt and sandstone with massive lenses of gypsum.
1300
1200
1100
1000
900
800
700
600
500
400
300
200
100
0
1
2
3
4
5
6
7
8
9
10
11

postdates sulfide precipitation and fills the open spaces (Figs. 1.6a-1.6d, 1.7g-1.7h). One exception is the "San Vicente Techo manto", which is located in the upper and northern margin of the main ore deposit, where WSD is largely lacking. Another attribute of this manto is the presence of massive pyrite, a mineral otherwise only present in traces.

Fontboté and Gorzawski (1990) proposed that San Vicente formed at a depth of about 2-3 km and a temperature range of about 70 to 160°C by influx of a metal-bearing saline brine characterized by radiogenic Sr and Pb. Extensive petrographic and isotopic (C, O, Sr, S, and Pb) information (Gorzawski, 1989; Fontboté and Gorzawski, 1990; Gorzawski et al., 1990) is available on San Vicente main deposit. The results of preliminary fluid inclusion studies indicate that the white sparry dolomite was precipitated from hot (115° to 162°C) and saline (up to 26 wt.% equivalent NaCl) fluids (Moritz et al, in press).

3.3 Host and gangue carbonates

The studied host and hydrothermal (syn- and post-ore) carbonates from San Vicente MVT district are listed in Table 3.1. It is possible to distinguish different generations of carbonates (Figs. 1.6a-1.6g). They include dark replacement dolomite (DRD, I), white sparry dolomite (WSD, II), late void-filling dolomite (LFD, IIId) or calcite (LFC, IIIc), and carbonate replacing evaporitic sulfate (EP).

The dark replacement dolomite is a fine- to medium-crystalline dolomite, with total organic carbon in the range of 0.07 % to 0.37 wt.% (Spangenberg, 1995) and occasionally relicts of primary depositional features (Fig. 1.7). Higher values of total organic carbon (up to 5.2 wt.%, Spangenberg et al., 1995) are also found in the vicinity of bituminous horizons. It presents different degrees of hydrothermal alteration which are expressed under the microscope, especially using cathodoluminescence, by dissolution and precipitation textures. This early dolomite has been classified into the following three groups which display an increasing degree of recrystallization and hydrothermal alteration: "Ivf" fine to very fine-grained (size from 15 to 60 µm, Figs. 1.7a, 1.7b), "If" fine-grained (size from 40 to 100 µm, Figs. 1.7c, 1.7d), and "Im" medium-grained (size from 100 to 400 µm, Figs. 1.7e, 1.7f). The very fine-grained DRD (Ivf) represents the best available approximation to the pre-ore host dolostone. In dolomites Ivf and If is possible to still recognize relicts of primary textures in particular ghost of former ooliths, whereas in the dolomite Im the primary texture preservation is poorer (Fig. 1.7).

In advanced stages of metasomatic alteration the white dolomite, replacing the dark host dolomite, has an increased grain size and coarse subhedral sparry dolomite (size from 0.4 to 2.5 mm; Fig. 1.7g) precipitates from the hydrothermal fluid in the available porosity. The resulting grayish coarse-grained replacement mottled dolomite forms millimetric spots of white dolomite and is comparable with the salt-and-pepper dolomite described by Ghazban et al. (1990) at Nanisivik MVT Zn-Pb deposit. This altered DRD is intergrown with the first generation of fine-crystalline anhedral sphalerite and occasionally with pyrite and micro-crystalline quartz.

White sparry dolomite (WSD, also called saddle dolomite) is the most extensive hydrothermal dolomite cement and is formed throughout the entire San Vicente belt. The WSD is a subhedral mostly grayish (due to inclusions of sulfides and organic matter) sparry dolomite that occurs as open-space filling in small spots, in millimetric to centimetric thick bands replacing the DRD, and as cement in hydraulic breccias. Alternating repetition of the bands of the DRD and the WSD, give rise to the characteristic zebra texture of the ore rock, a common feature of Mississippi Valley-type deposits (e.g., Arne et al., 1991; Beales and Hardy, 1980; Fontboté and Gorzawski, 1990; Fontboté, 1993; Landis and Tschauder, 1990). Six subgenerations of the ore-stage WSD were distinguished on the basis of their fabrics (Figs. 1.6c-1.6f): t1 = millimetric sized spots of WSD in mottled DRD, t2 = fine veinlets of WSD, t3 = ordered millimetric to centimetric thick bands of WSD , t4 = WSD in

Figure 3.2. Stratigraphic column of the Pucará units in the San Vicente mining area (modified after Rosas, 1994). 1=red sandstone; 2=marly limestone; 3=marly dolomite; 4=limestone; 5=dolomite; 6=dolomite with white sparry dolomite; 7=partly dedolomitized dolomite; 8=bituminous silty limestone; 9=volcanic rocks; 10=gypsum lenses; 11=ore.

Table 3.1. Studied host and gangue minerals from San Vicente MVT district. The paragenetic position of sphalerite (sl) and galena (gn) is shown schematically

Generation/ Subgeneration	Description	*Lithologic unit* sl	gn
San Judas Dolomite (SJD), San Vicente Dolomite (SVD), Alfonso Dolomite (AD)			
I	dark replacement dolomite (DRD)		
Ivf	very fine-grained DRD		
If	fine-grained DRD		
Im	medium-grained DRD		
Iom	organic matter associated to the DRD		
II	white sparry dolomite (WSD)		
IIt1	spots of WSD		
IIt2	fine veinlets of WSD		
IIt3	ordered bands of WSD		
IIt4	zebra texture		
IIt5	broad crosscutting veins of WSD		
IIt6	WSD in hydraulic breccia		
III	late-stage filling carbonate		
IIId	late-stage filling dolomite (LFD)		
IIIc	late-stage filling calcite (LFC)		
IIIbit	allochtonous hydrothermal bitumen		
EP	carbonate as evaporite pseudomorph		
EPd	dolomite replacing sulfate evaporites		
EPc	calcite replacing sulfate evaporites		
Uncush bituminous silty Limestone (UL)			
UL	host calcite		
ULom	organic matter associated to UL		

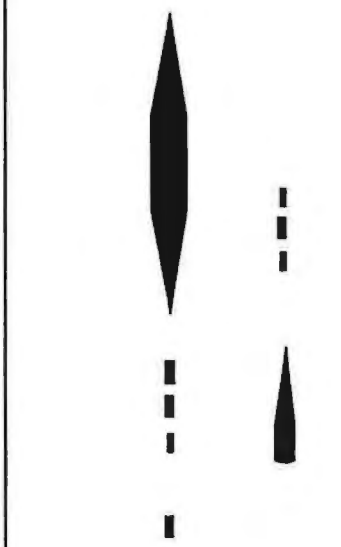

zebra rock, t5 = crosscutting veins of WSD, and t6 = white dolomite as oriented overgrowths of hydraulic breccias.

The late filling carbonate occurs as coarse or very coarse-grained, mainly anhedral, milky-white dolomite (LFD) or calcite (LFC) open-space fillings in the WSD. Where both late open-space filling carbonates are present, white calcite is apparently younger than dolomite.

A further carbonate phase occurs as sulfate pseudomorphs (EP) in the DRD. The main minerals replacing evaporitic sulfate evaporites (gypsum or anhydrite) are calcite, cherty quartz, and subordinate dolomite (Fig. 1.6g).

Most of the sphalerite occurs in the same paragenetic situation as white hydrothermal dolomite (Table 3.1): (1) as fine-crystalline anhedral sphalerite intergrown with recrystallized dolomite I; (2) as coarse open space-filling subhedral sphalerite predating and/or intergrown with the white sparry dolomite II on the pervasive altered dark dolomite (Figs. 1.7g, 1.7h); and (3) as very coarse euhedral crystals within the late filling white dolomite III in the cement of dissolution-breccias (Fig. 1.6b). Coarse-grained anhedral galena, and in a few places scarce native sulfur appear as open-space fillings throughout the district. Fine-grained native sulfur (up to 0.9 wt. % total sulfur) and occasionally aggregates of coarse-grained sulfur are intergrown with calcite in the sulfate pseudomorphs.

Solid bitumen occurs as open-space filling and appears to be slightly younger than the late vug carbonates (Fig. 1.6h). During the dissolution/recrystallization of host dolomite the released solid organic matter (kerogen) is trapped in the grain-boundaries and its thermal alteration generates (liquid and gaseous) hydrocarbons which are transported in the

hydrothermal fluids. These hydrocarbons migrate with the fluid and precipitate as solid bitumen after further thermal cracking, releasing light-molecular hydrocarbons (Sassen, 1988).

The Uncush bituminous silty Limestone (UL) is a black limestone rich in organic matter (total organic carbon ranges between 0.3 and 4.0 wt.%) and very-fine crystalline pyrite (total sulfur up to 1.2 wt.%) with shaly to silty intercalations. This unit (Fig. 3.2) overlies the major ore-bearing dolomitic unit (San Vicente Dolomite) and provides a stratigraphic reference horizon.

3.4 Methods

3.4.1 Sampling

Carbonate rocks from the San Vicente MVT district were sampled according to a hierarchical scheme comprising the following sampling scales: district, the San Vicente main deposit, manto, outcrop, and handspecimen. The results will be presented in two sections: district and mine scale.

The San Vicente district was studied at mineralized and barren areas in fourteen localities along a 27 km N-S traverse centered on the main deposit (Fig. 3.1). The aim of this district-scale sampling was to obtain information on regional isotopic trends in the host and gangue carbonates, which could reflect the flow path of the ore fluids. Sampling was performed at mined ore occurrences, surface outcrops, and exploration diamond-drill holes. District scale sampling was carried out in 14 profiles across the Pucará sequence. A total of 43 samples, mainly of the ore-bearing Dolomites (San Judas Dolomite, San Vicente Dolomite, and Alfonso Dolomite), have had stable isotope determinations.

An extensive multiple sampling was made at the San Vicente mining area. A total of 137 samples of several mantos from the three ore-bearing dolomitic units (SJD, SVD, AD) were analyzed. Two representative orebodies ("manto Alfonso", "manto San Vicente Techo") were sampled along two crosswise profiles in approximate direction NS and EW over an area of about 400x100 m^2 and 700x100 m^2 respectively. These profiles, with an irregular sampling step (between 5 and 50 m), cover the ore-bearing mantos and their barren projections in the same horizon. Thirty-two samples were collected in "manto Alfonso" and twenty-three in "manto San Vicente". The aim of this specific manto-scale sampling was to detect possible preferential orientation of the fluid path and hydrothermal alteration/ mineralization fronts. Finally the textural subgenerations of the DRD (Ivf to Im) and the WSD (IIt1 to IIt6) were studied in detail in selected outcrops and handspecimens (see Table 3.1).

Furthermore, three types of organic matter were isotopically investigated: total organic carbon (TOC) associated with the dark replacement dolomite (Iom), late hydrothermal bitumen (IIIom), and TOC associated with the bituminous Uncush limestone (ULom).

3.4.2 Analytical procedures

The different carbonate generations were selectively sampled from roughly polished slabs of more then 200 handspecimens by using a dental diamond-drill device. The mineralogical composition of a selected set of more than hundred samples was controlled by X-ray powder diffractometry at the University of Lausanne using a Philips® PW1710 goniometer. Only those samples which turned out to be pure dolomite or pure calcite were analyzed. C and O isotope analyses were performed at the University of Lausanne using a Finnigan MAT-251 mass spectrometer. CO_2 extraction was done at 50°C for dolomite and at 25°C for calcite following the conventional method by McCrea (1950). In a previous study (Spangenberg et al., 1995) we showed that the presence of organic matter and/or sulfur can disturb seriously the measured isotopic composition of the gangue carbonates from San Vicente deposit. Therefore, the carbonate samples containing organic matter were soaked in 5 % sodium hypochlorite solution for 15 h at room temperature to oxidize labile organo- and

organo-sulfur compounds. The CO_2 extracted from the carbonates was reacted with Ag_3PO_4 for 10 min before analysis, to eliminate the phosphoric acid-liberated sulfur species. Carbon and oxygen isotope values are reported conventionally as the variation in per mil (‰) relative to the PDB standard. Analytical uncertainty, monitored by daily replicate analysis of the laboratory standard Carrarra Marble for calcite and Binn Dolomite for dolomite, is no greater than ± 0.05 ‰ (1 s) for carbon and ± 0.1 ‰ for oxygen.

Organic matter was separated by a soft acid leaching (HCl 1N) of the powdered samples (DRD and Uncush limestones). The hydrothermal bitumen (IIIom) was sampled by hand-picking, and washed with HCl 1N solution. $\delta^{13}C$ values were measured in the CO_2 evolved by oxidation of the organic matter with vanadium pentoxide (V_2O_5) in sealed silica tubes at 900°C for 30 min. CO_2 was cleaned by a fractional sublimation in a cold trap, containing Ag_3PO_4. The analytical uncertainty, tested by analysis of the NBS-21 graphite standard ($\delta^{13}C$ = -28.10 ‰) and duplicate analysis of an inhouse graphite standard is better than ± 0.1 ‰ (1 s).

3.5 Results

3.5.1 San Vicente district

The carbon and oxygen isotope ranges determined in the DRD and the WSD in the studied localities of the San Vicente belt (values of the San Vicente deposit are given for comparison) are listed in Table 3.2. The $\delta^{13}C$ and $\delta^{18}O$ values of the DRD ($\delta^{13}C$ = 0.9 to 1.7 ‰; $\delta^{18}O$ = -10.0 to -7.4 ‰) and the WSD ($\delta^{13}C$ = 0.2 to 1.6 ‰; $\delta^{18}O$ = -11.4 to -7.4 ‰) vary within a rather close range for the different lithologic units all along the San Vicente district and are also similar to the isotopic ratios measured at the San Vicente main deposit (for the DRD: $\delta^{13}C$ = 0.5 to 2.5 ‰ and $\delta^{18}O$ = -9.6 to -6.4 ‰; for the WSD: $\delta^{13}C$ = -0.1 to 1.7 ‰; $\delta^{18}O$ = -11.8 to -7.3 ‰).

Table 3.2. Carbon and oxygen isotope composition of carbonates from deposits and ore-occurrences in the San Vicente Mississippi Valley-type district

Locality (abbreviation)	Lithologic unit (m, n)*	Ranges of isotopic ratios			
		$\delta^{13}C$ (‰)		$\delta^{18}O$ (‰)	
		DRD	WSD	DRD	WSD
Qbd. Piñon (QP)	SJD (-, 7)	-	1.0 to 1.4	-	-10.6 to -9.7
Rondayacu (RO)	SJD (-, 3)	-	0.8 to 0.9	-	-10.6 to -9.9
Yanachuro Sur (YS)	SJD (-, 2)	-	1.2 to 1.7	-	-10.2 to -9.7
Utcuyacu (UT)	SVD (-, 2)	-	1.1	-	-9.9 to -9.8
Qbd. Utcuyacu (QU)	SVD (-, 2)	-	0.5 to 1.1	-	-10.4 to -10.1
Aynamayo (AY)	SJD (2, 2)	1.6 to 1.7	1.1 to 1.3	-8.1 to -8.0	-10.0 to -9.9
	SVD (1, 2)	1.4	0.8 to 1.1	-7.6	-11.2 to -10.7
Chilpes (CH)	SJD (1, 2)	1.7	1.4 to 1.7	-7.8	-8.4 to -8.0
	SVD (2, 4)	1.0 to 1.6	0.7 to 1.0	-9.8 to -7.4	-10.0 to -9.5
Uncush Sur (US)	AD (-, 1)	-	1.3	-	-9.9
Afl. Campana (AC)	AD (-, 2)	1.5	0.9 to 1.4	-7.6	-8.2 to -8.7
San Vicente (SV)	SJD (2, 28)	1.1 to 1.7	0.6 to 1.6	-8.2 to -7.4	-10.5 to -8.0
	SVD (23, 90)	0.5 to 2.5	-0.1 to 1.6	-9.6 to -6.4	-11.8 to -7.3
	AD (4, 19)	1.2 to 1.7	0.8 to 1.7	-8.5 to -7.2	-10.0 to -8.1
Arcopunco (AR)	SVD (2, 4)	1.4	0.7 to 1.2	-9.0 to -7.4	-10.7 to -8.3
Machuyacu (MA)	SVD (-, 4)	-	0.7 to 0.9	-	-10.7 to -9.8
Palmapata (PA)	SVD (1, 2)	0.9	0.9 to 0.9	-10.0	-10.2 to -10.0
Puntayacu Junior (PJ)	SVD (-, 3)	-	0.2 to 0.5	-	-11.4 to -10.0
Pichita Sur (PS)	SVD (-, 1)	-	0.5	-	-10.8

*SJD=San Judas Dolomite, SVD=San Vicente Dolomite, AD=Alfonso Dolomite; m=number of analyzed samples of dark replacement dolomite (DRD); n=number of analyzed samples of white sparry dolomite (WSD)

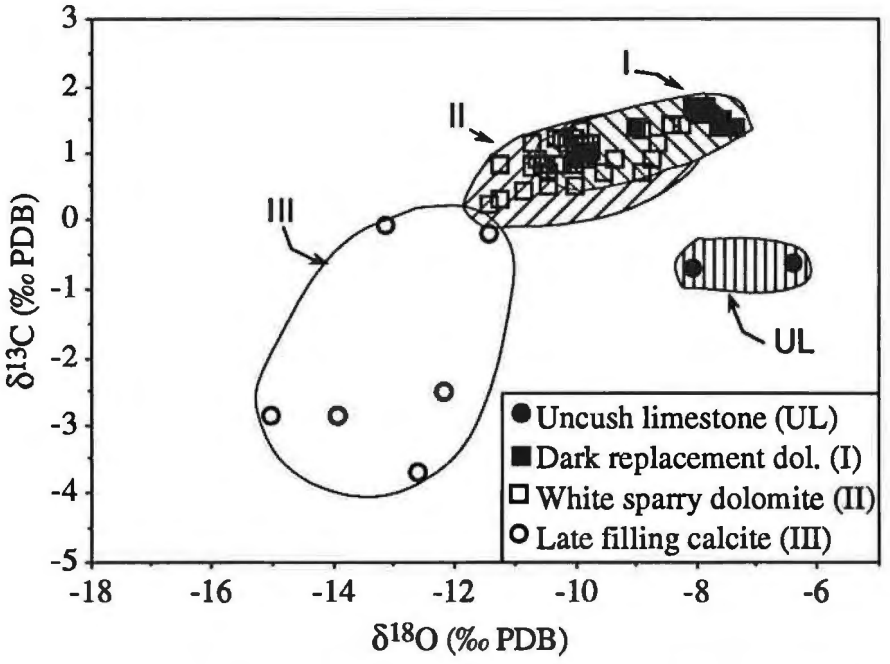

Figure 3.3. $\delta^{18}O$ versus $\delta^{13}C$ of the carbonates from the San Vicente district (without data from the San Vicente main deposit). Note the partial overlap between the fields of the DRD and the WSD.

At a textural scale the three main generations of carbonates (DRD, WSD and LFC) are well differentiated in $\delta^{13}C$ vs. $\delta^{18}O$ space (Fig. 3.3). The heaviest $\delta^{13}C$ and $\delta^{18}O$ end member is the DRD. The pervasively altered DRD (Im) is substantially depleted in ^{18}O (up to 3 ‰) and ^{13}C (up to 2 ‰). The hydrothermal sparry dolomites are isotopically similar to the neomorphized DRD (Fig. 3.3). The $\delta^{13}C$ and $\delta^{18}O$ values of five samples of late filling calcite are scattered from -3.7 to -0.1 ‰ and -15.0 to -11.4 ‰ respectively. The carbonate generations display a general tendency towards lighter isotopic compositions with advancing paragenetic stage. For each locality the isotopic shift from the DRD to the WSD is of the same order, ranging from 0.5 to 1 ‰ $\delta^{13}C$ and up to 4 ‰ $\delta^{18}O$ and show no significant zonation at the stratigraphic and the district scale (Table 3.2). The regional homogeneity of the isotopic composition of the altered-host and gangue dolomites suggests that the physicochemical conditions and the fluid-rock interaction processes were uniform and almost constant during host rock alteration and gangue precipitation. Note that the host DRD are significantly enriched in ^{13}C (up to 2.4 ‰) and depleted in ^{18}O (up to 3.6 ‰) relative to the Uncush limestones ($\delta^{13}C$= -0.7 to -0.6 ‰; $\delta^{18}O$= -8.1 to -6.4 ‰).

3.5.2 San Vicente main deposit

The results of the carbon and oxygen isotopic analyses of a representative subset comprising 140 samples of host and gangue minerals of the San Vicente mine are listed in Table 3.3, and the ranges determined with all the measurements (more than 250 samples) illustrated in Fig. 3.4.

3.5.2.1 Host and gangue carbonates

Carbon and oxygen isotopic compositions of Uncush limestones are restricted to a narrow range ($\delta^{13}C$ = 0.8 to 2.3 ‰, and $\delta^{18}O$ = -8.4 to -6.3 ‰). This carbonate phase represents the isotopic heaviest end member for calcite (Fig. 3.4). The different generations of gangue carbonates of the San Vicente deposit display a general tendency toward lighter isotopic composition in the following sequence: dark replacement dolomite -> white sparry dolomite -> late filling dolomite -> late filling calcite -> carbonates replacing evaporitic

Table 3.3. $\delta^{13}C$ and $\delta^{18}O$ values of host and gangue minerals from the San Vicente mine (representative values)

Sample name	Lith. Unit	Manto	Generation*	Description*	$\delta^{13}C$ ‰ PDB	$\delta^{18}O$ ‰ PDB
FSV-654	AD	Alfonso	If	DRD (If)	1.2	-8.5
			IIt3	ordered bands of WSD	1.0	-9.6
FSV-655	AD	Alfonso	IIt3	ordered bands of WSD	1.0	-9.8
FSV-665	AD	Alfonso	IIt6	WSD, hydraulic breccia	1.1	-8.7
			IIIc	LFC	-2.4	-13.4
FSV-667	AD	Alfonso	IIt5	crosscutting veins of WSD	1.4	-8.2
FSV-668	AD	Alfonso	IIt5	crosscutting veins of WSD	1.7	-9.2
FSV-801	AD	Alfonso	Ivf	DRD	1.3	-7.8
			IIt5	crosscutting veins of WSD	1.1	-9.9
			IIIc	LFC	-0.5	-9.8
			Iom	OM in DRD	-27.0	
FSV-803	AD	Alfonso	IIt6	WSD, hydraulic breccia	1.1	-9.7
FSV-804	AD	Alfonso	IIt6	WSD, hydraulic breccia	1.0	-9.9
FSV-805	AD	Alfonso	IIt6	WSD, hydraulic breccia	0.9	-10.0
FSV-806	AD	Alfonso	IIt6	WSD, hydraulic breccia	0.9	-9.3
FSV-807	AD	Alfonso	IIt6	WSD, hydraulic breccia	1.2	-9.6
			IIIc	LFC	-2.6	-11.9
FSV-808	AD	Alfonso	IIt5	crosscutting veins of WSD	1.5	-8.1
FSV-809	AD	Alfonso	IIt6	WSD, hydraulic breccia	1.0	-9.8
FSV-810	AD	Alfonso	IIt3	ordered bands of WSD	0.8	-9.9
FSV-811	AD	Alfonso	Ivf	1 DRD	1.7	-7.2
			If	2 DRD, py filling the oöliths	1.2	-7.3
			IIt5	crosscutting veins of WSD	1.2	-8.7
			Iom	TOC in DRD	-26.8	
FSV-816	AD	Alfonso	IIt3	ordered bands of WSD	1.6	-9.8
			IIt3	ordered bands of WSD	1.7	-9.2
			IIt5	crosscutting veins of WSD	1.4	-8.6
FSV-822	AD	Alfonso	IIIbit	hydrothermal bitumen	-23.0	
FSV-827	AD	Alfonso	IIIbit	hydrothermal bitumen	-23.3	
FSV-830	AD	Alfonso	IIt5	crosscutting veins of WSD	0.9	-9.8
FSV-15	UL		UL	Bituminous silty limestone	2.0	-6.3
FSV-18	UL		UL	Bituminous silty limestone	0.8	-7.6
FSV-1102	UL		UL	Bituminous silty limestone	1.2	-7.2
			ULom	TOC in UL	-27.2	
FSV-1103	UL		UL	Bituminous silty limestone	2.3	-6.6
			ULom	TOC in UL	-28.2	
FSV-671	SVD		Im	DRD, bituminous dolomite	0.9	-8.3
			IIIbit	hydrothermal bitumen	-24.0	
FSV-678	SVD		Im	DRD, bituminous dolomite	0.7	-10.8
			IIIbit	hydrothermal bitumen	-23.9	
FSV-851	SVD	SV techo	IIt6	WSD, hydraulic breccia	1.5	-8.0
			IIIc	LFC	-2.9	-11.8
FSV-852	SVD	SV techo	IIIc	LFC	0.3	-10.2
FSV-853	SVD	SV techo	If	DRD	1.1	-8.1
			Iom	TOC in DRD (Iom)	-26.4	
			IIIc	LFC calcite	0.0	-10.8
			IIIbit	hydrothermal bitumen	-27.7	
FSV-854	SVD	SV techo	IIIc	LFC	-2.8	-14.8
FSV-855	SVD	SV techo	IIt6	WSD, hydraulic breccia	0.8	-9.7
FSV-856	SVD	SV techo	Ivf	DRD	0.9	-7.6
			EPc	calcite replacing evaporite	-9.3	-12.1
FSV-857	SVD	SV techo	IIt6	WSD, hydraulic breccia	1.5	-8.0
			EPc	calcite replacing evaporite	-4.5	-10.9
FSV-860	SVD	SV techo	EPc	calcite replacing evaporite	-3.5	-9.5
FSV-861	SVD	SV techo	IIt6	WSD, hydraulic breccia	1.2	-7.5

continued

Table 3.3. Continued

Sample name	Lith. Unit	Manto	Generation	Description	$\delta^{13}C$ ‰ PDB	$\delta^{18}O$ ‰ PDB
FSV-862	SVD	SV techo	IIIc	LFC	0.2	-11.2
FSV-869	SVD	SV techo	IIt3	ordered bands of WSD	0.8	-8.9
			IIIc	LFC	0.5	-9.1
FSV-640	SVD	SV techo	EPc	calcite replacing evaporite	0.8	-12.5
			EPc	calcite replacing evaporite	0.2	-13.1
FSV-032	SVD	Jesus	IIt3	ordered bands of WSD	1.2	-8.2
FSV-033	SVD	Jesus	IIt4	WSD, zebra texture	0.9	-9.7
FSV-422	SVD	Jesus	IIt3	1 ordered bands of WSD	0.8	-10.3
			IIt4	2 WSD, zebra texture	1.0	-9.5
FSV-423	SVD	Jesus	Ivf	DRD, host dolostone	1.5	-6.4
			EPc	1 calcite replacing evaporite	-1.4	-10.6
			EPc	2 calcite replacing evaporite	-2.0	-9.9
			EPc	3 calcite replacing evaporite	-1.4	-10.3
FSV-673	SVD	Jesus	IIt6	WSD, hydraulic breccia	0.8	-8.6
			IIIc	LFC	0.7	-9.8
			IIIbit	hydrothermal bitumen	-27.0	
FSV-674	SVD	Jesus	IIt6	WSD, hydraulic breccia	1.0	-10.2
			IIIc	LFC	-0.5	-9.8
FSV-675	SVD	Jesus	IIIc	LFC with native sulfur	-0.3	-10.2
FSV-905	SVD	Jesus	If	DRD	1.6	-7.4
			IIt3	ordered bands of WSD	1.4	-8.5
			IIt2	fine veinlets of WSD	1.0	-9.8
			IIt2	fine veinlets of WSD	0.7	-10.4
			IIt1	spots of WSD in DRD	0.2	-11.2
			IIt1	spots of WSD in DRD	-0.1	-11.4
FSV-914	SVD	Ayala	Im	DRD	1.0	-9.5
			IIt3	ordered bands of WSD	1.2	-9.7
FSV-1	SVD	Ayala	IIt4	WSD, zebra texture	1.4	-8.7
FSV-662	SVD	Ayala	IIt4	WSD, zebra texture	1.3	-9.3
FSV-663	SVD	Ayala	IIt4	WSD, zebra texture	1.6	-8.5
FSV-664	SVD	Ayala	IIt6	WSD, hydraulic breccia	1.4	-9.4
FSV-4	SVD	3t	IIt5	crosscutting veins of WSD	1.2	-8.4
FSV-5	SVD	3t	Im	DRD , reticulate texture	0.5	-9.3
			IIt5	crosscutting veins of WSD	1.1	-10.2
			IIIc	LFC	0.6	-10.9
FSV-8	SVD	3t	IIt5	crosscutting veins of WSD	1.1	-9.3
FSV-213-2	SVD	3t	IIt4	WSD, zebra texture	1.3	-9.0
FSV-215	SVD	3t	IIt4	WSD, zebra texture	1.3	-8.7
FSV-20	SVD	3i	Ivf	DRD	2.1	-7.2
			IIt4	WSD, zebra texture	0.8	-10.8
FSV-31	SVD	3i	IIt4	WSD, zebra texture	1.1	-8.1
FSV-37	SVD	3i	IIt4	WSD, zebra texture	0.6	-9.8
FSV-22	SVD	3p	Im	DRD	0.8	-8.2
			EPd	1, dol replacing evaporite	0.3	-11.8
			EPd	2, dol replacing evaporite	0.3	-12.1
			EPd	3, dol replacing evaporite	0.5	-11.3
FSV-27	SVD	3p	IIt4	WSD, zebra texture	1.2	-8.7
FSV-29	SVD	3p	IIt5	crosscutting veins of WSD	0.8	-10.3
			EPd	1, dol replacing evaporite	1.0	-9.8
			EPd	2, dol replacing evaporite	0.6	-10.4
			EPd	3, dol replacing evaporite	-0.4	-12.1
			EPd	4, dol replacing evaporite	-0.1	-11.3
FSV-41	SVD	3p	IIt4	WSD, zebra texture	1.3	-7.8
FSV-656	SVD	3	IIt5	crosscutting veins of WSD	1.3	-9.9
			EPc	calcite replacing evaporite	-11.5	-12.5

continued

Table 3.3. Continued

Sample name	Lith. Unit	Manto	Generation	Description	$\delta^{13}C$ ‰ PDB	$\delta^{18}O$ ‰ PDB
FSV-657 B	SVD	3	IIt3	ordered bands of WSD	0.7	-10.0
			IIt3	ordered bands of WSD	0.8	-9.9
			IIt2	fine veinlets of WSD	1.0	-9.9
			IIt2	fine veinlets of WSD	0.8	-10.2
			IIt1	spot of WSD	0.4	-11.8
			IIt1	spot of WSD	0.7	-11.5
FSV-38	SVD	2	Im	DRD	1.8	-7.2
			IIt5	crosscutting veins of WSD	1.1	-8.1
			IIIc	LFC	-0.8	-9.8
			IIIbit	hydrothermal bitumen	-25.4	
FSV-39	SVD	2	IIt5	crosscutting veins of WSD	1.0	-9.4
FSV-205	SVD	2	IIt5	crosscutting veins of WSD	1.3	-7.3
FSV-658 A	SVD	2	IIt5	crosscutting veins of WSD	1.3	-8.3
FSV-658 B	SVD	2	IIt4	WSD, zebra texture	1.2	-7.8
FSV-42	SVD	1	IIt5	crosscutting veins of WSD	0.9	-8.5
FSV-659	SVD	1	Ivf	DRD	1.0	-7.1
			IIt5	crosscutting veins of WSD	1.1	-8.4
			IIIc	LFC	-0.1	-10.0
FSV-660	SVD	1	IIt6	WSD, hydraulic breccia	0.9	-9.9
FSV-713	SJD		If	DRD	1.7	-7.4
			IIt3	ordered bands of WSD	0.6	-9.4
FSV-714	SJD		IIt6	WSD, hydraulic breccia	1.2	-9.1
			IIId	1 LFD	1.0	-9.8
			IIId	2 LFD	0.3	-12.2
FSV-717	SJD	t	IIt6	WSD, hydraulic breccia	1.6	-8.0
FSV-718	SJD	m	Im	DRD	1.1	-8.2
			IIt6	WSD, hydraulic breccia	0.6	-9.8
FSV-719	SJD	p	IIt6	WSD, hydraulic breccia	1.1	-9.2
FSV-720	SJD	m	IIt6	WSD, hydraulic breccia	1.4	-8.3

*See table 1 for explanation of the abbreviations; TOC = total organic carbon.

sulfates (Fig. 3.4). This trend confirms previous C and O isotopic studies in San Vicente deposit (Fontboté and Gorzawski, 1990) and is similar to that found in studies on other MVT deposits (e.g., Frank and Lohmann, 1986; Ghazban et al., 1990; Farr, 1992; Nesbitt and Muehlenbachs, 1994) which report a lighter isotopic compositions in paragenetically late carbonates compared to the unaltered host carbonates. The carbonates exhibit an approximately positive covariation trend in the $\delta^{13}C$ vs. $\delta^{18}O$ space (trend AB, Fig. 3.5), that is interpreted as a result of precipitation by mixing of fluids of different isotopic composition. At the isotopically heavy end (A), the isotopic composition of the very fine-grained host DRD ($\delta^{13}C$ = 1.3 to 2.5 ‰; $\delta^{18}O$ = -7.8 to -6.4 ‰) overlaps partially the composition of the Uncush limestones. The very fine-grained DRD samples with the highest $\delta^{13}C$ and $\delta^{18}O$ are probably representative of original, unaltered host dolomite. The ore-stage dolomites (I, II) are strongly depleted in ^{18}O (up to 6 ‰) and less in ^{13}C (up to 2 ‰) and cluster together in a narrow field (Fig. 3.5). Note that the values of the samples from the main deposit coincide with the compositional range of the samples from the whole district. Two light extremes (B and C) can be distinguished; he end member-composition B is represented by calcite replacing evaporitic sulfate depleted in both $\delta^{13}C$ and $\delta^{18}O$, with values as low as -4.5 ‰ and -16.1 ‰ respectively. The endpoint C is characterized by two strongly ^{13}C-depleted calcite cements ($\delta^{13}C$ = -9.3 and -11.5 ‰) and slightly depleted in ^{18}O ($\delta^{18}O$ = -12.1 and -12.5 ‰). This indicates that extremely ^{13}C-depleted HCO_3^-, probably formed by degradation of organic matter (e.g., Carothers and Kharaka, 1980; Winter and Knauth, 1992), was dominant in the precipitation of these carbonate cements. It is also possible that mixing of formation fluids with fresh meteoric water modified the isotopic composition of the late open-space filling carbonates, because they typically occur in

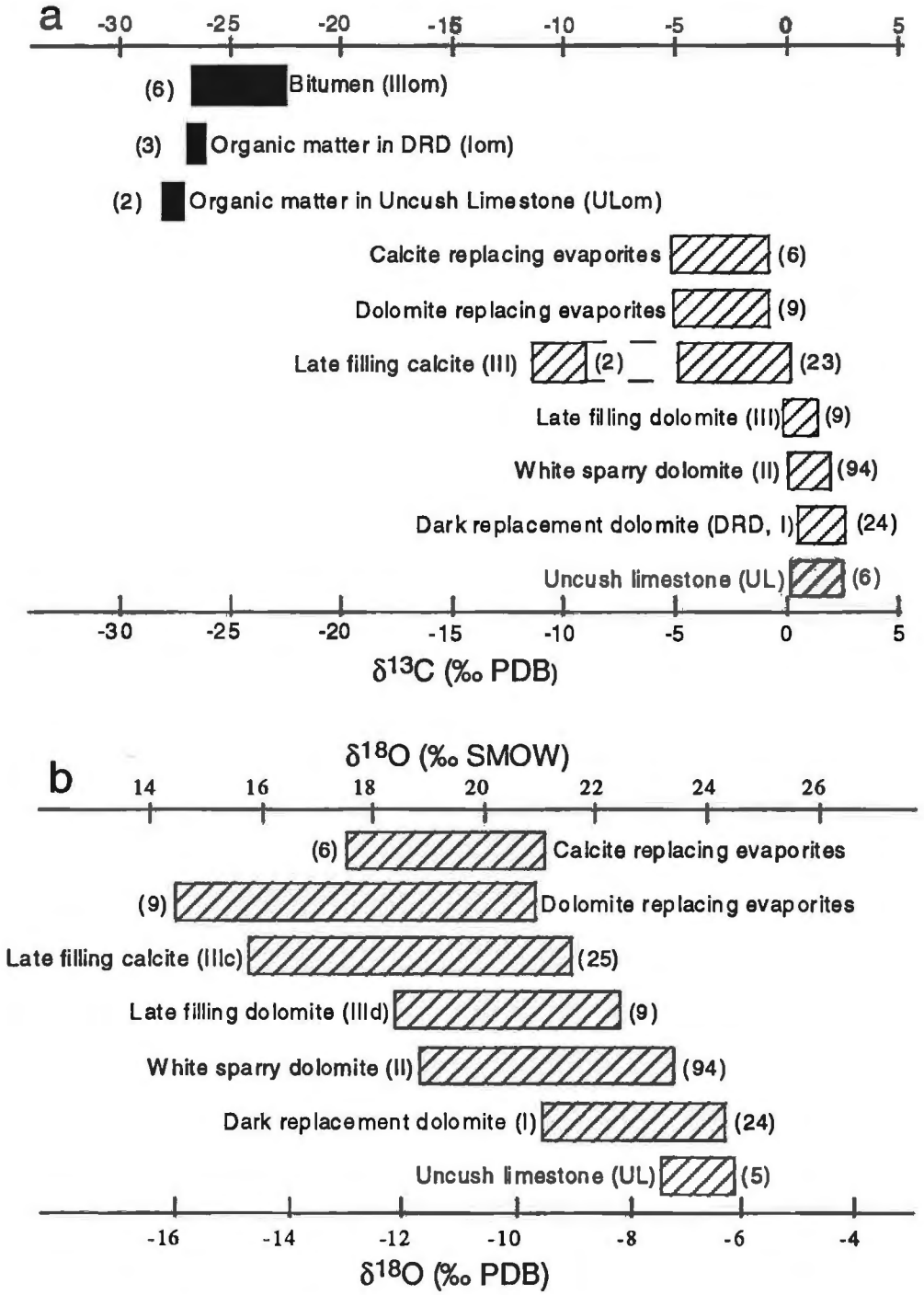

Figure 3.4. Carbon (a) and oxygen (b) isotope variations of host and gangue carbonates and associated organic matter in the San Vicente main deposit.

sites of high permeability with easy access to ground water. The wide isotopic ranges of the hydrothermal (i.e., from altered DRD to the LFC, see Table 3.1) carbonates can not be due to simple thermally-induced isotopic reequilibration (e.g., in San Vicente temperature changed between 60 and 160°C), which affects the oxygen more then the carbon isotopes. Therefore simple cooling can not account for the measured isotopic variations of the carbonates of San Vicente, indicating that multiple fluids were involved in their precipitation (see below).

The impermeable bituminous silty Uncush limestones from barren areas are substantially depleted in ^{13}C (≈3 ‰) relative to the same limestone from the San Vicente deposit (Fig. 3.5). This indicates that at San Vicente deposit the light-C pore waters (HCO_3^- liberated from the oxidation of the organic matter) of this limestone were diluted with the incoming ore solutions. It is, therefore, an evidence against considering the Uncush Limestone as a possible source for the ore components.

The isotopic composition of the carbonate generations and the associated organic matter in the three ore-bearing dolomitic units is summarized in Table 3.4. Note that no significant variation of the composition of the DRD, the WSD, and the LFC is related to the stratigraphic position.

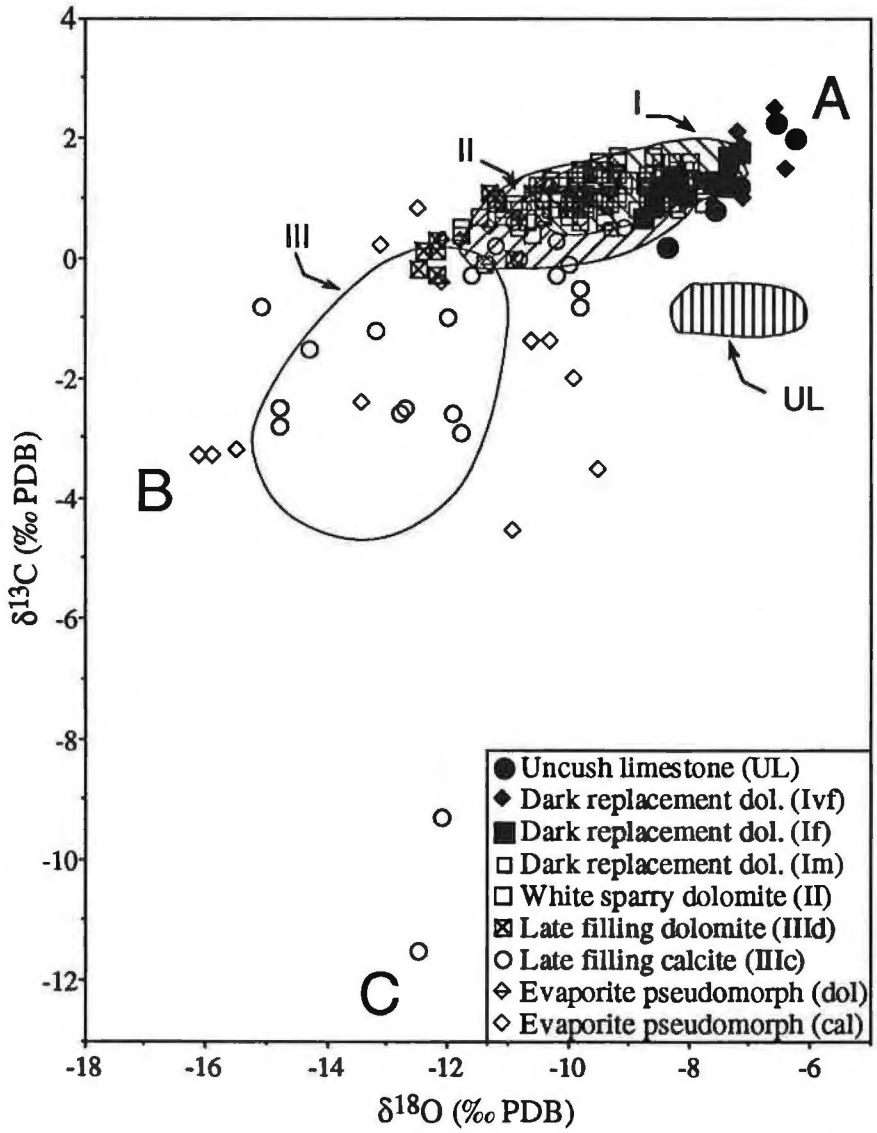

Figure 3.5. $\delta^{18}O$ versus $\delta^{13}C$ of the carbonates of the San Vicente deposit. The symbols are for samples of the San Vicente main deposit . The fields are for samples of the whole district (see Fig. 3.3). The isotopic composition of the mine-scale samples agree with that of the regional samples, except for the Uncush limestones.

3.5.2.2 Organic matter

The isotopic values of the total organic carbon in the Uncush limestones ($\delta^{13}C$= -28.2 to -27.2‰, Tab. 3.3) are similar those extracted from the DRD ($\delta^{13}C$= -27.0 to

-26.4‰, Fig. 3.4a). Assuming an identical kerogen source, we attribute the similar isotopic composition to a similar degree of thermal maturation. The $\delta^{13}C$ values of the hydrothermal bitumens ($\delta^{13}C$ -27.7 to -23.0 ‰, median = -24.0 ‰) are heavier than the organic matter disseminated in the host DRD. This isotopic shift is generally attributed to preferential loss of isotopically light low-molecular hydrocarbons (e.g., CH_4, C_2H_6) during the thermogenic breakdown of the native organic matter (e.g., Orr, 1974; Tissot et al., 1974). We can envisage that this bituminous material released from organic-rich host rocks (e.g., DRD, Uncush limestones) was probably further oxidized during transport in the ore fluids by heating or reaction with oxidants (e.g., sulfate), and precipitated later as an isotopically heavier solid bitumen. The $\delta^{13}C$ values of bitumen from other localities in San Vicente district, Aynamayo ($\delta^{13}C$ = -27.5 ‰), Chilpes ($\delta^{13}C$ = -26.9 ‰) and Arcopunco ($\delta^{13}C$ = -27.4 ‰) are about 3‰ lighter than the bitumen measured in the mining area (median = -24.0 ‰). The high $\delta^{13}C$ values of these bitumen at San Vicente may be diagnostic of intense hydrothermal alteration of the native organic matter associated to the host dolomite, not found in the studied smaller MVT deposits and occurrences in the area.

Table 3.4. Carbon and oxygen isotope composition from host and gangue minerals of the ore-bearing Dolomites (AD, SVD, SJD) in San Vicente deposit

	Medians and ranges of isotopic ratios (n)*					
	$\delta^{13}C$ (‰)			$\delta^{18}O$ (‰)		
Generation	AD	SVD	SJD	AD	SVD	SJD
DRD (Ivf)	1.5	1.7	1.7	-7.5	-7.1	-7.4
	1.3 to 1.7	0.9 to 2.5		-7.8 to -7.3	-7.6 to -6.4	
	(3)	(7)	(1)	(3)	(7)	(1)
WSD (II)	1.2	1.1	1.2	-9.4	-9.5	-9.2
	0.8 to 1.7	-0.1 to 1.6	0.6 to 1.6	-10 to -8.1	-11.8 to -7.3	-9.8 to -8.0
	(19)	(90)	(6)	(19)	(90)	(6)
LFD (IIId)		0.1	0.6		-11.8	-11.0
	-	-0.3 to 1.1	0.3 to 1.0	-	-12.5 to -10.6	-12.2 to -9.8
		(8)	(2)		(8)	(2)
LFC (IIIc)	-1.6	-0.8		-10.8	-11.6	-
	-2.6 to -0.5	-11.5 to 0.7	-	-11.0 to -9.8	-15.1 to -9.1	
	(2)	(23)		(2)	(23)	
EPd		0.3			-11.2	
	-	0.4 to 1.0	-	-	-12.1 to -9.8	-
		(7)			(7)	
EPc	-2.4	-2.6		-13.4	-11.7	-
		-4.5 to 0.8	-		-16.1 to -9.5	
	(1)	(10)		(1)	(10)	
Iom	-26.9	-26.4				
	-27.0 to -26.8		-			
	(2)	(1)				
IIIbit	-23.2	-25.4				
	-23.3 to -23.0	-27.0 to -23.9	-			
	(2)	(4)				

*See table 3.1 for explanation of the abbreviations; n=number of analyzed samples; - not analyzed.

3.5.3 Isotopic variation of gangue carbonates at outcrop and handspecimen scale

The different textural types of the altered DRD (Ivf, If, and Im, see section 3.3 and Table 3.1) and the WSD (t1 to t6) were sampled at selected mine-wall-showings of a few square meters in order to evaluate the isotopic variability at outcrop and rock scale. The results are summarized in Table 3.5. $\delta^{13}C$ and $\delta^{18}O$ values indicate two different isotopic trends at the textural scale. The data for the altered host replacement dolomites show a clear tendency toward lighter composition (isotopic shift up to 1.6 ‰ for $\delta^{13}C$ and 2.5 ‰ for $\delta^{18}O$). In the subgenerations of the WSD the isotopic trend is inverse, towards heavier isotopic composition from t1 towards t5 (Table 3.5). An enrichment in ^{13}C (up to 1.8 ‰) and ^{18}O (up to 3.3 ‰) records the evolution of the mineralizing fluid by interaction with the

Table 3.5. Carbon and oxygen isotope variation of the subgenerations of the dark replacement dolomite and the white sparry dolomite at outcrop and rock scale

Generation/	$\delta^{13}C$ (‰)		$\delta^{18}O$ (‰)	
Subgeneration (n)*	Range	Median	Range	Median
Dark replacement dolomite (I)				
Ivf (3)	1.7 to 2.5	1.9	-6.6 to -7.1	-7.1
If (6)	0.7 to 1.6	1.3	-8.8 to -7.4	-8.2
Im (6)	0.9 to 1.2	1.0	-9.6 to -7.8	-9.0
White sparry dolomite (II)				
IIt1 (3)	-0.1 to 0.7	0.4	-11.8 to -11.4	-11.6
IIt2 (4)	0.7 to 1.0	0.9	-10.4 to -9.8	-10.0
IIt3 (11)	0.9 to 1.6	1.2	-10.1 to -8.2	-9.5
IIt4 (14)	0.9 to 1.6	1.3	-10.9 to -8.0	-9.4
IIt5 (5)	1.0 to 1.7	1.2	-10.3 to -8.3	-8.9
IIt6 (13)	0.4 to 1.0	0.8	-11.8 to -9.4	-10.7

*See table 3.1 for explanation of the abbreviations; n=number of analyzed samples.

host dolomite. Note that the bands of WSD occurring in incipient zebra (t3), zebra ore (t4), or as crosscutting veins (t5) have indistinguishable isotopic compositions ranging from 0.9 to 1.6‰ $\delta^{13}C$ and -10.9 to -8.0 ‰ $\delta^{18}O$. Within a single sample, the early phases of WSD (t1) can show significant lower $\delta^{13}C$- and $\delta^{18}O$-values relative the more evolved textures (Fig. 1.6c, sample FSV-657B). This shift towards heavier $\delta^{13}C$ and $\delta^{18}O$ values already recognizable at handspecimen scale reflects the degree of isotopic exchange between the mineralizing fluid and the host dolomite with advancing stages of fluid-rock equilibration.

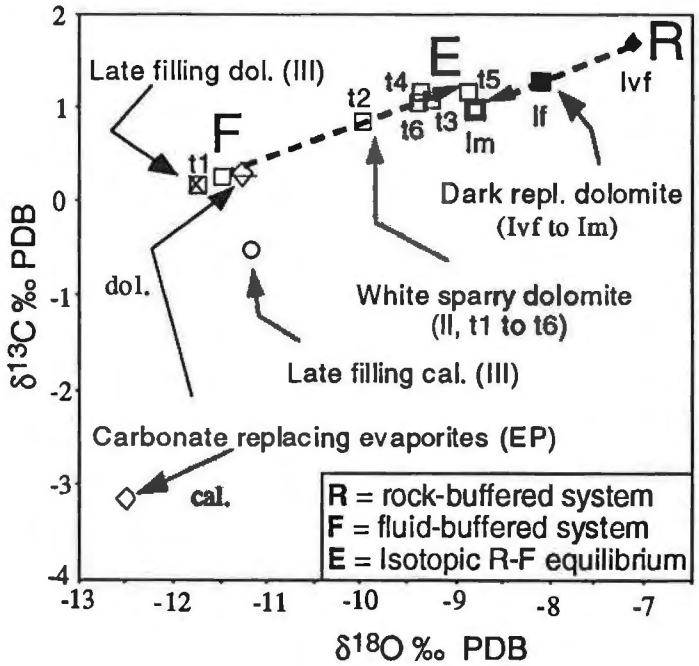

Figure 3.6. Median isotopic composition of the different generations and subgenerations of host and gangue carbonates from the San Vicente mine in $\delta^{18}O$ versus $\delta^{13}C$ space (Table 3.5). R = host-rock dominated system, F = fluid dominated system, E = equilibrium in the fluid-rock system.

The medians $\delta^{13}C$ and $\delta^{18}O$ of the host and gangue carbonate phases of all the samples from San Vicente deposit are shown in Fig. 3.6. Both the altered DRD and the WSD display a significant correlation in the $\delta^{13}C$ vs. $\delta^{18}O$ space. The very fine DRD (Ivf) represents the heaviest end member, in which the system composition is apparently

dominated by the host rock; the opposite situation of a fluid-buffered system is represented by the early spot-like (t1) white sparry dolomite (point F in Fig. 3.6). The trend R-E of DRD towards lighter isotopic composition reflects the progressive alteration by replacement of the host dolostone by the hydrothermal ore fluid. This is consistent with the widespread evidence of dissolution and porosity-enhancement of the host dolomite. These results confirm the validity of the criteria (color, grain size, presence of primary textural relicts) used for separation of the subgenerations of the DRD. The coupled and opposite compositional evolution of the ore fluid through interaction with the host rock is recorded by the C and O isotopic enrichment of the open space filling WSD textural subtypes t1 to t3-t5 (trend E-F in Fig. 3.6). Note, that the isotopic compositions of the late filling dolomite III and the dolomite in sulfate pseudomorphs are similar to the values of the early phase of WSD (t1). These open-space filling dolomites precipitate at constraint-free sites from a fluid not equilibrated with the host rock. It can, therefore, be assumed that these hydrothermal dolomites are representative of the incoming ore solution. Thus Fig. 3.6 illustrates how the isotopic composition of both the ore fluid and the host dolomite were progressively modified by processes of fluid-rock interaction until they attained isotopic equilibrium. The more evolved WSD subgenerations (t4, t5) and the more pervasive altered DRD (Im) with an isotopic composition intermediate between the host dolomite (Ivf) and the influxing ore fluid (t1) represent the situation of equilibrium in the fluid-rock system (point E in Fig. 3.6).

3.6 Discussion

In summary, the isotopic compositions of the carbonates and associated organic matter of the MVT-district of San Vicente display variation trends which are similar at regional and mine scale. These isotopic trends do not have any correlation with the stratigraphic sequence and do not exhibit any zonation at district or deposit scale, suggesting common mineralizing events. Further support is provided by studies of the maturation state of the organic matter in the host dolomite and hydrothermal bitumen, that indicate a similar degree of alteration of the native organic matter in the entire San Vicente belt (J.R. Disnar, pers. comm., 1994). Consequently we can conclude that ore and hydrothermal carbonates in the entire San Vicente district were precipitated from fluids of specific isotopic composition by regionally unvarying and stratigraphic independent geochemical mixing processes similar to those recorded in the main deposit. This also suggests the existence of a regional mineralizing hydrothermal system with interconnected plumbing.

3.6.1 Isotopic evolution of the hydrothermal carbonates

By explaining the C and O isotopic evolution San Vicente carbonates the following processes and parameters must be considered:

(1) Progressive changes in the isotopic composition of the host dolomite and the ore- and gangue-precipitating fluid due to mixing of different fluids, chemical exchange between rock and fluid, variations of temperature, f_{O_2}, pH, and salinity.

(2) Changes in fluid to rock ratio during ore and gangue precipitation. A small ratio does not produce any significant change in the host dolomite, and by contrast marked changes in the fluid; conversely in a fluid-dominated system the composition of the host and previously precipitated gangue dolomites tends towards that of the fluid.

(3) Kinetically-driven isotopic fractionation between carbonate and fluid can lead to situations of incomplete isotopic equilibrium in the fluid-rock system. Rapidly precipitating carbonates have the same isotopic composition as the solution; with slow precipitation the carbonates attain the equilibrium composition at the prevalent temperature (e.g., McCrea, 1950; O'Neil et al. 1969).

In the hydrothermal fluid the oxygen isotopic composition is largely controlled by H_2O at a given temperature and salinity (e.g., Taylor, 1979). On the contrary, the carbon isotope composition is controlled by the concentrations of the different carbon species (H_2CO_3 including aqueous CO_2, HCO_3^-, CO_3^{2-} and CH_4); the distribution of which is strongly dependent on changes in f_{O_2} and pH (Ohmoto, 1986). Therefore, the oxidized

carbon species in hydrothermal fluids that must be considered in isotopic mass balance calculations at low temperature (<350°C) are: H_2CO_3, HCO_3^-, and CO_3^{2-} (e.g., Ohmoto and Rye, 1979). The large isotopic fractionation factors between the different carbon species results in diagnostic variations of the $\delta^{13}C$ of carbon-bearing minerals. Consequently, the $\delta^{13}C$ variations of hydrothermal carbonates may provide valuable information on the physicochemistry of the ore-forming fluids (e.g., Matsuhisa et al., 1985; Shikazono, 1989; Zheng, 1990; Zheng and Hoefs, 1993).

Two end member situations can be distinguished during the interaction of the fluid and the carbonate wall rock. In the case of low fluid-rock ratio the hydrothermal system is buffered by the carbonate wall rock, and the most important dissolved carbon species is HCO_3^-. In contrast, if the system is buffered by the slightly acidic ore fluid the dominant carbon is carbonic acid (H_2CO_3).

In the following we discuss the genetic implications of changes in the pH of the ore fluid in the genesis of San Vicente deposit.

As emphasized by Anderson and Garven (1987) the H_2S produced by (biological or abiological) reduction of sulfate may liberate H^+ by means of precipitation of sulfides:

$$M^{2+} + H_2S = 2H^+ + MS \quad (1)$$

were M^{2+} represents divalent metals (in San Vicente M^{2+} is mainly Zn^{2+}), or (2) in the absence of metals by oxidation as the fluid encounter oxygenated ground waters:

$$H_2S + 2O_2 = 2H^+ + SO_4^{2-}. \quad (2)$$

Consequently the pH of the mineralizing H_2S-bearing fluid becomes more acid during ore precipitation or rising to the subsurface through tectonic or hydrothermal channel-ways. The (slightly) acidic fluid will dissolve the dolomite host rocks and produce CO_2:

$$CaMg(CO_3)_2 + 4H^+ = Ca^{2+} + Mg^{2+} + 2CO_2 + H_2O. \quad (3)$$

The liberated CO_2 increases the H_2CO_3 activity in the fluid, dissolving further carbonates until it reaches chemical equilibrium with the host dolostone. The fluid, saturated in Mg^{2+} and Ca^{2+} precipitates sparry dolomite and calcite. Moreover, the dissolution of the host rock dolomite may produce dissolution-brecciation. If one of the sulfide components (metal or hydrogen sulfide) is no longer available for ore precipitation reaction (1) stops, and the corrosive fluid will be progressively buffered by the carbonate host rocks. This accounts for the presence in the San Vicente main deposit of abundant dissolution-breccias at the boundaries of the orebodies. The cement in the breccias is white coarse-grained dolomite with subordinate sphalerite III, and in certain areas far from the main ore zone, mainly calcite. The presence of abundant dissolution-breccias in San Vicente indicate that the ore fluids in San Vicente were slightly acidic with H_2CO_3 as the dominant dissolved carbon species. This inference is in line with studies in the Ozark MVT-district, where thermodynamic calculations based on the chemical composition of dolomite-saturated fluid inclusions indicate pH-values of the ore fluids ranging between 4.2 to 5.0 (Leach et al., 1991).

The results also show that the late filling calcite and the calcite replacing evaporites are strongly depleted in ^{13}C and slightly in ^{18}O, indicating precipitation from a fluid with ^{13}C-deficient bicarbonate. Isotopically light carbon is generally interpreted as the result of oxidation of low molecular hydrocarbons. This interpretation is supported by the previously discussed ^{13}C-enrichment of the late bitumen relative to the organic matter in the host dolostone. Orr (1974, 1977) explained the breakdown of organic compounds by thermochemical sulfate reduction (TSR), a mechanism involving redox reactions between sulfate and organic matter with presence of hydrogen sulfide as an initiator to form native sulfur, H_2S, and HCO_3^-. The net reaction may be:

$$CaSO_4 + CH_4 = CaCO_3 + H_2S + H_2O \quad (4)$$

where methane represents the light hydrocarbons. If sufficient Mg^{2+} concentration is available the fluid precipitates dolomite:

$$2CaSO_4 + 2CH_4 + Mg^{2+} = CaMg(CO_3)_2 + 2H_2S + Ca^{2+} + 2H_2O\,. \quad (5)$$

Many studies invoke TSR during precipitation of MVT-ore and isotopically light sparry dolomite or calcite (Machel, 1987; Powel and Macqueen, 1984; Anderson and Garven, 1987; Ghazban et al., 1990; Leventhal, 1990; Anderson, 1991). In the San Vicente belt there exist various horizons with massive gypsum or anhydrite in the Red Sandstone at the base of the Pucará Group, as well as intercalated lenses with evaporite pseudomorphs in the dolomitic units. The association of massive sulfate lenses, sulfate pseudomorphs,

sulfides, elemental sulfur, extremely ^{13}C-depleted carbonates, altered organic matter in the host dolomite and isotopically heavier late solid bitumen points to thermochemical reduction of sulfate or thiosulfate; therefore TSR is suggested as the source of hydrogen sulfide in the ore fluid. Further work is necessary to determine in which form sulfur (sulfate or thiosulfate, e.g., Spirakis and Heyl, 1993) was transported in the ore fluid. We can nevertheless conclude that native organic matter in the host carbonate was certainly a main reductant in the processes of ore formation in San Vicente.

3.6.2 Quantitative modeling

The dissolution reactions of calcite and dolomite are exothermic, hence increasing temperature decreases the solubility (Holland and Malinin, 1979). Therefore the precipitation of the hydrothermal carbonates can not be occasioned by simple cooling of the hydrothermal fluids. Furthermore, the solubility of the carbonates is strongly influenced by the pH, CO_2-fugacity, and salinity of the fluid (Holland and Malinin, 1979). Thus, we have quantitatively modeled the isotopic composition of the carbonates of San Vicente main deposit using equations that take into account changes in pH of the precipitating fluid (different dominant dissolved carbon species) and the fugacity of CO_2 dissolved in the fluid.

The $\delta^{13}C$ and $\delta^{18}O$ isotope trends were simulated using the mass balance equations for fluid mixing and water-rock interaction of Zheng and Hoefs (1993) and the Rayleigh distillation equations for precipitation of carbonates during CO_2 degassing of Zheng (1990). All the carbon isotopic fractionation factors were taken from Ohmoto and Rye (1979), and for oxygen from Friedman and O'Neil (1977). The modeling parameters include the initial isotopic composition and temperature of wall rock and fluid, the dominant dissolved carbon species (H_2CO_3, HCO_3^-), and the cumulative fluid-rock ratio. Furthermore, the models account for temperature-dependent changes in the isotopic fractionation factor between rock and fluid by advancing fluid-rock interaction (increasing fluid-rock ratios). Isotopic equilibration between the rock and the fluid is assumed at the given temperature for each iteration. The limitations and usefulness of such a zero-dimensional approach, which ignore fluid-flow and kinetic constraints, were recently discussed by Blattner and Lassey (1990).

The quantitative models of the isotopic covariations of the hydrothermal carbonates of the San Vicente deposit are discussed in the following sections. Fluid-fluid mixing models for the precipitation of the hydrothermal calcite account for the geochemical evolution of the ore fluid (section 3.6.2.1.); water-rock interaction models match the isotopic shifts in the pervasive alteration of the host dark replacement dolomite and consequent precipitation of white dolomite (3.6.2.2.); finally models of CO_2 degassing (3.6.2.3.) explain the isotopic covariations of the hydrothermal dolomites (WSD, LFD).

3.6.2.1 Fluid-mixing

In the calculations of the mixing models we have considered calcite instead of dolomite for the following reasons: (1) calcite displays the largest range of isotopic variation in the $\delta^{13}C$ vs. $\delta^{18}O$ space (Fig. 3.5); and (2) the rate of dissolution/crystallization of calcite is very fast in comparison to the excessively-slow dissolving dolomite at low temperature (<90°C, e.g., Siebert, 1970; Holland and Malinin, 1979; Cole and Drumond, 1988).

The isotopic composition of the syn- and post-ore carbonate generations of San Vicente can be explained by a model with end member fluids (Fig. 3.7, Table 3.6). We assume that the isotopically heavy fluid (fluid A) is the native formation fluid, represented by the pore fluid of the unaltered host rock at a temperature of 60°C and with HCO_3^- as the dominant dissolved carbon species. The temperature correspond to a burial of 1.5 - 2 km and a normal geothermal gradient. The other fluid (fluid B) is the incoming mineralizing fluid at ≈150°C. This temperature is consistent with the measured homogenization temperatures of preliminary studies of fluid inclusions in the WSD (temperature of 115-162°C, salinities of 9.5-26 wt.% equivalent NaCl, Moritz et al. in press). The fluid is slightly acidic, with the dissolved carbon in form of H_2CO_3, and is represented by calcite cements in evaporitic sulfate pseudomorphs. This hot, acidic and saline fluid B can be considered as a thermally and compositional evolved meteoric water, whose chemistry was

Table 3.6. Fluids used in the fluid-mixing models of the isotopic covariations in the carbonates from San Vicente.

	Native formation fluid (fluid A)	Slightly acidic incoming fluid (fluid B)	TSR-dominated fluid (fluid C)
$\delta^{18}O$ (‰ SMOW)	2.5	0	5
$\delta^{13}C$ (‰ PDB)	1	-5	-15
Temperature (°C)	60	150	150
Dominant carbon specie	HCO_3^-	H_2CO_3	H_2CO_3
Total dissolved carbon (µg/g C)	500	200	250

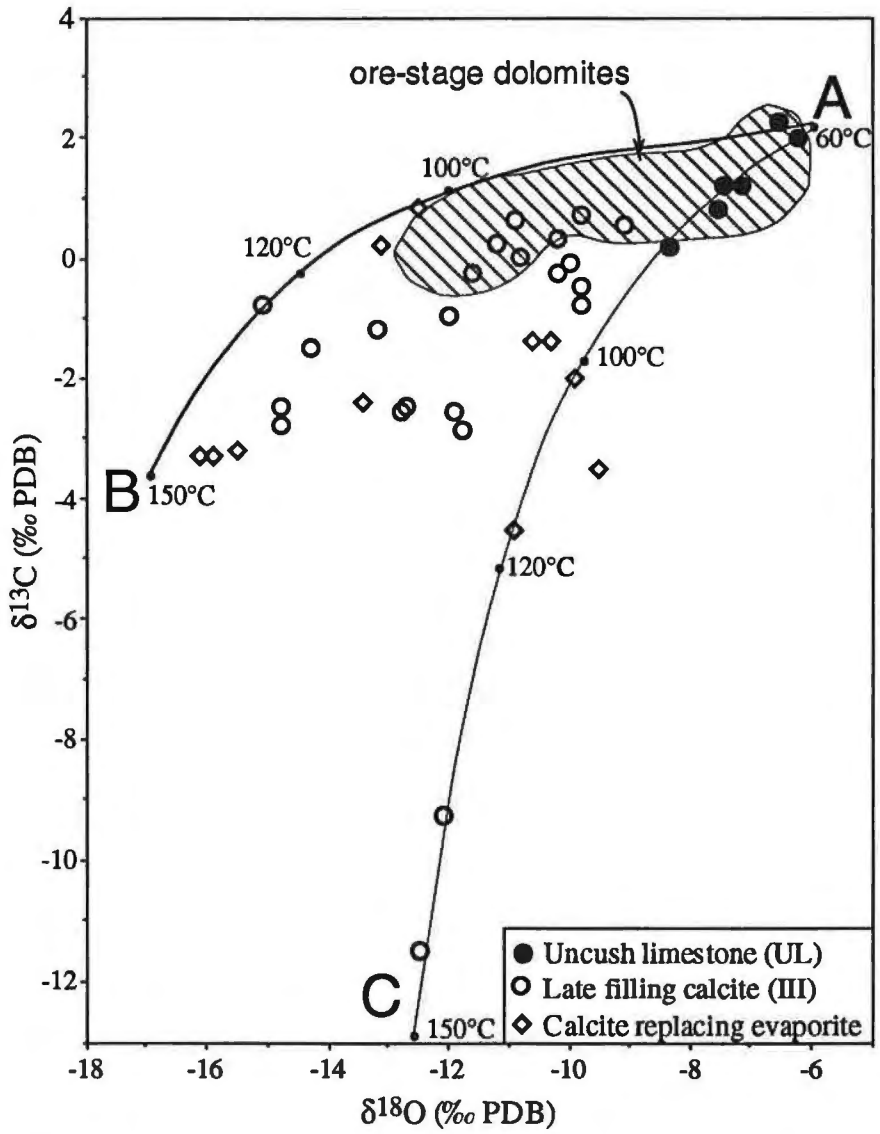

Figure 3.7. $\delta^{13}C$ versus $\delta^{18}O$ for calcites from the San Vicente mine. Theoretical curves for calcite precipitated during mixing of fluids. Fluid A: 60°C, $\delta^{13}C$ = 1‰ (PDB) and $\delta^{18}O$ = 2.5‰ (SMOW), with HCO_3- as the dominant dissolved carbon species; fluid B: 150°C, $\delta^{13}C$ = -5‰ (PDB) and $\delta^{18}O$ = 0‰ (SMOW), with H_2CO_3 as the dominant dissolved carbon species; fluid C: 150°C, $\delta^{13}C$ = -15‰ (PDB) and $\delta^{18}O$ = 5‰ (SMOW), with H_2CO_3 as the dominant dissolved carbon species (see also Table 3.6). The dashed field shows the area of composition of the ore stage DRD and WSD.

controlled during the transport by prolonged water-rock interaction and multiple mixing with different basinal fluids (e.g., connate marine waters, fresh meteoric water, and more evolved formation waters). The initial isotopic composition of fluid B was assumed to have a composition similar to the pore water of the late filling calcites at ≈150°C; $\delta^{13}C \approx -5‰$ and $\delta^{18}O \approx 0$ ‰ (SMOW). Part of the mineralizing fluid, because of decomposition of organic matter, is dominated by very light CO_2 (fluid C) and can be considered as an additional end member that is represented by the late-filling calcites with the lowest $\delta^{13}C$-values (Fig. 3.6). The $\delta^{13}C$-value (-15 ‰) of the fluid was estimated from the equilibrium isotopic fractionation between CH_4 and CO_2 at 150°C (Ohmoto and Rye, 1979), assuming that the composition of the CH_4 is similar to that of the analyzed bitumen ($\delta^{13}C \approx -25$ ‰). Mixing with heavy-carbon connate waters of the host carbonates was limited as evidenced by the mainly light-carbon hydrothermal calcites.

Most data points for calcites in Fig. 3.7 are enclosed in the field limited by the mixing curves AB and AC. Thus, the most likely process that accounts for the isotopic variation of the gangue carbonates of San Vicente is mixing of at least two different end member fluids: the native formation fluid A in equilibrium with the unaltered wall rock and an incoming corrosive (hot, slightly acidic and saline) mineralizing fluid B, which in part was strongly depleted in ^{13}C due to oxidation of organic matter (fluid C). The described fluid mixing model is the most direct way to account for simultaneous temperature and chemical (elemental and isotopic) evolution of the fluids involved in the hydrothermal system during ore formation.

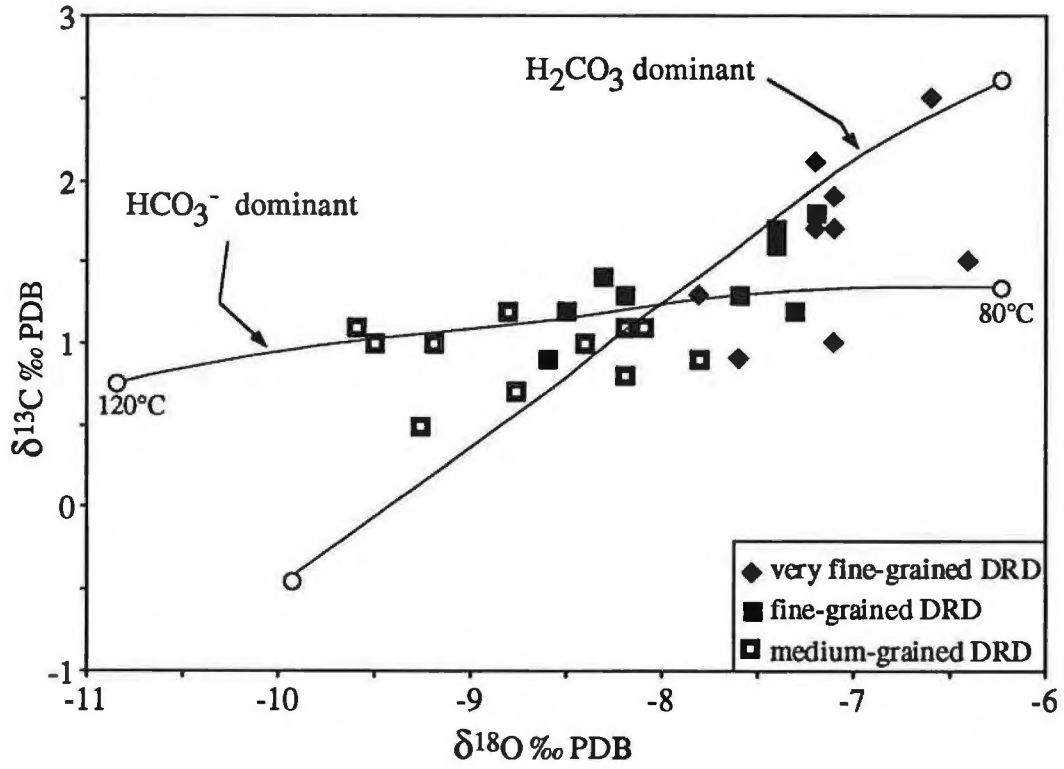

Figure 3.8. $\delta^{13}C$ versus $\delta^{18}O$ variations for the dark replacement dolomite (I) from the San Vicente mine. Calculated curves simulate precipitation of dolomite by fluid-rock interaction between 80°C and 120°C. The precursor very fine DRD has at 80°C $\delta^{13}C$ = 2.5‰ (PDB) and $\delta^{18}O$ = -6.5‰ (PDB). The inclined curve represent hydrothermal alteration by a fluid with $\delta^{13}C$ = -5‰ (PDB) and $\delta^{18}O$ = 0‰ (SMOW), and H_2CO_3 as the dominant dissolved carbon species; the horizontal curve represents the precipitation of DRD by interaction of the precursor dolomite and a fluid with HCO_3^- as the dominant dissolved carbon species, and $\delta^{13}C$ = -1.5‰ (PDB) and $\delta^{18}O$ = 0‰ (SMOW).

3.6.2.2 Fluid-rock interaction and alteration of the host dolostone

The isotopic evolution of the DRD matches models of fluid-rock interaction in terms of : (1) hydrothermal (isotopic) alteration of the host dolomite and previously precipitated carbonates, and (2) precipitation of white dolomite Im during fluid-rock interaction (Fig. 3.8). The inclined trend with a positive correlation between $\delta^{13}C$ and $\delta^{18}O$ ($r^2 = 0.92$) is explained by an alteration model of the host dolomite by a slightly acidic fluid with carbonic acid as the dominant dissolved carbon species. The isotopic composition of this fluid, $\delta^{18}O$ = 1.5‰ (SMOW) and $\delta^{13}C$ = -6.5‰, is controlled by the mixing of the end member fluids A, B and C. The roughly horizontal trend is explained by the concomitant dissolution/ precipitation of dolomite from a fluid (e.g., $\delta^{18}O \approx 0$‰ SMOW, $\delta^{13}C \approx -1.5$‰, dominant HCO_3^-) that evolves continually during exchange with the host dolomite ($\delta^{18}O$ = -7‰ PDB, $\delta^{13}C$ = 3‰). This model for fluid-rock interaction suggest that the isotopic covariation of the dark replacement dolomite records the combined processes of progressively cooling of the incoming corrosive fluid and of the pH-changes of the pore fluid of the host rock that explain the change of the dominant dissolved carbon species (HCO_3^- to H_2CO_3). Since sphalerite I is intergrown with the altered DRD, we infer that the main mechanism involved in the replacement/recrystallization of the DRD and the precipitation of sphalerite was fluid-rock interaction.

3.6.2.3 Precipitation of the ore-stage open-space filling dolomites

The above-modeled metasomatic interaction of the corrosive ore fluid with the host dolostone produced important dissolution of the host rock, thus enhancement of the porosity, fracturing, and pressure drop. The changes in the pore fluid pressure led to CO_2 outgassing and to the consequent decrease of the fluid acidity, and therefore to precipitation

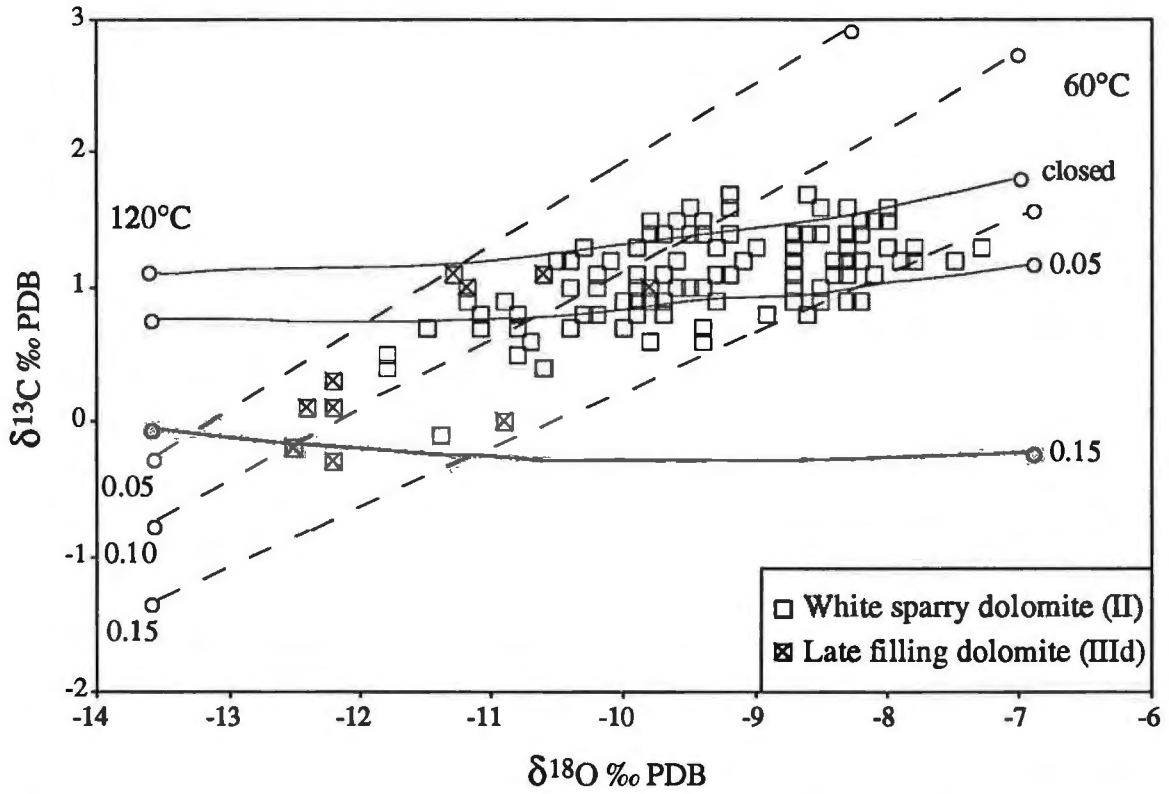

Figure 3.9. $\delta^{13}C$ versus $\delta^{18}O$ variations of the white sparry dolomite (II) and late filling dolomite (III) from the San Vicente mine. The theoretical curves represent the Rayleigh degassing-precipitation models for dolomite precipitated at temperatures between 60° to 120°C during CO_2 degassing. Inclined curves: fluid with dominant H_2CO_3, and $\delta^{13}C$ = -4.0‰ (PDB) and $\delta^{18}O$ = -1.0‰ (SMOW). Roughly horizontal curve: $\delta^{13}C$ =-1.5‰ (PDB) and $\delta^{18}O$ = -1.0‰ (SMOW). The mol fraction of carbon in the degassed CO_2 is given for each curve.

of the hydrothermal carbonates WSD and LFD in open spaces in zebra rocks and in dissolution-breccias.

Studies of fluid inclusion gas geochemistry suggested that CO_2 effervescence was a common phenomenon occurring during the deposition of ore sulfides and hydrothermal dolomite in southeast Missouri (Leach et al., 1991).

The covariations of $\delta^{13}C$ and $\delta^{18}O$ values in the white sparry dolomites and the late filling dolomites were modeled using combined Rayleigh distillation - carbonates precipitation equations (Fig. 3.9). The positive correlation array of the $\delta^{13}C$ vs. $\delta^{18}O$ values of the hydrothermal dolomites can be modeled by the combined CO_2 degassing and dolomite precipitation from a H_2CO_3-dominant fluid with $\delta^{13}C = -4$ ‰ PDB and $\delta^{18}O = -1.0$ ‰ (SMOW). The calculated models for CO_2 losses between 5 % to 15 % match the measured isotopic ratios between temperatures of about 60°C to 120°C (Fig. 3.9). The CO_2 removal from the fluid produce an increase in pH of the fluid that changes the dominant dissolved carbon species from H_2CO_3 to HCO_3^-. The roughly horizontal trends are modeled assuming a fluid dominated by HCO_3^-. The $\delta^{18}O$ value of this fluid is assumed to be the same as in the H_2CO_3 dominant fluid and the $\delta^{13}C$ value is taken as -1.5‰ PDB. Previous degassing of CO_2 and precipitation of WSD account for the significantly heavier C in the HCO_3^--dominated fluid. Note that the composition of the fluid is much like that the used in the model for DRD alteration. Very small CO_2 loss (less than 5%) is required to account for the isotopic changes of the WSD samples. The results of this model calculations lead to an interpretation of precipitation of dolomites II and III and the coexisting sphalerite generations during CO_2-degassing and cooling of the ore fluid.

3.7 Conclusions

The isotopic results, coupled with lithostratigraphic and petrographic considerations support the following conclusions.

1. Quantitative modeling of the isotopic covariations of the ore-stage dolomites provide insights on the two major mechanism of ore precipitation in the San Vicente belt: fluid-rock interaction and CO_2 degassing. Fluid-rock interaction processes explain the pervasive alteration of the host dolomite I and precipitation of sphalerite I. The WSD and the coexisting sphalerite II formed in previously prepared secondary porosity as overgrowths on the altered dolomite I by prolonged fluid-rock interaction and limited CO_2 degassing. Late filling dolomite III (or calcite) and the associated sphalerite III appear to have formed from the slightly acidic ore fluid during CO_2 degassing. Consequently, pressure variability plays a major role in the ore precipitation during the late hydrothermal events in San Vicente.
2. Precipitation of ore-stage carbonates occurred under relatively homogeneous conditions as indicated by the very constant isotopic composition of the WSD along San Vicente district. This suggests, that at a regional scale a uniform hydrothermal system with interconnected plumbing affected the whole San Vicente belt in a similar way.
3. At the ore site scale the chief flow type of the ore fluid was probably pervasive; consequently the spatial distribution of the ore-occurrences is controlled by the porosity (primary or secondary).
4. Heavier $\delta^{13}C$ values of the hydrothermal bitumen compared to the organic matter disseminated in the host dark replacement dolomite suggest that breakdown of the native organic matter provided the main reductant in the processes of ore formation in San Vicente.
5. The presence of native sulfur associated with extremely carbon-light calcites replacing evaporitic sulfates, altered native organic matter and heavier hydrothermal bitumen points to thermochemical reduction of sulfate and / or thiosulfate.

Acknowledgments

This research was supported by a grant of the Swiss National Science Foundation (Grant n. 20.36397.92) to L. Fontboté. This is a contribution to IGCP project n. 342 (Age and Isotopes of south American Ores). We are grateful to San Ignacio de Morococha S.A. Mining Company and the staff of the Geology Department of San Vicente mine for their help in the field work. We acknowledge discussions with L. Oldham. We thank Ph. Thélin and

F. Bussy of the University of Lausanne for XRD- and microprobe analyses and R. Martini of the University of Geneva for cathodoluminescence microscopy. J.S. and L.F. are grateful to J.R. Disnar of the University of Orléans for the Rock Éval analyses and valuable information on geochemical aspects of the organic matter associated to MVT deposits. We also thank G.M. Anderson for their critical comments and corrections on an earlier version of the manuscript.

References

Anderson, G.M.(1991) Organic maturation and ore precipitation in southeast Missouri. Economic Geology, v. 86, p. 909-926.

Anderson, G.M., and Garven, G. (1987) Sulfate-sulfide-carbonate associations in Mississippi Valley-Type lead-zinc deposits. Economic Geology, v. 82, p. 482-488.

Arne, D.C., Curtis, L.W., and Kissin, S.A. (1991) Internal zonation in a carbonate-hosted Zn-Pb-Ag deposit. Nanisivik, Baffin Island, Canada. Economic Geology, v. 86, p. 699-717.

Banner, J.L., and Hanson, G.N. (1990) Calculation of simultaneous isotopic and trace element variations during water-rock interaction with applications to carbonate diagenesis. Geochimica et Cosmochimica Acta, v. 54, p. 3123-3137.

Beales, F.W., and Hardy, J.L. (1980) Criteria for the recognition of diverse dolomite type with an emphasis on studies on host rocks for Mississippi Valley-Type ore deposits. In: D.H. Zenger, J.B. Dunham, and R.L. Ethington (Editors) Concepts and models of dolomitization. Society of Economic Paleontologists and Mineralogists Special Publication No. 28, p. 197-213.

Blattner, P., and Lassey, K.R. (1990) Transport of stable isotopes, kinetics, dispersive advection, and the "isotopic fronts" of Baumgartner and Rumble (1988). Contributions to Mineralogy and Petrology, v. 105, p. 486-490.

Carothers, W.W., and Kharaka, Y.K. (1980) Stable carbon isotopes of HCO3- in oil-field waters-implications for the origin of CO_2. Geochimica et Cosmochimica Acta, v. 44, p. 323-332.

Cole, D.R., and Drummond, S.E. (1988) Solubilities of calcite and dolomite in hydrothermal solutions. Abstracts with Programs. Geological Society of America, v. 20 (7), p. 41.

Disnar, J.R., and Héroux, Y. (1995) Dégradation et lessivage des hydrocarbures de la formation ordovicienne de Thumb Montain encaissant le gîte Zn-Pb de Polaris (TNW, Canada). Canadian Journal of Earth Sciences. (in press).

Farr, M.R. (1992) Geochemical variation of dolomite cement within the cambrian Bonneterre Formation, Missouri: evidence for fluid mixing. Journal of Sedimentary Petrology, v. 62, p. 636-651.

Fontboté, L. (1990) Stratabound ore deposits in the Pucará basin. An overview. In: Fontboté, L., Amstutz, G.C., Cardozo, M., Cedillo, E., and Frutos, J. (Editors) Stratabound ore deposits in the Andes. Springer, Heidelberg, p. 253-266.

Fontboté, L.(1993) Self-organization fabrics in carbonate-hosted ore deposits: the example of diagenetic crystallization rhythmites (DCRs). In: Fenoll Hach-Ali, P., Torres-Ruiz, J., and Gervilla, F. (Editors) Current research in geology applied to ore deposits. Proceedings of the Second Biennial SGA Meeting, Granada, Spain, Sept. 9-13, 1993, p. 11-14.

Fontboté, L., and Gorzawski, H. (1990) Genesis of the Mississippi Valley-type Zn-Pb deposit of San Vicente, Central Peru: geological and isotopic (Sr, O, C, S) evidences. Economic Geology, v. 85, p. 1402-1437.

Frank, M.H., and Lohmann, K.C. (1986) Textural and chemical alteration of dolomite: Interaction of mineralizing fluids and host rock in a Mississippi Valley-type deposit, Bonneterre Formation, Viburnum Trend. In: Hagni, R.D. (Editor) Process Mineralogy VI, The Metallurgy Society, Varrendale, PA, p. 103-116.

Friedman, I., and O'Neil, J.R. (1977) Compilation of stable isotope fractionation factors of geochemical interest. In: Fleischer, M. (Editor) Data of Geochemistry. 6th ed. U.S. Geological Survey Professional Paper 440-KK, 12 p. and 49 fig.

Garvin, P.L., and Ludvigson, G.A. (1993) Epigenetic sulfide mineralization associated with Pennsylvanian paleokarst in easter Iowa, U.S.A. Chemical Geology, v. 105, p. 271-290.

Ghazban, F., Schwarcz, H.P., and Ford, D.C. (1990) Carbon and sulfur isotope evidence for in situ reduction of sulfate, Nanisivik lead-zinc deposits, Northwest Territories, Baffin Island, Canada. Economic Geology, v. 85, p. 360-375.

Ghazban, F., Schwarcz, H.P., and Ford, D.C. (1991) Correlated strontium, carbon and oxygen isotopes in carbonate gangue at the Nanisivik zinc-lead deposits, northern Baffin Island, N.W.T. Canada. Chemical Geology (Isotope Geoscience Section), v. 87, p. 137-146.

Gorzawski, H. (1989) Isotopic, geochemical, and petrographic characterization of the diagenetic evolution in carbonate-hosted stratabound Zn-Pb-(F-Ba) deposits. Heidelberger Geowissenschaftliche Abhandlungen, v. 28, 250 p.

Gorzawski, H., Fontboté, L., Field, C.W., and Tejada, R. (1990) Sulfur isotope studies in the zinc-lead mine Vicente, Central Perú. In: Fontboté, L., Amstutz, G.C., Cardozo, M., Cedillo, E., and Frutos, J. (Editors) Stratabound ore deposits in the Andes. Springer, Heidelberg, p. 305-312.

Gregg, J.M. (1985) Regional epigenetic dolomitization in the Bonneterre Dolomite (Cambrian), southeastern Missouri. Geology, v. 13, p. 503-506.

Gregg, J.M., and Shelton, K.L. (1989) Geochemical and petrographic evidence for fluid sources and pathways during dolomitization and lead-zinc mineralization in Southeast Missouri: a review. Carbonates and Evaporites, v. 4, p. 153-175.

Gregg, J.M., and Shelton, K.L. (1989) Minor- and trace-element distribution in the Bonneterre Dolomite (Cambrian), southeast Missouri: evidence for possible multiple-basin fluid sources and pathways during lead-zinc mineralization.Geological Society of America Bulletin, v. 101, p. 221-230.

Haefner, R.J., Mancuso, J.J., Frizado, J.P., Shelton, K.L., and Gregg, J.M. (1988) Crystallization temperatures and stable isotope composition of Mississippi Valley-Type carbonates and sulfides of the Trenton limestone, Wyandot County, Ohio. Economic Geology, v. 83, p. 1061-1069.

Hannah, J.L., and Stein, H. (1984) Evidence for changing ore fluid composition: stable isotope analysis of secondary carbonates, Bonneterre Formation, Missouri. Economic Geology, v. 79, p. 1930-1935.

Holland, H.D, and Malinin, S.G. (1979) The solubility and occurrence of non-ore minerals. In: Barnes, H.L. (Editor) Geochemistry of hydrothermal ore deposits, 2nd Ed.,p. 461-508.

Landis, G.P. Tschauder, R.J. (1990) Late Mississippian karst caves and Ba-Ag-Pb-Zn mineralization in Central Colorado: Part II Fluid inclusion, stable isotope, and rock geochemistry data and a model of ore deposition. In: Beaty, D.W., Landis, G.P., and Thomson, T.B. (Editors) Carbonate-hosted sulfide deposits of the Central Colorado Mineral Belt. Economic geology, monograph 7, p. 339-366.

Leach, D.L., Plumlee, G.S., Hofstra, A.H., Landis, G.P., Rowan, E.L., and Viets, J.G. (1991) Origin of late dolomite cement by CO2-saturated deep basin brines: Evidence from the Ozark region, central United States. Geology, v. 19, p. 348-351.

Leventhal, J.S. (1990) Organic matter and thermochemical sulphate reduction in the Viburnum Trend, southeast Missouri. Economic Geology, v. 85, p. 622-632.

Machel, H.-G. (1987) Saddle dolomite as a by-product of chemical compaction and thermochemical sulfate reduction. Geology, v. 15, p. 936-940.

Matsuhisa, Y., Morishita, Y., and Sato, T. (1985) Oxygen and carbon isotope variations in gold-bearing hydrothermal veins in the Kushikino Mining Area, Southern Kyushu, Japan. Economic Geology, v. 80, p. 283-293.

McCrea, J.M. (1950) On the isotopic chemistry of carbonates and a paleotemperature scale. Journal of Chemical Physics, v. 18, p. 849-857.

Meyers, W.J. (1989) Trace element and isotope geochemistry of zoned calcite cements, Lake Valley Formation (Mississippian, New Mexico): insights from water-rock interaction modelling. Sedimentary Geology, v. 65, p. 355-370.

Moritz, R., Fontboté, L., Spangenberg, J. Rosas, S., Sharp, Z. and Fontignie, D. (in press) Sr, C and O isotope systematics in the Pucará Basin, Central Peru: comparison

between Mississippi Valley-type deposits and barren areas. accepted for publication in Mineralium Deposita.

Nesbitt, B.E. and Muehlenbachs, K. (1994) Paleohydrogeology of the Canadian Rockies and origins of brines, Pb-Zn deposits and dolomitization in the Western Canada Sedimentary Basin. Geology, v. 22, p. 243-246

O'Neil J.R., Clayton, R.N., and Mayeda, T.K. (1969) Oxygen isotope fractionation in bivalent metal carbonates. Journal of Chemical Physics, v. 51, p. 5547-5558.

Ohmoto, H., and Rye R.O. (1979) Isotopes of sulfur and carbon. In: Barnes, H.L. (Editor) Geochemistry of hydrothermal ore deposits, Wiley, New York, p. 509-567.

Orr, W.L. (1974) Changes in sulfur content and isotopic ratios of sulfur during petroleum maturation - study of Big Horn basin Paleozoic oils. American Association of Petroleum Geologists Bulletin, v. 58, p. 2295-2318.

Orr, W.L. (1977) Geologic and geochemical controls on the distribution of hydrogen sulfide in natural gas. In: Campos, R., and Goñi, J. (Editors) Advances in Organic Geochemistry 1975. ENADIMSA, Madrid, p. 572-597.

Orr, W.L. (1982) Rate and mechanism of non-microbial sulfate reduction. Geological Society of America, Abstracts with Programs, v. 14, p. 580.

Powell, T.G., and Macqueen, R.W. (1984) Precipitation of sulfide ores and organic matter: sulfate reactions at Pine Point, Canada. Science, v. 224, p. 63-66.

Qing, H., and Mountjoy, E. (1992) Large-scale fluid flow in the Middle Devonian Presqu'île barrier, Western Canada Sedimentary Basin. Geology, v. 20, p. 903-906.

Rosas, S. (1994) Facies, diagenetic evolution, and sequence analysis along a SW-NE profile in the southern Pucará Basin (Upper Triassic-Lower Jurassic), central Peru. Heidelberger Geowissenschaftliche Abhandlungen, v. 80, 337 p.

Sassen, R. (1988) Geochemical and carbon isotopic studies of crude oil destruction, bitumen precipitation, and sulfate reduction in the deep Smackover Formation. Organic Geochemistry, v. 12, p. 351-361.

Shikazono, N. (1989) Oxygen and carbon isotopic composition of carbonates from the neogene epithermal vein-type deposits of Japan: implication for evolution of terrestrial geothermal activity. Chemical Geology, v. 76, p. 239-247.

Siebert, R.M., Hostetler, P.B. (1970) The dissolution of dolomite below 100 degrees C. Abstracts with Programs. Geological Society of America, v. 2 (7), p. 682-683.

Spangenberg, J. (1995) Geochemical (elemental and isotopic) constraints on the genesis of the Mississippi Valley-type zinc-lead deposit of San Vicente, central Peru. [Ph.D. dissertation], University of Geneva, Switzerland (in press).

Spangenberg, J., and Fontboté, L. (1995) Rare earth element patterns in the host and gangue carbonates of the San Vicente zinc-lead deposit, Peru. Schweizerische Mineralogische und Petrographische Mitteilungen, v. 75, p. 271-275.

Spangenberg, J., Sharp, Z., and Fontboté, L. (1995) Apparent carbon and oxygen isotope variations of carbonate gangue minerals Mississippi Valley-type Zn-Pb of San Vicente deposit, central Peru: the effect of organic matter and sulphides. Mineralium Deposita, v. 30, p. 67-74.

Spirakis, C.S., and Heyl, A.V. (1993) Local heat, thermal convection of basinal brines and genesis of lead-zinc deposits of the Upper Mississippi Valley district. Transactions of the Institution of Mining and Metallurgy, Section B, v. 102, B201-B202.

Sverjensky, D.A. (1981) Isotopic alteration of carbonate host rocks as a function of water to rock ratio-An example from the Upper Mississippi Valley zinc-lead district. Economic Geology, v. 76, p. 154-172.

Sverjensky, D.A. (1986) Genesis of Mississippi Valley-type lead-zinc deposits. Annual Review of Earth and Planetary Sciences, v. 14, p. 177-199.

Taylor, H.P. (1979) Oxygen and hydrogen isotope relationships in hydrothermal mineral deposits. In: Barnes, H.L. (Editor) Geochemistry of hydrothermal ore deposits, Wiley, New York, p. 236-567.

Tissot, B., Durand, B., Espitalié, J, and Combaz, A. (1974) Influence of nature and diagenesis of organic matter in formation of petroleum. American Association of Petroleum Geologists Bulletin, v. 58, p. 499-506.

Winter, B.L., and Knaulth, L.P. (1992) Stable isotope geochemistry of carbonate fracture fills in the Monterey Formation, California. Journal of Sedimentary Petrology, v. 62, p. 208-219.

Zheng, Y.-F. (1990) Carbon-oxygen isotopic covariation in hydrothermal calcite during degassing of CO2: a quantitative evaluation and application to the Kushikino gold mining area in Japan. Mineralium Deposita, v. 25, p. 246-250.

Zheng, Y.-F., and Hoefs, J. (1993) Carbon and oxygen isotopic covariations in hydrothermal calcites. Theoretical modeling on mixing processes and application to Pb-Zn deposits in the Harz Mountains, Germany. Mineralium Deposita, v. 28, p. 79-89.

CHAPTER 4

RARE-EARTH AND TRACE ELEMENTS IN HYDROTHERMAL CARBONATES OF THE SAN VICENTE MISSISSIPPI VALLEY-TYPE DISTRICT, CENTRAL PERU

Abstract

The rare earth element (REE) and other trace element (Fe, Mn, Sr, Na, Ba, Zn) composition of the hydrothermal carbonates of the San Vicente Mississippi Valley-type district, hosted in the Triassic - Jurassic dolostones of the Pucará Group (central Peru), place constraints on the path-way of the ore fluid and changes in the Eh-pH conditions during mineralization. The ore-stage dark replacement dolomite and white sparry dolomite are depleted in Fe and REE, and enriched in Mn compared to the host dolomite. They display, in the samples of the main deposit, negative Ce and Eu anomalies. These results indicate that the incoming ore fluid was slightly oxidizing and acidic and poor in REE and Fe, which implies that the fluid flowed through a main aquifer, likely the detrital units at the base of the basin with limited interaction with the carbonate host rocks. Since the chemistry of the hydrothermal carbonates show a strong regional homogeneity, access of the corrosive ore fluid to the mineralization sites was likely by interconnected channel-ways (faults, basement highs) near the ore occurrences. This conclusion supports the hypothesis based on stable isotope data, suggesting that the whole San Vicente district was affected by a common hydrothermal system during the mineralization. The alteration of the native organic matter by the incoming fluid provides the local reducing conditions for thermochemical sulfate reduction and reduction of Eu^{3+} to Eu^{2+}. The ore-stage white sparry dolomite and associated sphalerite precipitated in acidic reducing fluid-buffered conditions. Mixing of the incoming fluid (slightly acidic, oxidizing, H_2CO_3 dominant) with native intra-formational fluids (alkaline, reducing, HCO_3^- dominant) explains the great scatter of the REE and other trace element analyses in the hydrothermal carbonates. The Fe-Mn covariations combined with the Eu anomalies of the hydrothermal carbonates are consistent with the change from reducing ore-stage to post-ore oxidizing conditions. The REE enrichment, the Mn depletion, and the positive Eu anomaly of the late-stage vug-filling carbonates indicate that the post-ore "residual" acidic fluid was again oxidizing due to continuous influx of fresh basinal waters. The precipitation of REE-rich late vug carbonates is probably due to CO_2 degassing caused by an enhanced hydrothermal porosity.

The results of this study match a parallel one based on stable isotopes and show that trace element geochemistry, including REE, of the hydrothermal carbonates from MVT-deposits may be also used as sensitive tracer of the ore-forming processes.

4.1 Introduction

Multiple fluid mixing and fluid rock interaction occurring during formation of Mississippi Valley-type (MVT) deposits induce changes in the composition of the fluid and the host carbonates. The chemical composition (elemental and isotopic) of the hydrothermal carbonates may record the nature and extent of these mixing processes.

Minor and trace element (excluding REE) compositions in carbonates have been commonly applied in studies of diagenesis (e.g., Bustillo et al., 1992; Brand and Veizer, 1980; Churnet and Misra, 1981; Erel and Katz, 1990; Land, 1980; Machel, 1987; Machel and Mountjoy, 1986, 1987; Meyers, 1989; Montañez and Read, 1992; Pingitore, 1978; Vahrencamp and Swart, 1990; Veizer, 1983a, 1983b). In particular, the areal Mg, Sr, Na, Fe, and Mn trends in carbonates may provide valuable information on the flow direction of dolomitizing (Machel, 1988) and mineralizing (Buelter and Guillemette, 1986; Farr, 1992; Gregg, 1988; Gregg and Shelton, 1989; Viets et al., 1983) fluids. Meyers (1989) has

shown that the Fe versus Mn covariations are strongly dependent of the extent of water-rock interaction combined with changes of the oxidation potential.

Rare earth elements (REE) have ionic radii similar to Ca^{2+} and extremely low concentrations in natural waters (<10^{-9} mol/l, Moldovanyi et al., 1990; see also deBaar et al., 1985; Elderfield and Greaves, 1982; Fleet, 1984). They have been used as tracers of diagenetic processes (Banner et al., 1988; Elderfield and Pagett, 1986; McDaniel et al., 1994; Moldovanyi, et al., 1990; Schieber, 1988) and precipitation of sediment-hosted Zn-Pb-(F) ores (e.g., Grant and Biss, 1983; Graf, 1984, 1988; Jones et al., 1991; Möller, 1983, 1991; Möller and Morteani, 1983; Möller et al., 1984; Shepherd et al., 1982; Zheng and Wang, 1991). The carbonate-fluid distribution coefficients of the REE are quite large (70 - 120, Palmer, 1985). Thus, extremely high water-rock ratios are required to alter the REE distribution in carbonates during diagenesis (Banner et al., 1988). Graf (1984), however, has documented that the altered host dolomite in the MVT district of Viburnum Trend was significantly depleted in light REE (LREE) compared to the unaltered host dolomite. He explained the differences in the REE patterns by interaction of the host rock with LREE depleted ore solutions.

The present communication is part of an extensive geochemical investigation of the gangue carbonates of the San Vicente MVT district hosted in the Upper Triassic - Lower Jurassic Pucará basin, central Peru. It includes C, O and Sr isotopic data, fluid inclusion studies, and geochemical data on the associated organic matter (Spangenberg, 1995; Spangenberg et al., 1994 and in prep.). The aim of this contribution is to discuss the constraints set by REE and other trace element (Fe, Mn, Sr, Na, Ba, Zn) contents of gangue carbonates on the source of the ore solutions, its transport, and the processes involved during sulfide precipitation at San Vicente. To our knowledge is the first time that REE have been integrated with other trace elements in a geochemical study of MVT mineralization.

Previous work on the San Vicente deposit includes Fontboté and Gorzawski (1990), Gorzawski et al. (1990), and Spangenberg et al. (1994, 1995a). Moritz et al. (in press) present Sr, C and O isotope data on mineralized and barren carbonate rocks at the scale of the Pucará basin. A lithogeochemical profile along the sedimentary sequence indicated that the carbonates in the ore-bearing units are enriched in manganese (Gonzalez, 1987, Fontboté and Gorzawski, 1990). Gorzawski (1989) noted that the hydrothermal white sparry dolomite is slightly enriched in manganese compared to the host dolomite.

4.2 Geological setting

The San Vicente Mississippi Valley-type (MVT) Zn-Pb district is located 300 km east of Lima in central Peru, between 1000 and 2500 m altitude, in the so-called "Ceja de Selva", i.e., the eastern flank of the Andes covered by tropical rain forest. It has an accumulated production and reserves of about 20 million metric tons ore of 10 wt. % zinc and 0.8 wt. % lead (Fontboté et al., 1995).

The Upper Triassic - Lower Jurassic Pucará basin, host of the San Vicente deposit and other non mined MVT occurrences (Fig. 4.1), is a carbonate platform at the western margin of the Brazilian Shield developed at the beginning of the Andean cycle by marine transgression over clastic sediments and volcanic and volcaniclastic rocks of the Upper Permian to Lower Triassic Mitu Group. Recent sedimentological, Sr, C and O isotope and metallogenetic studies of the Pucará basin are discussed in Fontboté (1990), Rosas (1994) and Moritz et al. (in press). The geology of the San Vicente main deposit was described in detail by Fontboté and Gorzawski (1990, and references therein). In the San Vicente mining area the carbonate sequence of the Pucará Group has a thickness of about 1300 m and range

Figure 4.1. Geological map of San Vicente belt showing the studied localities (barren and mineralized areas). QP = Quebrada Piñôn; RO = Rondayacu; YS = Yanachuro Sur; SI = Sillapata; UT = Utcuyacu; QU= Quebrada Utcuyacu; AY = Aynamayo; CH = Chilpes; AC = Afloramiento Campana; US = Uncush Sur; SV = San Vicente mine; VI = Vilcapoma; AR = Arcopunco; MA = Machuyacu; QS = Quebrada Seca; PA = Palmapata; PJ = Puntayacu Junior; SP = Sur Pichita; PI = Pichita.

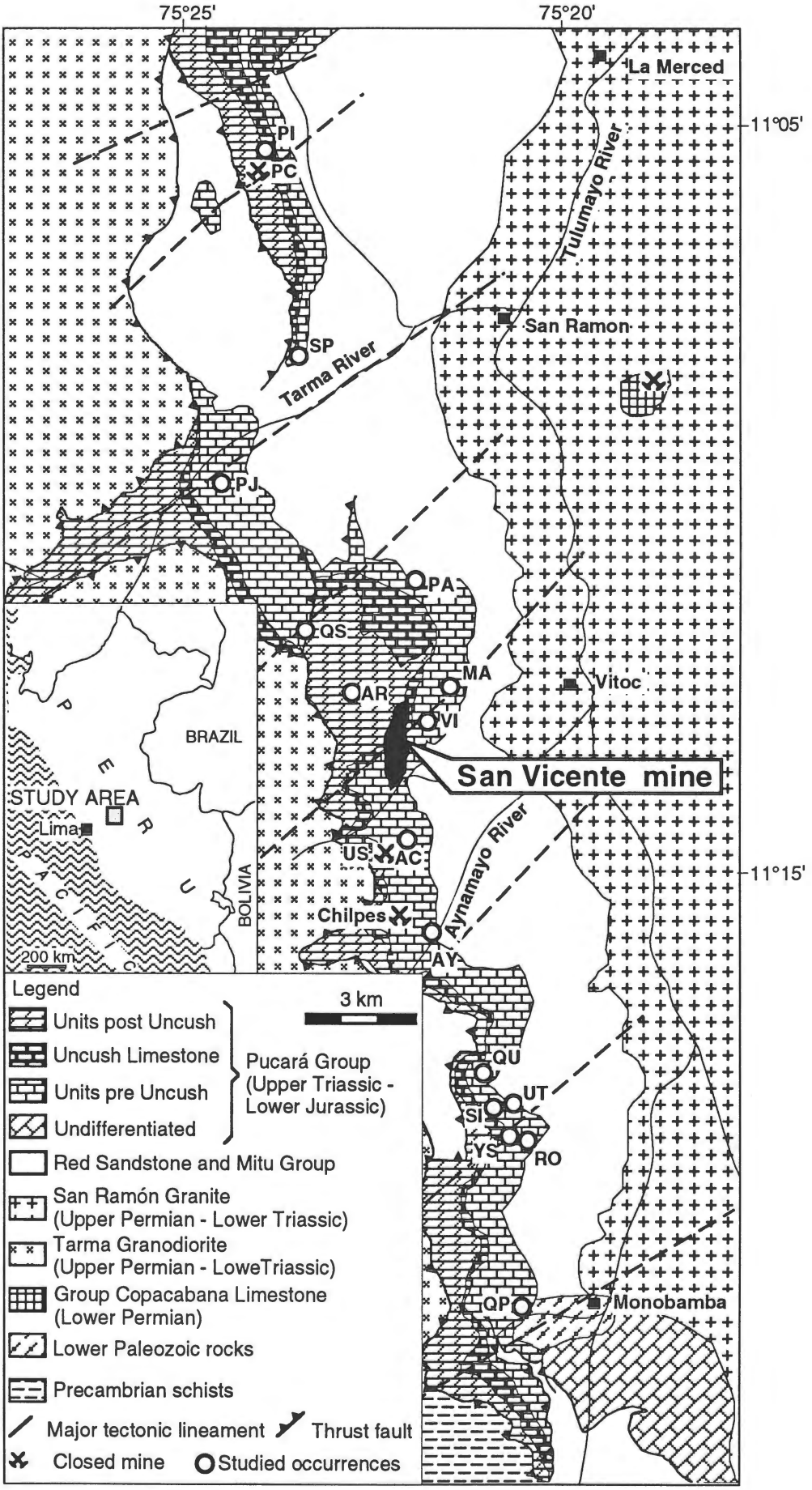
75°25'
75°20'
11°05'
11°15'
La Merced
Tulumayo River
San Ramon
Tarma River
PI
PC
SP
PJ
PA
QS
MA
AR
VI
Vitoc
San Vicente mine
BRAZIL
PERU
STUDY AREA
Lima
BOLIVIA
US
AC
Chilpes
Aynamayo River
AY
QU
UT
SI
YS
RO
QP
Monobamba
200 km
3 km
Legend
Units post Uncush
Uncush Limestone
Units pre Uncush
Undifferentiated
Pucará Group (Upper Triassic - Lower Jurassic)
Red Sandstone and Mitu Group
San Ramón Granite (Upper Permian - Lower Triassic)
Tarma Granodiorite (Upper Permian - LoweTriassic)
Group Copacabana Limestone (Lower Permian)
Lower Paleozoic rocks
Precambrian schists
Major tectonic lineament
Thrust fault
Closed mine
Studied occurrences

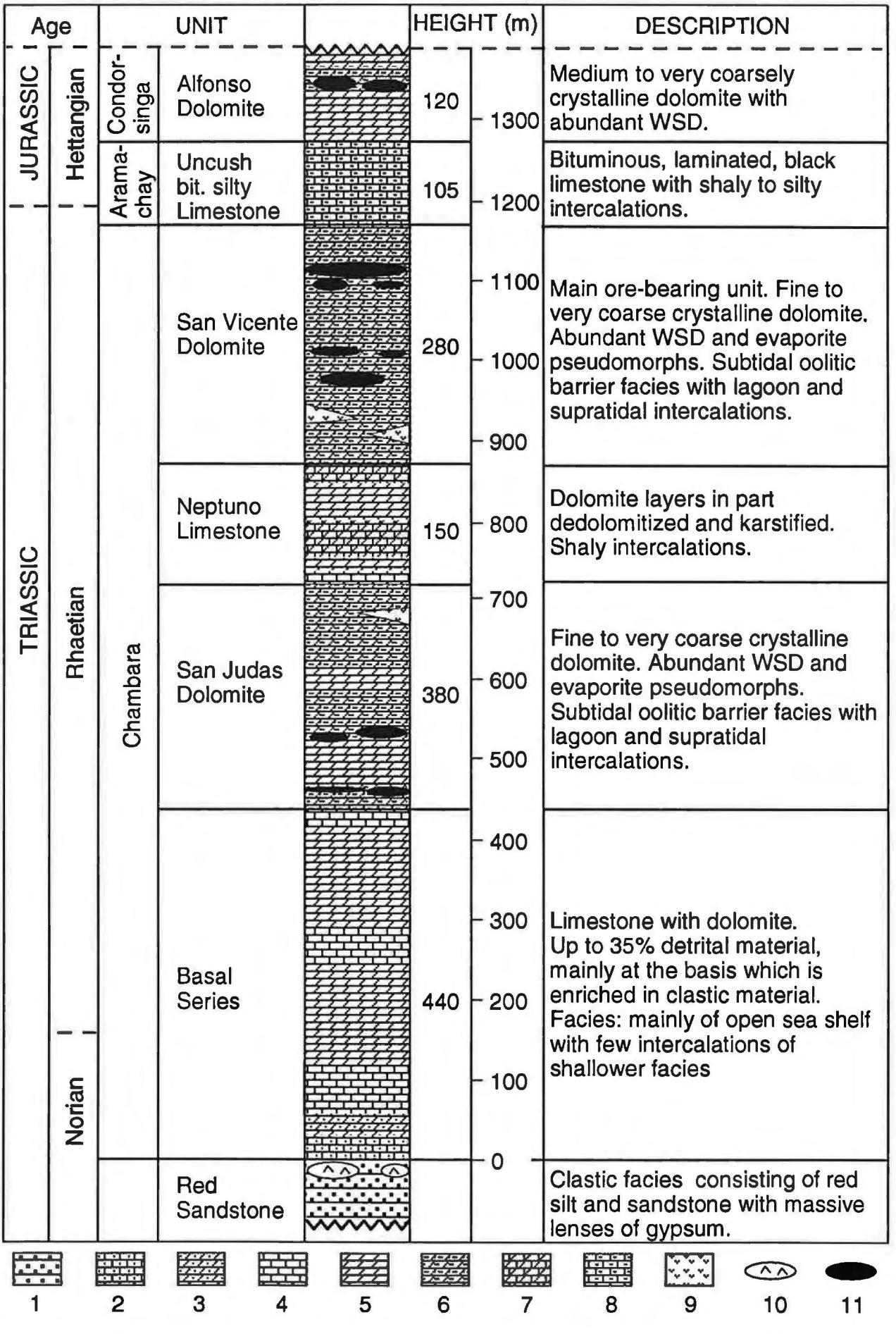
Age
UNIT
HEIGHT (m)
DESCRIPTION
JURASSIC
TRIASSIC
Hettangian
Rhaetian
Norian
Condor-singa
Arama-chay
Chambara
Alfonso Dolomite
Uncush bit. silty Limestone
San Vicente Dolomite
Neptuno Limestone
San Judas Dolomite
Basal Series
Red Sandstone
120
105
280
150
380
440
1300
1200
1100
1000
900
800
700
600
500
400
300
200
100
0
Medium to very coarsely crystalline dolomite with abundant WSD.
Bituminous, laminated, black limestone with shaly to silty intercalations.
Main ore-bearing unit. Fine to very coarse crystalline dolomite. Abundant WSD and evaporite pseudomorphs. Subtidal oolitic barrier facies with lagoon and supratidal intercalations.
Dolomite layers in part dedolomitized and karstified. Shaly intercalations.
Fine to very coarse crystalline dolomite. Abundant WSD and evaporite pseudomorphs. Subtidal oolitic barrier facies with lagoon and supratidal intercalations.
Limestone with dolomite. Up to 35% detrital material, mainly at the basis which is enriched in clastic material. Facies: mainly of open sea shelf with few intercalations of shallower facies
Clastic facies consisting of red silt and sandstone with massive lenses of gypsum.
1
2
3
4
5
6
7
8
9
10
11

in age from Norian to Hettangian (Fig. 4.2). Three dolomitic units, the San Judas Dolomite (SJD), the San Vicente Dolomite (SVD), and the Alfonso Dolomite (AD), host the orebodies. Most of the economic mineralization is contained within the San Vicente Dolomite. A series of normal faults and tectonic lineaments of general direction NE-SW, NW-SE, and N-S cut the carbonate units in the proximity to the orebodies (Fig. 4.1). These fault systems and basement highs may play an important role as channel pathways of the mineralizing solutions.

The ore occurs mainly as lens-shaped bodies (mantos) commonly conformable with bedding at the deposit scale. They are up to 1.3 km long, up to 200-300 m width, and up to several meters thick. The mineralization largely replaces dolomitized subtidal oolitic grainstones interlayered with dolomitized mudstones rich in organic matter and bearing evaporitic sulfate pseudomorphs (sabkha facies). It appears as zebra ore, replacements, and occasionally as cement in hydraulic breccias or veinlets (Fontboté and Gorzawski, 1990; Spangenberg et al., 1994). White sparry dolomite (WSD) is the main hydrothermal carbonate. Typically, WSD postdates sulfide precipitation and fills open spaces. One exception is the "San Vicente Techo manto", which is located in the upper and northern margin of the main ore deposit, where WSD is largely lacking. Another specificity of this manto is the presence of massive pyrite, a mineral otherwise only present in traces.

Fontboté and Gorzawski (1990) proposed that San Vicente formed at a burial depth of about 2-3 km and a temperature range of about 70 to 160°C by influx of a metal-bearing saline brine characterized by radiogenic Sr and Pb. The results of preliminary fluid inclusion studies indicate that the white sparry dolomite was precipitated from hot (115° to 162°C) and saline (up to 26 wt.% NaCl) fluids (Moritz et al, in press).

4.3 Host and gangue carbonates

Five different generations of carbonates can be distinguished in the ore-bearing dolostones of the San Vicente MVT district. They include dark replacement dolomite (DRD, I), white sparry dolomite (WSD, II), late void-filling dolomite (LFD, IIId) or calcite (LFC, IIIc), and carbonate replacing evaporitic sulfate (EP). The following classification of the carbonate generations is according to Spangenberg (1995).

The dark replacement dolomite is a fine- to medium-crystalline dolomite, with total organic carbon in the range of 0.07 % to 0.37 wt.% (Spangenberg, 1995). Higher values of total organic carbon (up to 5.2 wt.%, Spangenberg et al., 1995a) are also found in the vicinity of bituminous horizons. It presents different degrees of hydrothermal alteration which permits his classification into the following three groups: "Ivf" fine to very fine-grained (size from 15 to 60 µm, Figs. 1.7a, 1.7b), "If" fine-grained (size from 40 to 100 µm, Figs. 1.7c, 1.7d), and "Im" medium-grained (size from 100 to 400 µm, Figs. 1.7e, 1.7f). The very fine-grained is black-luminescent DRD (Ivf), indicating high Fe/Mn ratio (Figs. 1.7a, 1.7b). This dolomite represents the best available approximation to the pre-ore host dolostone. In dolomites Ivf and If is possible to still recognize relicts of primary textures in particular ghosts of former ooliths, whereas in the red-luminescent dolomite Im the primary texture preservation is poorer. The changes in the cathodoluminescence intensity indicate that the host dolomite was depleted in Fe and enriched in Mn during alteration.

In advanced stages of metasomatic alteration the white dolomite, replacing the dark host dolomite, increases its grain size and a coarse subhedral sparry dolomite (size from 0.4 to 2.5 mm) precipitates from the hydrothermal fluid in the available porosity. This altered DRD is intergrown with the first generation of fine-crystalline anhedral sphalerite and occasionally with pyrite and micro-crystalline quartz (Figs. 1.6g, 1.6h).

White sparry dolomite (WSD, also called saddle dolomite) is the most extensive hydrothermal dolomite cement and is formed throughout the entire San Vicente belt. The

Figure 4.2. Stratigraphic column of the Pucará Group in the San Vicente mining area (after Rosas, 1994). 1 = red sandstone; 2 = marly limestone; 3 = marly dolomite; 4 = limestone; % = dolomite; 6 = dolomite with white sparry dolomite; 7 = partly dedolomitized dolomite; 8 = bituminous silty limestone; 9 = volcanic rocks; 10 = lenses of gypsum; 11 = ore.

WSD is a subhedral white, mostly grayish (due to inclusions of sulfides and organic matter) sparry dolomite that occurs as open-space filling in small spots, in millimetric to centimetric thick bands replacing the DRD, and as cement in hydraulic breccias (Fig. 1.6). Alternating repetition of the bands of the DRD and the WSD, gives rise to the characteristic zebra texture of the ore rock, a common feature of Mississippi Valley-type deposits (e.g., Arne et al., 1991; Beales and Hardy, 1980; Fontboté and Gorzawski, 1990; Fontboté, 1993; Landis and Tschauder, 1990). The late filling carbonate occurs as coarse or very coarse-grained, mainly anhedral, milky-white dolomite (LFD) or calcite (LFC) open-space fillings in the WSD. Solid hydrothermal bitumen occurs as open-space filling and appears to be slightly younger than these late vug-filling carbonates.

A further carbonate phase occurs as sulfate pseudomorphs (EP) in the DRD (Fig. 1.6g). The main minerals replacing evaporitic sulfate (gypsum or anhydrite) are calcite, cherty quartz, and subordinate dolomite.

Most of the sphalerite occurs in the same paragenetic situation as white hydrothermal dolomite (Figs. 1.6a, 1.6b, 1.7g, 1.7h): (1) as fine-crystalline anhedral sphalerite intergrown with recrystallized dolomite I; (2) as coarse open space-filling subhedral sphalerite predating and/or intergrown with the white sparry dolomite II on the pervasive altered dark dolomite; and (3) as very coarse euhedral crystals within the late filling white dolomite III in cement of dissolution-breccias.

The Uncush bituminous silty Limestone (UL) is a black limestone rich in organic matter (total organic carbon ranges between 0.3 and 4.0 wt.%, Spangenberg , 1995) and very-fine crystalline pyrite (total sulfur up to 1.2 wt.%) with shaly to silty intercalations. This unit (Fig. 4.2) overlies the major ore-bearing dolomitic unit (San Vicente Dolomite) and provides a stratigraphic reference horizon (Fig. 4.1) .

4.4 Samples and analytical methods

4.4.1 Sampling

Carbonate host rocks from the San Vicente MVT district were sampled at district and mine scales in mineralized and barren areas along a 32 km N-S traverse centered in the main deposit (Fig. 4.1). Additional details of the sampling are given in Spangenberg (1995).
The district-scale samples come from nineteen localities, which include mined ore occurrences, surface outcrops, and exploration diamond-drill holes. A total of 42 samples, mainly of the ore-bearing dolomite units (Alfonso Dolomite, San Vicente Dolomite, and San Judas Dolomite) have been analyzed for major, minor and trace elements. Twenty two samples from seven ore occurrences were analyzed for REE.

Forty-three samples of the San Vicente mine were analyzed for major, minor and trace elements, and twenty-six for REE. They were sampled at different mantos from the three ore-bearing units (AD, SVD, SJD).

The stable isotope composition of these samples is presented in Spangenberg et al. (1995b) and Spangenberg (1995).

4.4.2 Sample preparation

Thin sections of representative samples were studied under the microscope to insure correct classification of the carbonate generations, in particular Ivf, If, and Im of the dark replacement dolomite (see Figs. 1.7a to 1.7f). Selected thin sections were examined under cathodoluminescence light, using the cold cathode luminescence Technosyn instrument model 8200 MKII of the University of Geneva (Martini et al., 1987).

The weathered and altered surface of the rock-samples was eliminated by sawing about 2 cm-thick slabs. These slabs were roughly polished, washed with distilled water, rinsed in acetone and dried. The different carbonate generations were separated using a diamond drill table-press, and ground in an agate mortar to less than 250 mesh. The fine powdered samples were analyzed by standard X-ray diffractometry methods at the University of Lausanne, to quantify the presence of non-carbonate minerals (quartz, clay

minerals, sulfides) and possible cross-contamination between distinct carbonate phases. Samples containing visible or XRD-detected sphalerite were discarded.

4.4.3 Major and trace element analysis

Five hundred mg of the dried sample powder were digested in 50 ml of HCl 1N at 50°C for 2 hours. Under these conditions dolomite reacts completely with the acid (e.g., Mazzucotelli et al., 1981; Robinson, 1980). After digestion the solution was filtered through a Whatman No. 42 filter. The filter was washed, ignited at 500 °C and weighed, to determine the wt.% insoluble residue (IR). The solutions were analyzed for Ca, Mg, Fe, Mn, Sr, Na, Zn and Ba using a Perkin-Elmer model 3005 inductively coupled plasma - atomic emission spectrometer (ICP-AES) of the Department of Mineral Chemistry of the University of Geneva. Multielemental calibration standards were prepared from single element *specpure* ICP-standard solutions. Replicate analysis of the geochemical reference samples JLs-1 (limestone), JDo-1 (dolomite), and NBS-88b (dolomitic limestone) indicate average reproducibilities for Ca and Mg better than ± 2 % (2 s), and for Mn, Fe, Sr, Zn of about ± 8 %. The reproducibility of barium (due to the very low concentrations) and sodium varied significantly between runs, exceeding occasionally ±15%.

The content in insoluble residue was used to correct the measured row data to 100 % acid-soluble (carbonate) fraction. The acid insoluble residue of the sample of the bituminous silty Uncush Limestone is up to 30 wt.%, whereas for the dark replacement dolomite ranges between 2 and 3 wt.% (up to 8 wt.% in very cherty samples) and for the hydrothermal carbonates only traces. XRD-analyses indicated that the main non-carbonate minerals were quartz and sulfides.

4.4.4 Rare earth element analysis

Rare earth elements and Y were analyzed by inductively coupled plasma - mass spectrometry (ICP-MS) at the XRAL-laboratories. The samples were digested using the same HCl 1N procedure described for the major and trace element analyses. Duplicate analyses yielded less than ± 10% variation of the measured values. The REE were determined in nine mine-scale sample by two methods, in the acid-soluble fraction by ICP-MS and in the whole-sample by instrumental neutron activation analysis (INAA). The aim of the determination of the REE using the two procedures was to evaluate the contribution of the non-carbonate (acid non-soluble) fraction to the total concentration of REE. The results are presented in the section 4.5.2.

4.5 Results

4.5.1 Major, minor, and trace elements

The major, minor and trace (excluding REE) element concentrations in the gangue carbonates from the main deposit and the studied occurrences in the San Vicente district are given in Table 4.1.

The hydrothermal dolomites (DRD, WSD, LFD) display a trend towards more stoichiometric Mg-concentration with advancing paragenetic stage (Fig. 4.3). The host very fine DRD (Ivf) is enriched in calcium, with $CaCO_3$ ranging between 55.9 and 60.2 mole % (median = 58.1 mole %), and depleted in Mg (39.5 to 43.5 mole % $MgCO_3$). The altered DRD (If, Im), and the open-space filling WSD and the LFD are slightly more stoichiometric, with $MgCO_3$ medians of 42.7%, 43.1%, 43.2%, and 43.4 mole % (Fig. 4.3). A similar trend was displayed by the $MgCO_3/CaCO_3$ ratio measured by electron microprobe analysis in selected samples of the ore-stage dolomites (Spangenberg, 1995).

The ranges of the trace element concentrations for the hydrothermal carbonates are shown in Fig. 4.4. The soluble fraction of the bituminous silty Uncush Limestone is poor in

Table 4.1. Geochemical composition of the acid soluble fraction from carbonates of the San Vicente district (including the San Vicente main deposit)

Sample	Loc[1]	Mant[2]	Lith[3]	Carbo.[4]	$CaCO_3$ (mole %)	$MgCO_3$ (mole %)	Fe (µg/g)	Mn (µg/g)	Na (µg/g)	Sr (µg/g)	Zn (µg/g)	Ba (µg/g)
FSV-984	QP		SVD	WSD	56.53	42.88	476	2358	436	93	12	
FSV-985	QP		SVD	WSD	57.40	42.00	1284	1674	551	74	3	
FSV-952	RO		SVD	WSD	56.30	43.43	262	982	303	113	41	5
FSV-953	RO		SVD	WSD	56.48	43.04	185	2022	399	72	24	6
FSV-953B	RO		SVD	WSD	56.43	43.08	628	1617	375	88	37	6
FSV-1001	YS		SVD	WSD	55.90	43.81	534	850	358	66	13	6
FSV-1003	YS		SVD	WSD	55.70	43.97	326	1275	283	92	60	5
FSV-956	UT		SVD	WSD	56.16	43.58	375	806	384	51	9	5
FSV-957	UT		SVD	WSD	56.43	43.34	555	535	327	60	8	6
FSV-652	QU		SVD	WSD	55.74	43.85	621	1247	330	107	26	7
FSV-653C	QU		SVD	WSD	56.62	42.76	1801	962	397	37	9343	2
FSV-1057	QU		UL		98.78	0.78	690	820	104	254	68	28
FSV-1059	QU		UL		98.58	1.10	728	262	169	625	5	49
FSV-988	AY		SJD	DRD (Im)	56.10	43.36	1657	982	415	68	19	
FSV-989	AY		SJD	DRD (Im)	55.56	43.66	2523	1213	402	97	90	7
FSV-988	AY		SJD	WSD	56.34	42.95	2251	1195	378	60	22	
FSV-989	AY		SJD	WSD	55.62	44.02	398	1299	364	67	44	6
FSV-992	AY		SVD	DRD (If)	56.35	43.22	988	1013	323	59	3581	71
FSV-990	AY		SVD	WSD	55.44	44.13	608	1409	349	136	48	19
FSV-992	AY		SVD	WSD	55.77	43.73	808	1558	517	102	164	12
FSV-754	CH		SJD	DRD (Im)	56.55	42.80	2103	1001	274	39	12	4
FSV-753	CH		SJD	WSD	56.38	43.14	1327	970	312	76	13	19
FSV-754	CH		SJD	WSD	56.26	42.67	3367	1768	377	44	12	3
FSV-754	CH		SJD	LFC	99.15	0.67	57	720	481	599	13	7
FSV-982	CH		SVD	DRD (Im)	56.02	43.18	2676	1230	418	57	19	
FSV-755	CH		SVD	DRD (Im)	56.24	43.19	366	2291	360	46	7	2
FSV-759	CH		SVD	DRD (If)	56.47	42.79	2558	1016	392	50		4
FSV-755	CH		SVD	WSD	56.33	43.31	234	1501	542	66		4
FSV-759	CH		SVD	WSD	56.26	43.00	2452	1134	289	49	7	2
FSV-761	CH		SVD	WSD	56.39	43.24	310	1412	537	56	6	3
FSV-982	CH		SVD	LFC	99.64	0.25	51	445	171	507	11	
FSV-981	AC		AD	DRD (If)	55.99	42.99	3899	1017	340	35	1476	
FSV-979	AC		AD	WSD	56.20	43.06	2532	1081	322	163	145	
FSV-981	AC		AD	WSD	55.92	43.09	3738	1070	422	34	1779	
FSV-976	US		AD	WSD	55.95	43.81	64	1095	378	49		
FSV-978	US		AD	LFC	99.18	0.70	48	480	129	249		
FSV-971	US		SJD	WSD	56.11	43.68	205	799	476	48		
FSV-972	US		SJD	WSD	56.39	43.36	435	767	456	49		
FSV-654	SV	Alfon.	AD	WSD	54.97	44.65	576	1189	483	57	80	4
FSV-665	SV	Alfon.	AD	WSD	56.91	43.09	2391	1082	282	70	137	3
FSV-665	SV	Alfon.	AD	LFC	99.41	0.48	50	422	127	473	3	1
FSV-801	SV	Alfon.	AD	DRD (Ivf)	60.20	39.48	746	605	581	67	263	2
FSV-806	SV	Alfon.	AD	WSD	57.05	42.60	429	1158	205	62	7	1
FSV-807	SV	Alfon.	AD	WSD	56.88	42.58	1204	1233	390	46	1362	1
FSV-807	SV	Alfon.	AD	LFC	89.68	10.14	323	522	184	320	16	
FSV-811	SV	Alfon.	AD	DRD (Ivf)	59.03	40.42	1609	566	160	56	22	2
FSV-811	SV	Alfon.	AD	DRD (If)	57.67	41.79	1797	682	286	44	760	1
FSV-816	SV	Alfon.	AD	WSD	58.20	41.56	302	757	373	51	12	1
FSV-830	SV	Alfon.	AD	WSD	58.06	41.32	643	2125	349	47	12	2
FSV-015	SV		UL		95.48	3.94	1448	300	161	1406	17	71
FSV-017	SV		UL		98.91	0.61	1436	379	212	793	1	32
FSV-1101	SV		UL		97.08	2.43	1104	168	88	566	2	21
FSV-1102	SV		UL		97.17	0.87	1446	154	146	393	5	6
FSV-1103	SV		UL		93.28	6.04	1484	414	151	1036	4	114
FSV-659	SV	1	SVD	WSD	56.76	41.77	4749	1991	480	73	2919	3
FSV-038	SV	2	SVD	DRD (If)	56.45	42.68	2778	1278	391	53	890	3
FSV-657B	SV	3	SVD	WSD	56.72	42.56	301	3022	455	83	8	9
FSV-020	SV	3i	SVD	DRD (Ivf)	57.23	42.08	1652	1259	318	73	134	2
FSV-022	SV	3i	SVD	WSD	57.61	41.18	3551	2031	446	92	3842	4
FSV-029	SV	3p	SVD	EPc	65.83	33.90	261	995	213	213	3656	7
FSV-213-2	SV	3t	SVD	WSD	56.26	42.39	4770	1486	448	42	149	2

continued

Table 4.1. Continued

Sample	Loc[1]	Mant[2]	Lith[3]	Carbonat 4	$CaCO_3$ (mole %)	$MgCO_3$ (mole %)	Fe (µg/g)	Mn (µg/g)	Na (µg/g)	Sr (µg/g)	Zn (µg/g)	Ba (µg/g)
FSV-913	SV	Ayala	SVD	WSD	54.92	43.81	3358	2207	314	56	22	2
FSV-914	SV	Ayala	SVD	WSD	55.15	44.42	696	1182	364	50	11	3
FSV-919	SV	Ayala	SVD	WSD	54.61	44.95	536	1349	366	61	129	3
FSV-919	SV	Ayala	SVD	LFD	55.65	43.94	30	1684	272	153	40	3
FSV-921	SV	Ayala	SVD	WSD	55.86	43.66	1075	1127	422	68	10646	3
FSV-004	SV	Ayala	SVD	WSD	54.67	44.67	1432	1514	299	45	32	2
FSV-902	SV	Jesus	SVD	LFC	99.18	0.76	12	277	171	305	2	2
FSV-904	SV	Jesus	SVD	EPc	99.31	0.64	75	126	391	391	14	3
FSV-905	SV	Jesus	SVD	DRD (If)	55.15	44.14	2147	1035	300	54	4	1
FSV-909	SV	Jesus	SVD	WSD	55.00	44.57	1309	569	456	35	17	1
FSV-423	SV	Jesus	SVD	DRD (Ivf)	55.88	43.53	2021	849	331	47		1
FSV-673	SV	Jesus	SVD	WSD	54.27	45.33	1296	527	330	89	4	4
FSV-673	SV	Jesus	SVD	WSD	54.32	44.93	1495	1794	377	53	5097	3
FSV-674	SV	Jesus	SVD	WSD	54.48	43.81	5226	2273	303	69	4979	2
FSV-675	SV	Jesus	SVD	LFC[5]	64.89	34.73	140	1504	221	190	26	4
FSV-851	SV	SV t	SVD	LFC	96.94	2.93	110	458	297	503	71	3
FSV-853	SV	SV t	SVD	DRD (If)	57.40	42.37	392	653	463	151	16	4
FSV-854	SV	SVt	SVD	LFC	88.90	10.96	119	471	308	347	774	2
FSV-856	SV	SV t	SVD	LFC	98.31	1.61	94	269	930	930	13	94
FSV-857	SV	SV t	SVD	LFC	99.79	0.12	104	285	141	1080		33
FSV-862	SV	SV t	SVD	WSD	57.10	42.54	503	1017	271	136	5104	4
FSV-713	SV		SJD	DRD (If)	57.14	42.37	1338	880	372	47	5	4
FSV-714	SV		SJD	WSD	56.14	43.19	1478	1618	417	53	4	2
FSV-714	SV		SJD	LFD	56.77	42.78	275	1757	516	54	7	4
FSV-718	SV	t	SJD	WSD	55.99	43.54	931	1206	379	41	1207	4
FSV-718	SV	m	SJD	DRD (Im)	55.69	43.40	2760	1383	355	58	998	4
FSV-719	SV	m	SJD	WSD	56.13	43.38	920	1375	346	74	6	4
FSV-779	AR		SVD	DRD (Im)	56.90	42.92	230	620	651	62		3
FSV-776	AR		SVD	WSD	57.31	41.95	2700	821	339	52	6	4
FSV-779	AR		SVD	WSD	56.50	43.22	384	909	511	69	5	2
Fsv-780	AR		SVD	WSD	56.43	43.11	1012	1115	270	54	14	5
FSV-959	MA		SVD	WSD	56.80	42.97	149	909	660	100	4	5
FSV-960	MA		SVD	WSD	57.52	42.26	287	722	531	58		4
FSV-964	PA		SVD	DRD (Im)	56.30	43.46	533	653	494	35	4039	3
FSV-964	PA		SVD	WSD	56.71	42.95	328	1266	521	41	5772	4
FSV-965	PA		SVD	WSD	56.53	43.22	405	763	458	37	251	1
FSV-967	PJ		SVD	WSD	56.75	42.82	279	1677	479	46	1	3
FSV-969	PJ		SVD	WSD	56.39	42.59	3506	1249	436	36		3
FSV-983	SP		SVD	WSD	56.42	43.34	418	769	579	53	7	

[1] Locality: abbreviations as in Fig. 4.1, SV = San Vicente main deposit.

[2] Manto name in the San Vicente main deposit (Alfon. = Alfonso; SVt = San Vicente techo)

[3] Lithologies: AD = Alfonso Dolomite; UL = Bituminous silty Uncush Limestone; SVD = San Vicente Dolomite; SJD = San Judas Dolomite

[4] DRD = dark replacement dolomite ("Ivf" very fine-grained, "If" fine-grained, "Im" medium-grained); WSD = white sparry dolomite (II); LFD = late filling dolomite (IIId); LFC = late filling calcite (IIIc); EPc = calcite replacing evaporitic sulfate
blank = not detected

[5] XRD results indicate a mixture of 75% dolomite and 25% calcite

iron, manganese, sodium, and zinc (1100 µg/g, 300 µg/g, 150 µg/g, 5 µg/g respectively) compared to the dolomite Ivf (1630 µg/g, 730 µg/g, 320 µg/g, 130 µg/g), and display the highest strontium (790 µg/g) and barium (30 µg/g) concentrations. This high Sr and Ba concentrations may indicate the contribution of the silicate minerals to the chemistry of the pore water (IR = 21.7 to 39.8 wt.%).

The content in Mn, Sr, Na, and Ba of the host dolomite (Ivf) increases during advancing alteration: from values of 730 µg/g, 60 µg/g, 320 µg/g, and 2 µg/g in the DRD (Ivf) to values of 1720 µg/g, 100 µg/g, 400 µg/g, and 4 µg/g in the LFD (Fig. 4.4). The enrichment in Sr of the LFD relative to the unaltered DRD coincides with the trend towards higher Mg concentrations.

Iron and zinc in the hydrothermal dolomites display more complex distribution trends

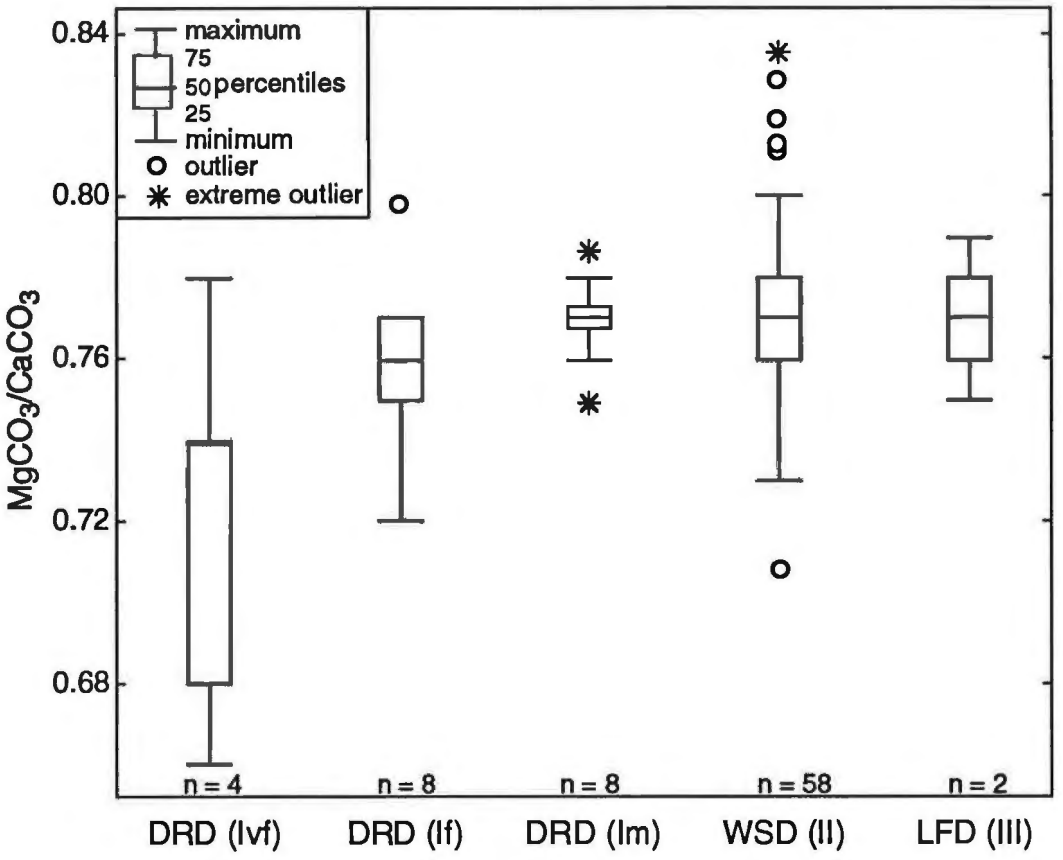

Figure 4.3. Ranges and medians of the $MgCO_3/CaCO_3$ ratio of the hydrothermal dolomites in San Vicente dolostones. DRD = dark replacement dolomite ("Ivf" very fine-grained, "If" fine-grained, "Im" medium-grained); WSD = white sparry dolomite (II); LFD = late filling dolomite (IIId); n = number of analyzed samples.

(Fig. 4.4), which can be summarized as follows: (i) the partially altered host dolomite has higher Fe and Zn values (1800 µg/g, 700 µg/g) than the host dolomite Ivf (1630 µg/g, 130 µg/g); (ii) the pervasive altered dolomite (Im) is poorer in Fe and Zn (1660 µg/g, 60 µg/g); and (iii) the concentrations of Fe in the WSD and LFD are very low (WSD: 620 µg/g , LFD: 160 µg/g Zn). Some samples of the WSD have extremely high Fe (> 2500 µg/g, up to 5230 µg/g) and Zn values (> 200 µg/g, up to 10650 µg/g) and are likely due to sphalerite leaching during the acid-digestion. Alternatively, the occurrence of Zn-dolomites, similar to those described by Kucha and Wieczorek (1984) in the Irish Navan Zn-Pb deposit, could explain the high values. However, this is considered as not possible because Zn-dolomites were not detected by XRD at San Vicente. Calcite pseudomorphs (EPc) display slightly higher Na and Ba (210 µg/g, 7 µg/g, up to 390 µg/g and 30 µg/g) compared to the late filling calcite (180 µg/g, 3 µg/g). This may indicate a local supply in both cations by the replaced sulfate.

In addition, the variation of the Fe and Mn concentrations in the hydrothermal dolomites support the cathodoluminescence evidence of increasing Mn/Fe ratios during dissolution and reprecipitation of the host dolomite.

Figure 4.4. Ranges and medians of the minor- and trace elements in the hydrothermal carbonates of San Vicente district. UL = bituminous silty Uncush limestone, n=7; DRD = dark replacement dolomite ("Ivf" very fine-grained, n=4; "If" fine-grained, n=8; "Im" medium-grained, n=8); WSD = white sparry dolomite (II), n=58; LFD = late filling dolomite (IIId), n=2; LFC = late filling calcite (IIIc), n=11; EPc = calcite replacing evaporitic sulfate, n=3. a) iron; b) manganese; c) strontium; d) sodium; e) barium; f) zinc.

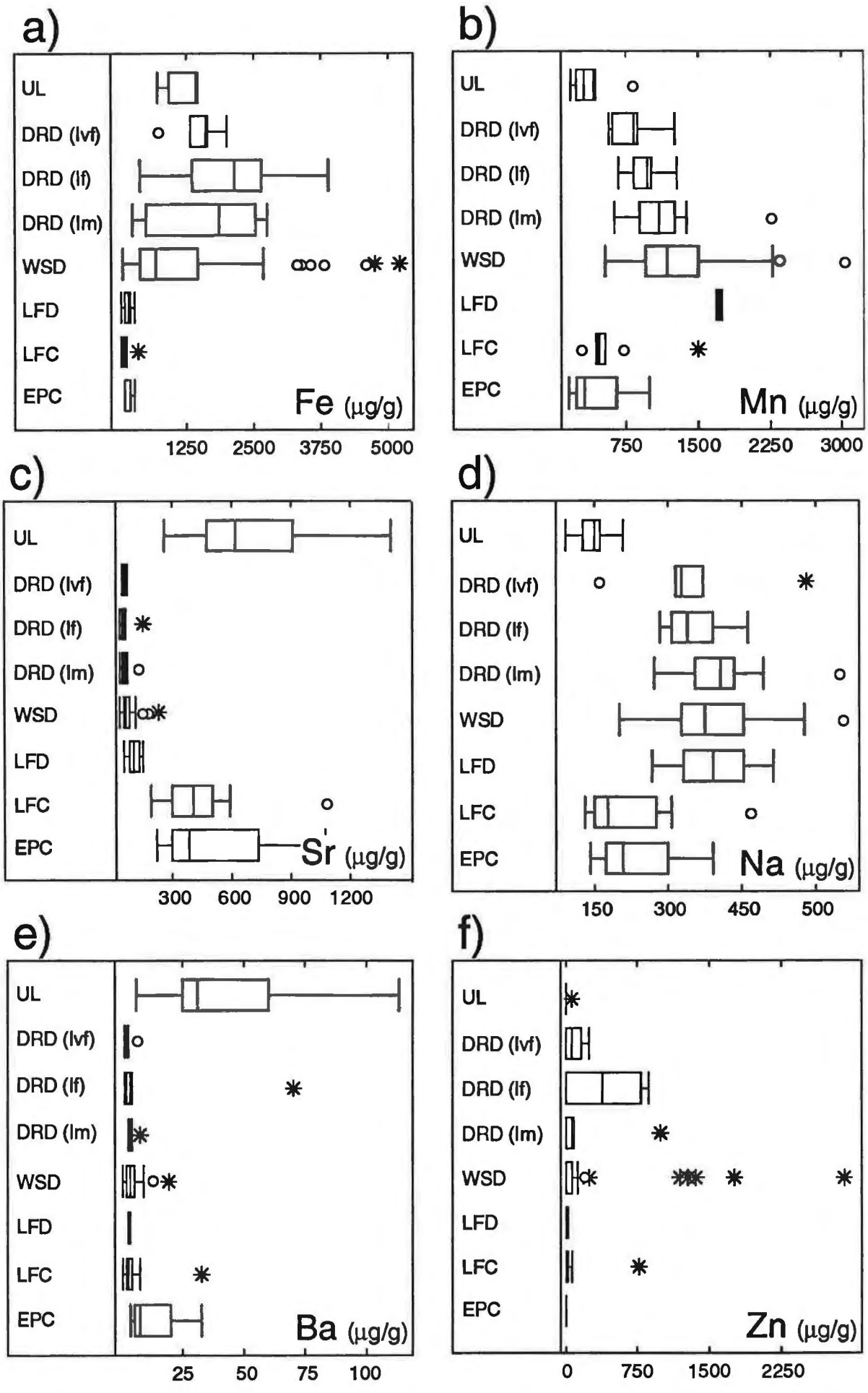
a)
UL
DRD (lvf)
DRD (lf)
DRD (lm)
WSD
LFD
LFC
EPC
Fe (µg/g)
1250 2500 3750 5000
b)
Mn (µg/g)
750 1500 2250 3000
c)
Sr (µg/g)
300 600 900 1200
d)
Na (µg/g)
150 300 450 500
e)
Ba (µg/g)
25 50 75 100
f)
Zn (µg/g)
0 750 1500 2250

The distribution of Fe, Mn, Na, Sr, Zn and Ba in hydrothermal dolomites at district scale is summarized in Table 4.2 and Fig. 4.5. The following features can be recognized: (1) Mn and Fe are enriched in the localities between San Vicente and "Quebrada Uncush"; (2) the highest values of Mn (up to 2360 µg/g) and Sr (up to 110 µg/g) were found in the localities south from "Chilpes", and show a significant areal correlation with major tectonic lineaments (e.g. localities "Yanachuro Sur", "Rondayacu") and the basement highs (e.g. Paleozoic rocks near "Quebrada Piñón"); (3) the locality of "Machuyacu" is characterized by anomalous values of Sr (up to 100 µg/g) and Na (up to 660 µg/g) and low values for Mn and Fe (820 µg/g and 220 µg/g); (4) the distribution of Na and Sr correlates roughly, and in contrast to Fe and Mn, do not show any clear trend. This may reflect that sodium (e.g., Bein and Land, 1983; Shukla, 1988) and likely Sr are enriched in hydrothermal carbonates as solid or fluid inclusions.

Table 4.2. Minor and trace element ranges and median values in the hydrothermal dolomites[1] of the San Vicente district

Locality[2] (n)	Fe (µg/g)	Mn (µg/g)	Na (µg/g)	Sr (µg/g)	Zn (µg/g)	Ba (µg/g)
QP	475 to 1283	1674 to 2358	436 to 551	74 to 93	3 to 9	-
(2)	(879)	(2016)	(493)	(84)	(7)	
RO	185 to 628	982 to 2022	302 to 398	72 to 113	24 to 41	5 to 6
(3)	(262)	(1617)	(375)	(87)	(37)	(6)
YS	326 to 534	850 to 1275	283 to 357	66 to 91	13 to 60	4 to 6
(2)	(430)	(1062)	(320)	(79)	(36)	(5)
UT	375 to 555	535 to 805	327 to 384	50 to 60	8 to 9	5 to 6
(2)	(465)	(670)	(356)	(55)	(8)	(6)
QU	620 to 1801	961 to 1247	320 to 397	37 to 107	25	2 to 7
(2)	(1104)	(1105)	(364)	(72)		(4)
AY	398 to 2522	982 to 1557	322 to 516	19 to 164	19 to 164	6 to 70
(7)	(988)	(1213)	(378)	(68)	(46)	(12)
CH	234 to 3367	970 to 2291	274 to 542	39 to 76	6 to 18	2 to 19
(9)	(2103)	(1230)	(377)	(50)	(12)	(4)
AC	2532 to 3899	1017 to 1080	322 to 421	34 to 163	144 to 1779	
(3)	(3758)	(1069)	(340)	(34)	(1476)	
US	65 to 435	766 to 1095	378 to 476	48 to 49		
(3)	(205)	(799)	(455)	(49)		
San Vicente	30 to 5226	527 to 3022	205 to 483	35 to 153	4 to 2919	1 to 9
(28)	(1325)	(1313)	(369)	(56)	(352)	(3)
AR	230 to 2700	619 to 1115	270 to 650	52 to 69	5 to 14	2 to 5
(4)	(698)	(865)	(425)	(58)	(6)	(3)
MA	149 to 87	722 to 909	531 to 660	58 to 100	4	4 to 5
(2)	(218)	(816)	(596)	(79)		(5)
PA	327 to 533	635 to 1266	457 to 520	35 to 41	250	1 to 4
(3)	(405)	(763)	(494)	(37)		(3)
PJ	279 to 3506	1249 to 1677	436 to 479	36 to 46		3
(2)	(1892)	(1463)	(458)	(41)		
SP	418	768	579	53	7	
(1)						

[1] Hydrothermal dolomites= altered dark replacement dolomite ("Im" medium-grained); white sparry dolomite (II) and late filling dolomite (IIId)

[2] Locality: abbreviations as in Fig. 4.1

n = number of analyzed samples; the median values are given in parentheses

Figure 4.5. Distribution of the minor- and trace elements in the ore-stage hydrothermal dolomites (DRD If, DRD Im, WSD) of the San Vicente district. **a)** iron; **b)** manganese; **c)** strontium; **d)** sodium. Zinc plot was not included because the high concentrations in this metal are probably due to contamination during the analysis

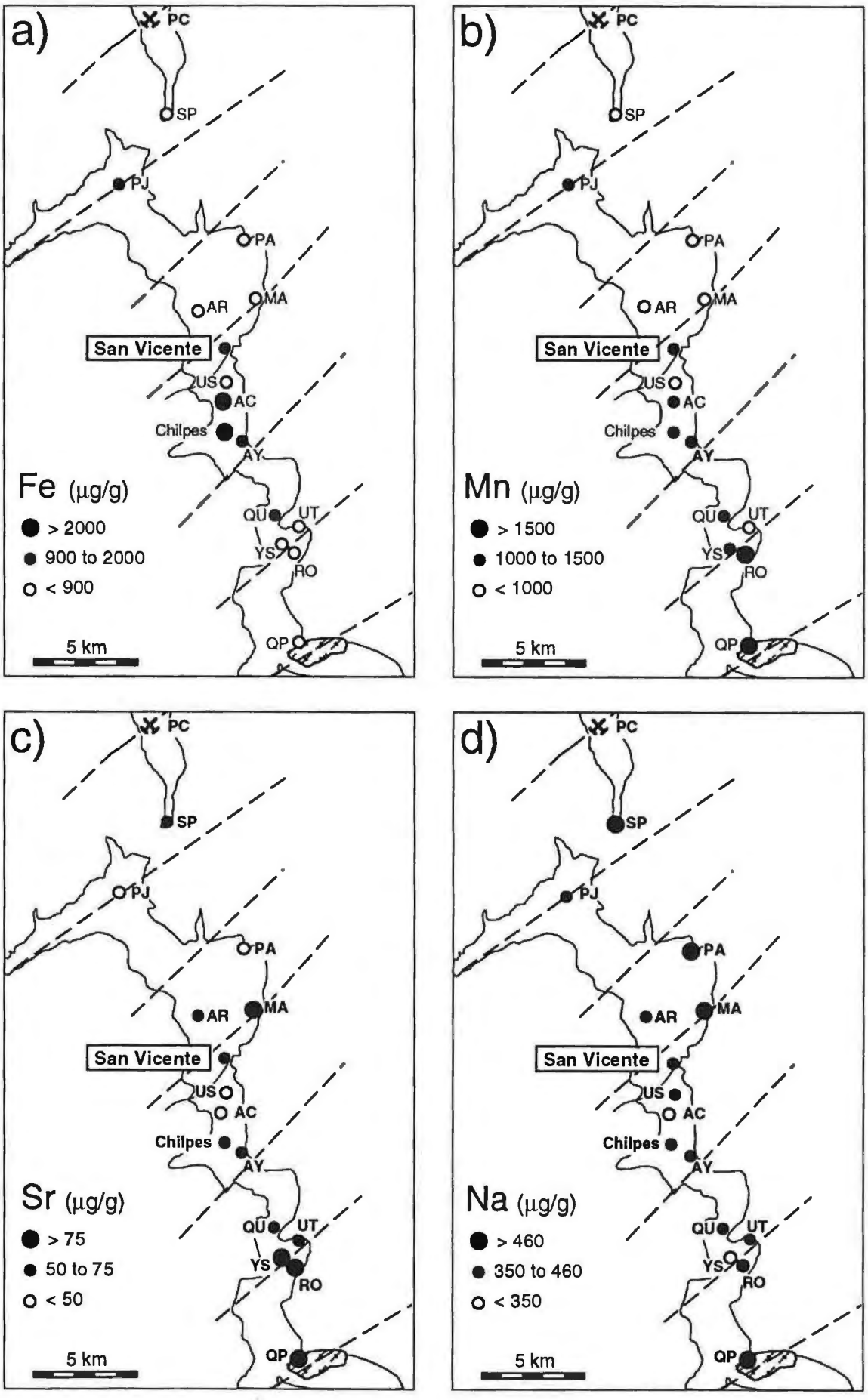
a)
PC
SP
PJ
PA
AR
MA
San Vicente
US
AC
Chilpes
AY
QU
UT
YS
RO
QP
Fe (µg/g)
> 2000
900 to 2000
< 900
5 km
b)
Mn (µg/g)
> 1500
1000 to 1500
< 1000
c)
Sr (µg/g)
> 75
50 to 75
< 50
d)
Na (µg/g)
> 460
350 to 460
< 350

4.5.2 Rare earth elements

The results of the comparative study between the ICP-MS-values of the acid soluble fraction and the whole-sample INAA-values are given in Table 4.3. The differences between the ICP-MS values and the INAA values roughly correlate with the wt.% IR (Table 4.3), reflecting the contribution of the non-carbonate fraction to the REE-INAA values. The REE results will be presented in two sections: San Vicente main deposit and San Vicente district.

4.5.2.1 San Vicente main deposit

The REE results of the acid-soluble fraction of the carbonates from San Vicente deposit are given in Table 4.4 and Table 4.5 (elemental ratios normalized to North American shales composite, values from Hanson, 1980). The distribution of the REE content in the different carbonate generations is illustrated in Fig. 4.6.

The bituminous silty Uncush limestone shows the highest REE concentration (ΣREE about 72 µg/g). In the other carbonate phases the REE content is lower than 12 µg/g. The concentration of REE in the ore stage dolomites decreases from the host DRD to the WSD (Ivf: 7.52 to 10.21 µg/g ; If: 4.05 to 6.03 µg/g; Im: 1.26 to 2.39 µg/g; II: 0.83 to 2.23 µg/g). The late filling carbonates show a large range of REE contents (LFD: 0.89 0 to 2.54 µg/g; LFC: 1.16 to 12.35 µg/g), which correlates with textural and paragenetic features. In order to discuss this broad range the late carbonates were subdivided as follows. Dolomites "IIIAd" occur in unmineralized cement of hydraulic breccias, dolomites "IIIBd" in dissolution breccias with sphalerite III at the boundaries of the orebodies (mainly in "1455 manto"). Calcites "IIIAc" are translucent filling of voids in dissolution porosity (mainly in "San Vicente techo manto"), and "IIIBc" white calcites fill large vein-like open spaces in hydraulic breccias. The dolomites have a similar REE content (IIIAd: 1.49 to 2.54 µg/g; IIIBd: 0.89 0 to 1.22 µg/g) but different REE patterns, whereas the calcites differ in the REE abundance (IIIAc: 1.16 0 to 2.24 µg/g; IIIBc: 8.18 0 to 12.25 µg/g) and patterns (see below).

The concentration in yttrium displays similar trends as those of the total REE contents (Table 4.4). In the Uncush limestone the concentration in Y ranges between 20.4 to 22 µg/g, and decreases in the ore-stage dolomites (DRD, WSD) in the order: Ivf (1.9 µg/g), If (0.7 µg/g), Im (0.6 µg/g), II (0.5 µg/g). The post-ore carbonates and the calcite replacing evaporitic sulfate are enriched in Y (IIIAd: 0.95 µg/g, IIIBd: 0.85, IIIAc: 0.85 µg/g, IIIBc: 16.5 µg/g, EPc: 4 µg/g).

The chondrite-normalized REE patterns of the different carbonate generations are illustrated in Fig. 4.7. The REE patterns of the calcite from the Uncush Limestone cluster within a narrow range and are parallel to the shale pattern (Fig. 4.7a). The REE patterns of the very fine-grained dark replacement dolomite (Ivf) are shaped similarly to those of the Uncush limestone, despite its lower elemental abundance (about 5 µg/g total REE). This suggests, that the bituminous silty Uncush limestone and the host dolomite inherited their REE patterns from Jurassic seawater and marine pore-water. The most significant feature of the REE distribution in the subgenerations of the DRD is a systematic depletion in Ce and generally, less pronounced, of all the REE, with advancing hydrothermal alteration (Figs. 4.7a, 1.7a to 1.7f). Moreover, the pervasive recrystallized dolomite Im displays a slightly flattened pattern compared to the unaltered dolomite Ivf. This is due to a more pronounced depletion in light REE (LREE, 7 to 14 times those of the dolomite Ivf), compared to the heavy REE (HREE, only 4 to 6 times).

The WSD are markedly depleted in LREE, particularly in Ce, and display REE patterns similar to that of the pervasive altered DRD (Fig. 4.7b). Similar LREE-depleted patterns compared to the host dolostones were found in hydrothermal carbonates at the MVT deposits in the Viburnum Trend, southeast Missouri (Graf, 1984). The late filling dolomite exhibits two types of REE patterns (Fig. 4.7b). One type (IIIAd) is essentially similar to the REE patterns of the white sparry dolomite, and the other type (IIIBd) shows a flatter HREE distribution without Ce anomaly. Furthermore, the La/Yb ratio of the hydrothermal dolomites (Table 4.5) decreases in the order: DRD, WSD, LFDA, LFDB (3.22, 2.62, 0.56, 0.08). This indicates a trend towards more fractionated precipitates with advancing mineralization. The REE patterns and abundances of the late filling calcite vary extensively in slope, from strongly negative to weakly positive (Fig. 4.7c). The differences in texture,

Table 4.3. REE concentrations (in μg/g) in carbonates from San Vicente measured by ICP-MS and by INAA

Sample	Carbonate[2]	Value[1]	La	Ce	Pr	Nd	Sm	Eu	Gd	Tb	Dy	Ho	Er	Tm	Yb	Lu	IR[2]
		a LLD	0.05	0.05	0.05	0.05	0.03	0.05	0.05	0.05	0.05	0.03	0.05	0.05	0.05	0.03	wt.%)
		b LLD	0.1	1		3	0.01	0.05		0.1					0.05	0.01	
FSV-1101	UL	a	16.1	26.4	3.45	13.3	2.86	0.53	2.80	0.42	2.44	0.48	1.44	0.19	1.22	0.18	39.9
		b	17.3	33	-	14	2.77	0.59	-	0.4	-	-	-	-	1.47	0.22	
		c	-7.4	-25.0		-5.2	3.2	-11.3		0					-20.5	-22.2	
FSV-1103	UL	a	17.7	26.5	3.43	13.1	2.76	0.58	2.72	0.42	2.46	0.50	1.45	0.19	1.22	0.18	36.1
		b	18.4	34	-	14	2.66	0.52	-	0.4	-	-	-	-	1.48	0.22	
		c	-4.0	-28.3		-6.9	3.6	10.3		0					-21.3	-22.2	
FSV-801	DRD (Ivf)	a	2.63	4.06	0.54	1.75	0.35	0.08	0.32		0.23	0.04	0.12		0.09		6.2
		b	2.8	5	-		0.43	0.14	-		-	-	-	-	0.05		
		c	-6.5	-23.2			-22.9	-75.0							44.4		
FSV-020	DRD (Ivf)	a	1.51	2.66	0.42	1.53	0.32	0.07	0.34	0.05	0.28	0.06	0.16		0.12		8.1
		b	1.5	3	-		0.34	0.18	-		-	-	-	-	0.14	0.02	
		c	0.7	-12.8			-6.3	-157							-16.7		
FSV-853	DRD (If)	a	1.45	2.43	0.37	1.06	0.22		0.19		0.14		0.08		0.09		2.7
		b	1.5	3	-		0.23	0.15	-		-	-	-	-	0.11	0.02	
		c	-3.4	-23.5			-4.5								-22.2		
FSV-905	DRD (Im)	a	0.79	0.81	0.20	0.35	0.07		0.08		0.07						2.1
		b	0.6	1	-		0.06	0.15	-		-	-	-	-			
		c	24.1	-23.5			14.3										
FSV-869	WSD (II)	a	0.61	0.66	0.20	0.41	0.11		0.10		0.09						1.2
		b	0.3		-		0.10	0.12	-		-	-	-	-	0.05		
		c	50.8				9.1								-15		
FSV-714	LFD (IIId)	a	0.68	0.82	0.20	0.41	0.09		0.10		0.10		0.07		0.07		0.0
		b	0.4	1	-		0.07	0.11	-		-	-	-	-	0.07	0.01	
		c	41.2	-22.0			22.2								0.0		
FSV-902m	LFC (IIIc)	a	0.30	1.70	0.30	1.80	0.60	0.17	0.70	0.10	1.00	0.22	0.60		0.60	0.09	0.0
		b	0.3	1	-		0.50	0.25	-	0.1	-	-	-	-	0.53	0.08	
		c	0.0	41.2			16.7	-47.1		0.0					11.7	11.1	

[1]UL = bituminous silty Uncush limestone; DRD = dark replacement dolomite ("Ivf" very fine-grained, "If" fine-grained, "Im" medium grained); WSD = white sparry dolomite (II); LFD = late filling dolomite (IIId); LFC = late filling calcite (IIIc); EPc = calcite replacing evaporitic sulfate.

[2] a = ICP-MS; b = INAA; LLD = lower limit of detection; c = relative difference = [(a-b)/a]·100.

[3] Insoluble residue

- = not analyzed

blank = not detected

Table 4.4. Rare earth element abundances (in μg/g) of the acid soluble fraction of the carbonates from the San Vicente deposit

Sample	Carbonate[1]	Lith.[2]	Manto[3]	Y	La	Ce	Pr	Nd	Sm	Eu	Gd	Tb	Dy	Ho	Er	Tm	Yb	Lu
Chon.[4]					*0.315*	*0.813*	*0.1*	*0.597*	*0.192*	*0.072*	*0.259*	*0.049*	*0.325*	*0.072*	*0.213*	*0.032*	*0.209*	*0.032*
NASC[5]				*27.0*	*32*	*73*	*7.9*	*33*	*5.7*	*1.24*	*5.2*	*0.85*	*5.8*	*1.04*	*3.4*	*0.5*	*3.1*	*0.48*
FSV-015	UL	UL		22.0	14.9	19.9	2.83	10.8	2.29	0.49	2.38	0.37	2.22	0.47	1.40	0.19	1.18	0.18
FSV-1101	UL	UL		20.4	16.1	26.4	3.45	13.3	2.86	0.53	2.80	0.42	2.44	0.48	1.44	0.19	1.22	0.18
FSV-1103	UL	UL		21.4	17.7	26.5	3.43	13.1	2.76	0.58	2.72	0.42	2.46	0.50	1.45	0.19	1.22	0.18
FSV-801	DRD (Ivf)	AD	Alfon.	1.5	2.63	4.06	0.54	1.75	0.35	0.08	0.32		0.23	0.04	0.12		0.09	
FSV-020	DRD (Ivf)	SVD	3i	2.4	1.51	2.66	0.42	1.53	0.32	0.07	0.34	0.05	0.28	0.06	0.16		0.12	
FSV-423	DRD (If)	SVD	1	0.7	1.10	1.52	0.28	0.64	0.13		0.13		0.13		0.06		0.06	
FSV-853	DRD (If)	SVD	SVt	0.7	1.45	2.43	0.37	1.06	0.22		0.19		0.14		0.08		0.09	
FSV-905	DRD (Im)	SVD	Ayala	0.5	0.79	0.81	0.18	0.35	0.07		0.08		0.07					
FSV-718	DRD (Im)	SJD	SJ	0.7	0.51	0.24	0.15	0.14	0.05		0.06		0.07					
FSV-654	WSD	AD	Alfon.	0.6	0.81	0.73	0.19	0.28	0.06		0.08		0.06					
FSV-806	WSD	AD	Alfon.		0.41	0.23	0.13	0.11	0.03									
FSV-661	WSD	SVD	Jesus	0.3	0.54	0.45	0.14	0.22	0.05		0.05							
FSV-919	WSD	SVD	Ayala	1.0	0.38	0.45	0.14	0.31	0.09		0.11		0.13		0.09		0.10	
FSV-869	WSD	SVD	SVt	0.5	0.61	0.61	0.20	0.41	0.11		0.13		0.09					
FSV-919	LFD (IIIAd)	SVD	Ayala	1.2	0.31	0.34	0.11	0.23	0.08		0.10		0.14	0.04	0.12		0.15	
FSV-714	LFD (IIIAd)	SJD	SJ	0.7	0.68	0.81	0.20	0.41	0.09		0.12		0.08		0.07		0.07	
FSV-695	LFD (IIIBd)	SVD	1455	0.7	0.07	0.33	0.07	0.17	0.07		0.08		0.09				0.09	
FSV-1092	LFD (IIIBd)	SVD	1455	1.0	0.09	0.30	0.07	0.21	0.05		0.09		0.18		0.10		0.07	
FSV-665	LFC (IIIAc)	AD	Alfon.	1.0	0.66	0.46	0.22	0.37	0.16		0.15		0.14		0.06			
FSV-857	LFC (IIIAc)	SVD	SVt	0.7	0.54	0.54	0.24	0.44	0.12		0.11		0.08					
FSV-856	LFC (IIIAc)	SVD	SVt	-	0.12	0.32	0.11	0.29	0.09	0.06	0.10		0.10					
FSV-902c	LFC (IIIBc)	SVD	Ayala	24.0	0.69	0.86	0.36	1.22	1.09	0.38	1.91	0.45	2.76	0.52	1.25	0.14	0.64	0.08
FSV-902m	LFC (IIIBc)	SVD	Ayala	9.0	0.34	1.71	0.32	1.79	0.57	0.17	0.70	0.09	1.01	0.22	0.62		0.60	0.09
FSV-423	EPc	SVD	Jesus	4.9	0.41	1.89	0.28	1.73	0.41	0.10	0.41		0.49	0.12	0.40		0.30	
FSV-904	EPc	SVD	Jesus	3.0	0.32	1.62	0.31	1.38	0.32	0.07	0.32		0.32	0.07	0.20		0.20	

[1]UL = bituminous silty Uncush limestone; DRD = dark replacement dolomite ("Ivf" very fine-grained, "If" fine-grained, "Im" medium grained); WSD = white sparry dolomite (II); LFD = late filling dolomite (IIId); LFC = late filling calcite (IIIc); EPc = calcite replacing evaporitic sulfate.

[2] Lithologies: AD=Alfonso Dolomite; UL=Bituminous silty Uncush Limestone; SVD=San Vicente Dolomite; SJD=San Judas Dolomite.

[3] Manto name in the San Vicente main deposit (Alfon. = Alfonso; SVt = San Vicente techo).

[4] Chondrite-normalizing values from Hanson (1980).

[5] North American shale composite values from Haskin et al. (1966).

- = not analyzed

blank = not detected

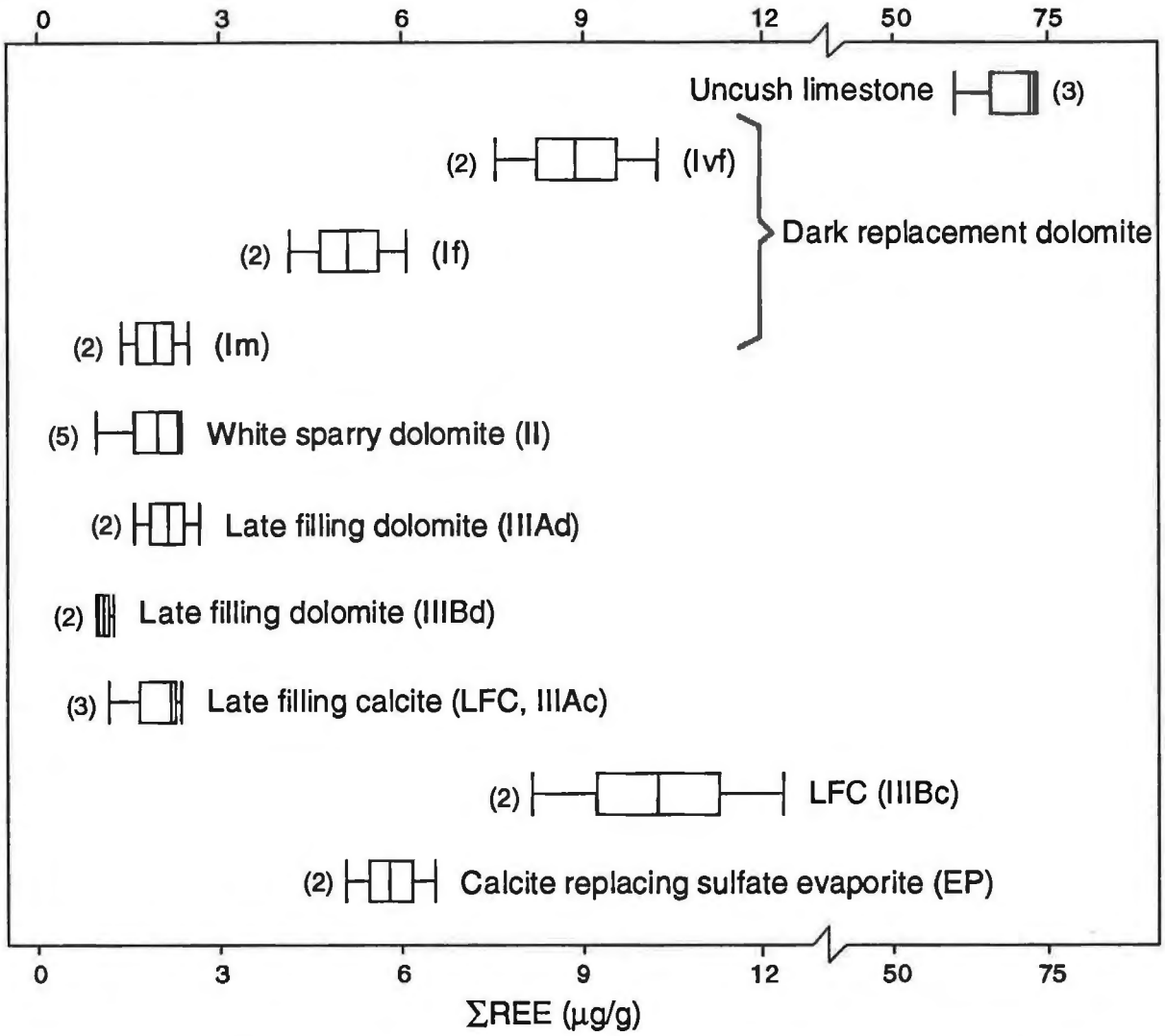

Figure 4.6. Ranges and medians of the total rare earth element abundance of the carbonates from San Vicente deposit. UL = bituminous silty Uncush limestone; DRD = dark replacement dolomite ("Ivf" very fine-grained, "If" fine-grained, "Im" medium-grained); WSD = white sparry dolomite (II); LFD = late filling dolomite (IIIAd and IIIBd); LFC = late filling calcite (IIIAc and IIIBc); EPc = calcite replacing evaporitic sulfate.

Figure 4.7. a) Chondrite-normalized REE abundances in Uncush limestone and subgenerations of dark replacement dolomite (DRD) from the San Vicente deposit. Compare to North American shale composite (NASC). The REE patterns of the host dolomite (Ivf) are similar in the different dolomite units: AD = Alfonso Dolomite; SVD = San Vicente Dolomite; SJD = San Judas dolomite. The REE-trend X-Y reflects the degree of replacement of the host dolomite. **b)** Chondrite-normalized REE abundances in the white sparry dolomite (II) and the late filling dolomite (IIId). Compared with the REE patterns of the host dark replacement dolomite (Ivf). Note that the HREE pattern of the late dolomite IIIA and IIIB have a positive slope. The dolomites IIIB are depleted in La. **c)** Chondrite-normalized REE abundances in the late filling calcites (IIIAc and IIIBc), and carbonates replacing evaporitic sulfates (EPc). Compare with the REE patterns of the host dark replacement dolomite (Ivf). The late calcites IIIB have a concave-up pattern. See text for explanation. **d)** Median REE patterns of the Uncush limestone, and the hydrothermal carbonates normalized to the very fine replacement dolomite (Ivf). WSD = white sparry dolomite (II); LFD = late filling dolomite (IIIAd and IIIBd); LFC = late filling calcite (IIIAc and IIIBc); EPc = calcite replacing evaporitic sulfate. See text for explanation.

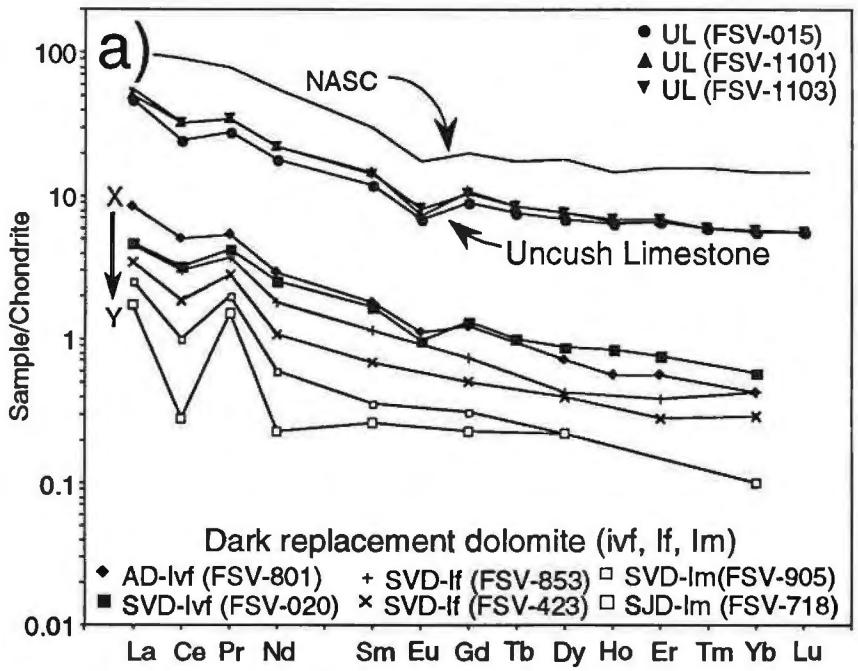
a)
NASC
UL (FSV-015)
UL (FSV-1101)
UL (FSV-1103)
X
Y
Uncush Limestone
Sample/Chondrite
Dark replacement dolomite (ivf, If, Im)
AD-Ivf (FSV-801)
SVD-Ivf (FSV-020)
SVD-If (FSV-853)
SVD-If (FSV-423)
SVD-Im(FSV-905)
SJD-Im (FSV-718)
La Ce Pr Nd Sm Eu Gd Tb Dy Ho Er Tm Yb Lu

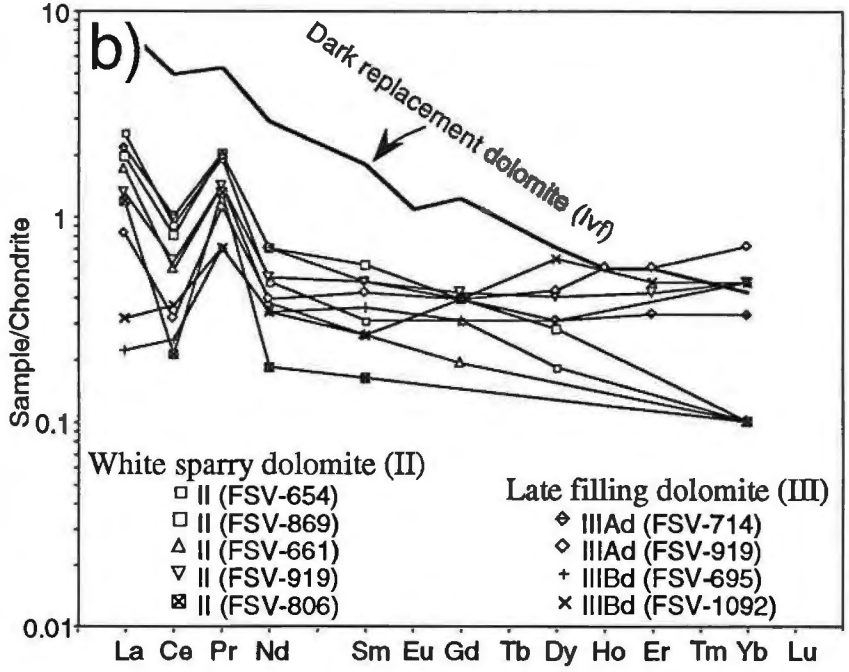
b)
Dark replacement dolomite (Ivf)
Sample/Chondrite
White sparry dolomite (II)
II (FSV-654)
II (FSV-869)
II (FSV-661)
II (FSV-919)
II (FSV-806)
Late filling dolomite (III)
IIIAd (FSV-714)
IIIAd (FSV-919)
IIIBd (FSV-695)
IIIBd (FSV-1092)
La Ce Pr Nd Sm Eu Gd Tb Dy Ho Er Tm Yb Lu

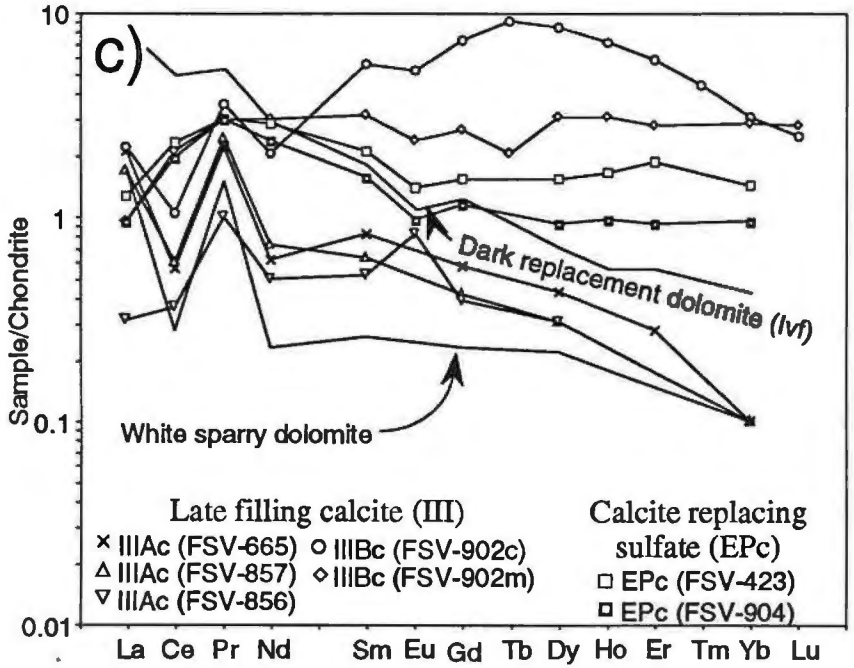
c)
Dark replacement dolomite (Ivf)
White sparry dolomite
Sample/Chondrite
Late filling calcite (III)
IIIAc (FSV-665)
IIIAc (FSV-857)
IIIAc (FSV-856)
IIIBc (FSV-902c)
IIIBc (FSV-902m)
Calcite replacing sulfate (EPc)
EPc (FSV-423)
EPc (FSV-904)
La Ce Pr Nd Sm Eu Gd Tb Dy Ho Er Tm Yb Lu

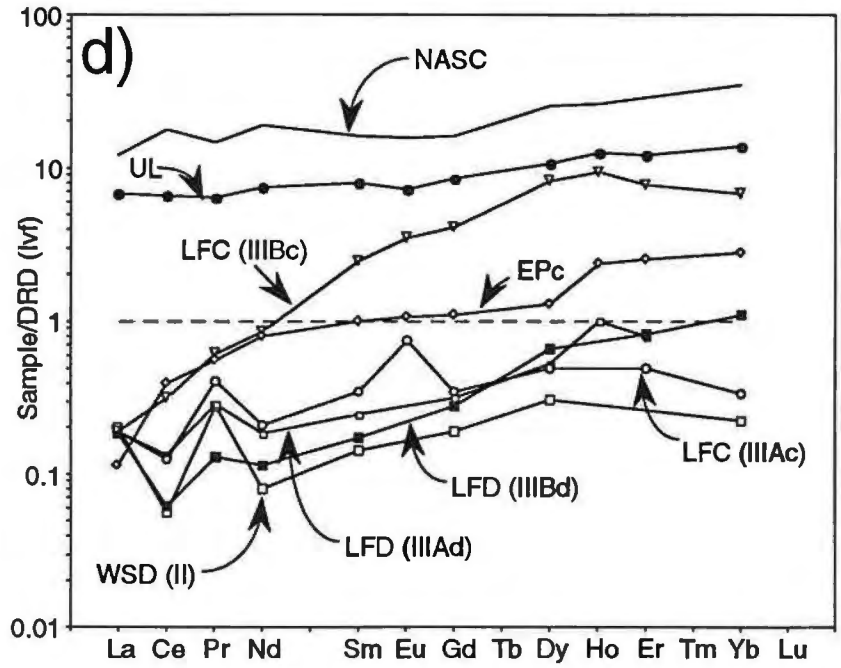
d)
NASC
UL
LFC (IIIBc)
EPc
LFC (IIIAc)
LFD (IIIBd)
LFD (IIIAd)
WSD (II)
Sample/DRD (Ivf)
La Ce Pr Nd Sm Eu Gd Tb Dy Ho Er Tm Yb Lu

color and mineralogical assemblages of these LFC correlate with the REE patterns. Three samples of the translucent calcite filling voids in the DRD (samples IIIAc in Fig. 4.7c and Table 4.4) have REE patterns roughly similar to those of the white sparry dolomite. Two of these samples (FSV-665 and FSV-857) are calcite intergrown with sphalerite III cementing dissolution-breccias. They are depleted in Ce ($Ce/Ce^* = 0.28$) and their Eu content is lower than the detection limit. The other sample (FSV-856) is also depleted in LREE ($La/Sm = 0.18$, $Ce/Ce^* = 0.52$) but has a significant positive Eu anomaly ($Eu/Eu^* = 2.63$). The calcite from a large vein in the hydraulic breccia (samples IIIBc in Fig. 4.7c and Table 4.4) shows a pronounced enrichment in REE, with REE contents 1 to 10 times greater than chondrite. In contrast to the other hydrothermal carbonates the REE patterns of these calcites are characterized by a steep increase of the LREE. Calcite sampled at the margin of the vein (sample FSV-902m), only few millimeters away from the contact with the host DRD, has a flat HREE pattern, in contrast to the calcite from the vein center (FSV-902c) which is strongly enriched in middle REE (MREE). In this latter sample enrichments in MREE and HREE are more pronounced than those in LREE, resulting in an overall concave-up REE pattern. In addition the calcite at the center of the vein exhibits a terbium maximum, and the calcite at the margin a minimum. As discussed by Möller (1983), the presence of a Tb maximum in Ca minerals point to an acidic parent solution, and the Tb minimums to an alkaline. Thus, the Tb enrichment indicate, that the calcite at the center was crystallized from a more acidic (less rock-buffered) fluid. The two samples show a slightly positive Eu anomaly ($Eu/Eu^* = 1.12$) compared to the North America shales composite (Table 4.5). The calcites replacing evaporitic sulfate have the flattest chondrite-normalized REE patterns (Fig. 4.7c), and are slightly enriched in Ce ($Ce/Ce^* = 1.03$) and Eu ($Eu/Eu^* = 1.06$). The REE signature is comparable to that of the late filling translucent calcites IIIB near the contact with the DRD. These calcites are characterized by a pronounced enrichment in MREE and HREE relative to LREE and a small but still significant positive Eu anomaly ($Eu/Eu^* = 1.02$ to 1.14). Tassé and Bergeron (1991) reported slight positive Eu anomalies ($Eu/Eu^* = 1.28$) in carbonates replacing anhydrite, likely formed during thermochemical sulfate reduction, in an evaporitic dolostone unit of the lower ordovician Beekmantown Group, Québec.

The REE patterns normalized to the average host dolostone (Ivf) are shown in Fig. 4.7d. This normalization procedure eliminates the REE distribution-characteristics inherited from the host rock. Thus the deviations of the REE distribution in the hydrothermal carbonates reflect the diagenetic processes, including the ore-forming events.

All the hydrothermal carbonates are markedly depleted in LREE compared to HREE. The WSD and LFD show pronounced negative Ce anomalies, suggesting that the incoming ore-fluid was depleted in LREE, and particularly in Ce. Furthermore, the extensive depletion of the ore-stage dolomites compared to the host dolomite indicate that no compositional resetting (REE enrichment) took place between the ore fluid and the REE-rich Uncush limestone. This is consistent with the stable isotope evidence against considering the less permeable bituminous silty Uncush Limestone as a source or channel-pathway of the ore fluid (Spangenberg, 1995).

4.5.2.2 San Vicente district

The REE concentrations and the NASC-normalized REE ratios for the carbonate samples from the San Vicente district are given in Table 4.6 and 4.7. The chondrite-normalized REE diagrams are shown in Fig. 4.8. The hydrothermal dolomites are extremely poor in most REE, and several values are below the analytical detection limit. Nevertheless, certain trends seem to be present.

The REE patterns of the Uncush limestone in "Vilcapoma" and "Quebrada Utcuyacu" have shapes similar to the samples of the same stratigraphic unit in the San Vicente mining area (Fig. 4.8a). The REE abundance of the UL is markedly higher in "Vilcapoma" relative to San Vicente and "Quebrada Utcuyacu" (VI: 126.2 µg/g, SV: 71.8 µg/g, QU: 67.9 µg/g). The REE patterns of the dark replacement dolomite from five localities are roughly parallel to the pattern of the San Vicente deposit (Fig. 4.8b). The altered DRD (If, Im) in the regional-scale samples do *not have a Ce anomaly*, differing in this strongly from the samples from San Vicente. The samples of "Vilcapoma" and "Sillapata" are characterized by higher REE abundance compared to the DRD in San Vicente mine, indicating a minor degree of hydrothermal alteration. The minimum in Tb in the DRD from "Sillapata" suggest more

Table 4.5. REE-ratios[1] for the different generations of carbonates in San Vicente deposit normalized to North American shale composite

Sample	Carbonate[2]	ΣREE (µg/g)	Ce/Nd (SN)	La/Yb (SN)	La/Sm (SN)	Sm/Yb (SN)	Ce/Ce* (SN)	Eu/Eu* (SN)	Eu* (SN)
FSV-015	UL	59.6	0.83	1.22	1.16	1.06	0.66	0.92	0.53
FSV-1101	UL	71.8	0.90	1.28	1.00	1.27	0.77	0.82	0.64
FSV-1103	UL	73.2	1.14	1.41	1.14	1.23	0.74	0.93	0.62
median	UL	71.8	0.90	1.28	1.14	1.23	0.74	0.92	
FSV-801	DRD (Ivf)	10.2	1.05	2.83	1.34	2.12	0.74	1.05	0.08
FSV-020	DRD (Ivf)	7.5	0.79	1.22	0.84	1.45	0.73	0.93	0.08
median	DRD (Ivf)	8.9	0.92	2.02	1.09	1.78	0.73	0.99	
FSV-423	DRD (If)	4.0	1.07	1.78	1.51	1.18	0.60		0.03
FSV-853	DRD (If)	6.0	1.04	1.56	1.17	1.33	0.72		0.05
median	DRD (If)	5.0	1.06	1.67	1.34	1.25	0.66		
FSV-905	DRD (Im)	2.4	1.05	3.83	2.01	1.90	0.44		0.02
FSV-718	DRD (Im)	1.3	0.74	2.62	1.92	1.36	0.18		0.02
median	DRD (Im)	1.8	0.90	3.22	1.96	1.63	0.31		
FSV-654	WSD (II)	2.23	1.18	3.92	2.40	1.63	0.41		0.02
FSV-806	WSD (II)	0.83	0.70	1.79	2.20	0.82	0.17		0.03
FSV-661	WSD (II)	1.47	0.92	2.62	1.92	1.36	0.36		0.02
FSV-919	WSD (II)	1.86	0.74	0.40	0.81	0.49	0.44		0.03
FSV-869	WSD (II)	2.20	0.73	2.95	0.99	2.99	0.41		0.03
median	WSD (II)	1.9	0.74	2.62	1.92	1.36	0.41		
FSV-919	LFD (IIIAd)	1.49	0.51	0.17	0.58	0.29	0.32		0.03
FSV-714	LFD (IIIAd)	2.54	0.90	0.94	1.35	0.70	0.48		0.03
median	LFD (IIIAd)	2.0	0.70	0.56	0.96	0.5	0.40		
FSV-695	LFD (IIIBd)	0.89	0.45	0.07	0.18	0.38	0.50		
FSV-1092	LFD (IIIBd)	1.22	0.68	0.10	0.36	0.27	0.69		
median	LFD (IIIBd)	1.0	0.56	0.08	0.27	0.32	0.59		
FSV-665	LFC (IIIAc)	2.24	0.56	3.20	0.73	4.35	0.26		0.05
FSV-857	LFC (IIIAc)	2.06	0.50	2.62	0.80	3.26	0.28		0.04
FSV-856	LFC (IIIAc)	1.06	0.45	-	0.18	-	0.52	2.63	0.03
median	LFC (IIIAc)	2.06	0.50	2.91	0.73	3.80	0.28	*2.63*	
FSV-902c	LFC (IIIBc)	12.35	0.32	0.10	0.11	0.93	0.35	1.10	0.47
FSV-902m	LFC (IIIBc)	8.18	0.43	0.05	0.09	0.54	0.98	1.14	0.21
median	LFC (IIIBc)	10.2	0.38	0.08	0.10	0.73	0.88	1.12	
FSV-423	EPc	6.52	0.51	0.13	0.18	0.73	1.03	1.10	0.13
FSV-904	EPc	5.04	0.52	0.15	0.18	0.82	0.93	1.02	0.10
median	EPc	5.8	0.51	0.14	0.18	0.78	1.03	1.06	

[1] $(Ce/Nd)_{SN}$ = extent of Ce depletion; $(La/Yb)_{SN}$ = fractionation of LREE from the HREE; $(La/Sm)_{SN}$ = fractionation of the LREE; $(Sm/Yb)_{SN}$ = fractionation of the HREE; $(Eu/Eu^*)_{SN} = Eu_{SN}/[0.5 \cdot (Sm_{SN} + Gd_{SN})]$ values >1 positive anomaly, <1 negative anomaly, =1 no anomaly; $(Ce/Ce^*)_{SN} = Ce_{SN}/[0.5 \cdot (La_{SN} + Pr_{SN})]$;

[2] UL = bituminous silty Uncush limestone; DRD = dark replacement dolomite ("Ivf" very fine-grained, "If" fine-grained, "Im" medium-grained); WSD = white sparry dolomite (II); LFD = late filling dolomite (IIId); LFC = late filling calcite (IIIc); EPc = calcite replacing evaporitic sulfate

acidic pore solutions.

The samples of WSD are extremely depleted in rare earth elements (1.6 to 2.7 µg/g) with REE concentrations mostly below the analytical detection limit (Fig. 4.8c). However, the following features can be recognized: (1) the REE contents and overall patterns of the district samples are roughly similar to the samples in the main San Vicente deposit; (2) the absence of negative Ce anomalies in the WSD of the district-samples (Ce/Ce* = 0.72 to 1.00) is the only outstanding difference with the WSD of the San Vicente deposit (Ce/Ce* = 0.17 to 0.44); (3) one sample of "Q. Piñón" shows a significant enrichment in MREE, which is characteristic of the late filling dolomites IIIB from San Vicente.

In summary, the REE patterns of the ore stage dolomites excepting the behavior of Ce and Eu are mostly similar in samples at district (Fig. 4.8) and deposit scale (Fig. 4.7). This supports the stable isotope evidence (Spangenberg et al., 1994, 1995b) of a common

Table 4.6. Rare earth element abundances (in μg/g) of the acid soluble fraction of the carbonates from the San Vicente district (excluding data from the San Vicente deposit)

Sample	Loc.[1]	Lith.[2]	Carbonate[3]	Y	La	Ce	Pr	Nd	Sm	Eu	Gd	Tb	Dy	Ho	Er	Tm	Yb	Lu
Chon.[4]					*0.315*	*0.813*	*0.1*	*0.597*	*0.192*	*0.072*	*0.259*	*0.049*	*0.325*	*0.072*	*0.213*	*0.032*	*0.209*	*0.032*
NASC[5]				*27.0*	*32*	*73*	*7.9*	*33*	*5.7*	*1.24*	*5.2*	*0.85*	*5.8*	*1.04*	*3.4*	*0.5*	*3.1*	*0.48*
FSV-684	QP	SVD	DRD (Ivf)	1	1.50	3.40	0.40	1.80	0.40	0.08	0.30		0.20		0.20		0.10	
FSV-685	QP	SVD	DRD (Ivf)	4	0.60	1.30	0.20	1.60	1.50	0.41	1.40	0.20	0.90		0.30		0.30	
FSV-984	QP	SVD	WSD (II)		0.10	0.30		0.20										
FSV-985	QP	SVD	WSD (II)	3	0.40	0.80	0.10	0.50	0.20	0.06	0.30		0.20		0.10			
FSV-681	SI	SVD	DRD (Ivf)	3	4.00	9.70	1.20	4.80	1.20	0.24	1.00	0.10	0.90	0.16	0.40		0.40	0.06
FSV-682	SI	SVD	EPc	1	2.00	4.20	0.50	1.60	0.20	0.08	0.30		0.20					
FSV-1059	QU	UL	UL	20	15.4	24.9	3.00	12.1	2.70	0.55	2.70	0.40	2.50	0.51	1.50	0.20	1.30	0.18
FSV-754	CH	SJD	DRD (Ivf)	1	0.40	0.70		0.50	0.10		0.20		0.10					
FSV-754	CH	SJD	WSD (II)		0.40	0.60		0.30										
FSV-754	CH	SJD	LFD (IIId)	11	8.00	24.2	3.30	13.4	2.70	0.85	2.30	0.30	1.70	0.33	0.90	0.10	0.70	0.09
FSV-759	CH	SVD	DRD (Ivf)			0.30		0.30	0.10		0.10		0.10					
FSV-759	CH	SVD	WSD (II)		0.30	0.80	0.10	0.50	0.10		0.10		0.10					
FSV-753	CH	SVD	WSD (II)			0.20		0.20	0.06		0.08		0.06				0.02	
FSV-982	CH	SVD	LFC (IIIc)		0.10	0.40		0.30										
FSV-1097	VI	UL	UL	55	17.4	33.3	7.20	33.3	7.80	1.55	7.80	1.20	7.30	1.49	4.00	0.50	2.90	0.43
FSV-1098	VI	SVD	DRD (Ivf)	9	2.50	7.90	1.30	6.60	1.90	0.40	1.80	0.30	1.70	0.32	0.80	0.10	0.60	0.09
FSV-891	QS	UL	UL	1	1.10	2.10	0.20	0.90	0.20		0.20		0.20		0.10			
FSV-689	PI	CD	DRD (Ivf)	2	0.80	1.70	0.20	1.00	0.20		0.20		0.20		0.10			
FSV-691	PI	CD	DRD (Ivf)		0.50	0.90	0.10	0.40	0.10									
FSV-693	PI	SVD	WSD (II)		0.30	0.50		0.20										
FSV-694	PI	SVD	WSD (II)		0.50	0.90		0.30										

[1] The location of the sample sites is shown in Fig. 1

[2] Lithologies: AD = Alfonso Dolomite; UL = Bituminous silty Uncush Limestone; SVD = San Vicente Dolomite; SJD = San Judas Dolomite

[3] UL = bituminous silty Uncush limestone; DRD = dark replacement dolomite ("Ivf" very fine-grained, "If" fine-grained, "Im" medium grained); WSD = white sparry dolomite (II); LFD = late filling dolomite (IIId); LFC = late filling calcite (IIIc); EPc = calcite replacing evaporitic sulfate

[4] Chondrite-normalizing values from Hanson (1980)

[5] North American shale composite values from Haskin et al. (1966)

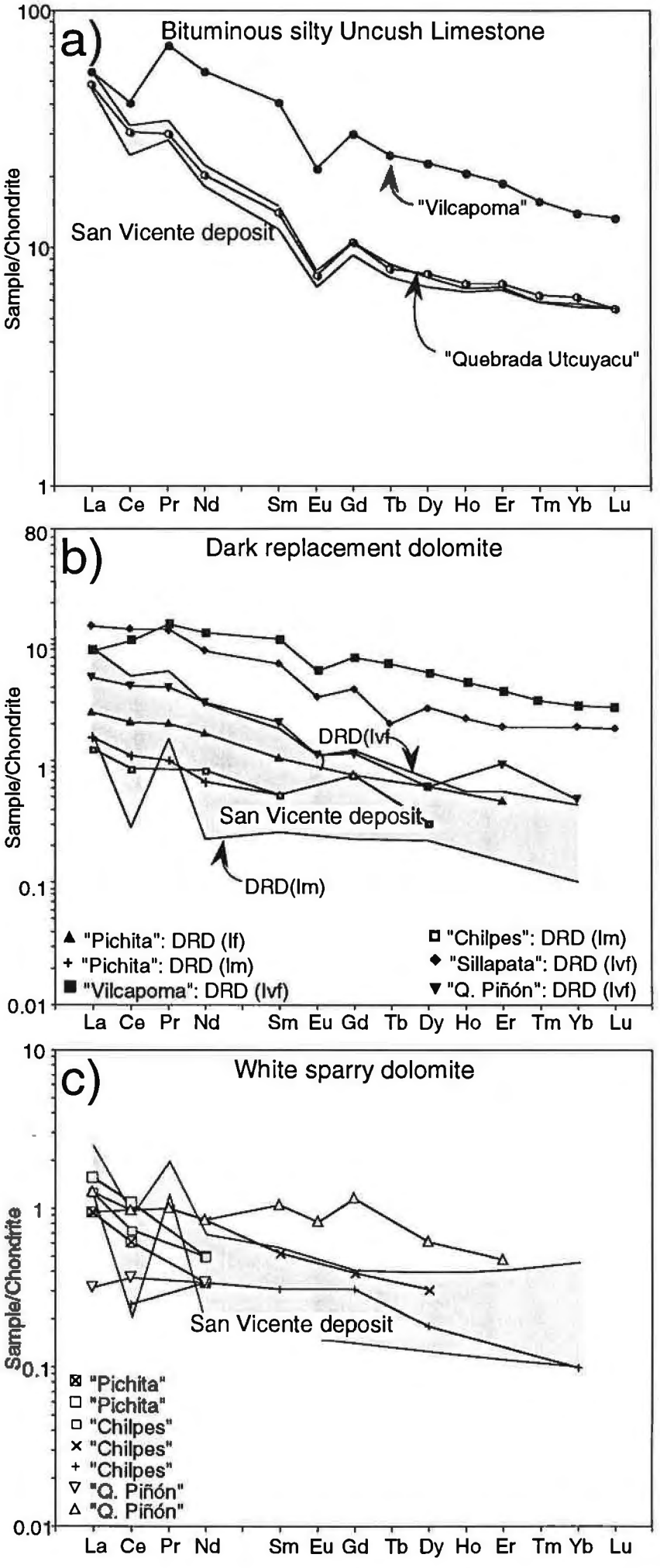
a)
Bituminous silty Uncush Limestone
Sample/Chondrite
100
10
1
San Vicente deposit
"Vilcapoma"
"Quebrada Utcuyacu"
La Ce Pr Nd Sm Eu Gd Tb Dy Ho Er Tm Yb Lu
b)
Dark replacement dolomite
80
10
1
0.1
0.01
DRD(lvf)
San Vicente deposit
DRD(lm)
"Pichita": DRD (lf)
"Pichita": DRD (lm)
"Vilcapoma": DRD (lvf)
"Chilpes": DRD (lm)
"Sillapata": DRD (lvf)
"Q. Piñón": DRD (lvf)
La Ce Pr Nd Sm Eu Gd Tb Dy Ho Er Tm Yb Lu
c)
White sparry dolomite
10
1
0.1
0.01
San Vicente deposit
"Pichita"
"Pichita"
"Chilpes"
"Chilpes"
"Chilpes"
"Q. Piñón"
"Q. Piñón"
La Ce Pr Nd Sm Eu Gd Tb Dy Ho Er Tm Yb Lu

hydrothermal system controlling the chemistry of the carbonates of the San Vicente district.

Depletion in LREE (La/Sm) and HREE (Sm/Yb) in carbonates do not show any clear regional trends within the San Vicente belt (Table 4.7). The great scatter shown by the elemental ratios La/Sm, Sm/Yb, and Ce/Nd of the hydrothermal dolomites (DRD, WSD) probably resulted of fluctuation of the pore-fluid chemistry (see below). Further work is necessary to explain the absence of negative Ce anomalies in the ore-stage dolomites at the district scale compared those found at the main deposit.

The depletion in LREE (La/Sm) and particularly in cerium (Ce/Nd) of the hydrothermal carbonates correlate with the carbon ($r_{(\delta^{13}C\text{-La/Sm})} = 0.53$, $r_{(\delta^{13}C\text{-Ce/Nd})} = 0.67$) and oxygen ($r_{(\delta^{18}O\text{-La/Sm})} = 0.53$, $r_{(\delta^{18}O\text{-Ce/Nd})} = 0.68$) isotope ratios (Table 4.8). Yttrium correlates positively with the total REE content ($r_{(\Sigma REE\text{-Y})} = 0.87$) reflecting the similar geochemical behaviour of Y and the REE.

4.6 Discussion

The incorporation of minor and trace elements (including REE) into Ca-Mg-carbonates is controlled by the distribution coefficient D_{TE}:

$$D_{TE} = (C_{TE}/C_M)_c/(C_{TE}/C_M)_f$$

where C is the concentration of the trace element (TE) or the major cation (M, Ca + Mg in the case of dolomites) in the carbonate (c) or in the fluid (f). If $D > 1$ the trace element is preferentially enriched in the precipitate relative to the major cation, whereas if $D < 1$ the trace element will concentrate in the fluid during progress of carbonate-precipitation (Veizer, 1983a). The few reliable distribution coefficients for carbonates at diagenetic temperatures which are available for minor and trace elements (Veizer, 1983b; Kretz, 1982) indicate that the coefficients of Fe, Mn, and Zn are greater than one ($D_{Fe} = 1.18\text{-}23.6$; $D_{Mn} = 6.37\text{-}38.1$; $D_{Zn} = 23.8\text{-}95.2$), and for Mg, Sr, Na, and Ba smaller than one ($D_{Mg} = 0.03\text{-}0.21$; $D_{Sr} = 0.012\text{-}0.2$; $D_{Na} \leq 0.00003$; $D_{Ba} = 0.05\text{-}0.22$). The apparent distribution values for the REE in foraminiferal calcite are greater than one, and generally (excluding Ce) they decrease with the ionic radii from $D_{La} = 125$ to $D_{Yb} = 73$ (Palmer, 1985). Moreover, the distribution of the trace elements is influenced by the sorption on the carbonate surface (Zachara et al., 1991), the concentration of the complexing ligands (Brookins, 1989; Cantrell and Byrne, 1987; Möller, 1991; Stanley and Byrne, 1990; Terakado and Masuda, 1988), and the precipitation rate (Lorens, 1981). Recently, Vahrencamp and Swart (1990) have suggested that Sr distribution coefficient in dolomite is dependent on the stoichiometry.

4.6.1 Mg, Fe, Mn, Sr, Na and Zn in the hydrothermal carbonates

The measured gain in Mg of the hydrothermal dolomites (Fig. 4.3) would require a high Mg/Ca ratio in the incoming fluid, suggesting that magnesium was incorporated into the fluid during interaction with the path-through rocks. Possible sources of Mg would be the conversion of high-Mg to low Mg-calcite, dedolomitization of Ca-rich dolomites, and conversion of smectite to illite (e.g., Pingitore, 1978; Richter, 1974; Leuchs, 1985; McHargue and Price, 1982). The incoming fluid is thought to have leached underlying detrital rocks (Fontboté and Gorzawsky, 1990, Moritz et al, in press), and breakdown of smectite could be the local source for Mg. The transformation of smectite to illite produce significant quantities of Fe^{2+} and Na^{+} (e.g., McHargue and Price, 1982). The depletion of iron and slightly enrichment of sodium ($D_{Fe} > 1$, $D_{Na} < 1$) of the hydrothermal dolomites (Fig. 4.4) support breakdown of smectite as a Mg source, whereby Fe of the smectite would be immobilized in oxidizing conditions (see below).

Figure 4.8. Chondrite-normalized REE abundances in the **a)** bituminous silty Uncush Limestone, **b)** dark replacement dolomite, **c)** white sparry dolomite from the San Vicente district. Compare with the field defined by the samples from San Vicente mine. See Fig. 4.1 for location of the sample sites.

Table 4.7. REE-ratios[1] of the carbonate samples from the San Vicente district normalized to North American shale composite. The median values of the carbonates from the San Vicente deposit are given for comparison

Sample	Loc.[2]	Carbonate[3]	ΣREE (µg/g)	La/Yb (SN)	La/Sm (SN)	Sm/Yb (SN)	Ce/Nd (SN)	Ce/Ce* (SN)	Eu/Eu* (SN)	Eu* (SN)
FSV-684	QP	DRD (Ivf)	8.4	1.45	0.67	2.18	0.85	0.94	1.01	0.08
FSV-685	QP	DRD (Ihb)	8.7	0.19	0.07	2.72	0.37	0.62	-	-
FSV-984	QP	WSD (II)	0.6	-	-	-	0.68	1.00	-	-
FSV-985	QP	WSD (II)	2.7	-	0.36	-	0.72	0.82	1.04	0.06
FSV-681	SI	DRD (Ihb)	24.2	0.97	0.59	1.63	0.91	1.01	0.96	0.25
FSV-682	SI	EPc	9.1	-	1.78	-	1.19	0.99	1.39	0.06
FSV-1059	QU	UL	67.9	1.15	1.02	1.13	0.93	0.77	0.89	0.62
FSV-754	CH	DRD (Ivf)	2.0	-	0.71	-	0.63	0.72	-	0.03
FSV-754	CH	WSD (II)	1.3	-	-	-	0.90	0.72	-	-
FSV-754	CH	LFD (IIId)	58.9	1.11	0.53	2.10	0.82	1.10	1.50	0.57
FSV-759	CH	DRD (Ivf)	0.9	-	-	-	0.45	-	-	0.02
FSV-759	CH	WSD (II)	2.0	-	0.53	-	0.72	0.97	-	0.02
FSV-753	CH	WSD (II)	0.6	-	-	1.63	0.45	-	-	0.02
FSV-982	CH	LFD (IIId)	0.8	-	-	-	0.60	1.07	-	-
SV-median	SV	UL	71.8	1.28	1.14	1.23	0.90	0.74	0.92	0.62
SV-median	SV	DRD (Ivf)	8.9	2.02	1.09	1.78	0.92	0.73	0.99	0.08
SV-median	SV	WSD (II)	1.9	2.62	1.92	1.36	0.74	0.41	-	0.03
SV-median	SV	LFD (IIIAd)	2.0	0.56	0.96	0.5	0.70	0.4	-	0.03
SV-median	SV	LFD (IIIBd)	1.0	0.08	0.27	0.32	0.56	0.59	-	-
SV-median	SV	LFC (IIIAc)	2.1	2.91	0.73	3.80	0.50	0.28	2.63	0.04
SV-median	SV	LFC (IIIBc)	10.2	0.08	0.10	0.73	0.38	0.88	1.12	0.34
SV-median	SV	EPc	5.8	0.14	0.18	0.78	0.51	1.03	1.06	0.11
FSV-1097	VI	UL	126.2	0.58	0.40	1.46	0.45	0.65	0.87	1.78
FSV-1098	VI	DRD (Ivf)	26.3	0.40	0.23	1.72	0.54	0.91	0.95	0.42
FSV-891	QS	UL	5.0	-	0.98	-	1.05	0.90	-	0.05
FSV-689	PI	DRD (Ivf)	4.4	-	0.71	-	0.77	0.87	-	0.05
FSV-691	PI	DRD (Im)	2.0	-	0.89	-	1.02	0.85	-	0.01
FSV-693	PI	WSD (II)	1.7	-	-	-	1.13	0.83	-	-
FSV-694	PI	WSD (II)	1.0	-	-	-	1.36	0.92	-	-

[1] $(Ce/Nd)_{SN}$ = extent of Ce depletion; $(La/Yb)_{SN}$ = fractionation of LREE from the HREE; $(La/Sm)_{SN}$ = fractionation of the LREE; $(Sm/Yb)_{SN}$ = fractionation of the HREE; $(Eu/Eu^*)_{SN} = Eu_{SN}/[0.5 \cdot (Sm_{SN} + Gd_{SN})]$ values >1 positive anomaly, <1 negative anomaly, =1 no anomaly; $(Ce/Ce^*)_{SN} = Ce_{SN}/[(1/3) \cdot (2La_{SN} + Sm_{SN})]$ since Pr was mostly not detected;

[2] The location of the sample sites is shown in Fig. 4.1.

[3] UL = bituminous silty Uncush limestone; DRD = dark replacement dolomite ("Ivf" very fine-grained, "If" fine-grained, "Im" medium-grained);
WSD = white sparry dolomite (II); LFD = late filling dolomite (IIId); LFC = late filling calcite (IIIc); EPc = calcite replacing evaporitic sulfate.

Iron II and zinc cations have the proper charge and ionic radii ($R_{Fe^{2+}} = 0.76$ Å, $R_{Zn^{3+}} = 0.74$ Å) to substitute for Mg ($R_{Mg^{2+}} = 0.65$ Å) in the dolomite lattice. Thus, iron rich dolomites are stoichiometrically depleted in magnesium (e.g., Gregg, 1988, Taylor and Sibley, 1986). The hydrothermal dolomites of San Vicente display roughly inverse trends of Fe and $MgCO_3/CaCO_3$ ratios (Figs. 4.4, 4.5), but no numerical correlation (r = -0.03).

Since Fe, Mn, and Zn have D > 1 the fluid would be depleted in these metals during precipitation of the dolomites unless externally recharged. In addition both metals, Zn and Fe, were extracted from the fluid during precipitation of sphalerite. Furthermore, the black non-cathodoluminescence of the dolomites I (Fig. 4.3) and the red luminescence of dolomite II indicate that the high iron host dolomite I was altered by a fluid with a high Mn/Fe ratio. Thus the measured decrease in Fe and increase in Mn (and likely Zn) in the late hydrothermal dolomites (IIId) suggests that the external supply in Mn to the ore fluid was unlimited, whereas probably constrained for Fe (and Zn). An external large source of Mn could be the detrital sediments and volcaniclastic rocks of the underlying Mitu Group, the Permo-Triassic intrusive rocks (San Ramón Granite and equivalent rocks) and the Lower Paleozoic rocks

near San Vicente. Leaching of these rocks would bring important amounts of Fe, Mn, and Mg into solution. Fluid migration in oxidizing conditions would explain the enrichment of the fluid in Mn compared to Fe (see section 4.6.3.1.). Furthermore the scarcity of pyrite in the San Vicente main deposit provides evidence for a Fe-poor ore fluid.

The enrichment in Sr of the ore- and post-ore carbonates (Figs. 4.4, 4.5) indicates that the incoming saline ore fluid was rich in Sr compared to the pore water of the host dolomite. Strontium isotope studies indicate that the Permo-Triassic intrusions in the Pucará basin, or their clastic derivatives in the Mitu Group, are a likely source of strontium (Moritz et al., in press).

In addition, a rapid precipitation (Lorens, 1981) of the ore- and post-ore carbonates would cause the uptake of unfavored (D < 1) trace cations, as Sr. Consequently, some chemical (elemental and isotopic) patterns of the hydrothermal carbonates could be kinetically controlled.

4.6.2 Fractionation of the REE during mineralization

The overall fractionation of the REE in hydrothermal carbonates can be explained in the Yb/Ca versus Yb/La space, according Parekh and Möller (1977), in terms of assimilation and remobilization during mineralization (Fig. 4.9). The vertical (Yb/Ca ratio) component indicates the extent of interaction ("assimilation") between the host dolomite and the fluid during increasing water-rock ratios, while the horizontal (Yb/La ratio) the overall REE-fractionation ("remobilization").

The hydrothermal carbonates (DRD, WSD, LFD, and LFC) of San Vicente display a roughly diagonal trend in the Yb/Ca - Yb/La diagram (Fig. 4.9), indicating that they were

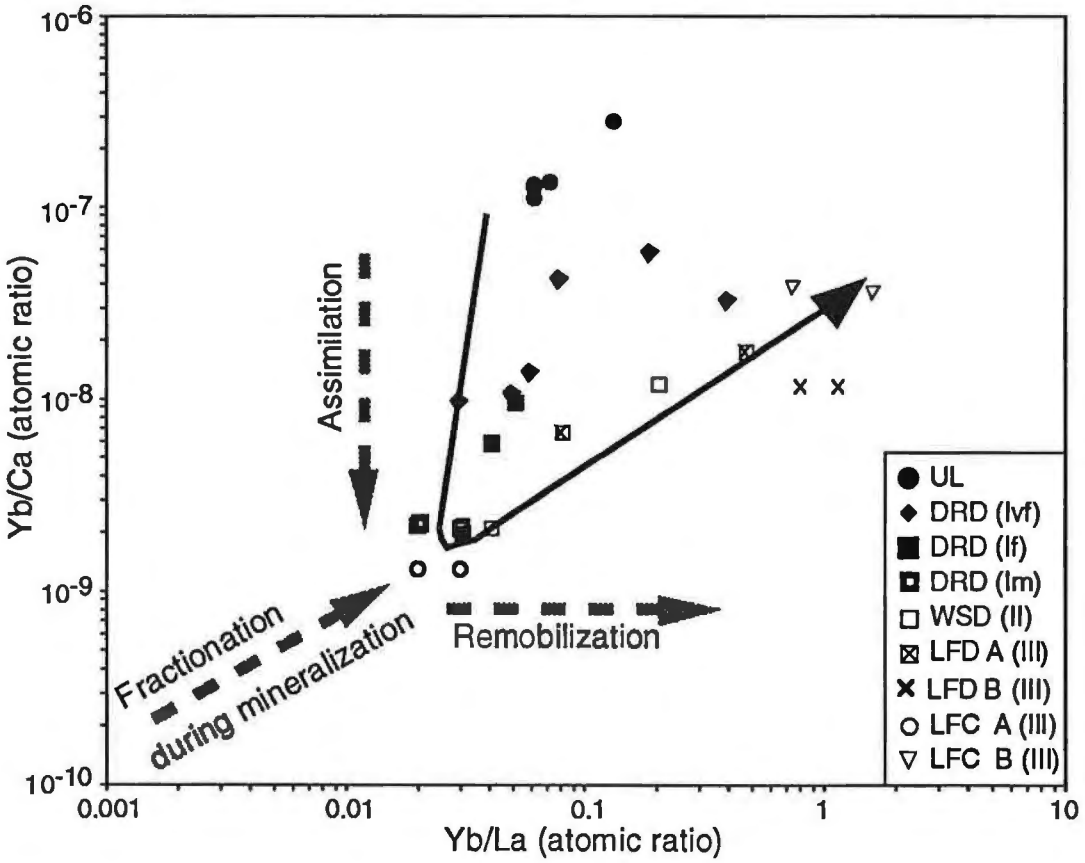

Figure 4.9. Yb/Ca versus Yb/La plot of the hydrothermal carbonates in the San Vicente district, showing the trends of REE fractionation during mineralization defined by Parekh and Möller (1977).

precipitated from a fluid whose REE fractionation increases during mineralization. The important horizontal component (Yb/La) to the overall trend indicates that the incoming fluid was complexing controlled. CO_2 partial pressure and pH control the stability of the hard REE-CO_3^{2-} complexes. Thus, the precipitation of sulfides, which acidifies the ore solution, and CO_2 degassing due to an enhanced hydrothermal porosity, would cause the precipitation of REE-rich late carbonates.

The pronounced depletion in LREE, and scatter in REE patterns of the ore-stage dolomites (Im, II) of San Vicente belt reflects alteration of the host rock by circulation of large amount of REE-poor solutions. McLennan (1989) states that, in contrast to other trace elements (such as Sr), extremely high fluid-rock ratios (e.g., F/R > 10^3) are required to modify the REE concentration of carbonates during diagenetic processes. The MREE and HREE enrichment of the late open-space filling carbonates (III) suggests that these carbonates precipitated in a fluid-buffered system. This enrichment in REE may be due to changes of pH and Eh without importing REE into the system. We conclude that the incoming mineralizing fluid (REE-poor) was not in chemical equilibrium with the carbonates of the Pucará Group. The same conclusion is attained through stable isotope data (Spangenberg et al., 1994, 1995b). This implies that the fluid flow was through a main aquifer, likely the detrital units at the base of the basin, without or with little interaction (e.g. small residence time) with the Pucará carbonates. Access to the ore sites was by interconnected channel-ways (faults, basement highs) near the ore occurrences. Mixing of the incoming fluid (mineralizing, slightly acidic, oxidizing, H_2CO_3 dominant) with native fluids (intra-formational, alkaline, reducing, HCO_3^- dominant) explains the great scatter of the REE and other trace elements in the hydrothermal carbonates.

4.6.3 Eh-pH considerations

The trace elements that occur in aqueous solutions in multiple oxidation states, e.g. Fe(II,III), Mn(II,IV), Ce(III,IV), Eu(II,III), are potential tracers of the Eh-pH changes during diagenetic processes. Thus, the distribution of Fe, Mn, Ce, and Eu in the hydrothermal carbonates of San Vicente will be discussed in terms of the redox conditions during ore precipitation.

4.6.3.1 Fe - Mn covariation

The Fe-Mn covariation (Fig. 4.10) of the hydrothermal dolomites of San Vicente display a roughly "L"-shaped trend, which is characterized by a vertical field (A-B) with Mn between 500 and 3000 µg/g and low Fe (<1500 µg/g) and an oblique ("dogleg", after Meyers, 1989) field (A-C) covering a wide range of both Fe (1500 to 5000 µg/g) and Mn (500 to 2250 µg/g). The dark replacement dolomite occurs in the horizontal field, whereas the WSD occurs in both fields. The two samples of the LFD fall in the vertical field.

Meyers (1989) interpreted the "L"-shape trend of the Fe-Mn covariation in the calcite cements of the Mississippian Lake Valley Formation in New Mexico by fluid-rock interaction combined with Eh changes. He pointed out, that a "dogleg" extension in the Mn-Fe space would indicate the case of unlimited Mn-supply, in which the limiting factor would be the water-rock exchanges.

In San Vicente, we assume that the incoming mineralizing fluid is *slightly acidic* (pH ≈ 5 to 6, see Spangenberg et al., 1995b) and *oxidizing*, at least at the early stages of migration, probably due to its migration through the oxidizing environment of the underlying Red Sandstones and other detrital units of the Pucará. Interaction of the corrosive fluid (F) with the host dolomite (R) decreases the fluid acidity and Eh (trend F-R in Fig. 4.11). The pH-changes are mainly controlled by carbonate dissolution until complete buffering by the host dolomite. Reducing conditions are provided by the light hydrocarbons liberated during alteration of the disseminated organic matter in the host dolomite (see organic matter - carbonate Eh-pH boundary in Fig. 4.11). These hydrocarbons are oxidized during thermochemical sulfate reduction (see sulfide-sulfate Eh-pH boundary in Fig. 4.11).

The concentrations of Mn^{2+} and Fe^{2+} in the incoming oxidizing fluid were very low (e.g. in the range of $<10^{-8}$ molar Mn^{2+} and $<<10^{-10}$ molar Fe^{2+}, see Fig. 4.11); this

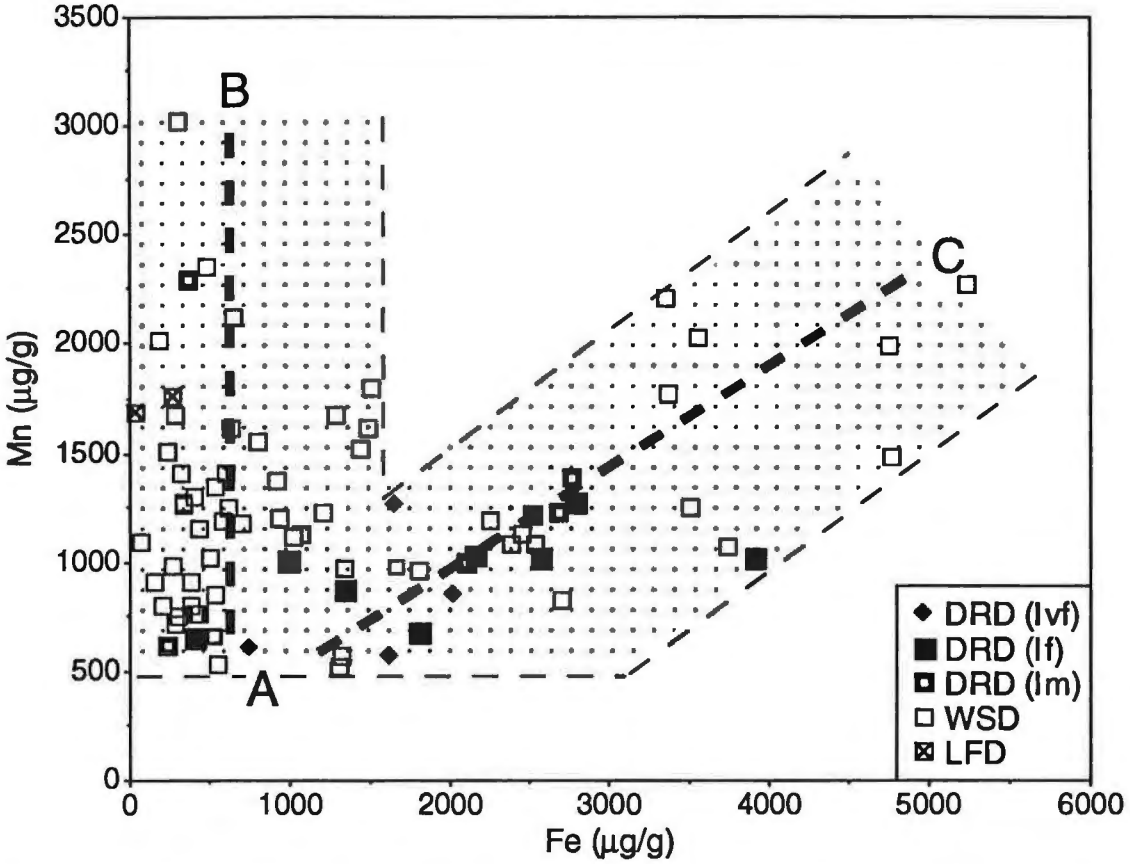

Figure 4.10. Mn versus Fe plot of the hydrothermal dolomites from the San Vicente district. There is an overall "L" shape trend, with a "dogleg" extension. See text for discussion.

explains that Fe and Mn were not incorporated in the dolomites in spite of the distribution coefficients greater than one. A decrease in the Eh would result in an increase of free Mn^{2+} in the fluid and limited or no increase in Fe^{2+} (e.g., trend F-F' in Fig. 4.11). In this Eh-pH field, Mn would be incorporated in the precipitates (WSD), whereas Fe remains as Fe^{3+} (trend A-B in Fig. 4.10). As the Eh continues to decrease, Fe^{3+} would be reduced to mobile Fe^{2+} (trend F'-F'' in Fig. 4.11). If the supply in Mn was unlimited, both divalent metals would be available in solution to coprecipitate with the carbonates ("dogleg" trend A-C in Fig. 4.10). If the supply in Mn or Fe was limited, the precipitated carbonates would be poor in Fe and Mn. Finally, the pervasive altered host dolomite become protected by the overgrowths of hydrothermal white dolomite, and could not further deliver reductants. Consequently, the recharge of the fluid-rock system with oxygenated basinal solutions would provide oxidizing conditions. Textural and stable isotope evidence (Spangenberg et al., 1994, Spangenberg, 1995) show that the late hydrothermal carbonates precipitated from a fluid-buffered system, and the low concentrations in Mn and Fe of the late filling dolomites support the hypothesis of return to oxidizing conditions in a fluid-buffered system.

4.6.3.2 Cerium anomalies

In a sedimentary environment Ce^{3+} may be oxidized to the 13.9 % smaller Ce^{4+} cation, which is largely adsorbed by hydrolizates or suspended matter (e.g., Piper, 1974; Palmer, 1985; Tlig and M'Rabet, 1985) or retained in solution as carbonate complexes (e.g., Möller, 1983; Möller et al., 1984); consequently, the precipitated carbonates will have a negative Ce anomaly.

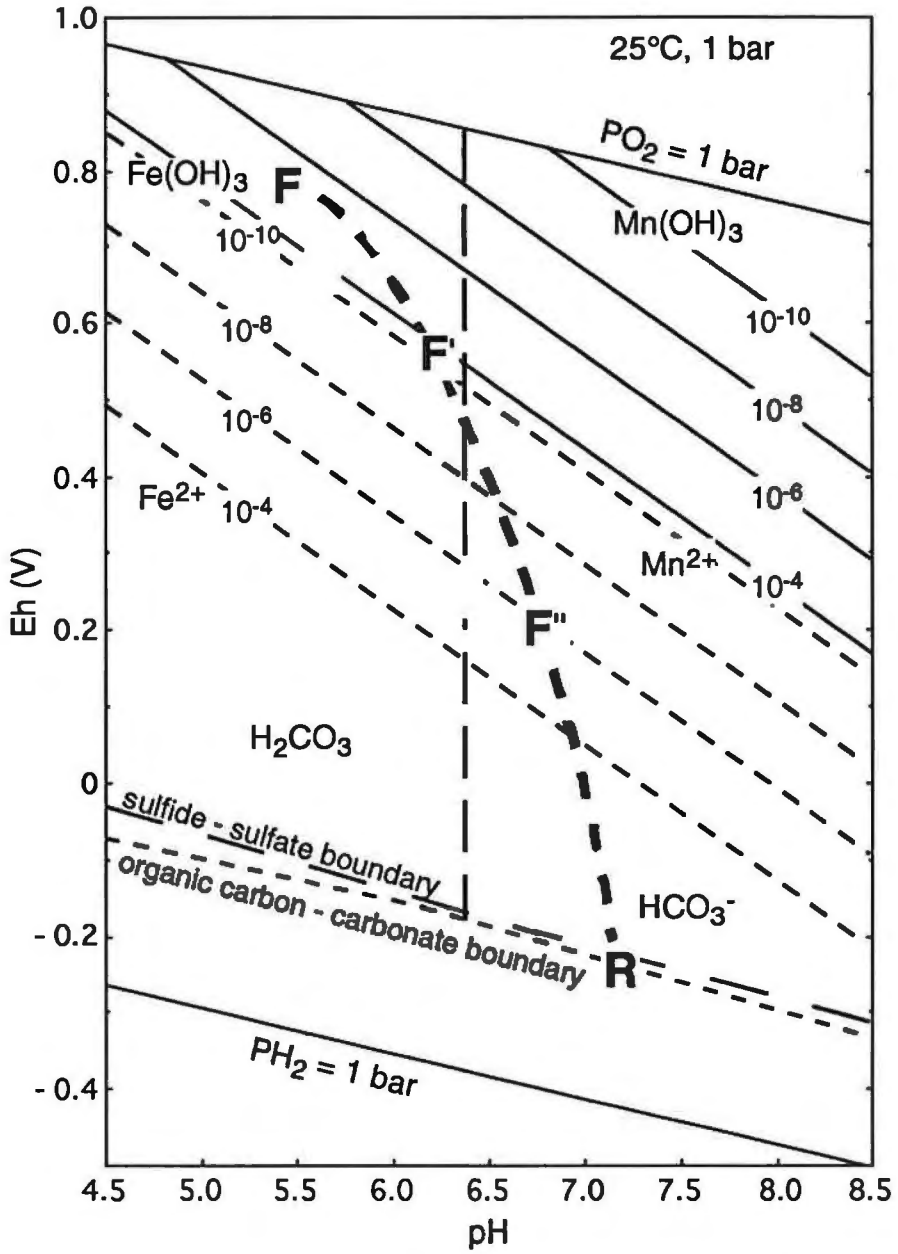

Figure 4.11. Eh-pH diagram for part of the system Fe-Mn-O-H, assuming $Fe_2(OH)_3$ and $Mn(OH)_3$ as stable phases for Fe (III) and Mn (III). Boundaries calculated for activities of Fe^{2+} and Mn^{2+} of 10^{-10}, 10^{-8}, 10^{-6}, and 10^{-4} after equations of Pourbaix (1963). The sulfide-sulfate boundary and organic carbon - carbonate are after Brookins (1988). F-R is a schematic representation at 25°C of the expected Eh-pH trend during interaction of the incoming fluid with the host dolomite.

The negative Ce anomaly in the ore-stage dolomite of the San Vicente deposit (Figs. 4.7a, 4.7b) supports early (pre-ore) circulation of the incoming fluid in oxidizing environment, in which Ce was depleted compared to the neighboring La and Pr.

4.6.3.3 Europium anomalies

The Eu behavior in the carbonates of the San Vicente deposit is summarized as follows (Table 4.5): (1) the bituminous silty Uncush limestone and the host dark replacement dolomite have a slightly negative Eu anomaly (Eu/Eu* = 0.82 - 0.93 for UL, 0.93-1.05 for DRD); (2) the Eu concentration in the ore-stage hydrothermal dolomites is

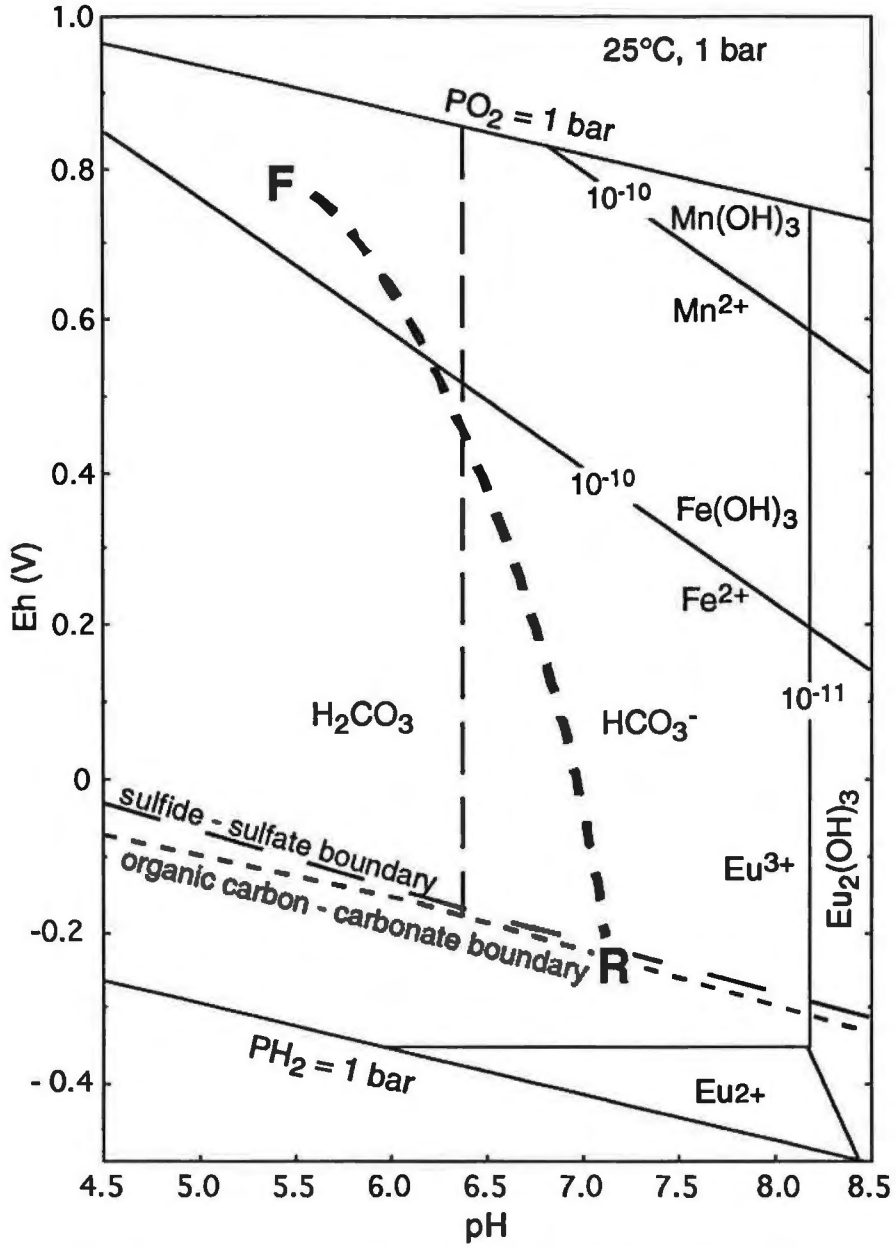

Figure 4.12. Eh-pH diagram for part of the system Eu-O-H (25°C, and 1 bar) assuming $Eu(OH)_3$ as stable phase for Eu (III). Boundaries calculated for total dissolved activities of 10^{-11}. The boundaries for Fe (II)-Fe (III) and MN (II) Mn (III) for activities of Fe^{2+} and Mn^{2+} of 10^{-10}, sulfide-sulfate boundary and organic carbon - carbonate are given for comparison. The Eh-pH boundaries were calculated after equations of Brookins (1988) an Pourbaix (1963).

always lower than the analytical detection limit; and (3) the late stage filling calcites have a significant positive Eu anomaly (1.10 - 2.63).

A negative Eu anomaly in the precipitates may indicates that the fluid was poor in total Eu or that Eu^{3+} was deficient in the fluid compared to Eu^{2+}. Europium +2 is too large (23.5 % larger than Eu^{3+}) to be retained by sorption/coprecipitation during fluid migration (e.g., McLennan, 1989); consequently, more mobile. In aqueous solutions at low temperature (<100°C) the chemistry of europium is dominated by the oxidation state +3, whereas Eu^{2+} occurs under extremely reducing conditions in alkaline fluids (e.g., Bau and Möller, 1991; Brookins, 1989, p. 211). In particular appreciable amounts of Eu^{2+} (activity

$>10^{-11}$ molar) in solutions at 25°C require Eh values lower than -0.36 V ($fO_2 \approx -80$) and pH ≈ 7-10 (Fig. 4.12). Such extreme reducing and alkaline conditions could be probably only encountered in the pore fluids of anoxic marine sediments (e.g. the bituminous silty Uncush Limestone).

At higher temperature (≈100°C) thermodynamic calculations by Sverjensky (1984) predict that hydrothermal fluids with oxidation state near those of the sulfide/sulfate boundary would contain significant Eu^{2+} (Fig. 4.13). He noted that strong preferential complexing (with highly charged ligands, such as CO_3^{2-} and SO_4^{2-}) of Eu^{3+}, at 100°C would move the Eu^{2+}/Eu^{3+} redox boundary towards lower fO_2. Europium could be largely as Eu^{2+} in the hot and slightly acidic ore fluid, which precipitated Eu-depleted white sparry dolomite in San Vicente district. The positive anomalies of the late calcites indicate that the fluid was enriched in the (mobile) Eu^{2+} during the main-mineralization stage; afterwards oxidized to Eu^{3+} which precipitated with the post-ore carbonates.

Thus, the Eu anomalies, and the Fe-Mn covariations of the hydrothermal carbonates record the change from reducing ore-stage to post-ore oxidizing conditions. These changes of the Eh-pH conditions of the ore fluid are interpreted to be due to mixing of the native intra-formational fluid (alkaline, reducing, HCO_3^- dominant) with the incoming mineralizing fluid (slightly acidic, oxidizing, H_2CO_3 dominant) in an open dynamic system.

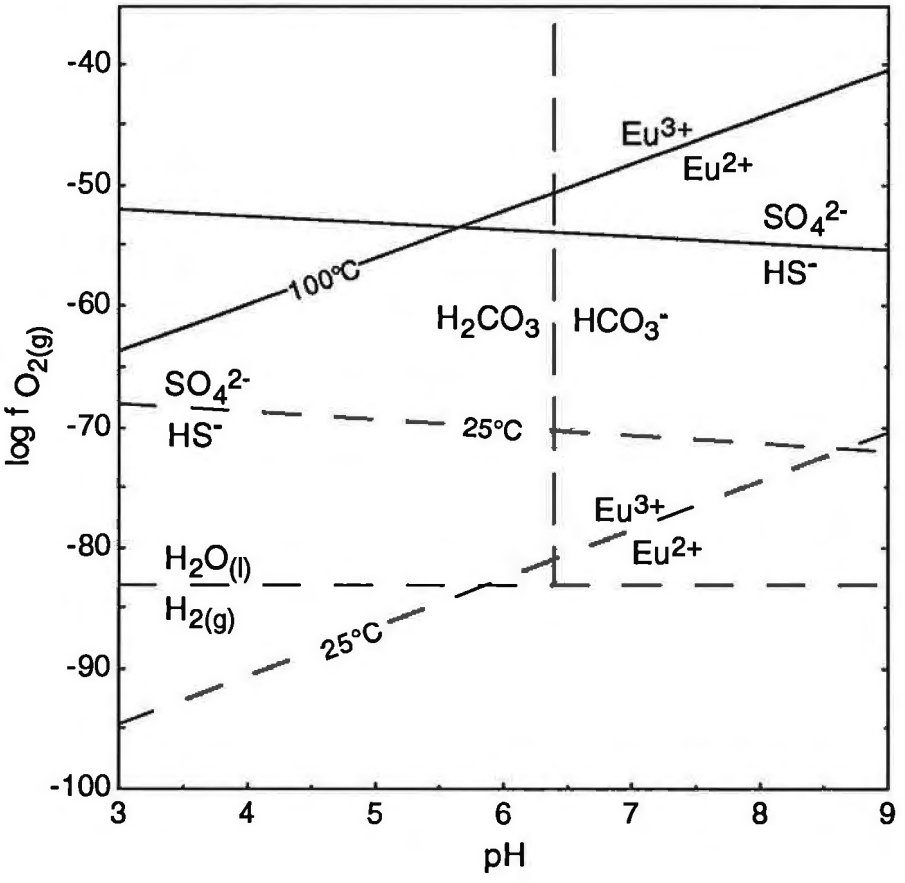

Figure 4.13. fO_2-pH diagram for equal activities of Eu^{2+} and Eu^{3+}, and SO_4^{2-}/HS^- at 25°C and 100°C. From Sverjensky (1984). Note that at temperature ≈100°C the solutions can contain significant Eu^{2+} also in the presence of oxidized sulfur.

4.7 Conclusions

The distribution of the REE and other trace elements in the hydrothermal carbonates of the San Vicente Mississippi Valley-type district set constraints on the chemistry of the ore fluid and the variation of the Eh-pH conditions during mineralization:

(1) The incoming mineralizing fluid was slightly acidic (pH ≈ 5), oxidizing, likely due to circulation through the underlying detrital rocks at the base of the Pucará Group,

(2) The regional geochemical homogeneity of the hydrothermal carbonates combined with the lack of geochemical equilibration between the incoming fluid and the carbonate rocks of the Pucará Group constrain the regional-scale fluid flow to high-permeability channel- ways (faults, basement highs) near the ore occurrences.

(3) The dissolution of the host dolomite by the corrosive incoming fluid provides the local redox conditions necessary to reduce sulfate to sulfide (and Eu^{3+} to Eu^{2+}). In this early rock-buffered stage the host dolomite was replaced by white dolomite and sphalerite I.

(4) Precipitation of open space-filling white sparry dolomite and sphalerite II occurred in acidic reducing fluid-buffered conditions, as indicated by the Mn uptake and REE-depletion of the WSD.

(5) The REE enrichment, the Mn depletion, and positive Eu anomaly of the late-stage vug-filling carbonates indicate that the post-ore "residual" acidic fluid, and likely again oxidizing (due to influx of fresh basinal waters), would extensively enhance the secondary porosity by carbonate dissolution until pH-buffering. CO_2 degassing would cause the precipitation of REE-rich late carbonates.

(6) The trace element signature of the San Vicente carbonates supports the genetic model proposed by quantitative modeling of the stable isotope covariations, which involve (a) mixing of native-intraformational fluid and an incoming slightly acidic ore fluid, and (b) interaction between the corrosive fluid and the host dolostone.

Acknowledgments

This study is supported by the Swiss National Science Foundation (Grant No. 20.36397.92). We are grateful to San Ignacio de Morococha S.A. Mining Company and the staff of the Geology Department of San Vicente mine for their help in the field work.
The authors thank J. Buffle, J.C. Negre and M. Martin (ICP-AES laboratory), and R. Martini (Cathodoluminescence microscopy) of the University of Geneva, and Ph. Thélin (XRD-analyses) and F. Bussy (Electron microprobe) of the University of Lausanne for their cooperation during the analytical work.

References

Arne, D.C., Curtis, L.W., and Kissin, S.A. (1991) Internal zonation in a carbonate-hosted Zn-Pb-Ag deposit. Nanisivik, Baffin Island, Canada. Economic Geology, v. 86, p. 699-717.

Banner, J.L., Hanson, G.N., and Meyers, W.J. (1988) Rare earth element and Nd isotopic variations in regionally extensive dolomites from the Burlington-Keokuk Formation (Mississippian): implications for REE mobility during carbonate diagenesis. Journal of Sedimentary Petrology, v. 58, n. 3, p. 415-432.

Bau, M, and Möller, P. (1991) REE systematics as source of information on minerogenesis. In: Pagel, M. and Leroy, J.L. (Editors) Source, transport and deposition of metals. Balkema, Rotterdam, p. 17-20.

Beales, F.W., and Hardy, J.L. (1980) Criteria for the recognition of diverse dolomite type with an emphasis on studies on host rocks for Mississippi Valley-Type ore deposits. In: Zenger, D.H., Dunham, J.B., and Ethington, R.L. (Editors) Concepts and models of dolomitization. SEPM Special Publication No. 28, p. 197-213.

Bein, A., Land, L.S. (1983) Carbonate sedimentation and diagenesis associated with Mg-Ca-chloride brines. Journal of Sedimentary Petrology, v. 53, p. 243-260.

Brand, U., and Veizer, J. (1980) Chemical diagenesis of a multicomponent carbonate system-1: Trace elements. Journal of Sedimentary Petrology, v. 50, n. 4, p. 1219-1236.

Brookins, D.G. (1988) Eh-pH diagrams for geochemists. Springer, New York, 176 p.

Brookins, D.G. (1989) Aqueous geochemistry of rare earth elements. Mineralogical Society of America, Reviews in Mineralogy. v. 21, p. 201-225.

Buelter, D.P., and Guillemettte, R.N. (1988) Geochemistry of epigenetic dolomite associated with lead-zinc mineralization of the Viburnum Trend, Southeast Missouri: a reconnaissance study. In: Shukla, V., and Baker, P.A. (Editors) Sedimentology and Geochemistry of Dolostones, SEPM, Special publication No.43, p. 85-93.

Bustillo, M., Fort, R., and Ordoñez, S. (1992) Genetic implications of trace-element distributions in carbonate and non-carbonate phases of limestones and dolostones from western Cantabria, Spain. Chemical Geology, v. 97, p. 273-283.

Cantrell, K.J., and Byrne, R.H. (1988) Rare earth element complexation by carbonate and oxalatre ions. Geochimica et Cosmochimica Acta, v. 51, p. 597-606.

Churnet, H.G., and Misra, K.C. (1981) Genetic implications of the trace element distribution pattern in the Upper Knox carbonate rocks, Copper Ridge District, East Tennessee. Sedimentary Geology, v. 30, p. 173-194.

De Baar, H.J.W., Bacon, M.P., and Brewer, P.G. (1985) Rare earth elements in the Pacific and Atlantic Oceans. Geochimica et Cosmochimica Acta, v. 49, p. 1943-1959.

Elderfield, H., and Greaves, M.J. (1982) The rare earth elements in seawater. Nature, v. 296, p. 214-219.

Elderfield, H. and Pagett, R. (1986) Rare earth elements in ichthyoliths: variations with redox conditions and depositional environment. The Earth of the Total Environment, v. 49, p. 175-197.

Erel, Y., and Katz, A. (1990) Trace-element distribution across calcite veins: a tool for genetic interpretation. Chemical Geology, v. 85, p. 361-367.

Farr, M.R. (1992) Geochemical variation of dolomite cement within the Cambrian Bonneterre Formation, Missouri: evidence for fluid mixing. Journal of Sedimentary Petrology, v. 62, p. 636-651.

Fleet, A. J. (1984) Aqueous and sedimentary geochemistry of the rare earth elements. In: Henderson, P. (Editor) Developments in geochemistry 2. Rare earth element geochemistry, Elsevier, p. 343 - 373.

Fontboté, L. (1990) Stratabound ore deposits in the Pucará basin. An overview. In: Fontboté, L. , Amstutz, G.C., Cardozo, M., Cedillo, E., and Frutos, J. (Editors) Stratabound ore deposits in the Andes. Springer, Heidelberg, p. 253-266.

Fontboté, L. (1993) Self-organization fabrics in carbonate-hosted ore deposits: the example of diagenetic crystallization rhythmites (DCRs). In: Fenoll Hach-Ali, P., Torres-Ruiz, J., and Gervilla, F. (Editors) Current research in geology applied to ore deposits. Proceedings of the Second Biennial SGA Meeting, Granada, Spain, Sept. 9-13, 1993, p. 11-14.

Fontboté, L., and Gorzawski, H. (1990) Genesis of the Mississippi Valley-type Zn-Pb deposit of San Vicente, Central Peru: geological and isotopic (Sr, O, C, S) evidences. Economic Geology, v. 85, p. 1402-1437.

Fontboté, L., Spangenberg, J., Oldham, L., and Davila, D. (1995) The Mississippi Valley-type zinc-lead mine of San Vicente, eastern Pucará basin, Peru. International Field conference on carbonate-hosted lead-zinc deposits. June 3-6, 1995, St. Louis, Missouri, USA. Abstracts volume, p. 83-86.

González, E. (1987) Petrographische und geochemische Untersuchungen an einem Gesamt-Profil durch die schichtgebundene Zn-Pb-Lagerstätte San Vicente, Perú. Unpub. M.Sc. thesis, Univ. Heidelberg, 128 p.

Gorzawski, H. (1989) Isotopic, geochemical, and petrographic characterization of the diagenetic evolution in carbonate-hosted stratabound Zn-Pb-(F-Ba) deposits. Heidelberger Geowissenschaftliche Abhandlungen, v. 28, 250 p.

Gorzawski, H., Fontboté, L., Field, C.W., and Tejada, R. (1990) Sulfur isotope studies in the zinc-lead mine Vicente, Central Perú. In: Fontboté, L. , Amstutz, G.C., Cardozo, M., Cedillo, E., and Frutos, J. (Editors) Stratabound ore deposits in the Andes. Springer, Heidelberg, p. 305-312.

Graf, J.L. (1984) Effects of Mississippi Valley-Type mineralization on REE patterns of carbonate rocks and minerals, Viburnum Trend, Southeast Missouri. Journal of Geology, v. 92, n. 3, p. 307-324.

Graf, J.L. (1988) Rare earth element studies of Mississippi Valley-Type (MVT), Pb-Zn-Cu deposits in Kansas, Oklahoma, and Missouri, USA. In: Pélissonier, H., and Sureau, J.F. (Editors) Mobilité et concentration des métaux de base dans les

couvertures sédimentaires. Manifestations, mécanismes, prospection. Document du BRGM n. 183, p. 75-88.

Grant, N.K., and Bliss, M.C. (1983) Strontium isotope and rare earth element variations in non-sulfide minerals from the Elmwood-Gordonsville mines, central Tennessee. In: Kisvarsanyi, G., Grant, S.K., Pratt, W.P., and Koenig, J.W. (Editors), International Conference on Mississippi Valley type lead-zinc deposits. Proc. Vol., Rolla, University of Missouri - Rolla. p. 206-210.

Gregg, J.M. (1988) Origins of dolomite in the offshore facies of the Bonneterre Formation (Cambrian), Southeast Missouri. In: Shukla, V., and Baker, P.A. (Editors) Sedimentology and Geochemistry of Dolostones, SEPM, Special publication No.43, p. 67-83.

Gregg, J.M., and Shelton, K.L. (1989) Geochemical and petrographic evidence for fluid sources and pathways during dolomitization and lead-zinc mineralization in Southeast Missouri: a review. Carbonates and Evaporites, v. 4, n.2, p. 153-175.

Hanson, G.N. (1980) Rare earth elements in petrogenetic studies of igneous systems. Annual Review of Earth and Planetary Sciences, v. 8, p. 371-406.

Jones, D.G, Plant, J.A., and Colman T.B. (1991) New evidence for Viséan-Namurian shales as the source of the Pennine mineralisation of England. In: Pagel, M., and Leroy, J.L. (Editors) Source, transport and deposition of metals. Balkema, Rotterdam, p. 309-312.

Kretz, R. (1982) A model for the distribution of trace elements between calcite and dolomite. Geochimica et Cosmochimica Acta, v. 46, p. 1979-1981. Kucha, H. and Wieczorek, A. (1984) Sulfide - Carbonate relationships in the Navan (Tara) Zn-Pb deposit, Ireland. Mineralium Deposita, v.19, p. 208-216.

Land, L.S. (1980) The isotopic and trace element geochemistry of dolomite: the state of the art. In: Zenger, D.H., Dunham, J.B., and Ethington, R.L. (Editors) Concepts of models of dolomitozation, Society of Economic Paleontologists and Mineralogists Special Publication, No. 28, p. 87-110.

Landis, G.P.Tschauder, R.J. (1990) Late Mississippian karst caves and Ba-Ag-Pb-Zn mineralization in Central Colorado: Part II Fluid inclusion, stable isotope, and rock geochemistry data and a model of ore deposition. In: Beaty, D.W., Landis, G.P., and Thomson, T.B. (Editors). carbonate-hosted sulfide deposits of the Central Colorado Mineral Belt. Economic geology, monograph 7, p. 339-366.

Leuchs, W. (1985) Beziehungen zwischen Verquarzung und Dolomitisierung der devonischen Riffkalke von Dornap bei Muppertal. Neues Jahrbuch für Geologie und Paläontologie - Abhandlungen, p. 129-152.

Lorens, R.B. (1981) Sr, Cd, Mn, and Co distribution coefficients in calcite as a function of calcite precipitation rate. Geochimica et Cosmochimica Acta, v. 45, p. 53-561.

Machel, H.-G. (1987) Saddle dolomite as a by-product of chemical compaction and thermochemical sulfate reduction. Geology, v. 15, p. 936-940.

Machel, H.G. (1988) Fluid flow direction during dolomitization as deduced from trace-element trends. In Sedimentology and Geochemistry of Dolostones, In: Shukla, V. and Baker, P.A. (Editors), SEPM, Special publication No. 43, p. 115-125.

Machel, H.-G., and Mountjoy, E.W. (1986) Chemistry and environments of dolomitization - A reappraisal. Earth Sciences Reviews, v. 23, p. 172-222.

Martini, R., Amieux, P., Gandin, A., and Zaminetti, L. (1987) Triassic foraminifers from Punt Tonnara (SW Sardinia) observed in cathodoluminescence. Revue de Paléobiologie, v. 6, p. 23-27.

Mazzucotelli, A., Vannucci, R., Vannucci, S., and Rubiera, R. (1981) Determinazione della composizione chimica della frazione carbonatica di calcari e dolomie mediante spettrofotometria in assorbimento atomico e cromatografia a scambio ionico. Rendiconti Società Italiana di Mineralogia e Petrologia, v. 37, n. 2, p. 913-920.

McDaniel, D.K., Hemming, S.R., McLennan, S.M., and Hanson, G.M. (1994) Resetting of neodymium isotopes and REEs during sedimentary processes: The Early Proterozoic Chelmsford Formation, Sudbury Basin, Ontario, Canada. Geochimica Cosmochimica Acta, v. 58, p. 931-941.

McHargue, T.R., and Price, R.C. (1982) Dolomite from clay in argillaceous or shale-associated marine carbonates. Journal of Sedimentary Petrology, v. 52, p. 873-886.

McLennan, S.M. (1989) Rare earth elements in sedimentary rocks: influence of provenance and sedimentary processes. In: Lipin, B.R., and McCay, G.A. (Editors), Geochemistry and mineralogy of rare earth elements. Reviews in Mineralogy, v. 21, p. 116-200.

Meyers, W.J. (1989) Trace element and isotope geochemistry of zoned calcite cements, Lake Valley Formation (Mississippian, New Mexico): insights from water-rock interaction modelling. Sedimentary Geology, v. 65, p. 355-370.

Moldovanyi, E.P., Walter, L.M., Brannon, J.C., and Podosek, F.A. (1992) New constraints on carbonate diagenesis from integrated Sr and S isotopic and rare earth element data, Jurassic Smackover Formation, U.S. Gulf Coast: a reply. Applied Geochemistry, v. 7, p. 93-97.

Möller, P. (1983) Lanthanoids as a geochemical probe and problems in lanthanoid geochemistry. Distribution and behavior of lanthanoids in non-magmatic-phases. In: Simha, S.P. (Editor) Systematics and the properties of the lanthanides. Reidel, p. 561-616.

Möller, P. (1991) REE fractionation in hydrothermal fluorite and calcite. In: Pagel, M., and Leroy, J.L. (Editors) Source, transport and deposition of metals. Balkema, Rotterdam, p. 91-94.

Möller, P., and Morteani, G. (1983) On the geochemical fractionation of rare earth elements during the formation of Ca-minerals and its application to problems of the genesis of ore deposits. In. Augustithis, S.S. (Editor) The significance of trace elements in solving petrogenetic problems and controversies. Thephrastus, Athens. p. 747-791.

Möller, P., Morteani, G., and Dulski, P. (1984) The origin of the calcites from Pb-Zn veins in the Harz Mountains, Federal Republic of Germany. Chemical Geology, v. 45, p. 91-112.

Montañez, I.P., and Read. J.F. (1992) Fluid-rock interaction history during stabilization of early dolomites, Upper Knox Group (Lower Ordovician), U.S. Appalachians. Journal of Sedimentary Petrology, v. 62, p. 753-778.

Moritz, R., Fontboté, L., Spangenberg, J. Rosas, S., Sharp, Z. and Fontignie, D. (in press) Sr, C and O isotope systematics in the Pucará Basin, Central Peru: comparison between Mississippi Valley-type deposits and barren areas. Mineralium Deposita.

Palmer, M.R. (1985) Rare earth elements in foraminifera tests. Earth and Planetary Science Letters, v. 73, p. 285-298.

Parekh, P.P., and Möller, P. (1977) Revelation of the genesis of minerals in paragenesiswith fluorites, calcites and phosphates via rare earth fractionation. In: Nuclear Techniques and Mineral Resources. International Atomic Energy Agency. Vienna. p. 353-369.

Pingitore, N.E. (1978) The behaviour of Zn+2 and Mn+2 during carbonate diagenesis: theory and applications. Journal of Sedimentary Petrology, v. 48, n. 3, p. 799-814.

Piper, D.Z. (1974) Rare earth elements in the sedimentary cycle: a summary. Chemical Geology, v. 14, p. 285-304.

Pourbaix, M. (1963) Atlas d'équilibres électrochimiques. Gauthier-Villars, Paris, 644 p.

Richter, D.K. (1974) Enstehund und Diagenese der devonischen und permotriassischen Dolomite in der Eifel. Contr. Sedimentology, v. 2, p. 1-101.

Robinson, P. (1980) Determination of calcium, magnesium, manganese, strontium, sodium and iron in the carbonate fraction of limestones and dolomites. Chemical Geology, v. 28, p. 135-146.

Rosas, S. (1994) Facies, diagenetic evolution, and sequence analysis along a SW-NE profile in the southern Pucará Basin (Upper Triassic-Lower Jurassic), central Peru. Heidelberger Geowissenschaftliche Abhandlungen, v. 80, 337 p.

Schieber, J. (1988) Redistribution of rare-earth elements during diagenesis of carbonate rocks from the mid-proterozoic Newland Formation, Montana, USA. Chemical Geology, v. 69, p. 111-126.

Shepherd, T.J., Darbyshire, D.P.F., Moore, G.R., and Greenwood, D.A. (1982) Rare earth element and isotopic geochemistry of the North Pennine ore deposits. Bulletin du BRGM (2), section II, n. 4, p. 371-377.

Shukla, V. (1988) Sedimentology and geochemistry of a regional dolostone: correlation of trace elements with dolomite fabrics. In: Shukla V., and Baker P.A. (Editors) Sedimentology and Geochemistry of Dolostones, SEPM, Special publication No. 43, p. 145-157.

Spangenberg, J., Fontboté, L., Sharp, Z., and Hunziker, J. (1994) Stable isotope (C, O) constraints on the genesis of the Mississippi Valley-type zinc-lead deposit of San Vicente, central Peru. 7° Congreso Geológico Chileno, 17-21 octubre de 1994, Concepción, Chile. Abstracts volume II, p. 1532-1536.

Spangenberg, J. (1995) Geochemical (elemental and isotopic) constraints on the genesis of the Mississippi Valley-type zinc-lead deposit of San Vicente, central Peru. [Ph.D. dissertation], University of Geneva, Switzerland, (in press)

Spangenberg, J., Sharp, Z., and Fontboté, L. (1995a) Apparent carbon and oxygen isotope variations of carbonate gangue minerals Mississippi Valley-type Zn-Pb of San Vicente deposit, central Peru. Mineralium Deposita, v. 30, p. 67-74.

Spangenberg, J., Fontboté, L., Sharp, Z., and Hunziker, J. (1995b) Carbon and oxygen isotope study of hydrothermal carbonates in the zinc-lead deposits of San Vicente, central Peru. (submitted)

Stanley, J.K., and Byrne, R.H. (1990) The influence of solution chemistry on REE uptake by Ulva lactuca L. in seawater. Geochimica et Cosmochimica Acta, v. 54, p. 1587-1595.

Sverjensky, D.A. (1984) Europium redox equilibrium in aqueous solution. Earth and Planetary Science Letters, v. 67, p. 70-78.

Tassé, N., and Bergeron, M. (1991) Geochemistry of REE in carbonate replacing sulfate evaporites in the lower ordovician Beeknantown Group, St. Lawrence Lowlands, Québec. Geological Association of Canada; Mineralogical Association of Canada; Canadian Geophysical Union, Joint Annual Meeting, 16. Abstracts, Toronto, May 27-29, p. 122.

Taylor, T.R., and Sibley, D.F. (1986) Petrographic and geochemical characteristics of dolomite in the Trenton Formation, Ordovician, Michigan Basin. Sedimentology, v. 33, p. 61-86.

Terakado, Y., and Masuda, A. (1988) The coprecipitation of rare-earth elements with calcite and aragonite. Chemical Geology, v. 69, p. 103-10.

Tlig, S., and M'Rabet, A. (1985) A comparative study of the rare earth element (REE) distribution within the Lower Cretaceous dolomites and limestones of Central Tunisia. Sedimentology, v. 32, p. 897-907.

Vahrenkamp, V.C., and Swart, P.K. (1990) New distribution coefficient for the incorporation of strontium into dolomite and its implications for the formation of ancient dolomites. Geology, v. 18, p. 387-391.

Veizer, J. (1983a) Chemical diagenesis of carbonates: theory and application of trace element technique. In: Arthur, A., Anderson, T., Kaplan, I., Veizer, J., and Land., S. (Editors) Stable isotopes in sedimentary geology. SEPM Short Course No. 10, p. 3.1-3.100.

Veizer, J. (1983b) Trace elements and isotopes in sedimentary carbonates. In: Reeder, R.J.(Editor) Carbonates: mineralogy and chemistry. Reviews in Mineralogy, v. 11, p. 265-299.

Viets, J.G., Mosier, E.K., and Erickson, M.S. (1983) Geochemical variations of major, minor, and trace elements in samples of the Bonneterre Formation from drill holes transectimg the Viburnum Trend Pb-Zn district of Southeast Missouri. In: Kisvarsanyi, G., Grant, S.K., Pratt, W.P., and Koenig, J.W. (Editors), International Conference on Mississippi Valley type lead-zinc deposits. Proc. Vol., Rolla, University of Missouri - Rolla. p. 174-186.

Zheng, M., and Wang, X. (1991) Genesis of the Daliangzi Pb-Zn deposit in Ichuan, China. Economic Geology, v. 86, p. 831-846.

Zachara, J.M., Cowan, C.E., and Resch, C.T. (1991) Sorption od divalent metals on calcite. Geochimica et Cosmochimica Acta, v. 55, p. 1549-1562.

CHAPTER 5

PRELIMINARY GEOCHEMICAL STUDY OF THE ORGANIC MATTER DISSEMINATED IN THE CARBONATES OF THE SAN VICENTE MISSISSIPPI VALLEY-TYPE DISTRICT, CENTRAL PERU

5.1 Introduction

In this chapter the results of a preliminary study of the geochemistry of organic matter (OM), including in particular pyrolysis of the whole carbonates samples is presented. Three "types" of OM are associated to the gangue carbonates of the San Vicente Mississippi Valley-type (MVT) district of San Vicente, central Peru. According to paragenetic and textural relationships they can be classified in: (1) OM disseminated in the bituminous silty Uncush limestone (UL); (2) OM disseminated in the dark replacement dolomite of the host dolostones (DRD, I); (3) and solid hydrothermal bitumen (IIIbit) occurring as open-space filling coating the late filling calcite or dolomite. The present study of the organic content in the carbonates of San Vicente is mainly based on Rock-Eval analysis performed by J.R Disnar at the University of Orléans.

The common association of bitumen with MVT deposits is widely documented (e.g. Anderson, 1991; Leventhal, 1990; Parnell et al., 1992, and references therein). The role of the OM in ore precipitation was discussed in terms of (1) carrier of the metals by organo-metallic complexing, (2) source or pre-concentrator of the ore components (metal and sulfur), (3) and thermochemical sulfate reduction (Anderson and Garven, 1987; Anderson and Mcqueen, 1988; Cannon and Orgeval, 1976; Giordano, 1993; Giordano and Barnes, 1981; Leventhal, 1990; Macqeen and Powel, 1983; Manning, 1986; Manning and Gize, 1993; Parnell, 1988; Powel and Mcqeen, 1984; Gize at al., 1991; Sverjensky, 1986; Spirakis, 1986).

Furthermore, recent organic geochemical and petrographic studies have shown that the degree of maturation/alteration of the OM (disseminated in the host carbonates) serves as a sensitive tracer of the flow-path of the ore fluid and the timing of the mineralizing events (Disnar and Héroux, 1995; Guize and Barnes, 1987; Henry et al., 1992; Leventhal, 1986; Marikos, 1986; Marikos et al., 1986). In addition, organic geochemistry may be used as a guide for hidden MVT-deposits (e.g., Disnar and Gauthier, 1988; 1989; Héroux and Tassé, 1990; Héroux et al., 1994; Spirakis and Heyl, 1992).

5.2 Methods

5.2.1 Samples

Thirty-seven samples were selected from a detailed sampling of the gangue carbonates from both the main deposit and mineralized and barren areas at the San Vicente district (Tab. 5.1, detailed description in chapter 1 and in Spangenberg et al., 1995). They comprise whole-rock samples of the bituminous silty Uncush Limestone (UL) and the ore-bearing dolomite units (Alfonso Dolomite, San Vicente Dolomite, San Judas Dolomite) and of solid hydrothermal bitumen in the latter units. Under "bituminous horizon" are included samples from a fractured zone within the San Vicente Dolomite roughly parallel to the major overthrust.

5.2.2 Analysis

Total organic carbon (TOC) and total sulfur was determined by LECO pyrolysis at the laboratories of XRAL. Twenty-five samples were analyzed for TOC. Total sulfur was

determined in 19 samples. Reported duplicate analysis indicate an uncertainty of ±1% (2s) for TOC and S. The values for TOC (Table 5.1) compare relatively well with those of Rock-Eval (excepting sample FSV-1059).

Rock-Eval pyolysis was performed at the Laboratoire de Géologie de la Matière Organique, University of Orléans by J. R. Disnar. Nineteen powdered whole-samples were directly pyrolised; six samples of the Uncush limestone were extracted with chloroform before pyrolysis. The analyses were performed using standard methods described in Espitalié et al. (1985a). The method consists in heating of a small sample (≈100 mg) in two steps. The first is the volatilization of the free hydrocarbons (HC) at 200°C (or 300°C) for 3 min; the second the conversion of the solid organic matter to hydrocarbons by increasing the temperature to 600°C at a rate of 25°C/min. The gases liberated during the pyrolysis are swept by a stream of helium gas to a flame ionization detector, which record typical peaks with increasing temperature. The following Rock-Eval parameters are derived from the area and shape of these peaks (Espitalie, 1985a, 1985b):

- S_1: is the amount of already existing mobile and free hydrocarbons (oil) that were volatized at 200°C or 300°C (in mg HC per g sample);
- S_2: is the amount of HC (in mg HC per g sample) liberated during the pyrolysis of the kerogen (i.e., non-soluble organic matter, Milles, 1994) and of extractable heavy compounds (asphaltenes, resines) between 300 and 600°C. S_2 indicates the hydrocarbons which could be produced during maturation by deeper burial or other thermal processes. During diagenesis the most important HC liberated is methane.
- T_{max}: is the temperature in °C at which the pyrolitic yield of HC from a rock sample (peak S_2) reaches its maximum. T_{max} is a maturation parameter which is dependent of the kerogen type and its cracking kinetics.
- TOC: is the total organic carbon, which is determined by summing the pyrolised organic carbon (S_1, S_2) with the residual organic carbon released by heating in air to 600°C the pyrolised sample.

Two maturity indicators are calculated using the Rock-Eval S_1, S_2 and TOC parameters (e.g. Espitalié, 1984b, Milles, 1994): the oil production index "OPI" and the hydrogen index "HI". The oil production index is the ratio of free HC to the total HC released during pyrolysis ($OPI = S_1/[S_1+S_2]$). The hydrogen index is a measure of the hydrogen richness of the kerogen, calculated from S_2 and TOC ($HI = S_2/TOC$, in mg HC per g TOC). It correlates well with the elemental ratio H/C and, therefore, can be used for characterizing the organic matter (Espitalié et al., 1977, 1985b). The most used maturity parameters derived from the pyrolysis Rock-Eval are T_{max}, HI, and OPI.

5.3 Results

The total organic carbon (TOC) and sulfur in the gangue carbonates of San Vicente are presented in Table 5.1, and summarized in Table 5.2. The bituminous silty Uncush limestone is rich in organic matter (0.28 to 4.01 wt.% TOC) and sulfur (0.03 to 1.4 wt.%). The relatively high sulfur concentrations is attributed to the presence of fine-grained diagenetic pyrite. The organic content of the dark replacement dolomite decreases with increasing grain size and alteration from 0.07 to 1.22 wt.% in the very-fine grained DRD (Ivf) to <0.01 wt.% in the pervasively altered DRD (Im). The TOC values in the white sparry dolomite range between <0.01 and 0.13 wt.% (median: 0.08 wt.%), and the S content between 0.07 and 0.08 wt.%. In the bituminous horizon at the "Jesús manto" the organic carbon content is up to 12.3 wt.%. The late filling carbonates have very low concentrations in organic matter and sulfur (TOC < 0.05 wt.%, S < 0.03 wt.%).

Similar contents in organic matter were reported by Maqueen and Powell (1983) in the bituminous limestone (0.80 to 7.5 wt.%) and the dolostones (0.13 to 1.8 wt.%) of the Middle Devonian barrier complex at the MVT district of Pine Point. Viets at al. (1983) documented that the organic content of the dolostones of the Upper Cambrian Bonneterre Formation is up to 0.2 wt.% TOC, which decreases by a factor of 3 to 5 near the ore deposits of Viburnum Trend. Recent studies precised that the TOC in these dolostones range from 0.05 to 0.47 wt.% (Henry et al., 1992).

The content of organic matter in the hydrothermal carbonates (DRD, WSD, LFD,

Table 5.1. Total organic carbon (TOC) and sulfur contents in the gangue carbonates from the San Vicente district

Sample	Loc.[1]	Lith.[2]	Carbonate[3]	TOC[4] (wt.%)		S[5] (wt.%)
				LECO	Rock-Eval	
FSV-015	SV	UL			2.17	
FSV-017	SV	UL			0.28	
FSV-1101	SV	UL		4.01	4.46	0.87
FSV-1102	SV	UL		2.62	2.73	1.17
FSV-1103	SV	UL			2.92	
FSV-1097	VI	UL		3.06		1.4
FSV-891	QS	UL		0.14	0.16	0.02
FSV-1133	QC	UL			2.89	
FSV-1136	QC	UL			2.89	
FSV-1059	QU	UL		2.02	0.72	0.91
FSV-020	SV	SVD	DRD (Ivf)		0.07	
FSV-684	QP	SVD	DRD (Ivf)	1.22		
FSV-685	QP	SVD	DRD (Ivf)	0.09		
FSV-801	SV	AD	DRD (Ivf)	0.37	0.35	0.42
FSV-811	SV	AD	DRD (Ivf)	0.31	0.26	2.07
FSV-423	SV	SVD	DRD (Ivf)	0.13		0.13
FSV-754	CH	SJD	DRD (Ivf)	0.15		
FSV-759	CH	SVD	DRD (Ivf)	0.22		
FSV-1098	VI	SVD	DRD (Ivf)	0.23		
FSV-689	PI	CD	DRD (Ivf)	0.07		
FSV-691	PI	CD	DRD (Ivf)	0.11		
FSV-905	SV	SVD	DRD (If)	0.09		0.07
FSV-919	SV	SVD	DRD (If)	0.09		0.25
FSV-811	SV	AD	DRD (If)	0.04		0.15
FSV-713	SV	SJD	DRD (If)		<0.01	
FSV-924	SV	SVD	DRD (Im)		<0.01	
FSV-718	SV	SJD	DRD (Im)		<0.01	
FSV-984	QP	SVD	WSD (II)	0.07		
FSV-924	SV	SVD	WSD (II)	0.06		
FSV-816	SV	AD	WSD (II)	0.09		0.07
FSV-661	SV	SVD	WSD (II)	0.13		0.07
FSV-914	SV	SVD	WSD (II)		0.01	
FSV-919	SV	SVD	WSD (II)	0.11		0.08
FSV-919	SV	SVD	LFD (IIId)	0.05		0.02
FSV-665	SV	AD	LFC (IIIc)	0.02		0.03
FSV-671	SV	SVD	IIIbit*		5.22	
FSV-678	SV	SVD	IIIbit*		12.34	
FSV-423	SV	SVD	EPc			0.05
FSV-029	SV	SVD	EPc			0.86
FSV-904	SV	SVD	EPc			0.02

[1] QP = Quebrada Piñón; QU = Quebrada Utcuyacu; CH = Chilpes; SV = San Vicente mine; VI = Vilcapoma; QS = Quebrada Seca; QC = Quebrada Cascas; PI = Pichita (see Fig. 4.1).

[2] Lithologies: AD = Alfonso Dolomite; UL = Bituminous silty Uncush Limestone; SVD = San Vicente Dolomite; SJD = San Judas Dolomite

[3] DRD = dark replacement dolomite ("Ivf" very fine-grained, "If" fine-grained, "Im" medium grained); WSD = white sparry dolomite (II); LFD = late filling dolomite (IIId); LFC = late filling calcite (IIIc); EPc = calcite replacing evaporitic sulfate; IIIbit = hydrothermal bitumen; IIIbit*=bituminous "horizon" in the DRD

[4] Lower limit of detection (LLD) : LECO pyrolysis = 0.01 wt.%, Rock-Eval pyrolysis = 0.01 wt.%

[5] LECO pyrolysis (LLD = 0.01 wt.%)

blank = not analyzed

LFC) roughly correlates (r^2=0.68) with the sulfur concentration (Fig. 5.1), suggesting a causal relationship between the ore sulfides and the organic matter. In the dark replacement dolomite sulfur is likely present as organo-sulfur compounds (Spangenberg et al., 1995).

Table 5.2. Ranges and median values of total organic carbon (TOC) and sulfur of the gangue carbonates from San Vicente district

Carbonate (m, n)	TOC (wt.%)	S (wt.%)
Uncush Limestone (10, 5)	0.28 to 4.01 (2.76)	0.02 to 1.4 (0.9)
Dark replacement dolomite Ivf (11, 3)	0.07 to 1.22 (0.15)	0.13 to 2.07 (0.42)
Dark replacement dolomite If (4, 3)	0.01 to 0.09 (0.04)	0.07 to 0.25 (0.15)
Dark replacement dolomite Im (2, 0)	<0.01	
Bituminous "horizon" (2, 0)	5.22 to 12.34 (8.8)	
White sparry dolomite II (6, 3)	<0.01 to 0.13 (0.08)	0.07 to 0.08 (0.07)
Late filling dolomite IIId (1, 1)	0.05	0.02
Late filling calcite IIIc (1, 1)	0.02	0.03
Calcite replacing evaporitic sulfate (0, 3)		0.02 to 0.86 (0.3)

m, n = number of analyzed samples (TOC, S)

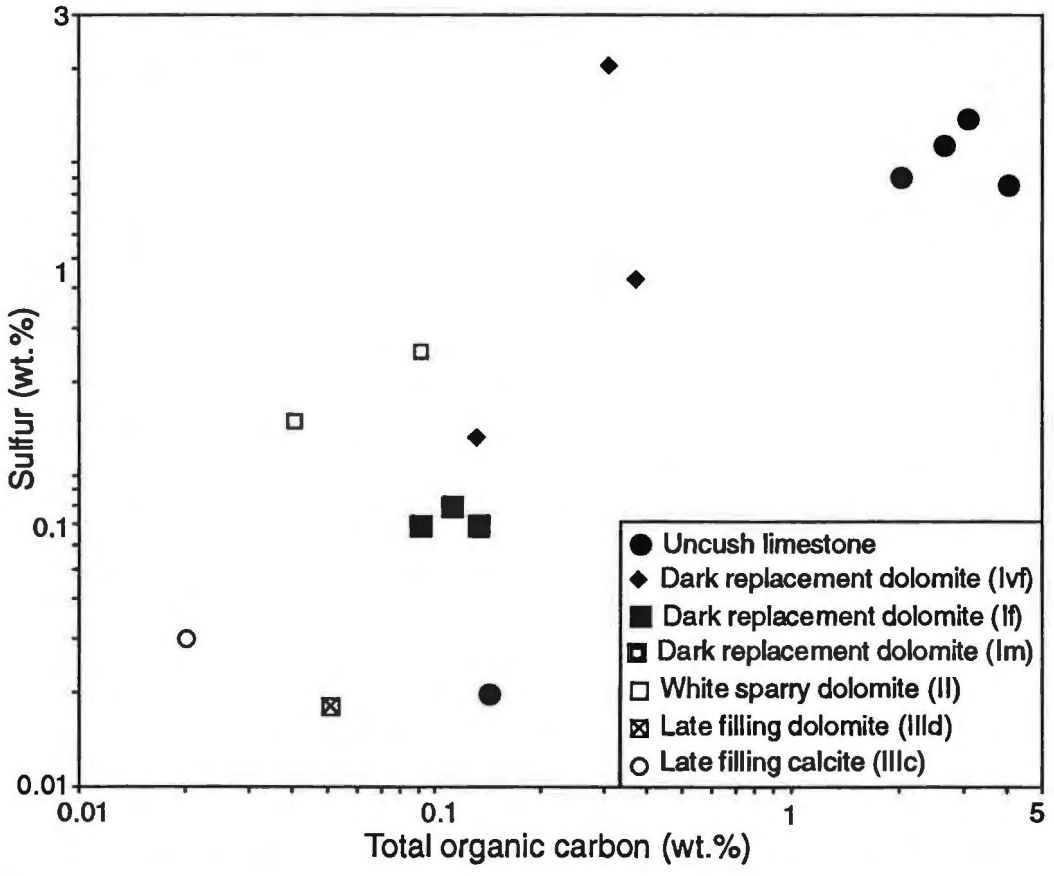

Figure 5.1. Total sulfur versus total organic carbon in gangue carbonates from the San Vicente Mississippi Valley-type district

The analyzed calcites replacing evaporitic sulfates contain traces of sulfur (0.02 and 0.9 wt.%) likely due to disseminated native sulfur. Occasionally, aggregates of coarse-grained native S overgrow calcite in the sulfate pseudomorphs.

The results of the Rock-Eval pyrolysis are given in Table 5.3. For S_1 and $S_2 < 0.2$ the parameters T_{max}, OPI, and HI are not significant (e.g. Espitalié et al., 1986). In Table 5.4 are summarized the raw data of the samples with TOC > 0.2 wt.%. Some features can be recognized (based in written communication of J.R. Disnar, 1994):

1) The Rock-Eval parameters of the bituminous silty Uncush limestone scatter greatly, with T_{max} ranging from 235°C to 480°C and HI from 8 to 103 mg HC/g TOC. This suggests the presence of different types of organic matter (Table 5.4). Thus, these samples were also analyzed by Rock-Eval pyrolysis after extraction with chloroform (samples a* and b* in Table 5.3), to remove the oil and oil-like products ("soluble bitumen"). The high S_1 (0.09 to 0.35 mg HC/g sample) and OPI (0.33 to 0.62) of the $CHCl_3$-extracted samples of the Uncush limestone (FSV-1101, FSV-1102, FSV-1103), and their higher TOC (3.86, 5.62, 3.46 wt.%) compared to the whole rock (4.36, 2.73, 2.92 wt.%) are interpreted to be due to residual chloroform. The T_{max} values of the $CHCl_3$-extracted Uncush limestone are higher (410 to 575°C, median: 515°C) than the measured in the whole rock (235 to 480°C, median: 285°C). This indicates that two types of organic matter occur in the Uncush Limestone: "OMI" and "OMII". OMI is an hyper-mature, likely autochthone, kerogen characterized by $T_{max} \approx 515$°C and poor in free HC (very low S_2 and HI), and is occasionally very abundant (e.g. 5.6 wt.% TOC in FSV-1102). OMII is likely an allochthonous soluble organic matter (bitumen) characterized by lower T_{max} (≈230°C) and high S_1 poor in free HC (very low S_2 and HI). The $CHCl_3$-extracted samples, excepting FSV-891, have markedly low HI values (8 - 60 mg HC/g TOC) in contrast to the non-extracted samples (2 - 19 mg HC/g TOC). This reflects, as expected, the loss of soluble bitumen during extraction.

2) In the samples of UL where the pyrolysis began at 300°C (FSV-891, FSV-1135, FSV-1136) the parameter $S_1 > S_2$. This indicates that thermally labile organic compounds (volatile at ≈300°C) were detected together with the free HC (oil, peak S_1). Thus, these light hydrocarbons are expressed in the peak S_1 but also in peak S_2, causing a shift of the measured T_{max} (about 326°C) toward the temperature of the beginning of the pyrolysis.

3) Some samples of the Uncush Limestone (FSV-015, FSV-1102, FSV-1103) have T_{max} values (415, 410, 420°C) close to the lower boundary of the oil window (about 435°C, Espitalié et al., 1985b, Milles, 1994). This suggests that the native organic matter in this samples was near the maturity state for oil generation. Leventhal (1990) reported similar T_{max} ranges (431 to 441°C) in the dolostones of the Bonneterre Formation at barren areas near the Viburnum Trend.

4) Dark replacement dolomite and white sparry dolomite have very low S_1 and S_2 values («0.2 mg HC/g sample); thus, the values of T_{max}, OPI and HI are unreliable (Table 5.3). However, the total organic carbon of the DRD (FSV-801, FSV-811) and the WSD (FSV-924) from the Alfonso Dolomite are relatively high (0.35, 0.26, 0.23 wt.%). This indicates that only very mature kerogen occurs in these ore-stage carbonates.

5) The bituminous "horizon" in the San Vicente Dolomite (FSV-671, FSV-678) has high S_1 values (0.59 and 0.69 mg HC/g sample), indicating significant amount of free oil (OMII), volatile at 200°C. These samples have also important amount of the mature kerogen OMI (5.2 and 12.3 wt.% TOC).

5.4 Discussion

The Rock-Eval results at San Vicente indicate that two types of organic matter are related to the mineralization: an autochthonous hyper - mature kerogen (OMI) and an allochthonous thermally labile chloroform-soluble bitumen (OMII). The presence of bitumen indicates temperatures have reached about 100°C (Tissot and Welte, 1978, p. 262), which is in line with fluid inclusions in the white sparry dolomite (Moritz et al., in press) suggesting that the ore fluid was at a temperature range of 115 to 162°C. Kerogen can produce oil at a temperature between 60 to 160°C, that matches the measured Rock-Eval T_{max} close to the boundary of the "oil window" (435 to 455°C, Miles, 1994). Thus, it is assumed that the

Table 5.3. Rock-Eval parameters and insoluble residue (IR) of the gangue carbonates of San Vicente district

Sample	Loc.[1]	Lit.[2]	Carbo.[3]	Ana.[4]	S_1 (mgHC/g)	S_2 (mgHC/g)	T_{max} (°C)	TOC (wt.%)	OPI	HI (mgHC/gOC)	IR (wt.%)
FSV-1059	QU	UL		a	0.14	0.56	237	0.72	0.20	77	29.1
FSV-015	SV	UL		a	0.38	0.39	418	2.17	0.53	16	31.7
FSV-017	SV	UL		a	0.04	0.27	481	0.26	0.13	103	
FSV-1101	SV	UL		a	0.22	1.32	240	4.46	0.14	28	39.8
FSV-1101	SV	UL		a*	*0.35*	*0.61*	*515*	*3.86*	*0.36*	*15*	
FSV-1102	SV	UL		a	0.25	1.64	243	2.73	0.13	60	
FSV-1102	SV	UL		a*	*0.29*	*0.60*	*411*	*5.62*	*0.33*	*10*	
FSV-1103	SV	UL		a	0.19	0.65	235	2.92	0.23	22	35.9
FSV-1103	SV	UL		a*	*0.34*	*0.68*	*419*	*3.46*	*0.33*	*19*	
FSV-891	QS	UL		b	0.04	0.03	523	0.16	0.67	15	
FSV-891	QS	UL		b*	*0.01*	*0.01*	*374*	*0.04*	*0.50*	*25*	
FSV-1135	QC	UL		b	1.00	0.29	327	2.89	0.78	9	
FSV-1135	QC	UL		b*	*0.10*	*0.07*	*523*	*3.09*	*0.62*	*2*	
FSV-1136	QC	UL		b	0.87	0.24	325	2.89	0.79	8	
FSV-1136	QC	UL		b*	*0.09*	*0.07*	*575*	*2.59*	*0.57*	*2*	
FSV-801	SV	AD	DRD Ivf	a	0.10	0.07	381	0.35	0.62	20	4.1
FSV-811	SV	AD	DRD Ivf	a	0.09	0.07	343	0.26	0.56	26	12.5
FSV-020	SV	SVD	DRD Ivf	a	0.10	0.06	371	0.07	0.62	85	10.4
FSV-713	SV	SJD	DRD If	a	0.10	0.07	370	<0.01	0.62	700	0.5
FSV-718	SV	SJD	DRD If	a	0.10	0.12	388	<0.01	0.45	1200	<0.05
FSV-924	SV	SVD	DRD Im	a	0.07	0.03	346	<0.01	0.70	300	
FSV-924	SV	SVD	WSD (II)	a	0.01	0.15	371	0.23	0.06	65	
FSV-914	SV	SVD	WSD (II)	a	0.01	0.16	356	<0.01	0.06		
FSV-671	SV	SVD	IIIbit	a	0.59	0.20	338	5.22	0.76	3	
FSV-678	SV	SVD	IIIbit	a	0.69	0.42	362	12.34	0.61	3	

[1] QU = Quebrada Utcuyacu; SV = San Vicente mine; QS = Quebrada Seca; QC = Quebrada Cascas (see Fig. 4.1).

[2] Lithologies: AD = Alfonso Dolomite; UL = Bituminous silty Uncush Limestone; SVD = San Vicente Dolomite; SJD = San Judas Dolomite (see Fig. 4.2)

[3] UL = bituminous silty Uncush limestone; DRD = dark replacement dolomite ("Ivf" very fine-grained, "If" fine-grained, "Im" medium grained; WSD = white sparry dolomite (II); IIIbit = hydrothermal bitumen

[4] Analytical procedure: a = first pyrolysis-step at a temperature of 200°C; b = first pyrolysis-step at a temperature of 300°C; * = analysis of the extract with chloroform

Rock-Eval parameters: S_1= free hydrocarbons (oil) in mg HC per g sample; S_2 = kerogen in mg HC per g sample; T_{max} in °C; TOC = total organic carbon in wt.%; OPI = oil production index (OPI = $S_2/[S_1+S_2]$), dimensionless; HI = hydrogen index = S_2/TOC in mg HC per g TOC); for S_1 and S_2 <0.2 T_{max} and OPI are not significative; for TOC<0.3 all parameter are unreliable

blank = mot analyzed

Table 5.4. Ranges and median values of the Rock-Eval parameters[1] of the gangue carbonates of San Vicente

Carbonate[2] (n)	S_1 (mg HC/g)	S_2 (mg HC/g)	T_{max} (°C)	TOC (wt.%)	OPI	HI (mg HC/g TOC)
UL	0.04 to 1.00	0.24 to 1.64	235 to 481	0.26 to 4.45	0.13 to 0.79	8 to 103
(8)	(0.24)	(0.48)	(284)	(2.81)	(0.21)	(25)
UL*	0.09 to 0.35	0.07 to 0.68	411 to 575	2.59 to 5.62	0.33 to 0.62	2 to 19
(5)	(0.29)	(0.60)	(515)	(3.46)	(0.36)	(10)
DRD Ivf	0.09 to 0.10	0.07	343 to 381	0.26 to 0.32	0.56 to 0.62	20 to 26
(2)	(0.09)		(362)	(0.30)	(0.59)	(23)
IIIbit	0.59 to 0.69	0.20 to 0.42	338 to 362	5.22 to 12.34	0.61 to 0.76	3
(2)	(0.64)	(0.31)	(350)	(8.78)	(0.68)	

[1] Only for samples with TOC<0.2: S_1 (OIL) = free hydrocarbons (HC) in mg HC per g sample; S_2 = kerogen in mg HC per g sample; T_{max} in °C; TOC = total organic carbon in wt.%; OPI = oil production index, (OPI = $S_2/[S_1+S_2]$), dimensionless; HI = hygrogen index = S_2/TOC in mg HC per g TOC)

[2] UL = bituminous silty Uncush limestone; * = analysis after extraction with chloroform; DRD Ivf = very fine-grained dark replacement dolomite; IIIbit = hydrothermal bitumen; n = analyzed samples

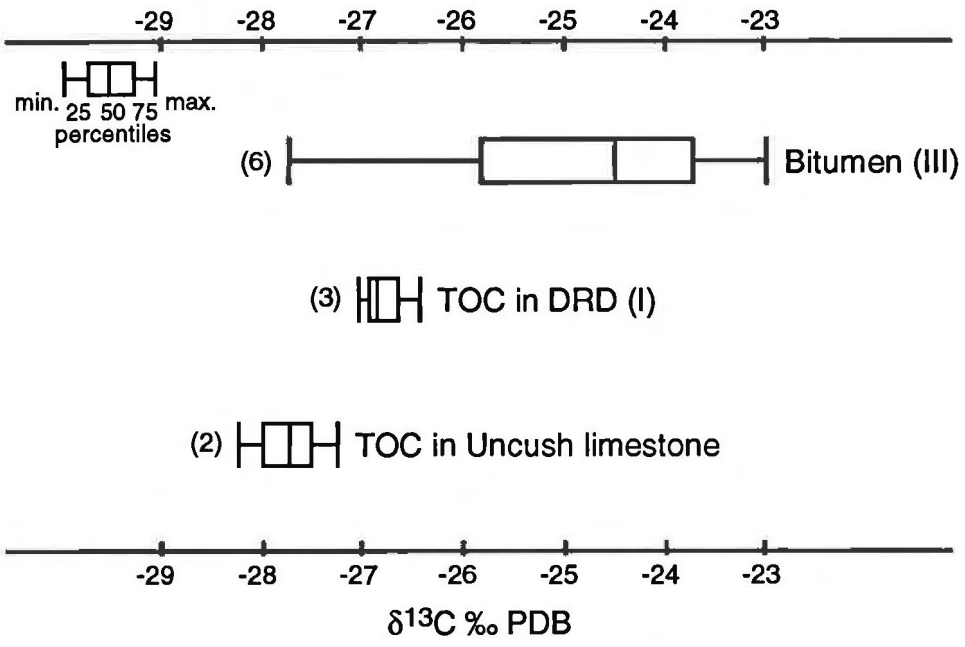

Figure 5.2. Variation of the $\delta^{13}C$ of the total organic carbon (TOC) associated to the gangue carbonates of San Vicente: TOC in the bituminous silty Uncush limestone, TOC in the dark replacement dolomite (DRD), and the late-stage hydrothermal bitumen (III); ($\delta^{13}C$ values in Spangenberg, 1995, chapter 3)

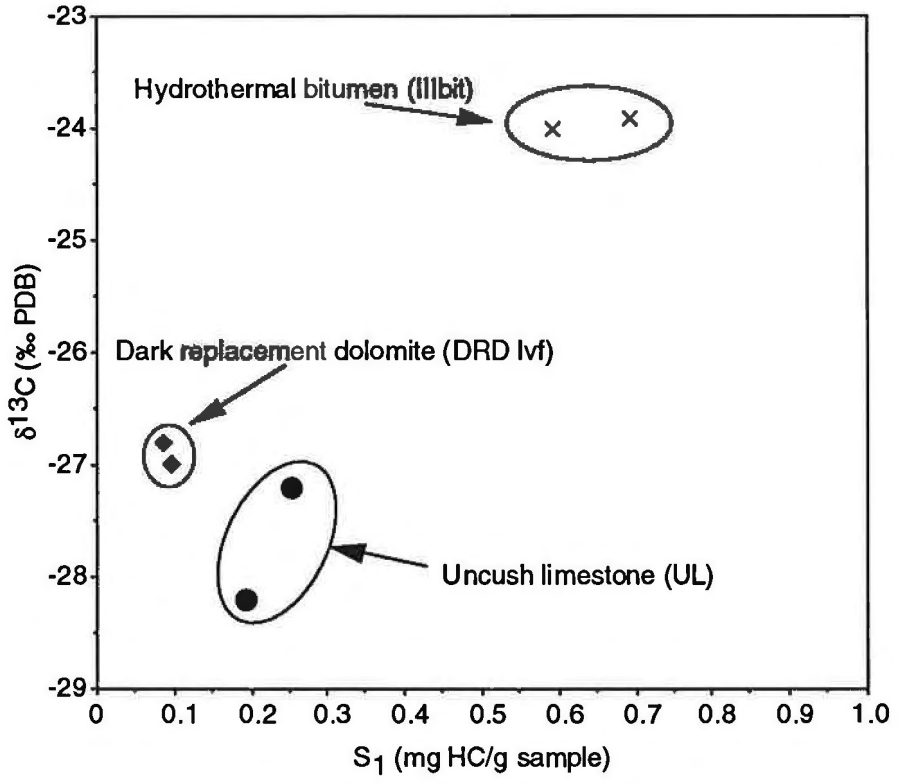

Figure 5.3. $\delta^{13}C$ versus the Rock-Eval parameter S_1 (oil) of the total organic carbon in the gangue carbonates of the San Vicente district

indigenous organic matter (kerogen) in the host dolomite of San Vicente produced oil during its alteration by the hot mineralizing fluid. The carbon isotope composition of the total organic carbon in gangue carbonates, and the hydrothermal bitumen suggest that alteration (thermal cracking, water-washing, and polymerization) of this oil produced isotopic-heavier solid bitumen (Fig. 5.2) and light gaseous hydrocarbons, mainly methane (e.g., Parnell, 1992; Sassen, 1988). The $\delta^{13}C$ versus S_1 diagrams illustrate that the total organic carbon of the hydrothermal solid bitumen is heavier than the altered "native" OM disseminated in the bituminous silty Uncush Limestone and the host dark replacement dolomite in spite of the slightly higher oil content of the solid bitumen (Fig. 5.3). The bitumen occurs as overgrowth of the late-filling carbonates, indicating that water-washing and polymerization, likely due to dilution and increase in pH and oxygen fugacity, occurred during the post-ore influx of basinal fresh waters. This conclusion is supported by the pH-Eh changes as deduced by the behaviour of Fe-Mn covariations and REE of the hydrothermal carbonates, that indicate that the post-ore environment was solution-buffered and oxidant (Spangenberg and Fontboté, 1995). In addition, the released hydrocarbons were likely involved in the thermochemical sulfate reduction, which causes the precipitation of low ^{13}C carbonates (e.g. Spangenberg et al., 1995).

5.5 Conclusions

The Rock-Eval results indicate that two types of organic matter occur in the gangue carbonates of San Vicente: a hyper-mature kerogen, which likely is thermally altered native organic matter, and an allochthonous thermally labile soluble bitumen. Alteration of the disseminated OM in the host dolomite by the incoming ore fluid released hydrocarbons which were precipitated as solid aggregates after further thermal cracking, water-washing, and polymerization. These results combined with carbon isotope data suggest that the native organic matter was the main source of reductants in the mineralizing fluid.

References

Anderson, G.M. (1991) Organic maturation and ore precipitation in southeast Missouri. Economic Geology, v. 86, p. 909-926.

Anderson, G.M. and Garven, G.(1987) Sulfate-sulfide-carbonate associations in Mississippi Valley-Type lead-zinc deposits. Economic Geology, v. 82, p. 482-488.

Anderson, G.M., and Macqueen, R.W. (1988) Mississippi Valley-type lead-zinc deposits. In: Roberts, R.G., and Sheahan, P.A. (Editors) Ore deposit models, Geoscience Canada, Reprint Series 3, p. 79-90.

Cannon, J. and Orgeval, J.J. (1976) Un example des reaction hydrocarbures - minéralisation: cas du filon de barytine de St. Privat (Bassin de Lodève, France). Bull. Centre Rech. Pau - SNPA, v. 10, p. 359-374.

Disnar, J.R. (1988) Apport de la géochimie organique a la comprehension de la genese des gîtes Zn-Pb en environnement sedimentaire. In: Pelissonnier, H., and Sureau, J.F. (Editors) Mobilité et concentration des metaux de base dans les couvertures sédimentaires. Manifestations, mécanismes, prospection. Document du BRGM, n. 183, p. 249-268.

Disnar, J.R., and Gauthier, B. (1989) Contribution of organic geochemistry to regional exploration and characterization of Mississippi Valley-type mineralization in the Causses basin (France). Journal of Geochemical Exploration, v. 32, p. 401-403.

Disnar, J.R., and Héroux, Y. (1995) Dégradation et lessivage des hydrocarbures de la formation ordovicienne de Thumb Montain encaissant le gîte Zn-Pb de Polaris (TNW, Canada). Canadian Journal of Earth Sciences, (in press).

Espitalié, J, Deroo, G., and Marquis, F. (1985a) La pyrolyse rock-eval et ses applications, première partie. Revue Institut français du Pétrole, v. 40, p. 563-579.

Espitalié, J, Deroo, G., and Marquis, F. (1985b) La pyrolyse Rock-Eval et ses applications, deuxième partie. Revue Institut français du Pétrole, v. 40, p. 755-784.

Espitalié, J, Deroo, G., and Marquis, F. (1986) La pyrolyse rock-eval et ses applications, troisième partie. Revue Institut français du Pétrole, v. 41, p. 73-89.

Espitalié, J, Laporte, J.L., Madec, M., Marquis, F., Leplat, P., Paulet, J., and Boutefeu, A. (1977) Méthode rapide de caractérisation des roches méres de leur potential pétrolier et de leur degré d'évolution. Revue Institut français du Pétrole, v. 32, p. 23-42.

Giordano, T.H. (1993) Metal transport in ore solutions by organic ligand complexation. In: Parnell, J., Ruffell, A.H., and Moles, N.R. (Editors) Geofluids '93, 4th-7th May 1993, Torquay, England, p. 413-416.

Giordano, T.H., and Barnes, H.L. (1981) Lead transport in Mississippi Valley-Type ore solutions. Economic Geology, v. 76, p. 2200-2211.

Gize, A.P., and Barnes, H.L. (1987) The organic geochemistry of two Mississippi Valley-Type lead-zinc deposits. Economic Geology, v. 82, p. 457-470.

Gize, A.P., Barnes, H.L., and Bell, J.S. (1991) A critical evaluation of organic processes in Mississippi Valley-Type genesis. In: Pagel, M., and Leroy, J.L. (Editors) Source, transport and deposition of metals. Balkema, Rotterdam, p. 527-530.

Henry, A.L., Anderson, G.M., and Héroux, Y. (1992) Alteration of organic matter in the Viburnum Trend lead-zinc district of southeastern Missouri. Economic Geology, v. 87, p. 288-309.

Héroux, Y., Chagnon, A., and Savard, M.M. (1994) Anomalies des propiétés de la matière organique et des assemblages argileux associés au gîte de Pb-Zn de Gays River, Nouvelle-Écocsse, Canada. Exploration Mining Geology, v. 3, p. 67-79.

Héroux, Y., and Tassé, N. (1990) Organic-matter alteration in an early Paleozoic basin: Zonaton around mineral showings compared to that around intrusions, St. Lawrence Lowlands, Quebec, Canada. Geological Society of America Bulletin, v. 102, p. 877-888.

Katz, B.J. (1983) Limitations of "Rock-Eval" pyrolysis for typing organic matter. Organic Geochemistry, v. 4, p. 195-199.

Leventhal, J.S. (1990) Organic matter and thermochemical sulphate reduction in the Viburnum Trend, southeast Missouri. Economic Geology, v. 85, p. 622-632.

Macqueen, R.W. (1986) Origin of Mississippi Valley-Type lead-zinc ores by organic matter-sulfate reactions: the Pine Point example. In: Dean, W.A.(Editor) Organics in ore deposits. Proceedings Denver Regional Exploration Geologists Society, p. 151-164.

Macqueen, R.W., and Powell, T.G. (1983) Organic geochemistry of the Pine Point lead-zinc ore field and region, Northwest Territories, Canada. Economic Geology, v. 18, p. 1-25.

Manning, D.A.C. (1986) Assessment of the role of organic matter in ore transport processes in low-temperature base-metal systems. Transactions Institution Mining and Metallurgy, sect. B, v. 95, p. 195-200.

Manning, D.A.C., and Gize, A.P. (1993) The role of organic matter in ore transport precesses. In: Engel, M.H., and Macko, S.A. (Editors) Organic geochemistry. Plenum Press, New York, p. 547-563.

Marikos, M.A. (1986) Relation of bitumen to ore in the Magmont West orebody, Viburnum Trend, Missouri. In: Dean, W.A.(Editor) Organics in ore deposits. Proceedings Denver Regional Exploration Geologists Society, p. 151-164.

Marikos, M., Laudon, R., and Leventhal, J. (1986) Solid insoluble bitumen in the Magmont west orebody, Southeast Missouri. Economic Geology, v. 81, p. 1983-1988.

Miles, J.A. (1994) Illustrated glossary of petroleum geochemistry. Clarendon, Oxfotd, 137 pp.

Moritz, R., Fontboté, L., Spangenberg, J. Rosas, S., Sharp, Z. and Fontignie, D. (in press) Sr, C and O isotope systematics in the Pucará Basin, Central Peru: comparison between Mississippi Valley-type deposits and barren areas. Mineralium Deposita.

Parnell, J. (1992) Introduction. In: Parnell, J. Kucha, H., and P. Landais (Editors) Bitumens in ore deposits. Spec. Pub. Nr. 6 of the SGA. Springer, Berlin. p. 1-7.

Parnell, J., Kucha, H., and Landais, P. (1992) Bitumens in ore deposits. Special Publication Nr. 6 of the SGA. Springer, Berlin.

Powell, T.G., and Macqueen, R.W. (1984) Precipitation of sulfide ores and organic matter: sulfate reactions at Pine Point, Canada. Science, v. 224, p. 63-66.

Sassen, R. (1988) Geochemical and carbon isotopic studies of crude oil destruction, bitumen precipitation, and sulfate reduction in the deep Smackover Formation. Organic Geochemistry, v. 12, p. 351-361.

Spangenberg, J., and Fontboté, L. (1995) Rare-earth and trace elements in hydrothermal carbonates of the San Vicente Mississippi Valley-type district, central Peru. (to be submitted)

Spangenberg, J, Fontboté, L., Sharp, Z., and Hunziker, J. (1995) Carbon and oxygen isotope study of hydrothermal carbonates in the zinc-lead deposits of San Vicente, central Peru. (to be submitted)

Spirakis, C.S. (1986) Occurrence of organic carbon in Mississippi Valley Deposits and an evaluation of processes involving organic carbon in the genesis of these deposits. In: Dean, W.A.(Editor) Organics in ore deposits. Proceedings Denver Regional Exploration Geologists Society, p. 85-92.

Spirakis, C.S., and Heyl, A.V. (1992) Organic matter (bitumen and other forms) as the key to localization of Mississippi Valley-Type Ores. In: Parnell, J. Kucha, H., and P. Landais (Editors) Bitumens in ore deposits. Spec. Pub. Nr. 6 of the SGA. Springer, Berlin. p. 381-398.

Sverjensky, D.A. (1986) Genesis of Mississippi Valley-type lead-zinc deposits. Annual Review of Earth and Planetary Sciences, v. 14, p. 177-199.

Tissot, B., Durand, B., Espitalié, J, and Combaz, A. (1974) Influence of nature and diagenesis of organic matter in formation of petroleum. American Association of Petroleum Geologists Bulletin, v. 58, 499-506.

Tissot, B. and Welte, D.H. (1978) Petroleum formation and occurrence. Springer, Berlin, 538 pp.

APPENDIX 1

CARBON AND OXYGEN ISOTOPIC COMPOSITION OF HOST AND GANGUE MINERALS

Abbreviations used in Appendix 1

Lab. mr.: internal laboratory number
St. sc.: study scale, OS = outcrop (including rock scale); MS = mine (including manto scale); RS = district scale
Unit: SJD = San Judas Dolomite; SVD = San Vicente Dolomite; UL = Bituminous silty Uncush Limestone; AD = Alfonso Dolomite
Stud. min.: studied mineral, DRD = dark replacement dolomite ("Ivf" very fine-grained, "If" fine-grained, "Im" medium-grained); WSD = white sparry dolomite (II); LFD = late-stage filling dolomite (IIId); LFC = late-stage filling calcite (IIIc); EPd, EPc = dolomite or calcite replacing sulfate evaporites; Iom = organic matter disseminated in the DRD; IIIbit = hydrothermal bitumen; ULom = organic matter disseminated in the bituminous silty Uncush limestone
WSD sub.: subgenerations of WSD = "t1" millimetric-sized spots of WSD; "t2" fine veinlets of WSD, "t3" ordered millimetric to centimetric thick bands of WSD; "t4" WSD in zebra rock; "t5" crosscutting veins of WSD; and "t6" white dolomite as oriented overgrowths of hydraulic breccias
E (m) and N (m): mine coordinates
d18O (PDB): $\delta^{18}O$ value in ‰ PDB
d13C (PDB): $\delta^{13}C$ value in ‰ PDB

Table A1.1. Carbon and oxygen isotopic composition of host and gangue minerals from the San Vicente district

Sample	Lab. nr.	St. sc.	Locality	Unit	Manto	Stud. min.	WSD sub.	E (m)	N (m)	d18O (PDB)	d13C (PDB)
FSV-901		OS	San Vicente N	SVD	Jesus	DRD (If)		19846	21566	-8.8	0.7
FSV-901		OS	San Vicente N	SVD	Jesus	EPc		19846	21566	-15.5	-3.2
FSV-902		OS	San Vicente N	SVD	Jesus	DRD (If)		19846	21566	-8.6	0.9
FSV-902		OS	San Vicente N	SVD	Jesus	WSD (II)	t6	19846	21566	-9.4	1.0
FSV-902	JS-46	OS	San Vicente N	SVD	Jesus	LFC (IIIc)		19846	21566	-12.7	-2.5
FSV-902		OS	San Vicente N	SVD	Jesus	LFC (IIIc)		19846	21566	-12.8	-2.6
FSV-903		OS	San Vicente N	SVD	Jesus	DRD (Im)		19846	21566	-7.8	0.9
FSV-903		OS	San Vicente N	SVD	Jesus	WSD (II)	t3	19846	21566	-8.3	1.2
FSV-904	JS-54	OS	San Vicente N	SVD	Jesus	EPc		19846	21566	-16.1	-3.3
FSV-904		OS	San Vicente N	SVD	Jesus	EPc		19846	21566	-15.9	-3.3
FSV-905	JS-26	OS	San Vicente N	SVD	Jesus	DRD (If)		19816	21392	-7.4	1.6
FSV-905		OS	San Vicente N	SVD	Jesus	WSD (II)	t3	19816	21392	-8.5	1.4
FSV-905		OS	San Vicente N	SVD	Jesus	WSD (II)	t2	19816	21392	-10.4	0.7
FSV-905		OS	San Vicente N	SVD	Jesus	WSD (II)	t1	19816	21392	-11.4	-0.1
FSV-905		OS	San Vicente N	SVD	Jesus	WSD (II)	t2	19816	21392	-9.8	1.0
FSV-905		OS	San Vicente N	SVD	Jesus	LFC (IIIc)		19816	21392	-11.2	0.2
FSV-906		OS	San Vicente N	SVD	Jesus	DRD (Ivf)		19816	21392	-7.1	1.9
FSV-906		OS	San Vicente N	SVD	Jesus	LFC (IIIc)		19816	21392	-14.3	-1.5
FSV-906		OS	San Vicente N	SVD	Jesus	LFC (IIIc)		19816	21392	-13.2	-1.2
FSV-906		OS	San Vicente N	SVD	Jesus	LFC (IIIc)		19816	21392	-15.1	-0.8
FSV-907		OS	San Vicente N	SVD	Jesus	WSD (II)	t3	19816.7	21337	-8.7	0.9
FSV-908		OS	San Vicente N	SVD	Jesus	DRD (If)		19816.7	21337	-7.6	1.3
FSV-908		OS	San Vicente N	SVD	Jesus	WSD (II)		19816.7	21337	-7.9	1.2
FSV-908		OS	San Vicente N	SVD	Jesus	LFC (IIIc)		19816.7	21337	-14.8	-2.5
FSV-909	JS-27	OS	San Vicente N	SVD	Jesus	WSD (II)	t3	19816.7	21337	-8.7	1.0
FSV-910		OS	San Vicente N	SVD	Jesus	WSD (II)	t3	19816	21312	-8.2	0.9
FSV-910		OS	San Vicente N	SVD	Jesus	LFC (IIIc)		19816	21312	-11.6	-0.3
FSV-911	JS-28	OS	San Vicente N	SVD	Jesus	DRD (Im)		19816	21312	-8.7	1.0
FSV-911		OS	San Vicente N	SVD	Jesus	WSD (II)	t4	19816	21312	-8.7	1.0
FSV-912		OS	San Vicente N	SVD	Jesus	DRD (Ivf)		19816	21312	-7.1	1.7
FSV-912		OS	San Vicente N	SVD	Jesus	LFC (IIIc)		19816	21312	-12.0	-1.0
FSV-913	JS-29	OS	San Vicente N	SVD	Ayala	WSD (II)	t6	19596.5	20598	-8.5	1.0
FSV-914		OS	San Vicente N	SVD	Ayala	DRD (Im)		19596.5	20598	-9.5	1.0
FSV-914		OS	San Vicente N	SVD	Ayala	DRD (Im)		19596.5	20598	-9.6	1.1
FSV-914		OS	San Vicente N	SVD	Ayala	WSD (II)	t3	19596.5	20598	-9.8	1.4
FSV-914		OS	San Vicente N	SVD	Ayala	WSD (II)	t3	19596.5	20598	-9.7	1.4
FSV-914		OS	San Vicente N	SVD	Ayala	WSD (II)	t3	19596.5	20598	-9.6	1.5
FSV-914	JS-30	OS	San Vicente N	SVD	Ayala	WSD (II)	t3	19596.5	20598	-10.1	1.2
FSV-914		OS	San Vicente N	SVD	Ayala	WSD (II)	t3	19596.5	20598	-9.5	1.6
FSV-914		OS	San Vicente N	SVD	Ayala	WSD (II)		19596.5	20598	-8.3	1.6
FSV-914		OS	San Vicente N	SVD	Ayala	WSD (II)		19596.5	20598	-8.6	1.4
FSV-914		OS	San Vicente N	SVD	Ayala	WSD (II)		19596.5	20598	-8.2	1.5
FSV-914		OS	San Vicente N	SVD	Ayala	LFD (IIId)		19596.5	20598	-11.2	1.0
FSV-914		OS	San Vicente N	SVD	Ayala	LFD (IIId)		19596.5	20598	-10.6	1.1
FSV-915		OS	San Vicente N	SVD	Ayala	WSD (II)	t4	19797	20600	-9.4	1.5
FSV-915		OS	San Vicente N	SVD	Ayala	WSD (II)	t4	19797	20600	-9.8	1.5
FSV-917		OS	San Vicente N	SVD	Ayala	WSD (II)	t4	19797	20600	-9.5	1.4

continued

Table A.1.1. Continued

Sample	Lab. nr.	St. sc.	Locality	Unit	Manto	Stud. min.	WSD sub.	E (m)	N (m)	d18O (PDB)	d13C (PDB)
FSV-918		OS	San Vicente N	SVD	Ayala	DRD (Ivf)		19797	20600	-6.6	2.5
FSV-916		OS	San Vicente N	SVD	Ayala	WSD (II)	t4	19797	20603	-10.1	1.2
FSV-916		OS	San Vicente N	SVD	Ayala	WSD (II)	t4	19797	20603	-9.7	1.4
FSV-916		OS	San Vicente N	SVD	Ayala	WSD (II)	t4	19797	20603	-9.9	1.3
FSV-916		OS	San Vicente N	SVD	Ayala	WSD (II)	t4	19797	20603	-9.2	1.4
FSV-919		OS	San Vicente N	SVD	Ayala	DRD (If)		19795	20562	-8.3	1.4
FSV-919		OS	San Vicente N	SVD	Ayala	DRD (If)		19795	20562	-8.2	1.3
FSV-919		OS	San Vicente N	SVD	Ayala	DRD (Im)		19795	20562	-9.2	1.0
FSV-919		OS	San Vicente N	SVD	Ayala	DRD (Im)		19795	20562	-8.8	1.2
FSV-919		OS	San Vicente N	SVD	Ayala	WSD (II)	t6	19795	20562	-10.8	0.7
FSV-919		OS	San Vicente N	SVD	Ayala	WSD (II)	t6	19795	20562	-10.7	0.6
FSV-919	JS-31	OS	San Vicente N	SVD	Ayala	WSD (II)	t6	19795	20562	-10.6	0.4
FSV-919		OS	San Vicente N	SVD	Ayala	WSD (II)	t6	19795	20562	-10.8	0.5
FSV-919		OS	San Vicente N	SVD	Ayala	WSD (II)	t6	19795	20562	-10.2	1.0
FSV-919		OS	San Vicente N	SVD	Ayala	WSD (II)	t6	19795	20562	-11.1	0.7
FSV-919		OS	San Vicente N	SVD	Ayala	WSD (II)	t6	19795	20562	-11.8	0.5
FSV-919		OS	San Vicente N	SVD	Ayala	WSD (II)	t6	19795	20562	-11.2	0.9
FSV-919		OS	San Vicente N	SVD	Ayala	WSD (II)	t6	19795	20562	-11.1	0.8
FSV-919		OS	San Vicente N	SVD	Ayala	WSD (II)	t6	19795	20562	-10.4	1.0
FSV-919		OS	San Vicente N	SVD	Ayala	WSD (II)	t6	19795	20562	-10.4	1.0
FSV-919		OS	San Vicente N	SVD	Ayala	LFD (IIId)		19795	20562	-10.9	0.0
FSV-919		OS	San Vicente N	SVD	Ayala	LFD (IIId)		19795	20562	-12.5	-0.2
FSV-919	JS-32	OS	San Vicente N	SVD	Ayala	LFD (IIId)		19795	20562	-12.4	0.1
FSV-919		OS	San Vicente N	SVD	Ayala	LFD (IIId)		19795	20562	-12.2	0.1
FSV-920		OS	San Vicente N	SVD	Ayala	WSD (II)	t4	19795	20562	-10.4	1.2
FSV-921	JS-33	OS	San Vicente N	SVD	Ayala	WSD (II)	t4	19795	20562	-9.2	1.6
FSV-922		OS	San Vicente N	SVD	Ayala	WSD (II)	t4	19795	20562	-10.5	1.2
FSV-922		OS	San Vicente N	SVD	Ayala	WSD (II)	t4	19795	20562	-8.0	1.3
FSV-923		OS	San Vicente N	SVD	Ayala	WSD (II)	t4	19795	20562	-10.9	0.9
FSV-923		OS	San Vicente N	SVD	Ayala	LFD (IIId)		19795	20562	-12.2	-0.3
FSV-924		OS	San Vicente N	SVD	Ayala	DRD (Im)		19797	20602	-8.4	1.0
FSV-924		OS	San Vicente N	SVD	Ayala	WSD (II)	t4	19797	20602	-8.3	1.1
FSV-924		OS	San Vicente N	SVD	Ayala	LFD (IIId)		19797	20602	-11.3	1.1
FSV-654		MS	San Vicente N	AD	Alfonso	DRD (If)		20011	19115	-8.5	1.2
FSV-654	JS-1	MS	San Vicente N	AD	Alfonso	WSD (II)	t3	20011	19115	-9.6	1.0
FSV-655		MS	San Vicente N	AD	Alfonso	WSD (II)	t3	20011	19110	-9.8	1.0
FSV-665	JS-2	MS	San Vicente N	AD	Alfonso	WSD (II)	t6	19579	21107	-8.7	1.1
FSV-665	JS-3	MS	San Vicente N	AD	Alfonso	LFC (IIIc)		19579	21107	-13.4	-2.4
FSV-667		MS	San Vicente N	AD	Alfonso	WSD (II)	t5	19805	21328	-8.2	1.4
FSV-668		MS	San Vicente N	AD	Alfonso	WSD (II)	t5	19875	21036	-9.2	1.7
FSV-801	JS-4	MS	San Vicente N	AD	Alfonso	DRD (Ivf)		19898.5	21869	-7.8	1.3
FSV-801		MS	San Vicente N	AD	Alfonso	WSD (II)	t6	19898.5	21869	-9.9	1.1
FSV-801		MS	San Vicente N	AD	Alfonso	LFC (IIIc)		19898.5	21869	-9.8	-0.5
FSV-801		MS	San Vicente N	AD	Alfonso	Iom		19898.5	21869		-27.0
FSV-803		MS	San Vicente N	AD	Alfonso	WSD (II)	t6	19859	21816	-9.7	1.1
FSV-804		MS	San Vicente N	AD	Alfonso	WSD (II)	t6	19836	21796	-9.9	1.0
FSV-805		MS	San Vicente N	AD	Alfonso	WSD (II)	t6	19825	21773	-10.0	0.9
FSV-806	JS-5	MS	San Vicente N	AD	Alfonso	WSD (II)	t6	19467	21402	-9.3	0.9

continued

Table A.1.1. Continued

Sample	Lab. nr.	St. sc.	Locality	Unit	Manto	Stud. min.	WSD sub.	E (m)	N (m)	d18O (PDB)	d13C (PDB)
FSV-807	JS-6	MS	San Vicente N	AD	Alfonso	WSD (II)	t6	19471	21375	-9.6	1.2
FSV-807	JS-7	MS	San Vicente N	AD	Alfonso	LFC (IIIc)		19471	21375	-11.9	-2.6
FSV-808		MS	San Vicente N	AD	Alfonso	WSD (II)	t5	19477	21352	-8.1	1.5
FSV-809		MS	San Vicente N	AD	Alfonso	WSD (II)	t6	19482	21327	-9.8	1.0
FSV-810		MS	San Vicente N	AD	Alfonso	WSD (II)	t3	19476	21451	-9.9	0.8
FSV-811	JS-8	MS	San Vicente N	AD	Alfonso	DRD (Ivf)		19457	21487	-7.2	1.7
FSV-811	JS-9	MS	San Vicente N	AD	Alfonso	DRD (If)		19457	21487	-7.3	1.2
FSV-811	JS-10	MS	San Vicente N	AD	Alfonso	WSD (II)	t5	19457	21487	-8.7	1.2
FSV-811		MS	San Vicente N	AD	Alfonso	Iom		19457	21487		-26.8
FSV-816		MS	San Vicente N	AD	Alfonso	WSD (II)	t5	19521	21208	-9.8	1.4
FSV-816		MS	San Vicente N	AD	Alfonso	WSD (II)	t3	19521	21208	-8.6	1.7
FSV-816	JS-11	MS	San Vicente N	AD	Alfonso	WSD (II)	t3	19521	21208	-9.2	1.6
FSV-822		MS	San Vicente N	AD	Alfonso	IIIbit		19825	21333		-23.0
FSV-827		MS	San Vicente N	AD	Alfonso	IIIbit		19905	21073		-23.3
FSV-830	JS-12	MS	San Vicente N	AD	Alfonso	WSD (II)	t3	19891	21167	-9.8	0.9
FSV-015	JS-13	MS	San Vicente N	UL		UL		19980	20140	-6.3	2.0
FSV-017	JS-14	MS	San Vicente N	UL		UL		20140	19260	-8.4	0.2
FSV-018		MS	San Vicente N	UL		UL		20140	19260	-7.6	0.8
FSV-1101	JS-48	MS	San Vicente N	UL		UL		20130	19245	-7.5	1.2
FSV-1102	JS-49	MS	San Vicente N	UL		UL		20133	19254	-7.2	1.2
FSV-1102		MS	San Vicente N	UL		ULom		20133	19254		-27.2
FSV-1103	JS-50	MS	San Vicente N	UL		UL		20141	19265	-6.6	2.3
FSV-1103		MS	San Vicente N	UL		ULom		20141	19265		-28.2
FSV-671		MS	San Vicente N	SVD	Jesus	WSD (II)		19767	21137	-8.3	0.9
FSV-671		MS	San Vicente N	SVD	Jesus	IIIbit		19767	21137		-24.0
FSV-678		MS	San Vicente N	SVD	Jesus	WSD (II)		19829	21148	-10.8	0.7
FSV-678		MS	San Vicente N	SVD	Jesus	IIIbit		19829	21148		-23.9
FSV-851		MS	San Vicente N	SVD	SV techo	WSD (II)	t6	19845	21702	-8.0	1.5
FSV-851	JS-15	MS	San Vicente N	SVD	SV techo	LFC (IIIc)		19845	21702	-11.8	-2.9
FSV-852		MS	San Vicente N	SVD	SV techo	LFC (IIIc)		19848	21686	-10.2	0.3
FSV-853	JS-16	MS	San Vicente N	SVD	SV techo	DRD (If)		19849	21681	-8.1	1.1
FSV-853		MS	San Vicente N	SVD	SV techo	Iom		19849	21681		-26.4
FSV-853		MS	San Vicente N	SVD	SV techo	LFD (IIId)		19849	21681	-10.8	0.0
FSV-853		MS	San Vicente N	SVD	SV techo	IIIbit		19849	21681		-27.7
FSV-854	JS-17	MS	San Vicente N	SVD	SV techo	LFC (IIIc)		19846	21693	-14.8	-2.8
FSV-855		MS	San Vicente N	SVD	SV techo	WSD (II)	t6	19852	21671	-9.7	0.8
FSV-856		MS	San Vicente N	SVD	SV techo	DRD (Ivf)		19650	21330	-7.6	0.9
FSV-856	JS-52	MS	San Vicente N	SVD	SV techo	LFC (IIIc)		19650	21330	-12.1	-9.3
FSV-857		MS	San Vicente N	SVD	SV techo	WSD (II)	t6	19925	21785	-8.0	1.5
FSV-857	JS-18	MS	San Vicente N	SVD	SV techo	LFC (IIIc)		19925	21785	-10.9	-4.5
FSV-860		MS	San Vicente N	SVD	SV techo	EPc		19925	21785	-10.9	-4.5
FSV-861		MS	San Vicente N	SVD	SV techo	EPc		19761.2	21168	-9.5	-3.5
FSV-862	JS-19	MS	San Vicente N	SVD	SV techo	WSD (II)	t6	19808.3	21718	-7.5	1.2
FSV-869		MS	San Vicente N	SVD	SV techo	LFC (IIIc)		19841.3	21775	-11.2	0.2
FSV-869	JS-20	MS	San Vicente N	SVD	SV techo	WSD (II)	t3	19967.3	21855	-8.9	0.8
FSV-640		MS	San Vicente N	SVD	SV techo	LFC (IIIc)		19967.3	21855	-9.1	0.5
FSV-640		MS	San Vicente N	SVD	SV techo	EPc		19365	19465	-12.5	0.8
FSV-032		MS	San Vicente N	SVD	SV techo	EPc		19365	19465	-13.1	0.2

continued

Table A.1.1. Continued

Sample	Lab. nr.	St. sc.	Locality	Unit	Manto	Stud. min.	WSD sub.	E (m)	N (m)	d18O (PDB)	d13C (PDB)
FSV-033		MS	San Vicente N	SVD	Jesus	WSD (II)	t3	19910	20490	-8.2	1.2
FSV-422		MS	San Vicente N	SVD	Jesus	WSD (II)	t4	19890	20430	-9.7	0.9
FSV-422		MS	San Vicente N	SVD	Jesus	WSD (II)	t4	19845	21010	-10.3	1.3
FSV-422		MS	San Vicente N	SVD	Jesus	WSD (II)	t4	19845	21010	-9.5	1.0
FSV-423		MS	San Vicente N	SVD	Jesus	WSD (II)	t4	19845	21010	-10.2	0.8
FSV-423	JS-51	MS	San Vicente N	SVD	Jesus	DRD (Ivf)		19810	21300	-6.4	1.5
FSV-423		MS	San Vicente N	SVD	Jesus	EPc		19810	21300	-10.6	-1.4
FSV-423		MS	San Vicente N	SVD	Jesus	EPc		19810	21300	-9.9	-2.0
FSV-661		MS	San Vicente N	SVD	Jesus	EPc		19810	21300	-10.3	-1.4
FSV-673	JS-21	MS	San Vicente N	SVD	Jesus	WSD (II)	t6	19834	21059	-9.4	0.7
FSV-673	JS-22	MS	San Vicente N	SVD	Jesus	WSD (II)	t6	19788.5	21177	-8.6	0.8
FSV-673		MS	San Vicente N	SVD	Jesus	LFC (IIIc)		19788.5	21177	-9.8	0.7
FSV-674		MS	San Vicente N	SVD	Jesus	IIIbit		19788.5	21177		-27.0
FSV-674	JS-23	MS	San Vicente N	SVD	Jesus	WSD (II)	t5	19828	21017	-10.2	1.0
FSV-675	JS-24	MS	San Vicente N	SVD	Jesus	LFC (IIIc)		19828	21017	-9.8	-0.5
FSV-001		MS	San Vicente N	SVD	Jesus	LFC (IIIc)		19969	21798	-10.2	-0.3
FSV-662		MS	San Vicente N	SVD	Ayala	WSD (II)	t4	19900	20360	-8.7	1.4
FSV-663		MS	San Vicente N	SVD	Ayala	WSD (II)	t4	19795	20650	-9.3	1.3
FSV-664		MS	San Vicente N	SVD	Ayala	WSD (II)	t4	19795	20560	-8.5	1.6
FSV-004	JS-25	MS	San Vicente N	SVD	Ayala	WSD (II)	t6	19745	20720	-9.4	1.4
FSV-005		MS	San Vicente N	SVD	3t	WSD (II)	t5	19850	20405	-8.4	1.2
FSV-005		MS	San Vicente N	SVD	3t	DRD (Im)		19870	20410	-9.3	0.5
FSV-005		MS	San Vicente N	SVD	3t	WSD (II)	t5	19870	20410	-10.2	1.1
FSV-008		MS	San Vicente N	SVD	3t	LFC (IIIc)		19870	20410	-10.9	0.6
FSV-213-2	JS-35	MS	San Vicente N	SVD	3t	WSD (II)	t5	19900	20610	-9.3	1.1
FSV-215	JS-34	MS	San Vicente N	SVD	3t	WSD (II)	t4	19810	20578	-9.0	1.3
FSV-020		MS	San Vicente N	SVD	3t	WSD (II)	t4	19810	20580	-8.7	1.3
FSV-020	JS-36	MS	San Vicente N	SVD	3i	DRD (Ivf)		19895	20580	-7.2	2.1
FSV-031		MS	San Vicente N	SVD	3i	WSD (II)	t3	19895	20580	-10.8	0.8
FSV-037		MS	San Vicente N	SVD	3i	WSD (II)	t4	20000	20420	-8.1	1.1
FSV-022	JS-37	MS	San Vicente N	SVD	3i	WSD (II)	t4	19907	20285	-9.8	0.6
FSV-022		MS	San Vicente N	SVD	3p	DRD (Im)		19985	20255	-8.2	0.8
FSV-022		MS	San Vicente N	SVD	3p	EPd		19985	20255	-11.8	0.3
FSV-022		MS	San Vicente N	SVD	3p	EPd		19985	20255	-12.1	0.3
FSV-027		MS	San Vicente N	SVD	3p	EPd		19985	20255	-11.3	0.5
FSV-029		MS	San Vicente N	SVD	3p	WSD (II)	t4	19985	20255	-8.7	1.2
FSV-029		MS	San Vicente N	SVD	3p	WSD (II)	t5	19930	20690	-10.3	0.8
FSV-029	JS-53	MS	San Vicente N	SVD	3p	EPc		19930	20690	-9.8	1.0
FSV-029		MS	San Vicente N	SVD	3p	EPc		19930	20690	-10.4	0.6
FSV-029		MS	San Vicente N	SVD	3p	EPc		19930	20690	-12.1	-0.4
FSV-041		MS	San Vicente N	SVD	3p	EPc		19930	20690	-11.3	-0.1
FSV-656		MS	San Vicente N	SVD	3p	WSD (II)	t4	20000	20420	-7.8	1.3
FSV-656		MS	San Vicente N	SVD	3	WSD (II)	t5	20195	19325	-9.9	1.3
FSV-657A		MS	San Vicente N	SVD	3	LFC (IIIc)		20195	19325	-12.5	-11.5
FSV-657B		MS	San Vicente N	SVD	3	WSD (II)	t3	20195	19325	-9.4	1.4
FSV-657B	JS-38	OS	San Vicente N	SVD	3	WSD (II)	t3	20195	19325	-10.0	0.7
FSV-657B		OS	San Vicente N	SVD	3	WSD (II)	t3	20195	19325	-9.9	0.8
FSV-657B		OS	San Vicente N	SVD	3	WSD (II)	t2	20195	19325	-9.9	1.0

continued

Table A.1.1. Continued

Sample	Lab. nr.	St. sc.	Locality	Unit	Manto	Stud. min.	WSD sub.	E (m)	N (m)	d18O (PDB)	d13C (PDB)
FSV-657B		OS	San Vicente N	SVD	3	WSD (II)	t2	20195	19325	-10.2	0.8
FSV-657B		OS	San Vicente N	SVD	3	WSD (II)	t1	20195	19325	-11.8	0.4
FSV-038		OS	San Vicente N	SVD	3	WSD (II)	t1	20195	19325	-11.5	0.7
FSV-038	JS-39	MS	San Vicente N	SVD	2	DRD (If)		20075	20495	-7.2	1.8
FSV-038		MS	San Vicente N	SVD	2	WSD (II)	t5	20075	20495	-8.1	1.1
FSV-038		MS	San Vicente N	SVD	2	LFC (IIIc)		20075	20495	-9.8	-0.8
FSV-039		MS	San Vicente N	SVD	2	IIIbit		20075	20495		-25.4
FSV-205		MS	San Vicente N	SVD	2	WSD (II)	t5	20075	20490	-9.4	1.0
FSV-658A		MS	San Vicente N	SVD	2	WSD (II)	t5	19900	20610	-7.3	1.3
FSV-659	JS-40	MS	San Vicente N	SVD	1	WSD (II)	t5	19985	19416	-8.5	0.9
FSV-659		MS	San Vicente N	SVD	1	DRD (Ivf)		20245	19340	-7.1	1.0
FSV-659		MS	San Vicente N	SVD	1	WSD (II)	t5	20245	19340	-8.4	1.1
FSV-660		MS	San Vicente N	SVD	1	LFC (IIIc)		20245	19340	-10.0	-0.1
FSV-713		MS	San Vicente N	SVD	1	WSD (II)	t6	20250	19468	-9.9	0.9
FSV-713	JS-41	MS	San Vicente N	SJD		DRD (If)		20315	19645	-7.4	1.7
FSV-714		MS	San Vicente N	SJD		WSD (II)	t3	20315	19645	-9.4	0.6
FSV-714	JS-47	MS	San Vicente N	SJD		WSD (II)	t6	20221	19677	-9.1	1.2
FSV-714	JS-42	MS	San Vicente N	SJD		LFD (IIId)		20221	19677	-9.8	1.0
FSV-717		MS	San Vicente N	SJD		LFD (IIId)		20221	19677	-12.2	0.3
FSV-718	JS-43	MS	San Vicente N	SJD	t	WSD (II)	t6	20360	19642	-8.0	1.6
FSV-718	JS-44	MS	San Vicente N	SJD	m	DRD (Im)		20321	19637	-8.2	1.1
FSV-719	JS-45	MS	San Vicente N	SJD	m	WSD (II)	t6	20321	19637	-9.8	0.6
FSV-720		MS	San Vicente N	SJD	p	WSD (II)	t6	20341	19647	-9.2	1.1
FSV-984	JS-125	RS	Qbd. Piñon	SVD		WSD (II)		23768	5750	-10.0	1.2
FSV-985	JS-126	RS	Qbd. Piñon	SVD		WSD (II)		23717	5750	-10.3	1.2
FSV-952	JS-104	RS	Rondayacu	SVD		WSD (II)		23346	9704	-9.9	0.9
FSV-953	JS-105	RS	Rondayacu	SVD		WSD (II)		23280	9767	-11.2	0.3
FSV-953B	JS-106	RS	Rondayacu	SVD		WSD (II)		23280	9767	-10.6	0.9
FSV-1001	JS-134	RS	Yanachuro S	SVD		WSD (II)		23346	9752	-10.2	1.2
FSV-1003	JS-135	RS	Yanachuro S	SVD		WSD (II)		23345	9702	-9.7	1.1
FSV-956	JS-102	RS	Utcuyacu	SVD		WSD (II)		23639	10674	-9.8	1.1
FSV-957	JS-103	RS	Utcuyacu	SVD		WSD (II)		23623	10722	-9.9	1.1
FSV-652	JS-100	RS	Qbd. Utcuyacu	SVD		WSD (II)		22520	11745	-10.4	0.5
FSV-653C	JS-101	RS	Qbd. Utcuyacu	SVD		WSD (II)		22460	11670	-10.1	1.1
FSV-1057	JS-149	RS	Qbd. Utcuyacu	UL		UL		22730	11070	-8.1	-0.7
FSV-1059	JS-150	RS	Qbd. Utcuyacu	UL		UL		22860	11320	-6.4	-0.6
FSV-988	JS-127	RS	Aynamayo	SJD		DRD (Im)		21344	15393	-8.1	1.7
FSV-989	JS-129	RS	Aynamayo	SJD		DRD (Im)		21240	15318	-8.0	1.6
FSV-988	JS-128	RS	Aynamayo	SJD		WSD (II)		21344	15393	-8.9	1.3
FSV-989	JS-130	RS	Aynamayo	SJD		WSD (II)		21240	15318	-10.0	1.1
FSV-992	JS-132	RS	Aynamayo	SVD		DRD (If)		21245	14695	-7.6	1.4
FSV-990	JS-131	RS	Aynamayo	SVD		WSD (II)		21189	14736	-10.7	1.1
FSV-992	JS-133	RS	Aynamayo	SVD		WSD (II)	t6	21245	14695	-11.2	0.8
FSV-1082		RS	Aynamayo	SVD		IIIbit		21135	15000		-27.5
FSV-754	JS-137	RS	Chilpes	SJD		DRD (Im)		21129	15744	-7.8	1.7
FSV-753	JS-136	RS	Chilpes	SJD		WSD (II)		21031	15693	-8.4	1.4
FSV-754	JS-138	RS	Chilpes	SJD		WSD (II)		21129	15744	-8.0	1.6
FSV-754	JS-139	RS	Chilpes	SJD		LFC (IIIc)		21129	15744	-11.4	-0.2

continued

Table A.1.1. Continued

Sample	Lab. nr.	St. sc.	Locality	Unit	Manto	Stud. min.	WSD sub.	E (m)	N (m)	d18O (PDB)	d13C (PDB)
FSV-982	JS-122	RS	Chilpes	SVD		DRD (Im)		20642.7	15520	-7.8	1.6
FSV-755	JS-140	RS	Chilpes	SVD		DRD (Im)		20469	15536	-9.8	1
FSV-759	JS-142	RS	Chilpes	SVD		DRD (If)		20614	15471	-7.4	1.4
FSV-755	JS-141	RS	Chilpes	SVD		WSD (II)		20469	15536	-9.7	1
FSV-759	JS-143	RS	Chilpes	SVD		WSD (II)		20614	15447	-10.0	0.8
FSV-761	JS-144	RS	Chilpes	SVD		WSD (II)		20642.7	15520	-9.5	0.7
FSV-982	JS-123	RS	Chilpes	SVD		LFC (IIIc)		20642.7	15520	-12.6	-3.7
FSV-759		RS	Chilpes	SVD		IIIbit		20614	15471		-26.9
FSV-976	JS-117	RS	Uncush S	AD		WSD (II)		20242	17125	-9.9	1.3
FSV-978	JS-118	RS	Uncush S	AD		LFC (IIIc)		20268	17127	-13.9	-2.9
FSV-977		RS	Uncush S	AD		LFC (IIIc)		20340	17127	-13.1	-0.1
FSV-971	JS-115	RS	Uncush	SJD		WSD (II)		20675	18860	-9.8	1.1
FSV-972	JS-116	RS	Uncush	SJD		WSD (II)		20635	18861	-9.8	1
FSV-972		RS	Uncush	SJD		WSD (II)		20635	18861	-10.5	0.8
FSV-981	JS-120	RS	Afl. Campana	AD		DRD (If)		20615	17815	-7.6	1.5
FSV-979	JS-119	RS	Afl. Campana	AD		WSD (II)		20430	17145	-8.7	0.9
FSV-981	JS-121	RS	Afl. Campana	AD		WSD (II)		20615	17815	-8.2	1.4
FSV-775		RS	Arcopunco	AD		EPc		19311.2	21807	-12.1	-2.5
FSV-779	JS-146	RS	Arcopunco	SVD		DRD (Im)		19311.2	21807	-9.0	1.4
FSV-776		RS	Arcopunco	SVD		DRD (Im)		19311.2	21807	-7.4	1.4
FSV-776	JS-145	RS	Arcopunco	SVD		WSD (II)		19311.2	21807	-8.6	1.1
FSV-779	JS-147	RS	Arcopunco	SVD		WSD (II)		19311.2	21807	-8.9	0.7
Fsv-780	JS-148	RS	Arcopunco	SVD		WSD (II)		19311.2	21807	-9.3	0.9
FSV-779		RS	Arcopunco	SVD		IIIbit		19311.2	21807		-28.4
FSV-776		RS	Arcopunco	SVD		LFC (IIIc)		19311.2	21807	-15.0	-2.9
FSV-959	JS-107	RS	Machuyacu	SVD		WSD (II)		21784.5	22024	-10.3	0.8
FSV-960	JS-108	RS	Machuyacu	SVD		WSD (II)		21745.5	22095	-10.4	0.7
FSV-962	JS-109	RS	Machuyacu	SVD		WSD (II)		21532	22055	-9.8	0.9
FSV-960		RS	Machuyacu	SVD		WSD (II)		21745.5	22095	-10.7	0.8
FSV-964	JS-110	RS	Palmapata	SVD		DRD (Im)		21139	25000	-10.0	0.9
FSV-964	JS-111	RS	Palmapata	SVD		WSD (II)		21139	25000	-10.0	0.9
FSV-965	JS-112	RS	Palmapata	SVD		WSD (II)		21139	25007	-10.2	0.8
FSV-967	JS-113	RS	Puntayacu	SVD		WSD (II)		15940	27550	-11.4	0.2
FSV-969	JS-114	RS	Puntayacu	SVD		WSD (II)		15950	27700	-10.0	0.5
FSV-983	JS-124	RS	Pichita	SVD		WSD (II)		19000	31200	-10.8	0.4

APPENDIX 2

RESULTS OF ELECTRON MICROPROBE ANALYSES OF THE GANGUE CARBONATES

Analytical techniques of microprobe analysis

138 electron microprobe analyses for Ca, Mg, Fe, Mn, Zn, Na, and Sr were made on eight samples of gangue carbonates of the San Vicente deposit using the CAMECA CAMABAX SX50 of the Laboratoire de micro-analyse électronique, Uni. Lausanne. Acceleration voltage and beam current were 12 kV and 10 nA, respectively. Beam diameter was 10 µm and a 20 second integration time were used. Natural minerals were used as standards: dolomite for Ca and Mg; siderite for Fe; rhodochrosite for Mn; albite for Na; strontionite for Sr; and sphalerite for Zn. Data reduction was completed with the ZAF matrix-correction schema.

The results of the microprobe analyses are given in Table A2.1 and A2.2.

Abbreviations used in Table A2.1.

Loc.: SV = San Vicente deposit; AR = Arcopunco
x-coor. and y-coor.: X and Y coordinates of the microprobe stepping device
Carbonate gen.: DRD = dark replacement dolomite ("Ivf" very fine-grained, "If" fine-grained, "Im" medium-grained); WSD = white sparry dolomite (II)
WSD sub.: subgenerations of WSD = "t1" millimetric-sized spots of WSD; "t2" fine veinlets of WSD, "t3" ordered millimetric to centimetric thick bands of WSD
blank = not detected

Table A2.1. Results of electron microprobe analyses of the gangue carbonates

Sample	Loc.	x-coor. (mm)	y-coor. (mm)	Carbonate gen.	WSD sub.	CaCO3 (mole%)	MgCO3 (mole%)	MnCO3 (mole%)	FeCO3 (mole%)	Zn (wt.%)	Na (wt.%)	Sr (wt.%)
FSV-905-A	SV	5756	20689	DRD (Im)		53.52	44.92	0.31	1.25		0.00	
FSV-905-A	SV	5839	20712	DRD (Im)		53.13	45.12	0.34	1.02	0.17	0.03	
FSV-905-A	SV	5661	20382	DRD (If)		54.52	44.36	0.34	0.77		0.00	
FSV-905-A	SV	5693	21590	DRD (Im)		53.49	45.44	0.22	0.80		0.02	
FSV-905-A	SV	6398	22803	WSD (II)	t2	53.84	44.27	0.47	1.07	0.18	0.01	0.009
FSV-905-A	SV	6540	23645	WSD (II)	t2	53.90	45.18	0.28	0.56	0.05		
FSV-905-A	SV	6973	25748	WSD (II)	t1	54.15	45.43	0.39			0.02	
FSV-905-A	SV	7054	26916	WSD (II)	t1	54.86	44.45	0.31	0.17	0.09	0.02	
FSV-905-A	SV	7414	31502	WSD (II)	t3	53.30	44.95	0.59	0.72	0.22	0.01	
FSV-905-A	SV	7391	32160	WSD (II)	t3	53.82	44.52	0.42	0.91	0.17	0.00	
FSV-905-A	SV	7378	32845	WSD (II)	t3	53.80	44.80	0.20	0.85	0.17	0.02	
FSV-905-A	SV	6831	33549	DRD (Im)		53.32	45.20	0.29	1.17		0.01	
FSV-905-A	SV	6183	34399	DRD (Im)		54.19	44.82	0.13	0.70	0.08	0.02	
FSV-905-A	SV	6098	36493	DRD (Im)		54.34	44.45	0.41	0.63	0.08	0.01	
FSV-905-A	SV	4182	37892	DRD (Im)		52.98	43.55	0.38	3.02		0.04	
FSV-905-A	SV	3957	37892	DRD (If)		54.60	44.14	0.40	0.83	0.02	0.00	
FSV-905-A	SV	2690	38339	DRD (Im)		53.62	44.77	0.38	1.22		0.00	
FSV-905-B	SV	14550	-25126	DRD (If)		54.19	44.55	0.47	0.80			
FSV-905-B	SV	13727	-25110	DRD (If)		53.71	44.95	0.17	1.15		0.01	
FSV-905-B	SV	11283	-25186	WSD (II)	t3	53.77	45.98	0.23			0.01	
FSV-905-B	SV	9687	-25186	WSD (II)	t3	53.89	45.51	0.18	0.08	0.15	0.03	
FSV-905-B	SV	9623	-25267	WSD (II)	t3	53.54	45.60	0.36	0.03	0.24	0.01	
FSV-905-B	SV	7746	-25101	WSD (II)	t3	54.37	45.32	0.07	0.19		0.02	
FSV-905-B	SV	5919	-25147	DRD (Im)		53.78	44.60	0.30	0.71	0.29	0.03	
FSV-905-B	SV	4697	-25143	DRD (If)		53.97	44.54	0.42	0.69	0.12	0.02	0.063
FSV-905-B	SV	3472	-25143	DRD (If)		53.89	44.50	0.31	1.25	0.03		
FSV-905-B	SV	1742	-25093	WSD (II)	t1	54.78	43.87	0.35	0.56	0.23	0.01	
FSV-905-B	SV	-334	-25251	WSD (II)	t2	53.97	45.05	0.47	0.42		0.05	
FSV-905-B	SV	-34	-25251	WSD (II)	t2	54.33	45.20	0.26	0.15		0.02	
FSV-905-B	SV	-1748	-25240	DRD (Im)		54.02	44.58	0.47	0.59	0.14	0.04	
FSV-905-B	SV	-3369	-25250	DRD (Im)		54.72	43.58	0.38	0.68	0.29	0.04	0.030
FSV-905-B	SV	-4678	-27768	WSD (II)	t2	53.85	45.86	0.19	0.06		0.02	
FSV-905-B	SV	-4971	-23164	WSD (II)	t2	53.95	45.08	0.21	0.73		0.01	
FSV-905-B	SV	-5292	-25028	WSD (II)	t2	53.98	45.22	0.30	0.30	0.09	0.02	
FSV-905-B	SV	-8086	-25028	DRD (If)		53.98	44.14	0.38	0.96	0.27	0.01	
FSV-905-B	SV	-8434	-25028	DRD (If)		53.98	44.30	0.41	0.95	0.17	0.02	
FSV-905-B	SV	-8642	-28326	WSD (II)	t2	54.51	45.00	0.35	0.14		0.00	
FSV-905-B	SV	-8642	-26191	WSD (II)	t2	54.07	44.58	0.32	0.74	0.12	0.03	
FSV-905-B	SV	-10018	-21744	WSD (II)	t1	54.83	44.99	0.12	0.00		0.03	
FSV-905-B	SV	-9104	-25917	WSD (II)	t2	53.64	45.41	0.27	0.65		0.02	
FSV-905-B	SV	-12685	-25344	DRD (If)		54.68	44.06	0.09	0.89	0.12	0.03	
FSV-905-B	SV	-12843	-26121	WSD (II)	t2	54.20	44.85	0.30	0.60		0.02	
FSV-905-B	SV	-12917	-26852	WSD (II)	t2	53.70	45.02	0.27	0.96		0.02	
FSV-905-B	SV	-10181	-20235	WSD (II)	t2	53.80	45.19	0.14	0.17	0.33		0.045
FSV-657B-A	SV	10425	36469	WSD (II)	t2	53.71	45.13	0.68	0.04	0.24		
FSV-657B-A	SV	9618	36110	WSD (II)	t2	53.88	45.18	0.47	0.09	0.18	0.02	
FSV-657B-A	SV	10103	31950	WSD (II)	t1	54.80	44.96	0.19			0.02	

continued

Table A2.1. Continued

Sample	Loc.	x-coor. (mm)	y-coor. (mm)	Carbonate gen.	WSD subgen	CaCO3 (mole%)	MgCO3 (mole%)	MnCO3 (mole%)	FeCO3 (mole%)	Zn (wt.%)	Na (wt.%)	Sr (wt.%)
FSV-657B-A	SV	9027	31950	WSD (II)	t1	54.18	45.10	0.27	0.39		0.03	
FSV-657B-A	SV	7664	30324	WSD (II)	t1	54.46	45.24	0.10	0.16		0.02	
FSV-657B-A	SV	6402	30645	WSD (II)	t1	54.31	45.11	0.40	0.15		0.02	
FSV-657B-A	SV	2743	29138	WSD (II)	t1	53.95	45.27	0.25	0.32	0.12		
FSV-657B-A	SV	2304	29090	WSD (II)	t1	54.54	45.26	0.14	0.06		0.00	
FSV-657B-A	SV	-12436	35074	DRD (If)		54.58	45.26		0.01	0.04	0.03	
FSV-657B-A	SV	-12739	33101	DRD (If)		54.34	44.73	0.18	0.13	0.32	0.02	
FSV-657B-A	SV	-11400	32842	DRD (If)		54.16	45.45	0.18	0.18		0.01	
FSV-657B-A	SV	-13474	32369	DRD (If)		54.63	45.12	0.12	0.04		0.04	
FSV-657B-B	SV	8163	-23276	DRD (Im)		54.89	44.48	0.50	0.14		0.00	
FSV-657B-B	SV	7544	-23276	WSD (II)	t1	54.42	44.96	0.49	0.13		0.00	
FSV-657B-B	SV	8176	-23662	WSD (II)	t1	54.20	44.70	0.49	0.02	0.29	0.03	
FSV-657B-B	SV	-8221	-21054	WSD (II)	t1	54.46	45.15	0.10		0.12	0.03	
FSV-657B-B	SV	-8331	-21112	WSD (II)	t1	54.69	44.99	0.09	0.18	0.03	0.00	
FSV-657B-B	SV	-2363	-26404	WSD (II)	t2	54.34	45.27	0.26	0.07		0.02	
FSV-657B-B	SV	-1848	-25486	WSD (II)	t2	54.13	45.41	0.33		0.05	0.03	
FSV-657B-B	SV	-82345	-21116	WSD (II)	t2	53.81	45.07	0.18	0.09	0.42	0.03	
FSV-657B-B	SV	-7321	-26632	WSD (II)	t2	53.78	45.71	0.19	0.06	0.12	0.02	
FSV-657B-B	SV	-8689	-21267	WSD (II)	t1	54.46	44.91	0.10	0.27	0.13	0.01	
FSV-657B-B	SV	-97914	-21586	WSD (II)	t3	53.96	45.64	0.33		0.05	0.00	
FSV-657B-C	SV	5159	26684	WSD (II)	t3	54.21	45.43	0.18	0.16		0.01	
FSV-657B-C	SV	8740	28835	WSD (II)	t3	53.64	45.35	0.92	0.09			
FSV-657B-C	SV	1588	27247	WSD (II)	t3	53.82	45.00	0.74	0.16	0.12	0.02	
FSV-657B-C	SV	747	27414	WSD (II)	t3	54.07	44.98	0.65	0.28		0.02	
FSV-657B-C	SV	-2900	26789	WSD (II)	t3	53.97	45.35	0.58	0.04		0.03	
FSV-657B-C	SV	-4142	26719	WSD (II)	t2	53.91	45.22	0.06		0.40	0.03	
FSV-657B-C	SV	-4780	26896	WSD (II)	t3	54.11	45.37	0.37	0.14		0.01	
FSV-657B-C	SV	-4845	26635	DRD (Im)		54.34	45.00	0.64	0.00		0.01	
FSV-657B-C	SV	-5249	26631	DRD (Im)		53.72	44.99	0.67	0.16	0.24	0.01	
FSV-657B-C	SV	-7117	26332	WSD (II)	t2	53.77	45.13	0.67	0.01	0.19	0.03	
FSV-657B-C	SV	-6967	25677	WSD (II)	t2	53.50	45.52	0.73	0.20		0.02	
FSV-657B-C	SV	-10692	25340	DRD (Im)		53.98	45.12	0.83			0.04	
FSV-657B-C	SV	-9638	23854	DRD (Im)		53.76	45.57	0.57	0.01		0.04	
FSV-657B-C	SV	-10590	23882	WSD (II)	t2	53.53	45.70	0.73			0.02	
FSV-657B-C	SV	-11350	25140	WSD (II)	t2	54.23	45.00	0.67		0.03	0.03	
FSV-657B-C	SV	-12158	25368	WSD (II)	t2	54.18	45.05	0.70			0.03	
FSV-657B-C	SV	-12962	25328	DRD (Im)		54.20	45.04	0.58	0.06	0.04	0.02	
FSV-657B-C	SV	-13676	25779	DRD (Im)		53.75	44.69	0.64	0.21	0.36	0.02	
FSV-657B-C	SV	-14316	25799	DRD (Im)		54.11	45.02	0.85	0.02		0.01	
FSV-657B-C	SV	-757	25733	DRD (Im)		53.95	45.14	0.71		0.09	0.01	
FSV-657B-C	SV	8138	25646	DRD (Im)		54.16	44.66	1.01		0.03	0.03	0.032
FSV-776-B	AR	13686	-23869	DRD (Im)		53.79	44.91	0.31	0.98		0.01	
FSV-776-B	AR	13996	-23869	DRD (Im)		54.11	44.70	0.10	1.06			0.014
FSV-776-B	AR	13562	-23859	DRD (Im)		53.75	44.07	0.58	1.59		0.02	
FSV-776-B	AR	10185	-22158	WSD (II)	t3	53.78	44.40	0.20	1.63			
FSV-776-B	AR	9347	-22158	WSD (II)	t3	53.59	44.21	0.20	1.60	0.21	0.01	
FSV-776-B	AR	9755	-23556	WSD (II)	t3	53.68	45.41	0.04	0.65	0.08	0.03	
FSV-776-B	AR	8441	-22940	WSD (II)	t3	53.26	44.85	0.21	1.36	0.16	0.01	

continued

Table A2.1. Continued

Sample	Loc.	x-coor. (mm)	y-coor. (mm)	Carbonate gen.	WSD subgen	CaCO3 (mole%)	MgCO3 (mole%)	MnCO3 (mole%)	FeCO3 (mole%)	Zn (wt.%)	Na (wt.%)	Sr (wt.%)
FSV-776-B	AR	7021	-22940	DRD (Im)		54.16	44.91	0.51	0.43			
FSV-776-B	AR	5242	-22940	DRD (Im)		53.87	45.22	0.09	0.38	0.21	0.02	
FSV-776-B	AR	3287	-22390	DRD (Im)		53.30	45.10	0.09	1.12	0.18	0.03	
FSV-776-B	AR	647	-21443	WSD (II)	t2	53.79	45.58	0.09	0.53		0.01	
FSV-776-B	AR	875	-23393	WSD (II)	t2	53.48	45.26	0.39	0.61	0.13	0.01	
FSV-776-B	AR	-1023	-23393	DRD (Im)		54.05	45.23	0.04	0.64		0.02	
FSV-776-B	AR	-2830	-23393	DRD (Im)		53.54	45.41	0.00	0.50	0.27	0.02	
FSV-776-B	AR	-4072	-23454	DRD (Im)		54.09	45.08	0.18	0.60		0.03	
FSV-776-B	AR	-5312	-23346	WSD (II)	t3	53.54	45.06	0.18	0.62	0.30	0.02	
FSV-776-B	AR	-6664	-23346	WSD (II)	t3	54.01	44.31	0.57	0.85	0.08	0.05	
FSV-776-B	AR	-9017	-23323	DRD (Im)		54.20	45.28	0.03	0.48		0.01	
FSV-776-B	AR	-9075	-24473	DRD (Im)		54.00	44.84	0.21	0.88	0.03	0.01	
FSV-776-B	AR	-9807	-31459	WSD (II)	t3	53.36	45.13	0.18	0.86	0.24	0.02	
FSV-776-B	AR	-8497	-31466	WSD (II)	t3	53.39	45.74	0.27	0.58		0.01	
FSV-776-B	AR	-8139	-32047	WSD (II)	t3	53.82	44.78	0.09	1.19	0.03	0.03	
FSV-776-B	AR	-2124	-30464	WSD (II)	t3	53.45	45.35	0.09	0.91	0.08	0.03	
FSV-776-B	AR	-1501	-30045	WSD (II)	t2	53.43	45.16	0.28	0.96	0.09	0.01	
FSV-776-B	AR	4055	-29474	WSD (II)	t2	53.94	44.85	0.43	0.79			
FSV-776-B	AR	3365	-28895	DRD (Im)		53.65	44.71	0.24	1.34	0.03	0.00	
FSV-776-B	AR	6982	-32019	DRD (Im)		53.87	44.74	0.17	0.89	0.15	0.02	
FSV-779-A	AR	8882	23543	WSD (II)	t1	55.16	44.17	0.35	0.17	0.06	0.02	
FSV-779-A	AR	8101	23823	DRD (Im)		53.71	45.03	0.24	0.99		0.02	
FSV-779-A	AR	8324	22505	WSD (II)	t2	55.26	44.41	0.18	0.10		0.02	
FSV-779-A	AR	4360	26700	WSD (II)	t2	54.26	45.22	0.24	0.26		0.01	
FSV-779-A	AR	5063	25848	WSD (II)	t1	54.95	44.24	0.42	0.36		0.01	
FSV-779-A	AR	3466	26923	WSD (II)	t2	54.54	44.57	0.34	0.56			
FSV-779-A	AR	-1478	21536	WSD (II)	t2	54.34	45.03	0.26	0.37		0.00	
FSV-779-A	AR	-1614	21610	WSD (II)	t2	54.46	44.87	0.24	0.43			
FSV-779-A	AR	-1540	22345	WSD (II)	t1	54.01	44.29	0.48	0.38	0.44	0.01	
FSV-779-A	AR	-2057	26006	WSD (II)	t2	53.61	44.39	0.42	0.87	0.34	0.03	
FSV-779-A	AR	-1320	26133	WSD (II)	t1	54.23	45.07	0.27	0.27	0.05	0.03	
FSV-779-A	AR	-2920	25997	WSD (II)	t2	53.86	44.97	0.26	0.68	0.12		
FSV-779-A	AR	-6256	25828	WSD (II)	t2	54.41	44.90	0.06	0.63			
FSV-779-A	AR	-4578	26779	WSD (II)	t1	54.45	44.82	0.22	0.19	0.16	0.01	
FSV-779-A	AR	-4030	26213	WSD (II)	t2	53.83	45.21	0.12	0.56	0.12	0.03	
FSV-856	AR	4361	-22033	DRD (Ivf)		53.94	44.11	0.44	1.50		0.02	
FSV-856	AR	5082	-22012	DRD (Ivf)		53.35	44.25	0.49	1.27	0.33	0.01	
FSV-856	AR	4471	-22380	DRD (Ivf)		54.01	45.50	0.33	0.16		0.00	
FSV-856	AR	-2307	-25659	DRD (Ivf)		53.91	45.08	0.57	0.08	0.18	0.02	
FSV-856	AR	-2122	-25746	DRD (Ivf)		53.46	44.96	0.38	1.17		0.02	
FSV-856	AR	-2235	-25744	DRD (Ivf)		53.33	45.02	0.40	1.15	0.03	0.01	
FSV-856	AR	-3849	-2767	DRD (Ivf)		54.00	44.48	0.39	0.95	0.08	0.02	
FSV-856	AR	-4699	-28417	DRD (Ivf)		54.14	44.40	0.37	1.12		0.00	0.007

blank = not detected

Table A2.2. Ranges and median values of major and minor elements (electron microprobe analyses) in the dolomites of the San Vicente deposit

Carbonate[1]	$CaCO_3$ (mole %)	$MgCO_3$ (mole %)	$FeCO_3$ (mole %)	$MnCO_3$ (mole %)	Sr (wt.%)	Zn (wt.%)	Na (wt.%)
DRD (Ivf)	53.33 to 54.14	44.11 to 45.50	0.08 to 1.50	0.33 to 0.57	0.007	0.03 to 0.33	0.01 to 0.02
(8)	(53.92)	(44.72)	(1.13)	(0.39)	-	(0.13)	(0.01)
DRD (If)	53.71 to 54.71	44.06 to 45.45	0.01 to 1.25	0.09 to 0.47	0.063	0.01 to 0.32	0.01 to 0.04
(13)	(54.19)	(44.54)	(0.80)	(0.32)	-	(0.12)	(0.02)
DRD (Im)	52.98 to 54.89	43.55 to 45.57	0.01 to 3.02	0.01 to 1.01	0.014 to 0.032	0.03 to 0.36	0.01 to 0.04
(35)	(53.87)	(44.92)	(0.69)	(0.34)	(0.030)	(0.15)	(0.02)
WSD	53.26 to 55.26	43.87 to 45.89	0.01 to 1.63	0.04 to 0.92	0.009 to 0.045	0.03 to 0.44	0.01 to 0.05
(82)	(53.96)	(45.07)	(0.34)	(0.31)	(0.027)	(0.13)	(0.02)

[1] DRD= dark replacement dolomite ("Ivf" very fine-grained, "If" fine-grained, "Im" medium-grained); WSD = white sparry dolomite (II)
n = number of analyzed samples; the median values are given in parentheses

The results can be summarized as follows:
(1) $MgCO_3$ values of the hydrothermal dolomites (Im = 44.9 wt.%, II = 45.1 wt.%) are slightly higher than of the very fine dark replacement dolomite (Ivf = 44.7);
(2) $FeCO_3$ content of the carbonates decreases in the order Ivf - If - Im - II (1.13, 0.80, 0.69, 0.34 wt.%);
(3) concentrations of Sr and Na are very low (<0.05 wt.%); (4) some Zn values in the WSD are very high (>0.4 wt.%) due to contamination by intergrown sphalerite indicated by petrographic observations.

The trends displayed by $MgCO_3$ and $FeCO_3$ are roughly similar to those of the ICP-AES results presented in chapter 4.

APPENDIX 3

COMPUTER PROGRAMS FOR MODELING OF THE CARBON AND OXYGEN ISOTOPE VARIATIONS DURING FLUID MIXING, WATER-ROCK INTERACTION, AND CO_2 DEGASSING

A. Computer program (EXCEL-Macro) for modeling of the carbon and oxygen isotope covariations in calcites and dolomite during water-rock interaction (after equations of Zheng and Hoefs, 1993)

B. Computer program (EXCEL-Macro) for modeling of the carbon and oxygen isotope covariations in calcites and dolomite during fluid mixing (after equations of Zheng and Hoefs, 1993)

C. Computer program (EXCEL-Macro) for modeling of the carbon and oxygen isotope covariations in calcites and dolomite during CO_2 degassing (after equations for batch and Rayleigh distillation after Zheng, 1990)

	A
1	**COMPUTER PROGRAM (EXCEL-MACRO) FOR MODELING OF THE CARBON AND OXYGEN ISOTOPE COVARIATIONS IN CALCITE AND DOLOMITE**
2	**DURING WATER-ROCK INTERACTION**
3	Written by J. Spangenberg (Dpt. Minéralogie, Uni. Genève) after equations of Zheng, Y.F. and Hoefs, J. (1993) Mineral. Deposita, 28, p. 78-89
4	*WRINTERACTION (W)*
5	=SET.NAME("CT";!$B$7)
6	=SET.NAME("CIR";!$B$9)
7	=SET.NAME("SC";!$B$14)
8	=SET.NAME("CFR";!$B$11)
9	=SET.NAME("OIW";!$B$15)
10	=SET.NAME("CIW";!$B$16)
11	=SET.NAME("TI";!$B$17)
12	=SET.NAME("TF";!$B$18)
13	=SET.NAME("WR";!$B$20)
14	=SET.NAME("N";!$B$21)
15	=SET.NAME("K";!$B$22)
16	=SET.NAME("OIR";!$B$27)
17	=SET.NAME("OFR";!$B$28)
18	=SET.NAME("TDB";!$B$29)
19	=SET.NAME("CD";!$B$30)
20	=SET.NAME("OD";!$B$31)
21	=SET.NAME("XC";!$B$32)
22	=SET.NAME("TG";!$B$33)
23	=WR/N
24	WR=A23
25	=IF(CT=1)
26	MWR=WR*100/18
27	NO=3
28	NC=1
29	O=0
30	=ELSE()
31	MWR=WR*183/18
32	NO=6
33	NC=2
34	O=3.8
35	=END.IF()
36	=FOR("I";0;N;1)
37	=I
38	=(1+I)*MWR
39	=I*WR
40	=TF+I*TG

	A
41	TR=A40
42	=TI-I*TG
43	TW=A42
44	=IF(SC=1)
45	=((-8.914*100000000)/((TR+273.2)*(TR+273.2)*(TR+273.2)))+((10.897*1000000)/((TR+273.2)*(TR+273.2)))-((38.27*1000)/(TR+273.2))+44.14
46	FCR=A45
47	=((2.78*1000000)/((TR+273.2)*(TR+273.2)))-2.89
48	FOR=A47
49	=((-8.914*100000000)/((TW+273.2)*(TW+273.2)*(TW+273.2)))+((10.897*1000000)/((TW+273.2)*(TW+273.2)))-((38.27*1000)/(TW+273.2))+44.14
50	FCW=A49
51	=((2.78*1000000)/((TW+273.2)*(TW+273.2)))-2.89
52	FOW=A51
53	=ELSE.IF(SC=2)
54	=((-8.914*100000000)/((TR+273.2)*(TR+273.2)*(TR+273.2)))+((8.737*1000000)/((TR+273.2)*(TR+273.2)))-((18.11*1000)/(TR+273.2))+8.44
55	FCR=A54
56	=((2.78*1000000)/((TR+273.2)*(TR+273.2)))-2.89
57	FOR=A56
58	=((-8.914*100000000)/((TW+273.2)*(TW+273.2)*(TW+273.2)))+((8.737*1000000)/((TW+273.2)*(TW+273.2)))-((18.11*1000)/(TW+273.2))+8.44
59	FCW=A58
60	=((2.78*1000000)/((TW+273.2)*(TW+273.2)))-2.89
61	FOW=A60
62	=ELSE()
63	=((-0.553*100000000)/((TR+273.2)*(TR+273.2)*(TR+273.2)))+((0.381*1000000)/((TR+273.2)*(TR+273.2)))-((0.45*1000)/(TR+273.2))+2.13
64	FCR=A63
65	=((2.78*1000000)/((TR+273.2)*(TR+273.2)))-2.89
66	FOR=A65
67	=((-0.553*100000000)/((TW+273.2)*(TW+273.2)*(TW+273.2)))+((0.381*1000000)/((TW+273.2)*(TW+273.2)))-((0.45*1000)/(TW+273.2))+2.13
68	FCW=A67
69	=((2.78*1000000)/((TW+273.2)*(TW+273.2)))-2.89
70	FOW=A69
71	=END.IF()
72	=OIW+FOR+(NO/MWR)*OD
73	=((A72-30.91)/1.03091)+O
74	=CIW+FCR+(NC/MWR*XC)*CD
75	=(OIW+FOR)-(OIW+FOR-OIR)*EXP(-MWR/NO)
76	=((A75-30.91)/1.03091)+O
77	=(CIW+FCR)-(CIW+FCR-CIR)*EXP(-MWR*XC/NC)
78	=(OIR+MWR/NO*(OIW+FOR))/(1+MWR/NO)
79	=((A78-30.91)/1.03091)+O
80	=(CIR+(MWR*XC/NC)*(CIW+FCR))/(1+MWR*XC/NC)

	A
81	=OIW+FOW
82	=((A81-30.91)/1.03091)+O
83	=CIW+FCW
84	OIR=A75
85	CIR=A77
86	=I/K
87	=IF(A86=INT(A86))
88	=FORMULA(A37)
89	=SELECT(;"RC[1]")
90	=FORMULA(A39)
91	=SELECT(;"RC[1]")
92	=FORMULA(A40)
93	=SELECT(;"RC[1]")
94	=FORMULA(A73)
95	=SELECT(;"RC[1]")
96	=FORMULA(A74)
97	=SELECT(;"RC[1]")
98	=FORMULA(A76)
99	=SELECT(;"RC[1]")
100	=FORMULA(A77)
101	=SELECT(;"RC[1]")
102	=FORMULA(A82)
103	=SELECT(;"RC[1]")
104	=FORMULA(A83)
105	=SELECT(;"RC[1]")
106	=FORMULA(A79)
107	=SELECT(;"RC[1]")
108	=FORMULA(A80)
109	=SELECT(OFFSET(ACTIVE.CELL();1;-10))
110	=END.IF()
111	=NEXT()
112	=RETURN()

CARBON AND OXYGEN ISOTOPE VARIATIONS IN CARBONATES ALTERED BY F/R INTERACTION DURING INCREASING F/R RATIO AND R-HEATING (modified from Zheng & Hoefs, 1993)
Worksheet for MACRO A

ROCK		
Calcite or dolomite? (Calcite:1; Dolomite:2) =	2	CT
Initial d18O of the rock (PDB) =	-7.0	
Initial d13C of the rock (PDB) =	3.0	OR
Final d18O rock (PDB) =	-8.0	
Final d13C rock (PDB) =	0.5	OFR
FLUID		
Dominant carbon specie (HCO3-:1;H2CO3:2;CO3=:3)=	1	SC
Initial d18O of the fluid (SMOW) =	0.5	OW
d13C of total dissolved carbon (TDC) =	-1.5	CW
Initial (highest) temperature of the fluid (°C) =	120	TI
Final (lowest) temperature of the fluid (°C) =	80	TF
TDC concentration as carbon (ppm) =	300	
Maxima Fluid/Rock weight fraction ratio =	200	WR
Number of iterations (<WR)=	50	N
Print results in what factor of iterations =	1	K
d18O fluid (SMOW) suggested	0.5	
d13C fluid (H2CO3 dominant) suggested	-6.5	
d13C fluid (HCO3- dominant) suggested	-2.1	
d13C fluid (CO3= dominant) suggested	-2.0	
Initial d18O of the rock (SMOW)	23.7	OIR
Final d18O of the rock (SMOW)	22.7	OFR
TDC concentration as bicarbonate (mg/l)	1525	TDB
Δ13C = d13Cinitial - d13Cfinal of the rock =	2.5	CD
Δ18O = d18Oinitial - d18Ofinal of the rock =	1	OD
Moles TDC/Moles water	0.00045	XC
Temperature gradient (°C) per iteration	1	TG

Carbon isotope fractionation factors (Ohmoto and Rye, 1979):

Δ13C (dol-CO2 or dol-H2CO3ap)	4.23000
Δ13C (cal-CO2 or cal-H2CO3ap)	2.89576
Δ13C (dol-HCO3-)	2.62936
Δ13C (cal-HCO3-)	1.29511
Δ13C (CH4-CO2)	-45.15057
Δ13C (CO3= vs. H2CO3(aq) or CO2)	-19.24284
Δ13C (HCO3- vs. H2CO3ap or CO2)	1.60064

Oxygen isotope fractionation factors (Friedman & O'Neil et al., 1977):

Δ18O (cal-H20)	15.09116

Oxygen isotope fractionation factors (Northrop & Clayton, 1966):

Δ18O (dol-H20)	18.69774

Oxygen isotope fractionation factors (Bottinga, 1968; Friedman & O'Neil,

Δ18O (CO2-H20)	25.66024

Oxygen isotope fractionation factors (Bottinga, 1968):

Δ18O (CO2g-cal)	12.54200

MWR = mol fluid/mol rock = (WR)*(mol. R/mol. F)

Iteration	Cum. W/R	T-°C(rock)	d18O-(F/R-op)	d13C-(F/R-op)	d18O-(alt-op)	d13C-(alt-op)	d18O-(F/R-cl)	d13C-(F/R-cl)	d18O-(pr. f)	d13C-(pr.f)
0	0	80.0	-6.74	1.41	-6.88	2.99	-11.06	1.13	-6.41	2.99
1	4	80.8	-6.84	1.40	-6.98	2.97	-10.99	1.13	-6.97	2.97
2	8	81.6	-6.94	1.38	-7.08	2.96	-10.92	1.13	-7.07	2.96
3	12	82.4	-7.03	1.37	-7.18	2.94	-10.84	1.13	-7.16	2.94
4	16	83.2	-7.13	1.36	-7.27	2.93	-10.77	1.13	-7.26	2.93
5	20	84.0	-7.22	1.35	-7.37	2.91	-10.70	1.13	-7.35	2.91
6	24	84.8	-7.32	1.34	-7.46	2.90	-10.63	1.13	-7.45	2.90
7	28	85.6	-7.41	1.33	-7.55	2.88	-10.55	1.13	-7.54	2.88
8	32	86.4	-7.50	1.32	-7.65	2.87	-10.48	1.13	-7.64	2.87
9	36	87.2	-7.60	1.31	-7.74	2.86	-10.40	1.13	-7.73	2.86
10	40	88.0	-7.69	1.30	-7.83	2.84	-10.33	1.13	-7.82	2.84
11	44	88.8	-7.78	1.29	-7.92	2.83	-10.25	1.13	-7.91	2.83
12	48	89.6	-7.87	1.28	-8.01	2.81	-10.18	1.14	-8.00	2.81
13	52	90.4	-7.96	1.27	-8.10	2.80	-10.10	1.14	-8.09	2.80
14	56	91.2	-8.05	1.26	-8.19	2.79	-10.02	1.14	-8.18	2.79
15	60	92.0	-8.14	1.25	-8.28	2.77	-9.94	1.14	-8.27	2.77
16	64	92.8	-8.23	1.24	-8.37	2.76	-9.87	1.15	-8.36	2.76
17	68	93.6	-8.32	1.24	-8.46	2.74	-9.79	1.15	-8.45	2.74
18	72	94.4	-8.40	1.23	-8.55	2.73	-9.71	1.15	-8.53	2.73
19	76	95.2	-8.49	1.22	-8.63	2.72	-9.63	1.16	-8.62	2.72
20	80	96.0	-8.58	1.21	-8.72	2.70	-9.55	1.16	-8.71	2.70
21	84	96.8	-8.66	1.21	-8.80	2.69	-9.47	1.16	-8.79	2.69
22	88	97.6	-8.75	1.20	-8.89	2.68	-9.39	1.17	-8.88	2.68
23	92	98.4	-8.83	1.20	-8.97	2.66	-9.30	1.17	-8.96	2.66
24	96	99.2	-8.91	1.19	-9.06	2.65	-9.22	1.18	-9.05	2.65
25	100	100.0	-9.00	1.18	-9.14	2.64	-9.14	1.18	-9.13	2.64
26	104	100.8	-9.08	1.18	-9.22	2.62	-9.06	1.19	-9.21	2.62
27	108	101.6	-9.16	1.17	-9.30	2.61	-8.97	1.20	-9.29	2.61
28	112	102.4	-9.24	1.17	-9.39	2.60	-8.89	1.20	-9.38	2.60
29	116	103.2	-9.32	1.17	-9.47	2.58	-8.80	1.21	-9.46	2.58
30	120	104.0	-9.41	1.16	-9.55	2.57	-8.72	1.21	-9.54	2.57
31	124	104.8	-9.49	1.16	-9.63	2.56	-8.63	1.22	-9.62	2.56
32	128	105.6	-9.57	1.15	-9.71	2.54	-8.55	1.23	-9.70	2.54
33	132	106.4	-9.64	1.15	-9.79	2.53	-8.46	1.24	-9.78	2.53
34	136	107.2	-9.72	1.15	-9.87	2.52	-8.37	1.24	-9.86	2.52
35	140	108.0	-9.80	1.14	-9.94	2.51	-8.28	1.25	-9.93	2.51
36	144	108.8	-9.88	1.14	-10.02	2.49	-8.19	1.26	-10.01	2.49
37	148	109.6	-9.96	1.14	-10.10	2.48	-8.10	1.27	-10.09	2.48
38	152	110.4	-10.03	1.14	-10.18	2.47	-8.01	1.28	-10.17	2.47
39	156	111.2	-10.11	1.13	-10.25	2.46	-7.92	1.29	-10.24	2.46
40	160	112.0	-10.18	1.13	-10.33	2.44	-7.83	1.30	-10.32	2.44
41	164	112.8	-10.26	1.13	-10.40	2.43	-7.74	1.31	-10.39	2.43
42	168	113.6	-10.33	1.13	-10.48	2.42	-7.65	1.32	-10.47	2.42
43	172	114.4	-10.41	1.13	-10.55	2.41	-7.55	1.33	-10.54	2.41
44	176	115.2	-10.48	1.13	-10.63	2.40	-7.46	1.34	-10.62	2.40
45	180	116.0	-10.56	1.13	-10.70	2.39	-7.37	1.35	-10.69	2.39
46	184	116.8	-10.63	1.13	-10.77	2.37	-7.27	1.36	-10.76	2.37
47	188	117.6	-10.70	1.13	-10.84	2.36	-7.18	1.37	-10.84	2.36
48	192	118.4	-10.77	1.13	-10.92	2.35	-7.08	1.38	-10.91	2.35
49	196	119.2	-10.85	1.13	-10.99	2.34	-6.98	1.39	-10.98	2.34
50	200	120.0	-10.92	1.13	-11.06	2.33	-6.89	1.41	-11.05	2.33

alt = hydrothermal alteration during F/R interaction
F/R = carbonate precipitated by F/R interaction
op = open system
pr. f = precipitated from initial fluid
cl = closed system
Δ = d-change of wallrock due to F/R interaction
d13C vs. PDB
d18O vs. PDB if nothing stated

	B
1	**COMPUTER PROGRAM (EXCEL-MACRO) FOR MODELING OF THE CARBON AND OXYGEN ISOTOPE COVARIATIONS IN CALCITE AND DOLOMITE**
2	**PRECIPITATED DURING MIXING OF TWO FLUIDS**
3	Written by J. Spangenberg (Dpt. Minéralogie, Uni. Genève) after equations of Zheng, Y.F. and Hoefs, J. (1993) Mineral. Deposita, 28, p. 78-89
4	*FLUIDMIXING (M)*
5	=SET.NAME("CA";I$B$7)
6	=SET.NAME("CB";I$B$15)
7	=SET.NAME("OA";I$B$6)
8	=SET.NAME("OB";I$B$14)
9	=SET.NAME("TA";I$B$8)
10	=SET.NAME("TB";I$B$16)
11	=SET.NAME("SA";I$B$9)
12	=SET.NAME("SB";I$B$17)
13	=SET.NAME("CS";I$B$20)
14	=SET.NAME("P";I$B$22)
15	=FOR("I";0;100;I$B$21)
16	=I
17	=I/100
18	=1-B17
19	Xb=B17
20	Xa=B18
21	=Xa*TA+(1-Xa)*TB
22	T=B21
23	=IF(CS=1)
24	O=0
25	=IF(SA=1)
26	=((-8.914*100000000)/((T+273.2)*(T+273.2)*(T+273.2)))+((10.717*1000000)/((T+273.2)*(T+273.2)))-((38.27*1000)/(T+273.2))+43.97
27	AF=B26
28	=((2.78*1000000)/((T+273.2)*(T+273.2)))-2.89
29	AD=B28
30	=ELSE()
31	=((-8.914*100000000)/((T+273.2)*(T+273.2)*(T+273.2)))+((8.557*1000000)/((T+273.2)*(T+273.2)))-((18.11*1000)/(T+273.2))+8.27
32	AF=B31
33	=((2.78*1000000)/((T+273.2)*(T+273.2)))-2.89
34	AD=B33
35	=END.IF()
36	=IF(SB=1)
37	=((-8.914*100000000)/((T+273.2)*(T+273.2)*(T+273.2)))+((10.717*1000000)/((T+273.2)*(T+273.2)))-((38.27*1000)/(T+273.2))+43.97
38	BF=B37
39	=((2.78*1000000)/((T+273.2)*(T+273.2)))-2.89
40	BD=B39

	B
41	=ELSE()
42	=((-8.914*100000000)/((T+273.2)*(T+273.2)*(T+273.2)))+((8.557*1000000)/((T+273.2)*(T+273.2)))-((18.11*1000)/(T+273.2))+8.27
43	BF=B42
44	=((2.78*1000000)/((T+273.2)*(T+273.2)))-2.89
45	BD=B44
46	=END.IF()
47	=ELSE.IF(CS=2)
48	O=3.8
49	=IF(SA=1)
50	=((-8.914*100000000)/((T+273.2)*(T+273.2)*(T+273.2)))+((10.897*1000000)/((T+273.2)*(T+273.2)))-((38.27*1000)/(T+273.2))+44.14
51	AF=B50
52	=((2.78*1000000)/((T+273.2)*(T+273.2)))-2.89
53	AD=B52
54	=ELSE()
55	=((-8.914*100000000)/((T+273.2)*(T+273.2)*(T+273.2)))+((8.737*1000000)/((T+273.2)*(T+273.2)))-((18.11*1000)/(T+273.2))+8.44
56	AF=B55
57	=((2.78*1000000)/((T+273.2)*(T+273.2)))-2.89
58	AD=B57
59	=END.IF()
60	=IF(SB=1)
61	=((-8.914*100000000)/((T+273.2)*(T+273.2)*(T+273.2)))+((10.897*1000000)/((T+273.2)*(T+273.2)))-((38.27*1000)/(T+273.2))+44.14
62	BF=B61
63	=((2.78*1000000)/((T+273.2)*(T+273.2)))-2.89
64	BD=B63
65	=ELSE()
66	=((-8.914*100000000)/((T+273.2)*(T+273.2)*(T+273.2)))+((8.737*1000000)/((T+273.2)*(T+273.2)))-((18.11*1000)/(T+273.2))+8.44
67	BF=B66
68	=((2.78*1000000)/((T+273.2)*(T+273.2)))-2.89
69	BD=B68
70	=END.IF()
71	=END.IF()
72	=(Xa*(CA+AF)+P*(1-Xa)*(CB+BF))/(P+Xa-P*Xa)
73	=Xa*(OA+AD)+(1-Xa)*(OB+BD)
74	=((B73-30.91)/1.03091)+O
75	=(Xa*CA+P*Xb*CB)/(P*Xb+Xa)
76	=(Xa*OA+Xb*OB)/(Xa+Xb)
77	=FORMULA(B18)
78	=SELECT(;"RC[1]")
79	=FORMULA(B21)
80	=SELECT(;"RC[1]")

	B
81	=FORMULA(B76)
82	=SELECT(;"RC[1]")
83	=FORMULA(B75)
84	=SELECT(;"RC[1]")
85	=FORMULA(B74)
86	=SELECT(;"RC[1]")
87	=FORMULA(B72)
88	=SELECT(OFFSET(ACTIVE.CELL();1;-5))
89	=NEXT()
90	=RETURN()
91	
92	
93	
94	
95	
96	
97	
98	
99	
100	
101	
102	
103	
104	
105	
106	
107	
108	
109	
110	
111	
112	

CARBON AND OXYGEN ISOTOPE VARIATIONS IN CARBONATES PRECIPITATED BY FLUID MIXING (modified from Zheng & Hoefs, 1993) Worksheet for MACRO B

Fluid A

d18O (SMOW) =	-2.3	OA
d13C (PDB) =	-0.8	CA
Temp. (°C) =	60	TA
Dominant carbon specie? (HCO3-=1; H2CO3=2)	1	SA
TDC concentration as C (ppm) =	500	
TDC as bicarbonate (mg/l) =	2542	

Fluid B

d18O (SMOW) =	0.0	OB
d13C (PDB) =	-5.0	CB
Temp. (°C) =	150	TB
Dominant carbon specie? (HCO3-=1; H2CO3=2)	2	SB
TDC concentration as C (ppm) =	200	
TDC as bicarbonate (mg/l)	1017	
Precipitation of Calcite (1) or Dolomite (2)? =	2	CS
% increments of fluid B to the mixing =	2	MA
C proportion in both fluids (CB/CA)	0.4	P

M fract. fluid A	T-mix. (°C)	dO18 -SMOW (fluid)	d13C -PDB (fluidl)	dO18 -PDB (rock)	d13C -PDB (rock)
1.00	60.00	-2.30	-0.80	-6.93	2.54
0.98	61.80	-2.25	-0.83	-7.14	2.50
0.96	63.60	-2.21	-0.87	-7.36	2.46
0.94	65.40	-2.16	-0.90	-7.56	2.42
0.92	67.20	-2.12	-0.94	-7.77	2.38
0.90	69.00	-2.07	-0.98	-7.97	2.34
0.88	70.80	-2.02	-1.02	-8.16	2.30
0.86	72.60	-1.98	-1.06	-8.35	2.26
0.84	74.40	-1.93	-1.10	-8.54	2.22
0.82	76.20	-1.89	-1.14	-8.73	2.18
0.80	78.00	-1.84	-1.18	-8.91	2.14
0.78	79.80	-1.79	-1.23	-9.09	2.10
0.76	81.60	-1.75	-1.27	-9.26	2.06
0.74	83.40	-1.70	-1.32	-9.43	2.01
0.72	85.20	-1.66	-1.37	-9.60	1.97
0.70	87.00	-1.61	-1.41	-9.76	1.92
0.68	88.80	-1.56	-1.47	-9.93	1.88
0.66	90.60	-1.52	-1.52	-10.08	1.83
0.64	92.40	-1.47	-1.57	-10.24	1.78
0.62	94.20	-1.43	-1.63	-10.39	1.73
0.60	96.00	-1.38	-1.68	-10.54	1.67
0.58	97.80	-1.33	-1.74	-10.69	1.62
0.56	99.60	-1.29	-1.80	-10.83	1.56
0.54	101.40	-1.24	-1.87	-10.97	1.50
0.52	103.20	-1.20	-1.93	-11.11	1.44
0.50	105.00	-1.15	-2.00	-11.25	1.37
0.48	106.80	-1.10	-2.07	-11.38	1.30
0.46	108.60	-1.06	-2.14	-11.51	1.23
0.44	110.40	-1.01	-2.22	-11.64	1.15
0.42	112.20	-0.97	-2.29	-11.77	1.07
0.40	114.00	-0.92	-2.38	-11.89	0.99
0.38	115.80	-0.87	-2.46	-12.01	0.90
0.36	117.60	-0.83	-2.55	-12.13	0.81
0.34	119.40	-0.78	-2.64	-12.25	0.71
0.32	121.20	-0.74	-2.73	-12.36	0.60
0.30	123.00	-0.69	-2.83	-12.48	0.49
0.28	124.80	-0.64	-2.93	-12.59	0.38
0.26	126.60	-0.60	-3.04	-12.70	0.25
0.24	128.40	-0.55	-3.15	-12.80	0.12
0.22	130.20	-0.51	-3.26	-12.91	-0.02
0.20	132.00	-0.46	-3.38	-13.01	-0.17
0.18	133.80	-0.41	-3.51	-13.11	-0.33
0.16	135.60	-0.37	-3.65	-13.21	-0.50
0.14	137.40	-0.32	-3.79	-13.30	-0.67
0.12	139.20	-0.28	-3.93	-13.40	-0.87
0.10	141.00	-0.23	-4.09	-13.49	-1.07
0.08	142.80	-0.18	-4.25	-13.58	-1.29
0.06	144.60	-0.14	-4.42	-13.67	-1.52
0.04	146.40	-0.09	-4.60	-13.76	-1.77
0.02	148.20	-0.05	-4.80	-13.85	-2.04
0.00	150.00	0.00	-5.00	-13.93	-2.33

	C
1	**COMPUTER PROGRAM (EXCEL-MACRO) FOR MODELING OF THE CARBON AND OXYGEN ISOTOPE COVARIATIONS**
2	**IN CALCITE AND DOLOMITE PRECIPITATED DURING CO2 DEGASSING (Rayleigh distillation equations)**
3	Written by Jorge Spangenberg (Dpt. Minéralogie, Uni. Genève) after equations of Zheng, Y.F. (1990) Mineral. Deposita, 25, p. 246-250
4	*DEGASSING (D)*
5	=SET.NAME("OF";!$B$7)
6	=SET.NAME("CF";!$B$8)
7	=SET.NAME("TI";!$B$9)
8	=SET.NAME("TF";!$B$10)
9	=SET.NAME("SC";!$B$11)
10	=SET.NAME("MC";!$B$12)
11	=SET.NAME("MO";!$B$13)
12	=SET.NAME("FdT";!$B$14)
13	=SET.NAME("CT";!$B$15)
14	=IF(CT=1)
15	DO=0
16	=ELSE()
17	DO=3.8
18	=END.IF()
19	=(TI-TF)/100
20	TG=C19
21	=FOR("I";0;100;FdT)
22	=I
23	=TI-(I*TG)
24	T=C23
25	=((2.78*1000000)/((T+273.2)*(T+273.2)))-3.39
26	OR=C25
27	=16.6*1000/(T+273.2)-15.19
28	OC=C27
29	=IF(SC=1)
30	=IF(CT=1)
31	=((-8.914*100000000)/((T+273.2)*(T+273.2)*(T+273.2)))+((10.717*1000000)/((T+273.2)*(T+273.2)))-((38.27*1000)/(T+273.2))+43.97
32	RB=C31
33	=((-2.16*1000000)/((T+273.2)*(T+273.2)))+((20.16*1000)/(T+273.2))-35.7
34	CB=C33
35	=ELSE()
36	=((-8.914*100000000)/((T+273.2)*(T+273.2)*(T+273.2)))+((10.897*1000000)/((T+273.2)*(T+273.2)))-((38.27*1000)/(T+273.2))+44.14
37	RB=C36
38	=((-2.16*1000000)/((T+273.2)*(T+273.2)))+((20.16*1000)/(T+273.2))-35.7
39	CB=C38
40	=END.IF()

	C
41	=OF+(1-2*MO)*OR+MO*OC
42	=((C41-30.91)/1.03091)+DO
43	=CF+(1-2*MC)*RB-MC*CB
44	=OF+LN(1-MO)*OC+(1+LN(1-2*MO))*OR
45	=((C44-30.91)/1.03091)+DO
46	=CF+LN(1-MC)*CB+(1+LN(1-2*MC))*RB
47	=FORMULA(C23)
48	=SELECT(;"RC[1]")
49	=FORMULA(C42)
50	=SELECT(;"RC[1]")
51	=FORMULA(C43)
52	=SELECT(;"RC[1]")
53	=FORMULA(C45)
54	=SELECT(;"RC[1]")
55	=FORMULA(C46)
56	=SELECT(OFFSET(ACTIVE.CELL();1;-4))
57	=ELSE.IF(SC=2)
58	=IF(CT=1)
59	=((-8.914*100000000)/((T+273.2)*(T+273.2)*(T+273.2)))+((8.557*1000000)/((T+273.2)*(T+273.2)))-((18.11*1000)/(T+273.2))+8.27
60	CR=C59
61	=ELSE()
62	=((-8.914*100000000)/((T+273.2)*(T+273.2)*(T+273.2)))+((8.737*1000000)/((T+273.2)*(T+273.2)))-((18.11*1000)/(T+273.2))+8.44
63	CR=C62
64	=END.IF()
65	=OF+(1-2*MO)*OR+MO*OC
66	=((C65-30.91)/1.03091)+DO
67	=CF+(1-2*MC)*CR
68	=OF+(LN(1-MO))*OC+(1+LN(1-2*MO))*OR
69	=((C68-30.91)/1.03091)+DO
70	=CF+(1+LN(1-2*MC))*CR
71	=FORMULA(C23)
72	=SELECT(;"RC[1]")
73	=FORMULA(C66)
74	=SELECT(;"RC[1]")
75	=FORMULA(C67)
76	=SELECT(;"RC[1]")
77	=FORMULA(C69)
78	=SELECT(;"RC[1]")
79	=FORMULA(C70)
80	=SELECT(OFFSET(ACTIVE.CELL();1;-4))

	C
81	=ELSE()
82	=IF(CT=1)
83	=((-0.553*100000000)/((T+273.2)*(T+273.2)*(T+273.2)))+((0.381*1000000)/((T+273.2)*(T+273.2)))-((0.45*1000)/(T+273.2))+2.13
84	RB=C83
85	=((-8.361*100000000)/((T+273.2)*(T+273.2)*(T+273.2)))+((8.196*1000000)/((T+273.2)*(T+273.2)))-((17.66*1000)/(T+273.2))+6.14
86	CB=C85
87	=ELSE()
88	=((-0.555*100000000)/((T+273.2)*(T+273.2)*(T+273.2)))+((0.541*1000000)/((T+273.2)*(T+273.2)))-((0.45*1000)/(T+273.2))+2.3
89	RB=C88
90	=((-8.361*100000000)/((T+273.2)*(T+273.2)*(T+273.2)))+((8.196*1000000)/((T+273.2)*(T+273.2)))-((17.66*1000)/(T+273.2))+6.14
91	CB=C90
92	=END.IF()
93	=OF+(1-2*MO)*OR+MO*OC
94	=((C93-30.91)/1.03091)+DO
95	=CF+(1-2*MC)*RB-MC*CB
96	=OF+LN(1-MO)*OC+(1+LN(1-2*MO))*OR
97	=((C96-30.91)/1.03091)+DO
98	=CF+LN(1-MC)*CB+(1+LN(1-2*MC))*RB
99	=FORMULA(C23)
100	=SELECT(;"RC[1]")
101	=FORMULA(C94)
102	=SELECT(;"RC[1]")
103	=FORMULA(C95)
104	=SELECT(;"RC[1]")
105	=FORMULA(C97)
106	=SELECT(;"RC[1]")
107	=FORMULA(C98)
108	=SELECT(OFFSET(ACTIVE.CELL();1;-4))
109	=END.IF()
110	=NEXT()
111	=RETURN()
112	

CARBON AND OXYGEN ISOTOPE VARIATIONS IN CARBONATES PRECIPITATED DURING CO2-DEGASSING AND COOLING (modified from Zheng, 1990) Worksheet for MACRO C

Fluid:

d18O (SMOW) =	0.5	OF
d13C (PDB) =	-2.5	OF
Initial Temp. (°C) =	100	TI
Final Temp. (°C) =	80	TF
Dominant carbon specie? (HCO3-=1;H2CO3=2;CO3=3)=	1	SC
Mol fraction of C in degassed CO2 (<0.5) =	0.100	MC
Mol fraction of O in degassed CO2 (<<0.5) =	0.001	MO
Factor of temperature increment (1, 2, 3...) =	3	FdT
Calcite (=1) or Dolomite (=2)?	2	CT

BM = model based on batch distillation equations
RM = model based on Rayleigh distillation equations

T-mix. (°C)	dO18 -PDB (BM)	d13C -PDB (BM)	dO18 -PDB (RM)	d13C -PDB (RM)
100.0	-9.63	-0.63	-9.69	-0.71
99.4	-9.57	-0.63	-9.62	-0.71
98.8	-9.50	-0.63	-9.56	-0.71
98.2	-9.44	-0.63	-9.50	-0.71
97.6	-9.38	-0.63	-9.43	-0.71
97.0	-9.31	-0.63	-9.37	-0.71
96.4	-9.25	-0.63	-9.31	-0.71
95.8	-9.19	-0.63	-9.24	-0.71
95.2	-9.12	-0.63	-9.18	-0.71
94.6	-9.06	-0.63	-9.11	-0.71
94.0	-8.99	-0.63	-9.05	-0.71
93.4	-8.93	-0.63	-8.98	-0.71
92.8	-8.86	-0.63	-8.92	-0.71
92.2	-8.79	-0.63	-8.85	-0.71
91.6	-8.73	-0.63	-8.79	-0.71
91.0	-8.66	-0.63	-8.72	-0.71
90.4	-8.59	-0.63	-8.65	-0.71
89.8	-8.53	-0.62	-8.59	-0.71
89.2	-8.46	-0.62	-8.52	-0.71
88.6	-8.39	-0.62	-8.45	-0.70
88.0	-8.32	-0.62	-8.38	-0.70
87.4	-8.25	-0.62	-8.31	-0.70
86.8	-8.18	-0.61	-8.24	-0.70
86.2	-8.11	-0.61	-8.17	-0.70
85.6	-8.04	-0.61	-8.11	-0.70
85.0	-7.97	-0.61	-8.04	-0.69
84.4	-7.90	-0.60	-7.96	-0.69
83.8	-7.83	-0.60	-7.89	-0.69
83.2	-7.76	-0.60	-7.82	-0.69
82.6	-7.69	-0.60	-7.75	-0.68
82.0	-7.62	-0.59	-7.68	-0.68
81.4	-7.55	-0.59	-7.61	-0.68
80.8	-7.47	-0.59	-7.54	-0.67
80.2	-7.40	-0.58	-7.46	-0.67